

1985

Strengthening of simple span composite bridges by post-tensioning

Kenneth Frederick Dunker
Iowa State University

Follow this and additional works at: <https://lib.dr.iastate.edu/rtd>

 Part of the [Civil Engineering Commons](#)

Recommended Citation

Dunker, Kenneth Frederick, "Strengthening of simple span composite bridges by post-tensioning" (1985). *Retrospective Theses and Dissertations*. 12055.
<https://lib.dr.iastate.edu/rtd/12055>

This Dissertation is brought to you for free and open access by the Iowa State University Capstones, Theses and Dissertations at Iowa State University Digital Repository. It has been accepted for inclusion in Retrospective Theses and Dissertations by an authorized administrator of Iowa State University Digital Repository. For more information, please contact digirep@iastate.edu.

INFORMATION TO USERS

This reproduction was made from a copy of a document sent to us for microfilming. While the most advanced technology has been used to photograph and reproduce this document, the quality of the reproduction is heavily dependent upon the quality of the material submitted.

The following explanation of techniques is provided to help clarify markings or notations which may appear on this reproduction.

1. The sign or "target" for pages apparently lacking from the document photographed is "Missing Page(s)". If it was possible to obtain the missing page(s) or section, they are spliced into the film along with adjacent pages. This may have necessitated cutting through an image and duplicating adjacent pages to assure complete continuity.
2. When an image on the film is obliterated with a round black mark, it is an indication of either blurred copy because of movement during exposure, duplicate copy, or copyrighted materials that should not have been filmed. For blurred pages, a good image of the page can be found in the adjacent frame. If copyrighted materials were deleted, a target note will appear listing the pages in the adjacent frame.
3. When a map, drawing or chart, etc., is part of the material being photographed, a definite method of "sectioning" the material has been followed. It is customary to begin filming at the upper left hand corner of a large sheet and to continue from left to right in equal sections with small overlaps. If necessary, sectioning is continued again—beginning below the first row and continuing on until complete.
4. For illustrations that cannot be satisfactorily reproduced by xerographic means, photographic prints can be purchased at additional cost and inserted into your xerographic copy. These prints are available upon request from the Dissertations Customer Services Department.
5. Some pages in any document may have indistinct print. In all cases the best available copy has been filmed.

**University
Microfilms
International**

300 N. Zeeb Road
Ann Arbor, MI 48106

8524645

Dunker, Kenneth Frederick

STRENGTHENING OF SIMPLE SPAN COMPOSITE BRIDGES BY POST-TENSIONING

Iowa State University

PH.D. 1985

University
Microfilms
International 300 N. Zeeb Road, Ann Arbor, MI 48106

Strengthening of simple span composite bridges by post-tensioning

by

Kenneth Frederick Dunker

A Dissertation Submitted to the
Graduate Faculty in Partial Fulfillment of the
Requirements for the Degree of
DOCTOR OF PHILOSOPHY

Department: Civil Engineering

Major: Structural Engineering

Approved:

Signature was redacted for privacy.

In ~~Charge~~ of Major Work

Signature was redacted for privacy.

For the Major Department

Signature was redacted for privacy.

For the Graduate College

Iowa State University
Ames, Iowa

1985

TABLE OF CONTENTS

	PAGE
1. INTRODUCTION	1
1.1. Iowa Composite Bridges	1
1.2. Objectives	7
1.3. Literature Review	10
1.3.1. Prestressed steel structures	10
1.3.2. Prestressed composite structures	13
1.3.3. Bridge strengthening by post-tensioning	15
1.3.4. Bridge deck behavior and analysis	18
1.3.4.1. Live load distribution in right-angle bridges	18
1.3.4.2. Live load distribution in skewed bridges	20
1.3.4.3. Composite beam and bridge deck analysis	24
1.3.5. Summary	27
2. BEHAVIOR OF POST-TENSIONED COMPOSITE BEAMS	32
2.1. Beam Description	33
2.2. Elastic Analytical Model	43
2.2.1. Equilibrium analysis	43
2.2.2. Secondary effects	44
2.2.3. Model verification	48
2.3. Elastic Finite Element Model	54
2.3.1. SAP IV elements	55
2.3.2. Model assembly	59
2.3.3. Model verification	66
2.4. Inelastic Analytical Model	81
2.4.1. Model development	81
2.4.2. Model verification	83
3. BEHAVIOR OF POST-TENSIONED COMPOSITE BRIDGES	91
3.1. Bridge Descriptions	92
3.1.1. Model bridge	92
3.1.2. Bridge 1	95
3.1.3. Bridge 2	98
3.1.4. Post-tensioning details	100
3.2. Elastic Finite Element Model	103
3.2.1. Model development	103
3.2.2. Quarter symmetry model	110
3.2.3. Complete model	112
3.2.4. Model verification	115

3.2.4.1.	Model bridge	115
3.2.4.2.	Bridge 1	130
3.2.4.3.	Bridge 2	144
4.	POST-TENSIONING DISTRIBUTION	160
4.1.	Distribution Fractions	161
4.2.	Iowa Standard Bridge Designs	171
4.3.	Multiple Linear Regression	176
4.3.1.	Bridge variables	176
4.3.2.	Midspan distribution fractions	177
4.3.2.1.	Three-beam bridges	182
4.3.2.2.	Four-beam bridges	185
4.4.	Distribution Fraction Interpolation and Verification	187
5.	DESIGN METHODOLOGY	192
5.1.	Design Procedure	192
5.2.	Design Example	194
5.2.1.	Bridge description	195
5.2.2.	Loads and load distribution fractions	197
5.2.3.	Moments	197
5.2.4.	Section properties	199
5.2.5.	Post-tensioning design	202
5.2.6.	Stress checks and bracket location	212
5.2.7.	Brackets and anchorages	225
5.2.8.	Additional design considerations	225
6.	SUMMARY AND CONCLUSIONS	227
6.1.	Summary	227
6.2.	Conclusions	231
7.	ACKNOWLEDGMENTS	234
8.	REFERENCES	236
9.	APPENDIX. DERIVATION OF ΔT FORMULA FOR POST-TENSIONED BEAM WITH PARTIAL-LENGTH COVERPLATE	244

LIST OF TABLES

	PAGE
TABLE 1. Physical properties of concrete for composite beams (Dedic)	41
TABLE 2. Physical properties of steel for composite beams (Dedic)	42
TABLE 3. Experimental and computed midspan deflections and strains for prestressed composite beams -- elastic analytical model	51
TABLE 4. Experimental and computed ΔT forces, midspan deflections, and midspan strains for loaded prestressed composite beams -- elastic analytical model	52
TABLE 5. SAP IV analysis runs for post-tensioned composite beams . .	67
TABLE 6. Experimental and computed midspan deflections, midspan strains, and ΔT forces for Beam 2 -- elastic finite element models	71
TABLE 7. Experimental and computed midspan deflections, midspan strains, and ΔT forces for Beam 3 -- elastic finite element models	73
TABLE 8. Experimental and computed midspan deflections, ΔT forces, and flexural strengths -- inelastic analytical model	87
TABLE 9. Experimental and computed midspan coverplate strains for post-tensioned model bridge -- elastic finite element model	109
TABLE 10. Experimental and computed midspan deflections for post-tensioned model bridge -- elastic finite element model .	111
TABLE 11. Bridges included in multiple linear regression analysis for distribution fractions	174
TABLE 12. Dead and long-term dead loads	198

TABLE 13. Dead, long-term dead, and live load moments for exterior beam	200
TABLE 14. Dead, long-term dead, and live load moments for interior beam	201
TABLE 15. Section properties for exterior beam	203
TABLE 16. Section properties for interior beam	204
TABLE 17. Section properties with respect to composite bridge neutral axis	205
TABLE 18. Tension stresses in exterior beam coverplate at midspan .	207
TABLE 19. Distribution fractions	209
TABLE 20. Required post-tensioning tendon force	211
TABLE 21. Stress checks for exterior beam at midspan	213
TABLE 22. Stress checks for exterior beam with coverplate at coverplate cutoff	214
TABLE 23. Stress checks for exterior beam without coverplate at coverplate cutoff	215
TABLE 24. Stress checks for interior beam at midspan	216
TABLE 25. Stress checks for interior beam with coverplate at coverplate cutoff	217
TABLE 26. Stress checks for interior beam without coverplate at coverplate cutoff	218
TABLE 27. Bracket bolt location	219
TABLE 28. Stress checks for exterior beam at anchorage ($y = 4$ feet)	221

LIST OF FIGURES

	PAGE
FIGURE 1. 50 ft. by 30 ft. I-beam bridge, Dickinson County	3
FIGURE 2. Post-tensioned exterior bridge beam	6
FIGURE 3. Typical Iowa composite bridge	8
FIGURE 4. Prestressed composite beams (Stras)	37
FIGURE 5. Post-tensioned composite beams (Dedic)	39
FIGURE 6. Equilibrium analysis of a post-tensioned composite beam	45
FIGURE 7. Secondary effects due to post-tensioning	47
FIGURE 8. ΔT for post-tensioned composite beam with coverplate	49
FIGURE 9. Single element tests for SAP IV thin plate and shell element	57
FIGURE 10. Convergence tests for a simply supported plate with a central concentrated load	60
FIGURE 11. SAP IV finite element models for post-tensioned composite beams	62
FIGURE 12. SAP IV finite element models for shear connectors	65
FIGURE 13. SAP IV quarter symmetry, post-tensioned composite beam models	69
FIGURE 14. Longitudinal membrane stresses in deck for post- tensioning, Beam 2	75
FIGURE 15. Longitudinal membrane stresses in deck for post- tensioning and vertical load, Beam 2	76
FIGURE 16. Shear flow and shear connector forces, Beam 2	78
FIGURE 17. Shear flow and shear connector forces, Beam 3	80

FIGURE 18. Prestressed composite beams -- inelastic analytical model	84
FIGURE 19. Model bridge	93
FIGURE 20. Bridge 1	97
FIGURE 21. Bridge 2	99
FIGURE 22. Post-tensioning details	101
FIGURE 23. SAP IV finite element model for post-tensioned composite bridge beam	105
FIGURE 24. SAP IV bridge model details	106
FIGURE 25. Equivalent nodal loads	113
FIGURE 26. SAP IV quarter symmetry model for Bridge 1	114
FIGURE 27. SAP IV complete model for Bridge 2	116
FIGURE 28. Midspan strains and deflections for model bridge with post-tensioned exterior beams	119
FIGURE 29. Quarterspan strains and deflections for model bridge with post-tensioned exterior beams	120
FIGURE 30. Midspan strains and deflections for model bridge with one post-tensioned exterior beam	122
FIGURE 31. Deflected shape for model bridge with post-tensioned exterior beams	124
FIGURE 32. Midspan strains and deflections for model bridge with concentrated load at midspan of exterior beam	125
FIGURE 33. Deflected shape for model bridge with concentrated load at midspan of exterior beam	126
FIGURE 34. Midspan strains and deflections for model bridge with concentrated load at midspan of interior beam	128
FIGURE 35. Change in tendon force for vertically loaded, post-tensioned model bridge	129
FIGURE 36. Guard rail and end restraints for Bridge 1	131

FIGURE 37. Midspan strains and deflections for Bridge 1 with post-tensioned exterior beams	134
FIGURE 38. Bottom flange and coverplate strains for Bridge 1 with post-tensioned exterior beams	136
FIGURE 39. Midspan and end strains for Bridge 1 with post-tensioned exterior beams	138
FIGURE 40. Deflected shape for Bridge 1 with post-tensioned exterior beams and simple supports	140
FIGURE 41. Deflected shape for Bridge 1 with post-tensioned exterior beams and fixed supports	141
FIGURE 42. Midspan strains and deflections for Bridge 1 with eccentric truck load	142
FIGURE 43. Deflected shape for Bridge 1 with eccentric truck load	143
FIGURE 44. Midspan strains and deflections for Bridge 1 with central truck load	145
FIGURE 45. Deflected shape for Bridge 1 with central truck load	146
FIGURE 46. Midspan strains and deflections for Bridge 2 with post-tensioned exterior beams	148
FIGURE 47. Quarterspan strains and deflections for Bridge 2 with post-tensioned exterior beams	149
FIGURE 48. Bottom flange and coverplate strains for Bridge 2 with post-tensioned exterior beams	150
FIGURE 49. Midspan and end strains for Bridge 2 with post-tensioned exterior beams	153
FIGURE 50. Deflected shape for Bridge 2 with post-tensioned exterior beams	154
FIGURE 51. Midspan strains and deflections for Bridge 2 with eccentric truck load	155
FIGURE 52. Deflected shape for Bridge 2 with eccentric truck load	156
FIGURE 53. Midspan strains and deflections for Bridge 2 with central truck load	158
FIGURE 54. Deflected shape for Bridge 2 with central truck load	159

FIGURE 55. Distribution fractions for axial force and moment . . .	162
FIGURE 56. Post-tensioning distribution at midspan for Bridge 1 . . .	165
FIGURE 57. Force, eccentric force, and moment distribution at midspan for Bridge 1	168
FIGURE 58. Moment distribution at selected span locations for Bridge 1	169
FIGURE 59. Effects of span and anchorage location on moment distribution	170
FIGURE 60. Effects of relative beam stiffness and skew on moment distribution	172
FIGURE 61. Bridge variables	178
FIGURE 62. Transformation for aspect ratio vs. moment fractions for four-beam bridges	181
FIGURE 63. Multiple linear regression models for four-beam bridge distribution fractions	183
FIGURE 64. Midspan distribution fractions for three-beam bridges . .	184
FIGURE 65. Midspan distribution fractions for four-beam bridges . .	186
FIGURE 66. Interpolation for distribution fractions at locations other than midspan	188
FIGURE 67. Stresses for Bridge 1 with post-tensioning of 100 kips on each exterior beam	190
FIGURE 68. Four-beam composite bridge (Bridge 1)	196
FIGURE 69. Tendon elevation and eccentricity	208
FIGURE 70. Stress diagrams for steel bridge beams	223
FIGURE 71. Post-tensioning design	224

1. INTRODUCTION

1.1. Iowa Composite Bridges

During the period 1930 to 1960, a considerable number of single span, composite steel beam and concrete deck bridges were constructed in Iowa. The bridges were one- or two-lanes wide, were constructed with rolled steel, wide flange shapes, and were constructed for spans of approximately 20 to 80 feet. The Iowa State Highway Commission designed these bridges on the state highway system individually for each span length and bridge site and provided counties with series of standard plans for use in the design of bridges for the county road systems.

The bridges and standard plans designed by the Iowa State Highway Commission met the then-current American Association of State Highway Officials (AASHO) bridge design standards. Those AASHO standards permitted exterior beams to be designed for a wheel load fraction considerably smaller than the fraction for interior beams. As a consequence, the composite one- and two-lane bridges designed in Iowa had exterior steel beams with depths 2 or 3 inches less than the interior steel beams.

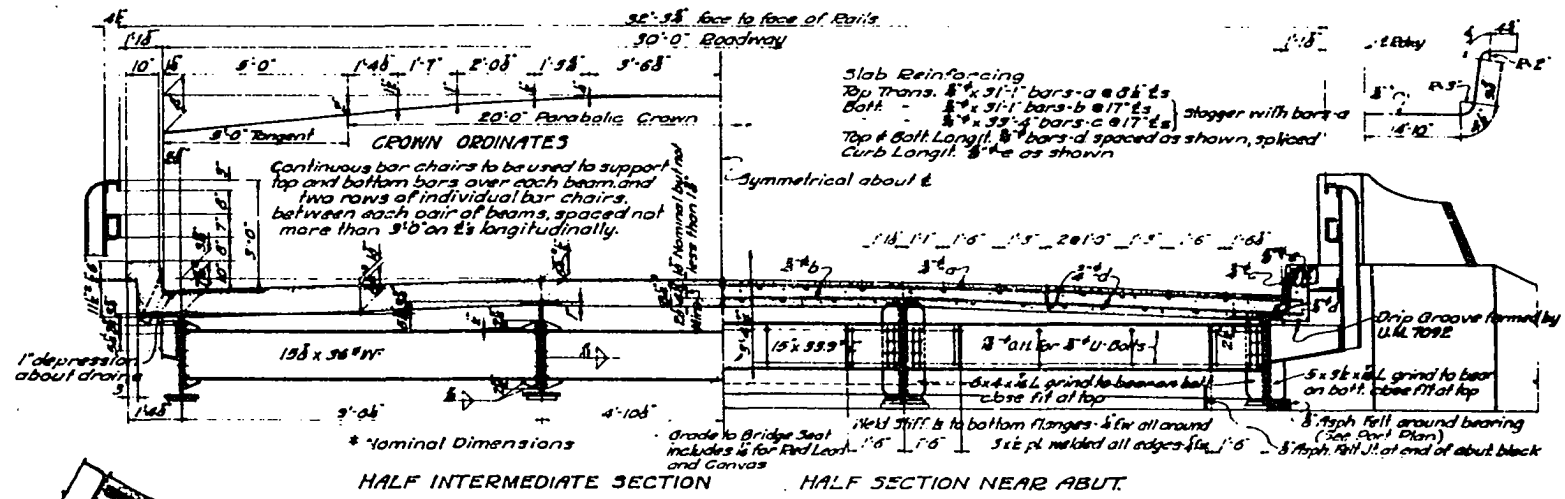
One of the typical Iowa bridge designs with small exterior beams is illustrated in Figure 1 [47]. The cross sections and the structural steel layout reproduced in the figure specify that exterior beams be nominally 27 inches deep and that interior beams be 30 inches deep. Because all beams were placed on the abutments at approximately the same

bearing elevation, the 3-inch difference in beam depths causes a transverse crown in the bridge deck.

The Seventh Edition of Standard Specifications for Highway Bridges [4] issued by AASHO in 1957 increased the wheel load distribution fraction for exterior beams for this bridge type. The increase was substantial -- approximately 40% for the two-lane, four-beam bridge shown in Figure 1. As a result, after 1957, when the Iowa composite bridges with smaller exterior beams were rated, they were found to be no longer adequate for their design loads.

In 1980, the Iowa State Legislature passed legislation (House File 747) [46] which increased legal loads in the state. The increases in legal gross weights were especially large for truck lengths (extreme distances between two or more consecutive axles) of 8 to 45 feet. These shorter trucks in most cases control the rating of the 20- to 80-foot span composite bridges. The increase in legal loads widened the gap between the rated strength of the older bridges and current rating standards.

A bridge which cannot be rated to carry legal loads must either be posted for restricted loads (embargoed), strengthened, or replaced. Posting a bridge, although the least expensive alternative, requires trucks and other heavy vehicles to travel extra distances, if drivers obey the embargo, and does not provide safety, if drivers disobey the embargo. Replacing a bridge is the most expensive alternative and does not utilize the full 40- or 50-year planned life of the bridge. The



a. Transverse cross sections and wing wall section

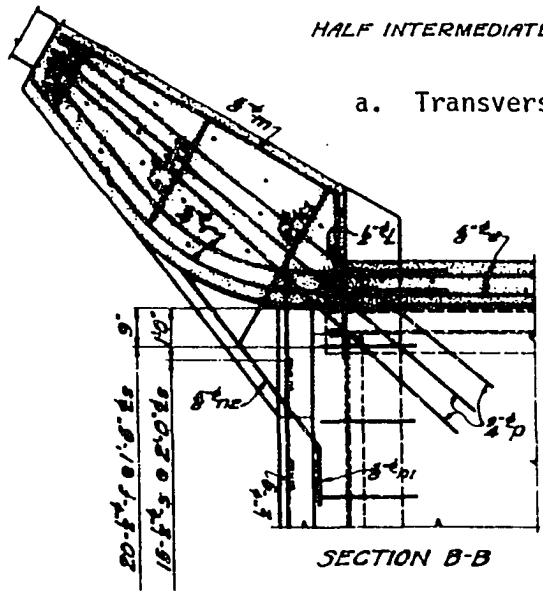


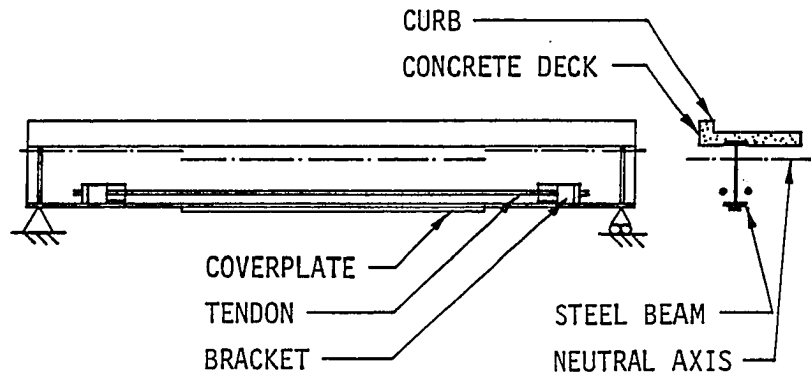
FIGURE 1. 50 ft. by 30 ft. I-beam bridge, Dickinson County

most desirable alternative, then, is to extend the life of the bridge and provide safety at a reasonable cost by strengthening.

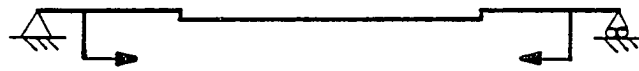
The bridges in question are generally found to be understrength because of flexural overstress at the bottoms of the small, exterior beams. This flexural overstress can be corrected by conventional methods such as addition of coverplates. Welding characteristics of the steel in older bridges often is unknown, however, which increases the difficulty and expense for adding coverplates.

An alternative, less expensive strengthening method -- post-tensioning of the exterior beams -- could remove the flexural overstress without welding. One arrangement for post-tensioning proposed by the Iowa Department of Transportation (Iowa DOT) is illustrated in Figure 2. The exterior beam in Figure 2a has steel brackets bolted to the beam on each side of the web, above the bottom flange, near the supports. When the tendons are stretched and anchored at the brackets, the tendons apply eccentric forces to the beam as shown in Figure 2b. For analysis purposes, the eccentric forces are statically equivalent to the sum of the axial forces and moments in Figure 2c and 2d. The post-tensioning illustrated will apply axial and flexural compression stresses to the bottom of the exterior beam to relieve tension overstress within the post-tensioned length.

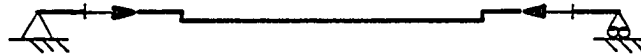
A major drawback to post-tensioning of the exterior beams has been the unknown distribution of the post-tensioning to the interior beams of a composite bridge. If only the exterior beams are post-tensioned, one



a. Post-tensioned beam



b. Idealized beam with applied eccentric forces



c. Idealized beam with applied axial forces



d. Idealized beam with applied moments

FIGURE 2. Post-tensioned exterior bridge beam

cannot assume that the resulting forces and moments remain only on the exterior beams. A composite bridge behaves as a single, three-dimensional structure. The shear connection between the steel beams and concrete deck, and the transverse stiffness of the bridge deck and diaphragms provide a path through which the post-tensioning on any one beam is distributed to the remainder of the bridge.

The typical Iowa composite bridge in need of strengthening is complex in terms of structural variables. The composite bridge illustrated in Figure 3 is a variably stiffened, orthotropic plate. Variations in longitudinal stiffness are due to the wide spacing of beams, differences in beam size, differences in coverplate size, differences in location of coverplate cutoff, and use of curbs integral with the deck. Variations in transverse stiffness are due to the use and placement of diaphragms. Accurate analysis of the typical composite bridge for post-tensioning distribution requires relatively complex theories for two- or three-dimensional structures.

1.2. Objectives

In 1980, because of the lack of engineering information on strengthening by post-tensioning and distribution of post-tensioning, the Iowa DOT identified the need for a feasibility study of strengthening the Iowa composite bridges with small exterior beams. The research conducted for this dissertation is part of the feasibility study and follow-up studies conducted by Engineering Research Institute

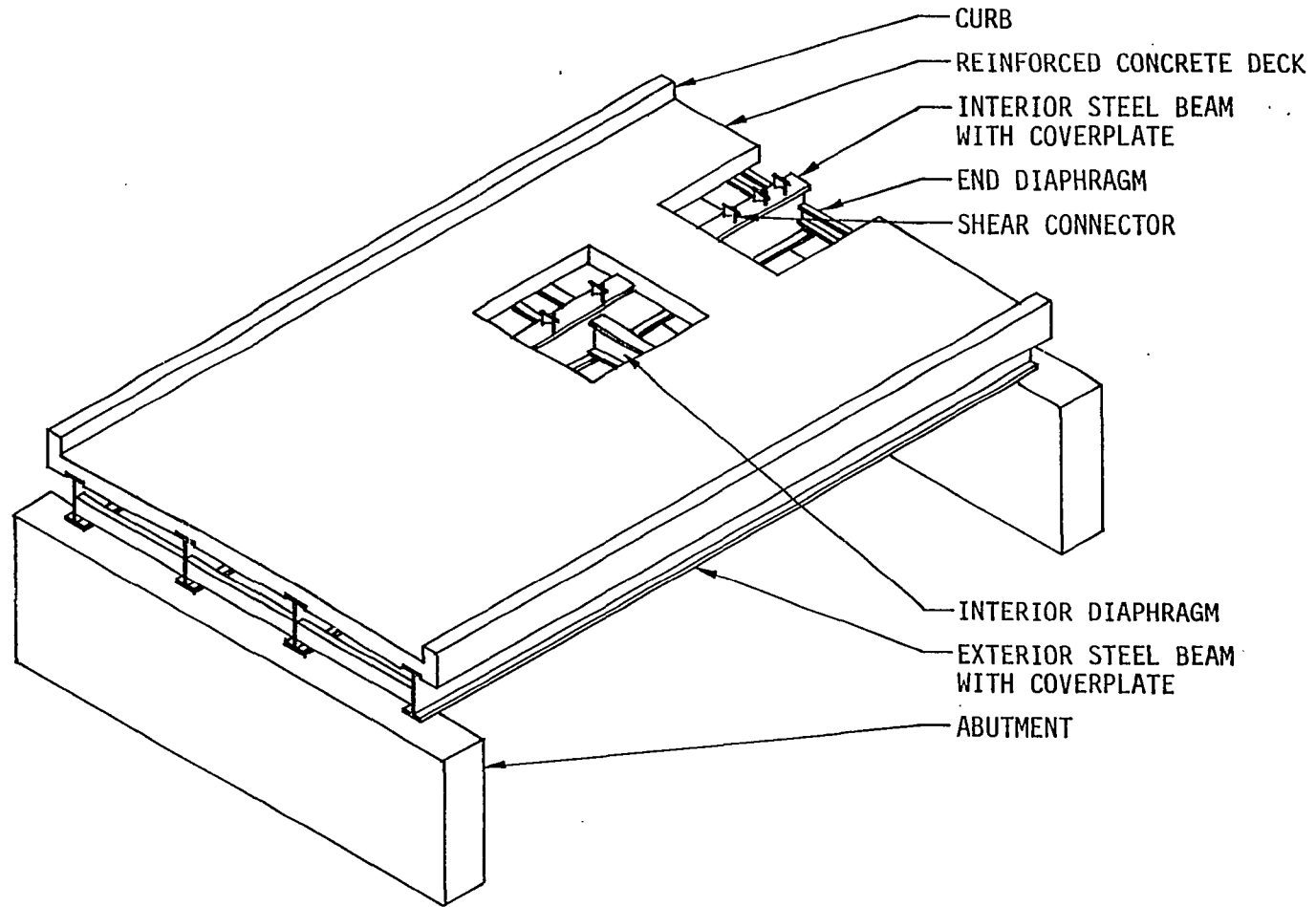


FIGURE 3. Typical Iowa composite bridge

of Iowa State University and sponsored by the Highway Division, Iowa DOT and the Iowa Highway Research Board. The overall goals of the research projects begun in 1980 were to determine the feasibility of strengthening by post-tensioning [55], to design and install the post-tensioning for two Iowa bridges [54], and to monitor the strengthened bridges and develop a simplified design methodology [28,29].

The overall objective for this research study was to develop the design methodology for strengthening of composite bridges by post-tensioning. More specific objectives established for the study were:

- To conduct a literature review for information regarding prestressed steel and composite structures, bridge strengthening by post-tensioning, and bridge deck behavior and analysis for right-angle and skewed bridges.
- To select and develop analysis methods for the elastic behavior of post-tensioned composite beams and bridges.
- To select and develop approximate analysis methods for determining the ultimate flexural strength of post-tensioned composite beams.
- To verify the analysis methods by checking them with examples from the literature, a half-scale model bridge constructed in the Iowa State University Structures Laboratory, and the two Iowa bridges strengthened in the field.
- To develop a simplified design methodology for strengthening composite bridges by post-tensioning, which accounts for the

distribution of the post-tensioning and is compatible with the American Association of State Highway and Transportation Officials (AASHTO) Service Load Design Method [3].

1.3. Literature Review

The literature review which follows has been organized into four main topics: prestressed steel structures, prestressed composite structures, bridge strengthening by post-tensioning, and bridge deck behavior and analysis. An effort was made to seek information on techniques for application of post-tensioning, on actual and potential problems with post-tensioning, and on available post-tensioning analysis and design methods. Because the distribution of post-tensioning could be similar to the distribution of bridge live loads, research studies of bridge deck behavior and analysis were reviewed to identify important variables and applicable analysis methods.

1.3.1. Prestressed steel structures

Prestressed metal structures have been proposed since 1837, when Squire Whipple in the United States learned to compensate for the poor tensile capacity of cast-iron members through prestressing [86]. Whipple placed ties in such a way as to precompress truss tension members, thereby protecting the cast-iron members from tension stress and potential brittle fracture.

In the late 19th and early 20th centuries, many U.S. bridges were constructed with trussed floor beams [11]. The king post or queen post

truss arrangement induced upward forces on floor beams in order to counteract downward forces due to dead and live loads. The upward forces were controlled by tightening turnbuckles in the tension rods and could be adjusted after construction to induce the desired amount of prestress.

Dischinger in Germany, beginning in 1935 [34], began to conceive much wider applications for prestressed steel. His proposals included highway and railway bridges utilizing prestressed plate girders, box girders, trusses and other structural forms [27].

In 1950, Magnel [63] reported experimental results from a steel truss prestressed by post-tensioning of the tension chord. Strands were placed inside the hollow chord and tensioned against anchorages at the ends of the chord. A 1954 article [62] described one of Magnel's projects, a prestressed long span roof truss for a Belgian aircraft hangar. Magnel stated that prestress loss was only 9% (which is relatively low compared to losses for prestressed concrete).

As a result of the European work in prestressed steel, Coff [22] in the United States proposed a 250-foot span prestressed steel plate girder bridge. Coff later patented a prestressed composite system. According to Stras [76], another U.S. patent was granted to Naillon in 1961 for prestressing of a steel beam by cables.

Barnett [12], in 1957, returned to the queen post truss concept in suggesting the use of prestressed steel "truss beams". For economy, Barnett recommended that the tension rod be placed below the beam,

thereby increasing the depth of the structure. He claimed weight savings of as much as 30% for his method.

A rather extensive testing program for a 90-foot span prestressed steel truss was reported by Finn and Needham [33] in England in 1964. During testing, prestressing bars failed several times, apparently as a result of faulty material.

Subcommittee 3 of the Joint ASCE-AASHTO Committee on Steel Flexural Members reviewed the state of the art in prestressed steel in 1968 [31]. For prestressing with steel wires or bars, Subcommittee 3 noted that combined secondary $P-\Delta$ (increase in beam moment due to axial force and bending deflection) and ΔT (increase in prestressing force due to bending deflection) effects can be as large as 20%. The subcommittee estimated loss of prestress due to steel relaxation to be less than 5%. For symmetrical I-sections, the subcommittee suggested that prestressing of new structures to counteract positive moments would not be economical, unless the prestressing tendons were placed below the I-section. Several potential problems which the subcommittee noted were corrosion, bending deflection, and lateral stability.

During the early 1970s, Ferjencik [32] and Tochacek and Amrhein [81] described progress in prestressed steel design in Czechoslovakia. Research was begun in 1960, and actual design specifications were adopted as a result of that research. Ferjencik described a rather extensive catalog of applications of prestressing, including applying it to girders and trusses. Tochacek and colleagues [81,82] pointed out

that the safety factor for the portions of prestressed steel structures subjected to a range of both tension and compression can be reduced by up to 20% under a working stress design. In order to give an adequate and consistent safety factor, he suggested use of load factor design.

In 1984, Bonasso [74] proposed a prefabricated, prestressed steel bridge as a replacement for an existing bridge near Mannington, West Virginia. The "tension arch" bridge would be constructed by stretching cables between bridge abutments, placing steel tubes with stiffeners to hold the cables in an approximately parabolic shape, tensioning the cables, and adding precast concrete deck sections. Bonasso's original proposal for the bridge called for precast concrete tubes, but he substituted steel tubes to make the bridge easier to construct.

1.3.2. Prestressed composite structures

Apparently as a result of the European work in the late 1940s and early 1950s, and as a result of his own interest in prestressed steel [22], Coff extended the concept of prestressing to composite structures. According to Stras [76], Coff obtained a U.S. patent for a composite concrete slab and steel beam system. The system was prestressed by cables attached to the ends of the slabs and draped along the steel beams, with pin attachments to the steel beams.

Szilard [77] proposed a similar composite system in 1959, but with tendons anchored to the steel beam rather than to the slab. The concrete slab was to be placed after prestressing of the steel beam and was attached to the steel beam with ordinary headed stud shear connectors.

In 1963, Hoadley [41] analyzed the behavior of composite concrete slab and steel beam members, including the ΔT effect in the prestressing tendon and the performance of the members up to and including ultimate load. The ΔT analysis neglected P- Δ secondary effects since those effects were estimated to be only 5 to 10%. Hoadley's analysis showed an increase in ultimate load capacity for efficient use of prestressing.

Stras [76] reported several tests to ultimate load of prestressed composite beams in 1964, and the tests later were correlated with an incremental strain analysis by Reagan [69]. After analyzing a series of bridge and building beams, Reagan concluded that failure generally occurred by crushing of the concrete rather than by fracture of the tendon. Reagan also noted that unbonded tendons do not significantly affect the resistance of the beam to deflection, since the prestressing tendons do not affect the moment of inertia of the beam.

Several U.S. bridges constructed during the early 1960s utilized prestressed composite beams and trusses. Hadley designed two such bridges in Washington state. The first was a 99-foot span composite, precast concrete slab placed on steel trusses with prestressed lower chords [37]. The second bridge was a 150-foot span, composite slab and post-tensioned delta girder bridge [38]. A skewed bridge with prestressed steel wide flange beams was also constructed in Pennsylvania [23]. The prestressing tendons were placed the full length of the bridge, above the bottom flanges of the beams. Headed shear connectors welded to the top flanges of the beams provided the connection between

beams and slab. All three bridges were constructed so that the bridge deck was made composite after prestressing.

The multiple-span Bonners Ferry Bridge in Idaho, completed in 1984, was designed by T. Y. Lin International [73] according to AASHTO Load Factor Design [3]. Prestressed steel plate girders for the bridge were made composite with the concrete deck during construction. In negative moment regions, the plate girders were prestressed in two stages. Prestressing was applied to the top flanges to control the dead load stresses which would result when the concrete deck was placed. Later, the concrete deck was prestressed to control live load stresses and to provide composite action over the entire length of the bridge. The negative moment region prestressing reduced the required amount of structural steel, limited the tension stress range, reduced deflection, and provided multiple tension stress paths to increase redundancy.

1.3.3. Bridge strengthening by post-tensioning

Since the early 1950s there have been many reports of bridges strengthened by post-tensioning. In 1952, Lee [60] reported the strengthening of British steel highway and railway bridges by post-tensioning. Both beam and truss bridges were strengthened. Berridge and Lee [17] described strengthening of a steel truss bridge in 1956, and Knee [56] mentioned strengthening of British steel railway bridges by post-tensioning as if it were a fairly common practice.

Sterian [75] reviewed Rumanian practice prior to 1969 in strengthening bridges by various methods, including post-tensioning by

cables or rods. Although Sterian described several methods of strengthening, including the addition of coverplates, he viewed post-tensioning as having the most potential. It is interesting to note that a research and model-testing program was completed in Rumania before any bridges actually were post-tensioned.

A proposal by Kandall [52] in 1969 for strengthening steel structures by post-tensioning was unique because he recommended adding material to the compression regions of members. The additional material had to be carefully fitted through or around cross members, making for a relatively complicated strengthening operation.

Vernigora et al. [84] reported the successful strengthening of a five-span, reinforced concrete bridge in Ontario, Canada. The five, simple spans were post-tensioned by means of draped cables so as to make the repaired bridge continuous over the supports.

Belenya and Gorovskii [15] of the Soviet Union presented a rather complete analysis of steel beams strengthened by post-tensioning. According to their analysis, prestressing could add up to 90% capacity (under allowable stress design) to an unstressed steel beam. They recommended a tendon length of 50 to 70% of the span length and recommended considering $P-\Delta$ effects only when the depth/span ratio is less than $1/20$.

During the past fifteen years, several Minnesota bridges have been strengthened by post-tensioning. A prestressed concrete bridge damaged by vehicle impact was repaired using post-tensioning [67]. It appears

that at least two Minnesota steel bridges have been repaired temporarily using post-tensioning [43]. In one case, salvaged cable and timber were utilized for strengthening. The strengthening was checked by means of instrumentation and a truck load.

During the 1970s, T. Y. Lin International strengthened a multiple-span steel plate girder bridge in Puerto Rico by post-tensioning. The post-tensioning scheme removed approximately 6 inches of dead load deflection at midspan.

In 1983, Lamberson [59] reported numerous examples of strengthening by post-tensioning in the United States. The Indiana Department of Highways post-tensioned the girders in a reinforced concrete bridge using threadbars harped at midspan of each girder, using essentially a king-post truss concept. The Illinois Department of Transportation utilized a similar harped tendon arrangement to strengthen the transverse steel floor beams in a steel truss bridge. Eleven other examples, including one of the bridges strengthened as a part of the research at Iowa State University, also are described. The threadbars utilized in the examples have been protected by either epoxy coatings, grouted pipes, or grouted plastic tubes.

A four-beam, two-lane composite bridge in Pasco County, Florida was repaired and strengthened in 1984 [14]. The post-tensioning designed by Howard Needles Tammen and Bergendoff (Orlando, Florida office) by the AASHTO Service Load Design Method [3] was similar to that illustrated in Figure 2a, and was applied to all four beams in each of three simple

spans. The post-tensioning raised the rated capacity of the bridge from an H 15-44 to an HS 20-44 at a cost of approximately \$ 20,000.

California has strengthened seven steel bridges [64] by post-tensioning in the period from 1979 to 1984 and is planning to strengthen at least twelve more. Since all of the beams in each bridge are of the same size, and since all of the beams are being post-tensioned equally, lateral distribution of the post-tensioning is not a major problem. To date, all of the California bridges have been strengthened using strand that is enclosed in galvanized pipe and grouted after post-tensioning. All prestressing systems and anchorage hardware must be tested and approved by the Caltrans Transportation Laboratory prior to installation.

1.3.4. Bridge deck behavior and analysis

This topic has been subdivided into: live load distribution in right-angle bridges, live load distribution in skewed bridges, and composite beam and bridge deck analysis.

1.3.4.1. Live load distribution in right-angle bridges For purposes of bridge design, the three-dimensional bridge structure usually is assumed to consist of a series of parallel, one-dimensional beams to which live load is distributed on the basis of wheel load fractions. The current AASHTO bridge design specifications [3] require that wheel load fractions for distributing truck loads to bridge beams be based on the following variables: type of bridge, number of lanes, spacing of beams, and classification of beam -- exterior or interior.

The simplified AASHTO wheel load fractions for computation of beam moments do not permit consideration of beam properties, deck properties, diaphragms, bridge span, bridge width, skew or other factors. The same wheel load fractions are required for both AASHTO Service Load Design and Load Factor Design methods.

Some variables not considered in the AASHTO wheel load fractions are of minor importance. Researchers have shown, for example, that typical diaphragms do not significantly affect live load distribution at service loads for beam and slab bridges [7,58,78,85]. With the variety of bridge design options currently available, however, the simple AASHTO wheel load fractions may be inaccurate or unconservative for some bridges.

— Many researchers have studied the live load distribution within bridge decks with the objective of improving accuracy beyond that of the AASHTO wheel load fractions. Researchers who have analyzed bridges by orthotropic plate theory have considered a comprehensive set of variables which account for most bridge properties. Orthotropic plate theory requires the use of beam properties, deck properties, diaphragms, bridge span, and bridge width in computation of θ , the flexural parameter, and α , the torsional parameter. Sanders and Elleby [71] proposed revisions to the AASHTO wheel load fractions which considered the variables currently in the AASHTO specifications and the variables which are used in computation of the orthotropic plate parameters.

Bakht et al. [8] in developing the Ontario Highway Bridge Design Code also considered individual bridge properties by means of orthotropic plate theory. Separate studies during the development of the code indicated that widths of design vehicles affected load distribution, and the edge distance between a wheel load and the exterior beam had a very significant effect on the distribution of moment to the exterior beam. Bakht et al. also found that the load distribution within the center 60% of the bridge was relatively constant.

A recently proposed finite element method for load distribution [19] considers all of the individual bridge variables which can be included in a finite element model. The load distribution factor is decomposed into the product of three ratios. The first ratio, the linear-idealization ratio, accounts for the discrepancy between the three-dimensional bridge structure and a simplified, one-dimensional model of each beam. The second ratio, the symmetric-load ratio, accounts for the number of loaded lanes, and the third ratio, the eccentric-load ratio, accounts for eccentricity of load. The proposed method is an alternative to the AASHTO wheel load fractions and can more accurately account for the properties of an individual bridge structure.

1.3.4.2. Live load distribution in skewed bridges The AASHTO wheel load fractions do not account for skew, and the orthotropic plate studies described above were unable to account for skew, although Bakht et al. [8] state that their results are applicable for bridges with

skews of 15 degrees or less. Because bridges are often constructed with skews of 30 or 45 degrees, skew should either be considered in analysis or neglected only after a thorough check of its effects on a bridge.

Skew generally has a greater effect on isotropic bridge decks than on orthotropic bridge decks. A rather comprehensive review of skew effects on prestressed slab bridge decks is contained in a publication by Clark and West [21]. The authors tested two 45-degree skewed, solid slab bridge deck models and compared the model results with separate grillage and finite element analyses. The models represented bridge decks which were essentially isotropic except for longitudinal post-tensioning.

Clark and West separated the prestressing into axial and bending components for purposes of analysis. Although the axial component could be treated on a simple force per unit area basis, the bending component could not be treated so simply. Because a portion of the bending component was dispersed in the slab as torsional and transverse bending stresses, a simple treatment of the bending component applied to a slab strip of unit width would overestimate the effects of the bending component. Increasing skew and increasing aspect ratio (width to length) increased bending component losses, whereas increasing orthotropy (longitudinal to transverse strength) decreased losses.

Due to the post-tensioning, obtuse corners of the bridge deck were subject to uplift, if not tied down. Downward reactions due to application of live load tended to concentrate in the obtuse corners.

Minor differences in behavior occurred depending on the sequence of post-tensioning of a slab bridge deck.

For slab bridge decks, Lee and Chaplin [61] reiterated several of the conclusions reached by Clark and West, namely that prestressing could cause uplift at obtuse corners, that maximum reactions due to live load occurred in obtuse corners, and that beam and slab (orthotropic) bridge decks would have reduced skew effects. Lee and Chaplin also noted that, for slab bridges, moments were large in obtuse corners and that the directions of principal moments were dependent on the position of a live load. The variation in direction of principal moments therefore requires additional quantities of reinforcing, beyond that required for right-angle bridges.

—Newmark et al. [66] tested both 30- and 60-degree skewed, quarter-scale composite beam and slab (orthotropic) bridge models and compared them with previously tested right-angle bridge models. For a 30-degree skewed bridge model, deflections and live load distribution to beams were essentially the same as for a right-angle bridge model. Beam strains in the skewed model were up to 5% larger than in a right-angle bridge model.

For the 60-degree skewed model, differences between the skewed and right-angle models became quite apparent. Smaller deflections were measured in the 60-degree skewed model, and deflections and load distributions were less uniform. Beam strains were up to 14% less. The change in performance could be explained by partial restraint at beam ends and increased torsional stiffness of the bridge deck.

Hondros and Marsh [42] tested a series of right-angle and 30-degree skewed, composite bridge models. They found that in the 30-degree skewed model, strains and deflections were approximately 17% less. It appeared to them that the proportion of load to each beam remained essentially the same for right-angle and 30-degree skewed bridge models.

Gustafson and Wright [36] utilized finite element analysis to analyze the effects of skew on an 80-foot span, two-lane steel girder and concrete slab composite bridge. Their analysis showed almost no change in distribution of moment to the girders for angles of skew less than 30 degrees, and no significant change unless the skew angle exceeded 45 degrees. They found that exterior girders were less sensitive to skew than interior girders. Influence lines for girder reactions which they plotted indicated that exterior girders carried a large percentage of midspan concentrated loads -- even when interior rather than exterior girders were loaded.

DeCastro and Kostem [26] conducted a rather extensive finite element analysis of composite, prestressed concrete I-beam bridges of moderate span. Their results were quite comparable to those of Gustafson and Wright. Exterior beams were less affected by skew than were interior beams, and the effect of skew was not significant until the angle of skew exceeded 45 degrees. For relatively closely spaced beams, the authors found that the distribution factor actually increased slightly. The effect of skew decreased as the span of the bridge increased.

Kennedy and Gupta [53] correlated orthotropic plate theory (modified to account for skew) with model tests. They concluded that for orthotropic plates, skew had a greater effect for uniform load than for a concentrated load. For a concentrated load at midspan, their charts can be interpreted to show results similar to those contained in other research reviewed above. For an interior beam, skew had the effect of decreasing moment to the beam, and the reduction became significant at angles of skew greater than 45 degrees. For an exterior beam, the charts indicated a slight increase in moment with increasing skew.

1.3.4.3. Composite beam and bridge deck analysis The analysis of composite bridge beams which are idealized as one-dimensional parts of the bridge structure must account for the following: shear lag in the concrete deck, relative properties of the concrete deck and steel beam, and properties of the mechanical shear connection which anchors the concrete deck to the steel beam. The effect of shear lag within the concrete deck, which reduces longitudinal stresses in the deck as the distance from the beam increases, generally is simplified by limiting the width of the concrete deck. The width of deck considered to be effective with the steel beam is set so that the actual stresses and the computed stresses at the location of the steel beam are approximately the same.

The effective width of the concrete deck is known to vary with type of load and position of load on the span. Variation in effective width

along the beam span usually has little effect on steel and concrete stresses [57]. For design purposes the AASHTO bridge design specifications [3] require the effective width to be the smallest of the widths computed by three simple rules. The AASHTO rules are different from those contained in foreign bridge design specifications [57] and may not be accurate for research purposes. A finite strip analysis [20] found the AASHTO rules to be conservative. However, recent research with respect to load factor design [18,40] has determined that, although the exterior girder deck widths are conservative, the interior deck widths are unconservative and that, beyond service load levels, both widths should be reduced.

For service load design, the relative properties of concrete deck and steel beam are adjusted through the use of the modular ratio, defined by AASHTO as the ratio of the modulus of elasticity of steel to the modulus of elasticity of concrete. The modular ratio is used to reduce the area of the effective concrete deck and transform the section properties for the composite beam to those of an equivalent steel beam.

AASHTO requires use of two modular ratios -- a theory-based ratio for live load and an arbitrarily increased ratio for long-term dead load. The ratio for long-term dead load is the theory-based ratio multiplied by three, which estimates the effect of creep in the concrete deck. In positive moment regions, where concrete is under compression, as the concrete creeps, stresses in the concrete deck are reduced, but stresses in the steel beam are increased [57]. The increased modular

ratio decreases the contribution of the concrete deck to the composite section, thereby reducing the moment of inertia and increasing the computed steel stresses. Another factor which may have the same effect as creep is concrete shrinkage. An experimental study [42] indicated that the shrinkage reduced moment of inertia as if the area of the concrete deck were reduced.

When composite bridge beams were designed by the Iowa State Highway Commission in the 1940s, part of the shear connection was assumed to be bond between the concrete deck and top flange of the steel beam [47]. That practice is no longer permitted by AASHTO, and shear connectors must have the capacity to fully transfer the shear between deck and beam. AASHTO requires that shear connectors be designed for two strength conditions: fatigue strength for shear range at service load and strength at ultimate load [3].

Ultimate strengths for shear connectors are computed from rules based on push-out tests. Stiffnesses or load-slip values can be obtained from push-out tests for elastic analysis of the shear connection. Johnson [51] states that elastic behavior occurs up to about half of the ultimate load for a connector.

For simple span beams, the stiffness of shear connectors may be as large as twice that indicated by push-out tests, however in negative moment regions of continuous spans, where the deck is in tension, the connector stiffness is less than that indicated by push-out tests [51]. Any slip which connectors permit between deck and beam generally has

little effect on elastic stresses and deflections for the composite beam. Therefore, the section properties transformed by the modular ratio are accurate enough for design purposes [51,87].

For elastic finite element analysis, the shear connection can be modeled in various ways, including a shear connector linkage assembly developed by Tumminelli and Kostem [83]. The model can give individual connector forces, of interest for fatigue design of connectors. Although connector spacing and stiffness has an effect on elastic forces on shear connectors, connector spacing and stiffness has little effect on the ultimate strength of a composite beam [87].

For analyzing the entire three-dimensional bridge superstructure, relatively complex methods are required. The bridge deck analysis methods in recent use include: grillage analysis [24,35,39], orthotropic plate theory [6,9,10,24,35,71], finite differences [24], folded plate theory [24,39], finite elements [19,24,39], finite strips [24] and others. All of the methods readily account for bending moments in the bridge structure, but only finite element analysis can account for axial forces in the bridge structure.

1.3.5. Summary

Although prestressed structures have been a design option for more than a century, their use has been limited until recently by available materials. Due to the tensile weakness of concrete and associated advantages of prestressing, prestressing has been applied more widely to concrete structures than to steel or composite structures.

Engineers have begun to realize, however, that prestressing of steel or composite bridges can lead to construction cost savings and, in some cases, better bridges. Prestressing for new structures has been applied as parallel, eccentric forces by means of straight tendons as illustrated in Figure 2a, or as parallel and perpendicular forces by means of harped tendons. For greatest economy, it is generally recommended that straight tendons be placed above beam sections in negative moment regions and below beam sections in positive moment regions, in order to increase eccentricity and, therefore, moment effects.

Although prestressing with unbonded tendons can significantly alter elastic stresses, unbonded tendons do not significantly stiffen a structure since the tendons do not have a direct effect on beam moment of inertia. By widening the range of elastic stresses to which a structure is subjected without increasing the ultimate strength by a corresponding amount, prestressing lowers the factor of safety. As a consequence, the load factor design method is recommended for new prestressed steel or composite structures. Although prestressing may lower the factor of safety, it did increase the ultimate strength in the applications reported in the literature.

Prestressing does have secondary effects which may range to 20%. For relatively shallow and flexible beams with depth-span ratios less than $1/20$, $P-\Delta$ effects should be considered in analysis. ΔT effects also are important for flexible structures and have a beneficial effect

since the ΔT effect increases the prestressing force when the structure is loaded. When applied prestressing causes compression stress in a region of a steel beam, potential lateral buckling of the beam must be considered.

Prestressing losses are generally small for steel structures. Relaxation loss in the tendons can be expected to be on the order of 5%. The actual loss during one post-tensioning operation was reported as 9%. Because unbonded tendons for steel or composite beams are exposed, the tendons must be protected from corrosion by coatings or grouted tubes. Not directly reported in the literature, but a definite safety concern nevertheless, is the need to prevent tendons from breaking during stressing or the planned lifetime of the structure.

— Many engineers have recognized the potential of bridge strengthening by post-tensioning as opposed to addition of coverplates and other methods. The reported strengthening applications avoided the distribution problem since all beams were of equal size and the post-tensioning for each beam was of equal magnitude. Thus, there is a definite need for a study of post-tensioning distribution.

Live load distribution in the current AASHTO bridge design specifications is based on very simple rules which account only for the type of bridge, number of loaded lanes, spacing of beams and classification of beam -- interior or exterior. These rules do not account for many bridge properties, and researchers have questioned the safety and economy of the rules. Advanced analysis methods such as

orthotropic plate theory and finite element analysis can account for the bridge properties neglected by the simple rules, and should be used to determine the live load distribution for complex bridge structures. The current AASHTO rules also assume a constant distribution over the entire span which research has shown to be accurate for the center 60% of the span.

Generally skew, which is sometimes neglected in bridge design, has minimal effect on orthotropic beam and slab bridges, as opposed to other bridge types. Skew has virtually no effect for angles less than 30 degrees and significant effect only for angles greater than 45 degrees. Skew tends to cause partial restraint of bridge beams, increased torsional stiffness of the bridge deck, and larger reactions and stresses in obtuse corners of the deck. Interior beams are affected more than exterior beams by skew, and short-span bridges are affected more than long-span bridges by skew.

One study which involved the prestressing of isotropic, skewed bridge deck models indicated that the sequence of prestressing had little overall effect on the final forces and moments. For analysis purposes, it was shown that the axial force and moment components should be treated separately.

Composite beam analysis, for design purposes, can be conducted with AASHTO rules for effective slab width, modular ratios, and shear connector capacity and spacing. For research purposes, however, the AASHTO rules should be considered generalizations which may be

conservative or unconservative for a given test condition. Effective flange width, for example, varies depending on type of load and location on the composite beam span. Shear connector slip can be expected to vary depending on whether the concrete deck is in compression or tension, and the slip is not likely to be the same in a composite beam as in push-out tests.

Although the analysis of a composite bridge for live load distribution could be conducted by any of a variety of advanced analysis methods, those methods can account only for bending moment. For the axial force component of prestressing, only finite element analysis can solve for the distribution. Finite element analysis also has the advantage for the Iowa composite bridges of being able to account for the partial-length coverplates and other variations in the bridge superstructure.

The literature points to a definite need for a research study of the distribution of post-tensioning in a bridge which has only exterior beams post-tensioned. Post-tensioning with eccentric, straight tendons should be analyzed as a combination of separate, axial force and moment components. For accuracy, as well as analysis of the axial force components, finite element analysis is the preferred method.

2. BEHAVIOR OF POST-TENSIONED COMPOSITE BEAMS

A design methodology for strengthening composite bridges by post-tensioning, which is applicable to current engineering practice, must be referenced to individual bridge beams. It is quite logical to examine the behavior of individual beams before examining the more complex behavior of the entire bridge superstructure. For both reasons, this research study has been organized in the following manner. First, the behavior of prestressed composite beams is examined by means of analytical and finite element models with the objective of developing a suitable elastic finite element model for individual beams. Then, the finite element beam model is extended to an entire bridge superstructure in order to examine the elastic behavior of the bridge. From the bridge behavior, the post-tensioning distribution is determined. Finally, the elastic post-tensioning distribution is referenced back to individual bridge beams. Although it would be desirable also to have the post-tensioning distribution for inelastic bridge behavior, that was beyond the scope of this research study.

At the time the bridge strengthening feasibility study was begun in 1980, a very limited number of tests of prestressed composite beams had been conducted by Stras [76]. Elastic and inelastic analysis methods by Stras and Reagan [68] and a ΔT elastic analysis method by Hoadley [41] were available for modeling the behavior of prestressed composite beams. The previous experimental and analytical information provided guidance for the development of a testing and analysis program for a model bridge

constructed in the Iowa State University Structural Research Laboratory in 1980. The model bridge was constructed as a half-size model of the superstructure for a composite bridge in Appanoose County, Iowa. The superstructure for the Appanoose County bridge is identical to the superstructure illustrated in Figure 1.

After the model bridge was tested extensively, it was sawed into four composite beams in 1982, which were tested with post-tensioning at service loads and at ultimate loads by Dedic [54]. The beams tested by Stras and Dedic provide the experimental data with which the analytical and finite element models developed in this chapter are verified. Computations by Reagan for the Stras beams and for a hypothetical bridge beam provide further verification of the models.

2.1. Beam Description

The behavior of a prestressed composite beam is dependent on the sequence in which the beam is constructed and prestressed. The composite beams in the Iowa bridges in need of strengthening were constructed without shoring. Each steel beam, with a coverplate welded to the bottom flange and shear connectors welded to the top flange, was placed on the bridge abutments. Each diaphragm was placed and connected to the steel beams to complete the basic steel frame for the bridge. Concrete forms were fastened to the steel beams. Deck reinforcing was placed, and the concrete deck was poured. The steel beams, at that time, supported their own weight as well as the weight of the concrete

deck. Approximately half of the allowable stress capacity of the steel beams was used before the deck became composite with the beams.

The steel guard rails may have been placed with the steel bridge frame, and the integral curbs may have been placed with the deck, or the guard rails and the curbs may have been placed after the deck. For purposes of this research study, curbs were assumed to be placed with the deck, and guard rails were assumed to be added later. The guard rails then stress the composite beams, and any vehicle which passes over the bridge stresses the composite beams. Therefore, the concrete deck is stressed longitudinally with a small amount of long-term dead load and a large amount of live and impact load. Any overstress in the steel beams would occur when a vehicle passes over the bridge.

— The Iowa bridge beams are of A7 steel, and the concrete is specified as Class A, which for rating purposes is interpreted by the Iowa Department of Transportation to have a minimum strength of 3000 psi. Although coverplates and shear connectors were welded to the steel beams during fabrication, field welding to the same beams for purposes of strengthening may not be convenient or possible. Thus, post-tensioning of the composite beams was planned with bolted connections.

The angle-plus-bar shear connectors in Figure 1b were apparently unique to Iowa, Minnesota, and Wisconsin. The connectors were stiffer and shallower than the channel or stud connectors currently in use. One probable reason for the minimal height of the connectors is that the steel beams were recessed approximately one inch into the concrete deck,

apparently in an effort to aid shear transfer by bond between the deck and top beam flange. Since no published information could be found for the angle-plus-bar connectors, Dedic conducted push-out tests for half-size and full-size connectors as part of the overall program of bridge strengthening research [54].

For the Iowa bridges to be strengthened, post-tensioning would be applied to steel beams which are already composite with the concrete deck and curbs. About half of the allowable stress capacity of the steel beams is utilized for dead load stresses. That stress condition can be quite different from the stress condition in a steel beam to be prestressed as part of a new structure.

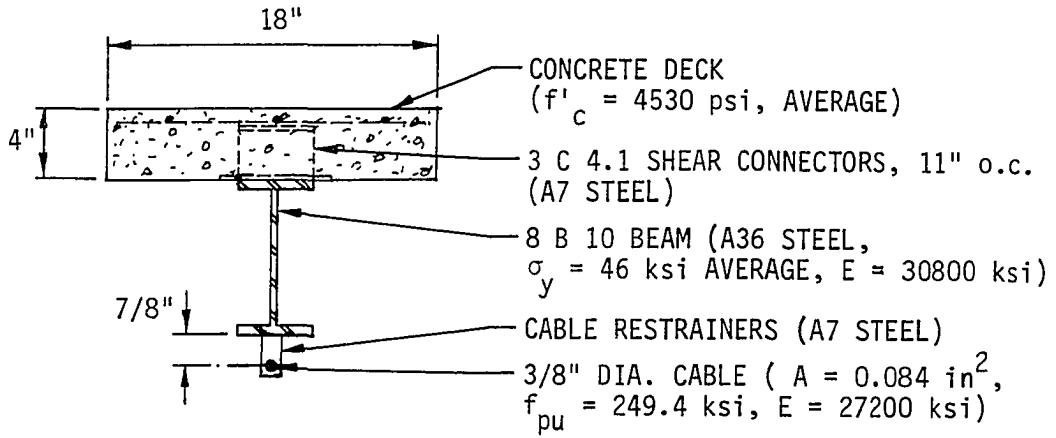
Stras tested three beams, Beams A, B, and C, all of which had the configuration shown in Figure 4. Those beams and the beams analyzed by Reagan were intended to model prestressed composite beams for new building or bridge structures. Construction sequence for the Stras beam in Figure 4 was as follows. Channel shear connectors were welded to the top flange, and the beam was prestressed with the steel cable. The prestressing created axial compression and negative moment flexural stresses equal to approximately one-third of the allowable stress capacity of the steel beam. Then, the concrete deck was cast on the unshored beam and, as it cured, became composite with the prestressed steel beam. The size of the deck was such that the actual width would be considered the effective width under AASHTO rules for composite beams. Presumably the intent of the prestressing was to reduce or

eliminate the tension stress in the bottom flange of the steel beam due to dead load. The steel beam would be essentially unstressed at critical locations before live loads were placed on the member.

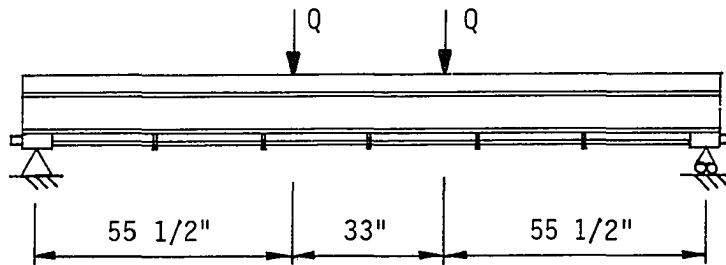
The three beams of the configuration in Figure 4, had attached restrainers through which the prestressing cable was threaded. The restrainers maintained a constant eccentricity between the tendon and the neutral axis regardless of the deflection of the beam. The prestressing tendon was placed below the beam for maximum efficiency, and the tendon ran the full length of the beam.

Equal vertical loads, Q , were applied to the beam to simulate live load. The loads were increased, and the behavior of the beam was monitored until failure occurred. Because of problems with construction and testing of the beams, it is likely that most of the prestressing was lost before the steel beam became composite with the deck and before vertical loading commenced.

As noted previously, the beams tested by Dedic were cut from the half-size laboratory model of an Iowa composite bridge. At the time the beams were cut from the bridge model they were approximately two years old. All of the deck sections on the beams were cracked due to previous testing and due to shrinkage of the small-aggregate concrete. The curbs for the exterior beams, Beam 1 in Figure 5b and Beam 4 in Figure 5e, were of higher strength than the deck as listed in Table 1. The curbs were added to the model bridge several months after the deck was cast. The deck sections with the exterior beams were narrow enough so that the



a. Cross section for Beams A, B, and C



b. Elevation

FIGURE 4. Prestressed composite beams (Stras)

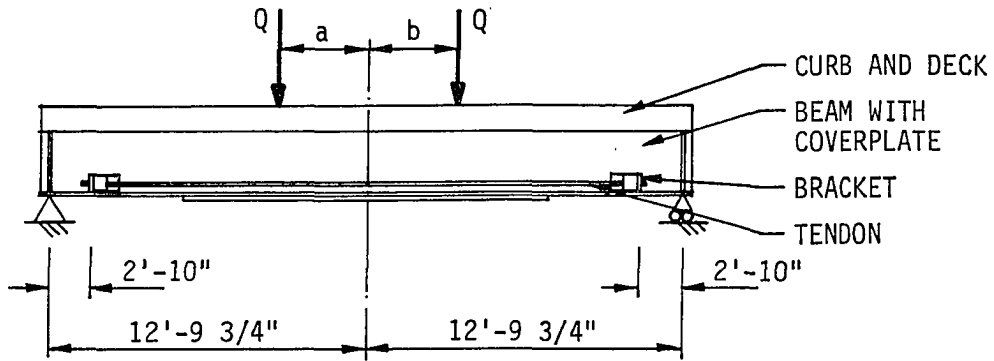
actual width could be considered the effective width according to AASHTO rules. The model exterior beams did not have attached guard rails since the rails would not be considered part of the primary bridge structure.

The deck for the model bridge had a 2-inch crown (not shown in Figure 5), which simulated the crown in the Appanoose County composite bridge. Interior beams, Beam 2 in Figure 5c and Beam 3 in Figure 5d, had relatively wide deck sections which exceeded the effective width according to the AASHTO rules. At the time the beams were tested in the elastic range with vertical loads, Q , the beams were post-tensioned with forces approximately equal to forces scaled for a full-size bridge after distribution losses. The post-tensioning was applied by means of 5/8-inch diameter threadbars with the properties listed in Table 2. For the ultimate load tests, the post-tensioning forces were increased above those applied for the elastic tests. Although the beams were constructed in essentially the same sequence as an Iowa composite bridge, because of the scale, the dead load stresses in the beams were only half those for a full-size bridge.

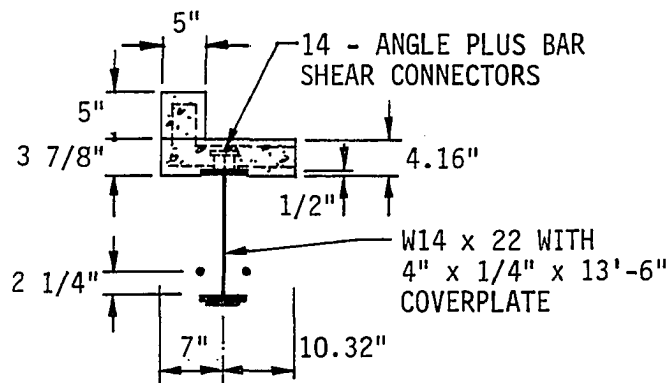
Two of the beams, Beams 3 and 4, had additional 1/2-inch diameter, double-nutted high strength bolt shear connectors. The shear connector size and placement was scaled to approximate the additional shear connection required to upgrade a full-size Iowa composite bridge beam so that all shear would be transferred through connectors.

The Dedic beams accurately model beams in the Iowa bridges to be strengthened. The tests of those beams and the tests of the Stras beams

BEAM	a, in	b, in
1	39 3/4	40
2	40	40
3	38 7/8	40 1/2
4	39 1/2	39 3/4

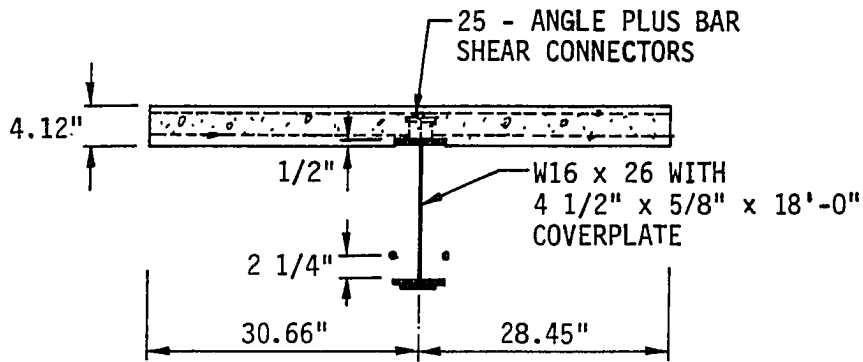


a. Elevation

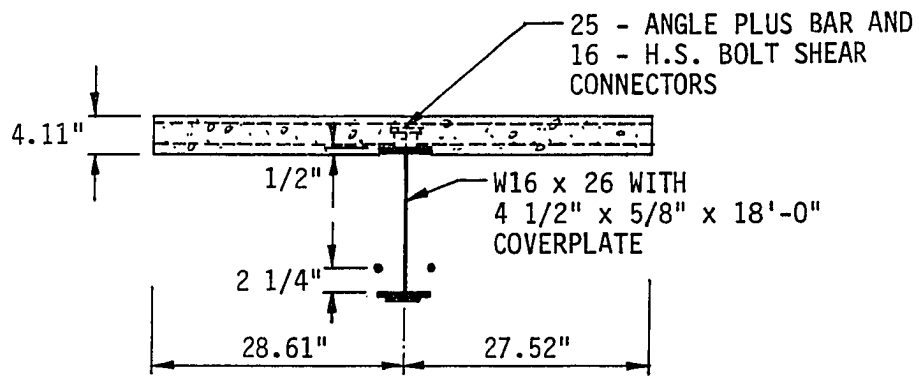


b. Beam 1 cross section

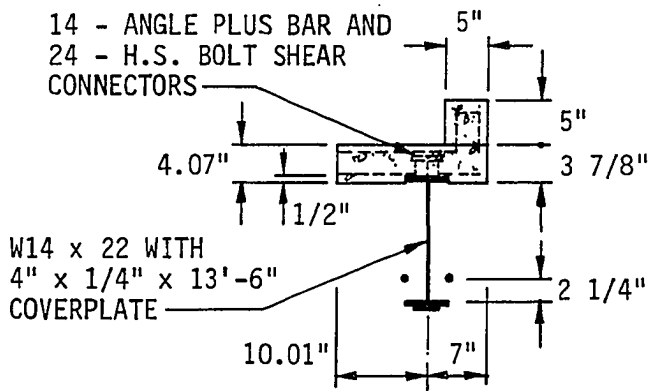
FIGURE 5. Post-tensioned composite beams (Dedic)



c. Beam 2 cross section



d. Beam 3 cross section



e. Beam 4 cross section

FIGURE 5 (Continued)

TABLE 1. Physical properties of concrete
for composite beams (Dedic)

	f'_c psi	E ksi
Deck	3300	2830
Curb	7450	5080

TABLE 2. Physical properties of steel for composite beams (Dedic)

	σ_y ksi	σ_u ksi	E ksi
#3 reinforcing bar	69.8	110.8	29,110
#4 reinforcing bar	70.8	109.7	-
5/8 inch diameter threadbar	-	156.1	24,100
W14 x 22	44.7	69.4	28,990
W16 x 26	44.1	66.9	29,990

provide a reasonable amount of experimental data for both elastic and inelastic beam behavior, against which to check analytical and finite element models of prestressed composite beams.

2.2. Elastic Analytical Model

The first model developed in this chapter for prestressed composite beams is an extension of classical beam theory. The effect of shear lag in the concrete deck is approximated by means of the AASHTO effective width rules, and the difference in elastic properties between concrete deck and steel beam is approximated through use of a theoretical modular ratio, with which the concrete deck is transformed to an equivalent steel area.

The elastic analytical model does not consider slip between deck and beam and, therefore, all computed stresses and deflections are based on full interaction. Shear deflections, which may be significant in a composite beam because of its relatively large depth, are not included in the model. Also, shrinkage cracking and tension cracking of the concrete deck, which would cause larger stresses and deflections, is not explained by the model, since the model assumes that concrete is a continuous, elastic material with equivalent compression and tension behavior.

2.2.1. Equilibrium analysis

After a composite beam is transformed to an equivalent steel beam by means of the modular ratio, forces, moments, and resulting stresses

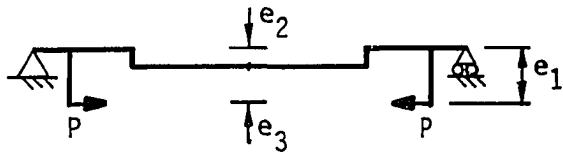
can be computed from classical beam theory. A post-tensioned composite beam, such as the beam illustrated in Figure 5a, can be idealized as shown in Figure 6a. The tension in the tendons, T , causes applied forces, P , which are eccentric with respect to the neutral axis of the beam. At the tendon anchorages, the applied forces are eccentric by an amount, e_1 . Over the central region of the beam, where the coverplate is welded to the bottom flange, the neutral axis is shifted downward, and the eccentricity is reduced by an amount e_2 to e_3 .

For purposes of analysis, the applied eccentric forces can be separated into applied axial forces and applied moments. The applied axial forces are shown in Figure 6b, and the corresponding axial force diagram is shown in Figure 6c. Applied moments, M_1 , are constant near the tendon anchorages, but are reduced by the moment, M_2 , to M_3 over the central, coverplated region of the beam. The final moments are illustrated in the moment diagram in Figure 6f.

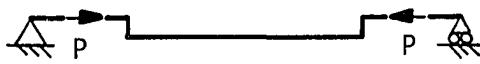
The analysis described above will give the primary forces and moments for a composite beam during application of the post-tensioning. The analysis does not, of course, account for secondary $P-\Delta$ effects or secondary ΔT effects.

2.2.2. Secondary effects

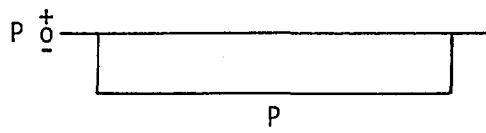
Deflections of a prestressed composite beam cause two secondary effects -- the $P-\Delta$ effect and the ΔT effect. The applied moments shown in Figure 6d cause bending deflections. For an unrestrained tendon, the eccentricity of the tendon with respect to the neutral axis will change



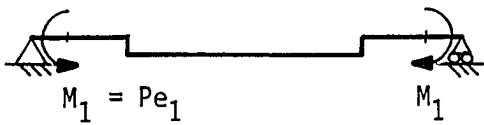
a. Applied eccentric forces



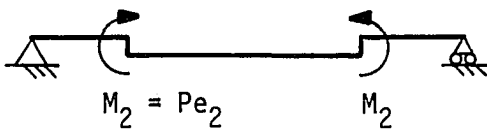
b. Applied axial forces



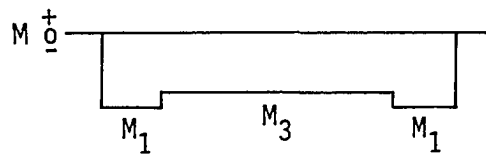
c. Axial force diagram



d. Applied moments



e. Induced moments due to shift in neutral surface at coverplate



f. Moment diagram

FIGURE 6. Equilibrium analysis of a post-tensioned composite beam

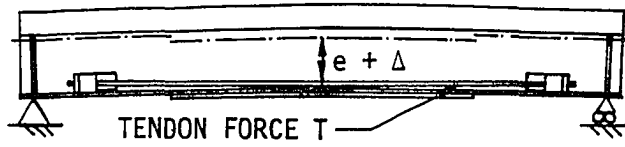
by the amount of the deflection at any cross section within the post-tensioned region. Because the deflection, Δ , increases the eccentricity, there will be an increase in the bending moment at the cross section equal to the axial force, P , multiplied by Δ .

The upward bow in the post-tensioned beam in Figure 7a causes the $P-\Delta$ effect illustrated on the moment diagram in Figure 7b. The $P-\Delta$ effect is beneficial in this case because it increases post-tensioning stresses, and increases those stresses the maximum amount at midspan, the usual critical point for the rating or design of the beam.

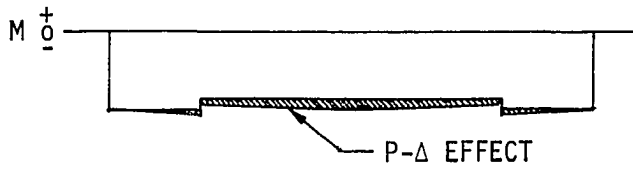
After the tendons are anchored to the composite beam, the beam becomes a first-degree indeterminate structure, and another secondary effect will occur as the beam is subjected to vertical load. When the beam is loaded and deflects downward, the tendon anchorages will move farther apart, thereby stretching the tendon and adding an increment, ΔT , to the tendon force.

If the vertical loading is such that the composite beam returns to its original shape, the $P-\Delta$ effect will disappear. At the same time, however, the tendon force will increase by ΔT . The ΔT effect increases both the post-tensioning moment as shown in Figure 7d and the axial compression force.

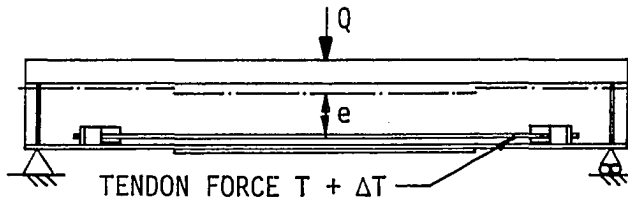
For the simply supported, post-tensioned beam, both $P-\Delta$ and ΔT effects are beneficial since both effects increase the post-tensioning stresses. $P-\Delta$ effects can be computed by determining the deflection of the beam caused by the eccentric forces and multiplying that deflection



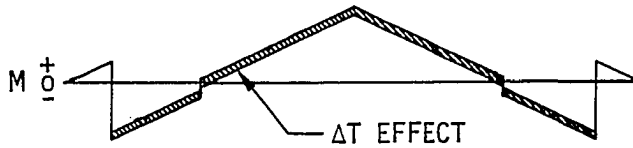
a. Post-tensioned beam



b. Moment diagram with P-Δ effect



c. Loaded post-tensioned beam



d. Moment diagram with ΔT effect

FIGURE 7. Secondary effects due to post-tensioning

by the force, P . Because the deflection of a composite beam due to post-tensioning typically is small within the elastic range, the corresponding $P-\Delta$ effect also will be small.

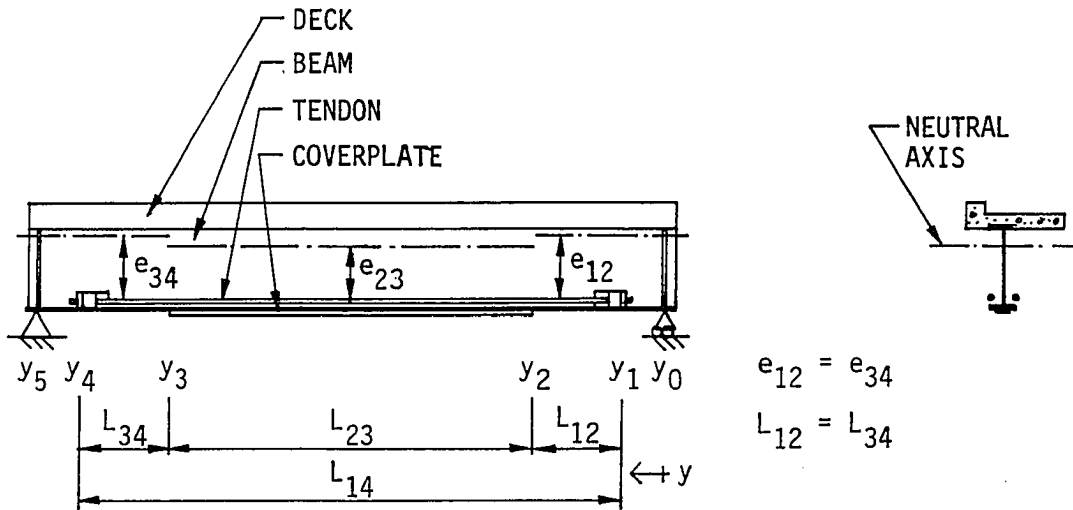
The change in tendon force, ΔT , must be computed through the use of an indeterminate analysis method. By means of the principle of strain energy (Castigliano's Theorem), Hoadley derived a formula for ΔT [41]. Hoadley's derivation was for a beam of constant cross section.

Because the beams in a typical Iowa composite bridge have partial-length coverplates, Hoadley's formula does not apply. Consequently, in the appendix, a new ΔT formula has been derived which accounts for a partial-length coverplate. The new formula is presented in Figure 8b. As the formula indicates, the change in tendon force is dependent on the moments caused by loads applied after post-tensioning, but is independent of the original post-tensioning force.

ΔT tends to be small, as will be demonstrated in Section 2.3.3. The computed ΔT is subject to the same limitations as classical beam theory. Shear connector slip and shear deflections are not considered in the ΔT formula derivation.

2.2.3. Model verification

Classical beam theory, as noted previously, does have limitations. The extent of the differences between the elastic analytical model based on classical beam theory and the actual behavior of prestressed composite beams can be determined from Tables 3 and 4. Table 3 is for the application of prestressing to the beams tested by Stras and Dedic.



a. Post-tensioned composite beam

$$\Delta T = \frac{\frac{e_{12}}{EI_{12}} \left[\int_{y_1}^{y_2} M \, dy + \int_{y_3}^{y_4} M \, dy \right] + \frac{e_{23}}{EI_{23}} \int_{y_2}^{y_3} M \, dy}{\frac{2e_{12}^2 L_{12}}{EI_{12}} + \frac{e_{23}^2 L_{23}}{EI_{23}} + \frac{2L_{12}}{A_{12}E} + \frac{L_{23}}{A_{23}E} + \frac{L_{14}}{A_R E_R}}$$

WHERE M = MOMENT FOR LOADS APPLIED AFTER POST-TENSIONING

e = ECCENTRICITY OF TENDON

A = AREA OF TRANSFORMED COMPOSITE SECTION

I = MOMENT OF INERTIA OF TRANSFORMED COMPOSITE SECTION

E = MODULUS OF ELASTICITY OF TRANSFORMED COMPOSITE SECTION

A_R = AREA OF POST-TENSIONING TENDONS

E_R = MODULUS OF ELASTICITY OF POST-TENSIONING TENDONS

NOTE: DERIVATION OF THE FORMULA IS GIVEN IN THE APPENDIX.

b. ΔT formula

FIGURE 8. ΔT for post-tensioned composite beam with coverplate

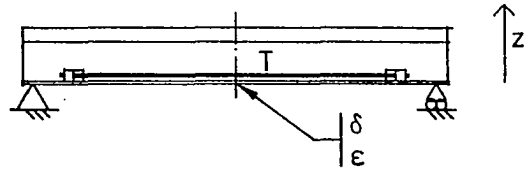
For the Stras beams, the prestressing was applied only to the steel beam, whereas for the Dedic beams, the prestressing was applied to the composite beam section.

For prestressing of the Stras beams, the computed and experimental strains in the bottom flange at midspan are in excellent agreement. For post-tensioning of the Dedic beams, computed midspan deflections, on the average, are 10% below experimental values, and computed midspan, coverplate strains are 18% below experimental values. The computed values for the Stras beams should be more accurate than the computed values for the Dedic beams since the Stras beams were steel, whereas the Dedic beams were composite.

The elastic analytical model does not consider shear deflection, shear connector slip, or reduced deck section due to concrete cracking. All of these factors could cause increased deflections and increased strains. During the first few months of testing the model bridge from which the Dedic beams were eventually cut, it was noticed that the bridge gradually responded in a more flexible manner. Quite probably the increased flexibility was due to concrete shrinkage and loss of bond between concrete deck and steel beams.

In order to examine the possible effect of concrete cracking, the area of the deck for Beam 2 was arbitrarily reduced by taking the modular ratio, n , to be three times the theoretical value. The increased n did little to alter the midspan deflection and strains for post-tensioning, as shown in Table 3. The reduction in transformed deck

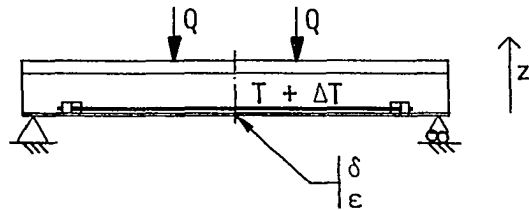
TABLE 3. Experimental and computed midspan deflections and strains for prestressed composite beams -- elastic analytical model



T = prestressing force in tendon
 δ = midspan deflection
 ϵ = midspan strain in bottom flange or coverplate
 Subscripts: e = experimental
 c = computed

TEST	T kips	δ_e in	δ_c in	$\frac{\delta_e}{\delta_c}$	ϵ_e $\mu\text{in/in}$	ϵ_c $\mu\text{in/in}$	$\frac{\epsilon_e}{\epsilon_c}$
Beams A, B, C (Stras)	8.47	-	0.056	-	-258	-266	0.97
Beam 1 (Dedic)	24.09	0.120	0.114	1.05	-196	-167	1.17
Beam 2 (Dedic)	31.66	0.102	0.095	1.07	-171	-147	1.16
Beam 2, 3n (Dedic)	31.66	0.102	0.094	1.09	-171	-148	1.16
Beam 3 (Dedic)	32.22	0.102	0.096	1.06	-179	-150	1.19
Beam 4 (Dedic)	24.25	0.143	0.115	1.24	-203	-169	1.20

TABLE 4. Experimental and computed ΔT forces, midspan deflections, and midspan strains for loaded prestressed composite beams -- elastic analytical model



Note: Strains and deflections do not include effects of T.

T = prestressing force in tendon
 ΔT = change in prestressing force
 Q = vertical load
 δ = midspan deflection
 ϵ = midspan strain in bottom flange or coverplate
 Subscripts: e = experimental, c = computed

TEST	Q kips	ΔT_e kips	ΔT_c kips	$\frac{\Delta T_e}{\Delta T_c}$	δ_e in	δ_c in	$\frac{\delta_e}{\delta_c}$	ϵ_e $\mu\text{in/in}$	ϵ_c $\mu\text{in/in}$	$\frac{\epsilon_e}{\epsilon_c}$
Beams A, B, C (Stras)	6.07	1.03	1.14	0.90	-0.209	-0.184	1.14	763	742	1.03
Beam 1 (Dedic)	9.0	4.69	4.11	1.14	-0.520	-0.380	1.37	543	491	1.11
Beam 2 (Dedic)	14.8	4.64	4.39	1.06	-0.510	-0.389	1.31	577	542	1.06
Beam 2, 3n (Dedic)	14.8	4.64	4.36	1.06	-0.510	-0.549	0.93	577	591	0.98
Beam 3 (Dedic)	15.1	4.60	4.49	1.02	-0.515	-0.398	1.29	594	554	1.07
Beam 4 (Dedic)	9.1	4.75	4.18	1.14	-0.544	-0.390	1.39	548	500	1.10

area raised the neutral axis of the composite section, thereby increasing the eccentricity of the post-tensioning force, at the same time it decreased the area and moment of inertia of the cross section. The two effects compensated, and the computed deflections and strains remained essentially the same.

In Table 4, experimental and computed values are compared for the same Stras and Dedic beams with applied vertical loads. The values in Table 4 are not cumulative with the values in Table 3. For the Stras beams, the computed ΔT force is 10% greater than the measured force, but for the Dedic beams, the computed ΔT forces average 9% less than the measured forces. Computed midspan deflections for all beams are less than the measured deflections and, for the Dedic beams, the differences range to 39%. Computed midspan strains are less than experimental strains, but differ by a maximum of 11%.

The elastic analytical model for Beam 2 with the increased modular ratio did bring the computed midspan deflections and strains closer to experimental values. For the vertical loading condition in Table 4, the reduced transformed deck area reduced the area and moment of inertia of the composite beam, but did not have any effect on the applied force or moment, as it did with post-tensioning.

All of the experimental or computed midspan deflections in Tables 3 and 4 represent 3% or less of the eccentricity of the prestressing tendons. Therefore, any $P-\Delta$ effects will also be 3% or less. $P-\Delta$ corrections would have minor but generally positive effects on the differences between experimental and computed values.

The elastic analytical model agrees well, usually within 10%, with experimentally determined prestressing deflections, tendon force changes, and vertical load strains. The model does not agree as well with experimentally determined prestressing strains and vertical loading deflections. The factors neglected by classical beam theory are the probable cause of the differences between the elastic analytical model and actual behavior of prestressed composite beams. Finite element models presented later in the next section will correlate better with the experimental results for the prestressed composite beams.

2.3. Elastic Finite Element Model

At the time this research was begun, there were three finite element programs for elastic, static analysis available at Iowa State University: SAP IV, SAP 6, and ANSYS. ANSYS was restricted to classroom use for relatively small problems and, therefore, was not available for research purposes. SAP 6 seemed to offer no significant advantage over SAP IV for static problems and was less convenient to use at Iowa State University than SAP IV. Consequently, SAP IV [13] was selected for the finite element analysis of the post-tensioned composite beams and bridges.

Because no graphics programs were available for SAP IV at Iowa State University, the author wrote several Fortran programs for plotting finite element models, deflected shapes, and stress diagrams. The author also wrote Fortran programs to generate SAP IV models for quarter

symmetry post-tensioned composite beams, quarter symmetry post-tensioned composite bridges, and complete post-tensioned composite bridges.

2.3.1. SAP IV elements

A finite element model for any structure is constructed by establishing a matrix of nodes connected by finite elements which have the properties of small segments of the structure. For each SAP IV node, six displacement degrees of freedom (dof), three translations and three rotations, can be set as active or non-active degrees of freedom for the structure. Also, a SAP IV node can be defined as a master node with one or more slave nodes. Each slave node degree of freedom is then dependent on the corresponding master node degree of freedom. The master-slave node option models a rigid link in the structure.

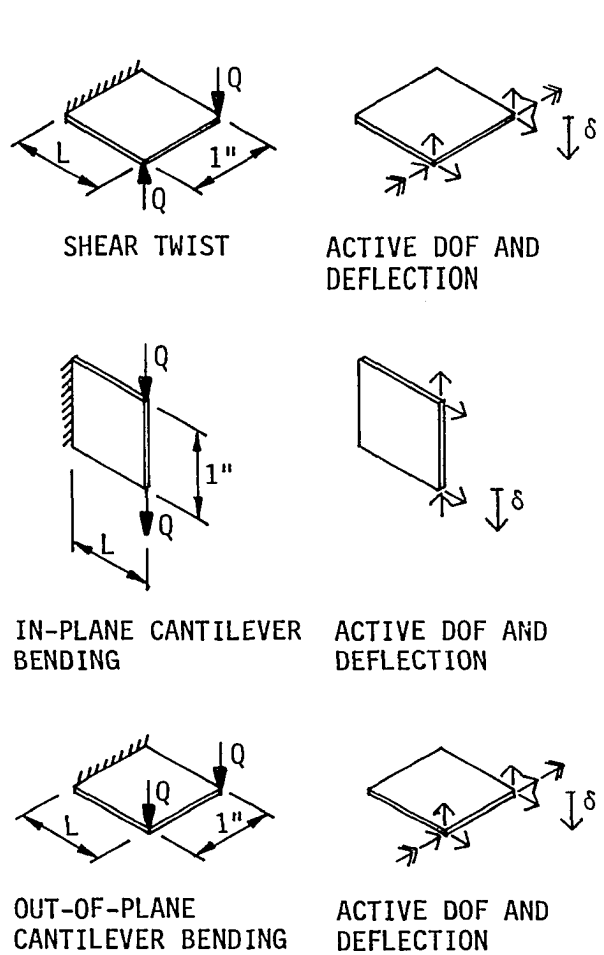
For modeling the post-tensioned composite beams, three elements from the SAP IV element library were chosen: a three-dimensional truss element, a three-dimensional beam element, and a thin plate and shell element. The truss and beam elements are not unique to SAP IV but are common to large, standard finite element programs. The beam element may be given the ability to deform in bending alone or to deform in both bending and shear by including a non-zero shear area with the element properties.

The thin plate and shell element, unique to SAP IV and a few related programs, is a quadrilateral of arbitrary geometry assembled from four compatible triangles. The element uses four constant strain triangles to represent membrane behavior and four LCCT9 elements to

represent bending behavior. The central node of the quadrilateral is located at the average of the coordinates of the four corner nodes. The stiffness associated with rotation normal to the plane of the element is not defined and should not be included in analysis. For shells or plates with small curvatures, boundary elements with arbitrary rotational stiffnesses must be located at the corner nodes of the thin plate and shell element in order to avoid numerical problems.

Thin plate or shell elements, such as the one in the SAP IV element library, can be formulated from displacement or stress fields using various techniques. Each different formulation gives the element certain properties which control its behavior when it is used alone or in combination with other elements. For evaluation and comparison purposes, Robinson [70] has proposed a series of relatively severe individual element tests and convergence tests for plate or shell elements. Those tests can be used to explore the behavior of a given element or to compare the behavior of various elements with the objective of selecting the best element.

In order to explore the behavior of the SAP IV element, three of Robinson's single element tests, extended to aspect ratios of less than one, are given in Figure 9. In the figure, each test is illustrated to the left and then defined in terms of active degrees of freedom. To the right, the deflections of the SAP IV element are given as fractions of theoretical deflections and with respect to the aspect ratio of the element.



$t = 0.05 \text{ in}$
 $E = 10 \times 10^3 \text{ ksi}$
 $G = 4 \times 10^3 \text{ ksi}$
 $\nu = 0.25$

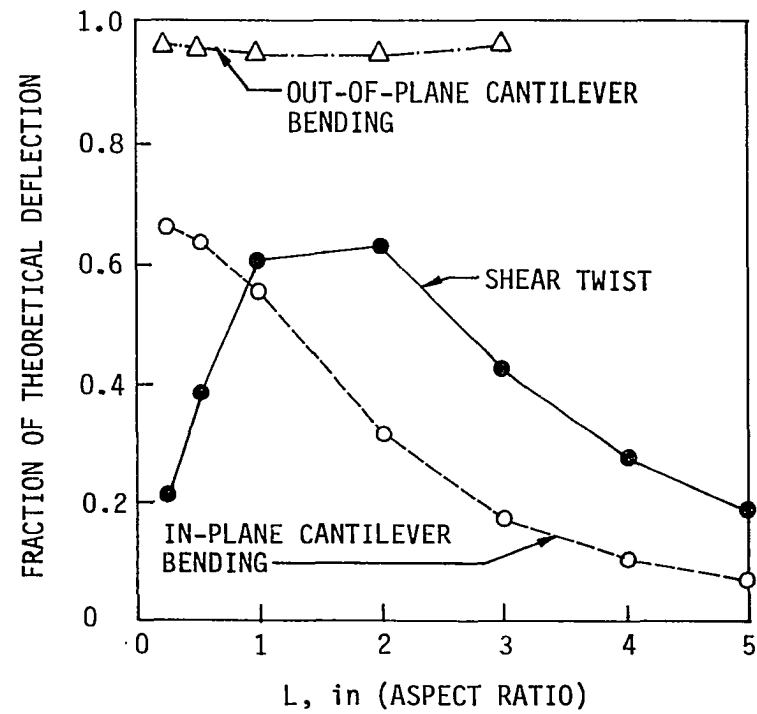


FIGURE 9. Single element tests for SAP IV thin plate and shell element

Since the thin plate and shell element is formulated to model out-of-plane bending, the element should perform well in the out-of-plane cantilever bending test. As shown in the graph, the element not only performs well but also is insensitive to aspect ratio.

The shear twist and in-plane cantilever bending tests, however, indicate some problems with the element. In shear twist, the SAP IV element is very sensitive to aspect ratio and, even at best, with aspect ratios of one or two, is considerably stiffer than membrane theory [79] would predict. The in-plane cantilever bending test, which at small aspect ratios consists primarily of shear, shows the element to have reasonable accuracy at small aspect ratios but poor accuracy for aspect ratios above two. Even with small aspect ratios, the element is stiffer than predicted by theory [80].

The single element tests show that, for greatest accuracy, the SAP IV thin plate and shell element should be given aspect ratios near one. Even at an aspect ratio of one, however, the element will be stiffer than predicted by theory.

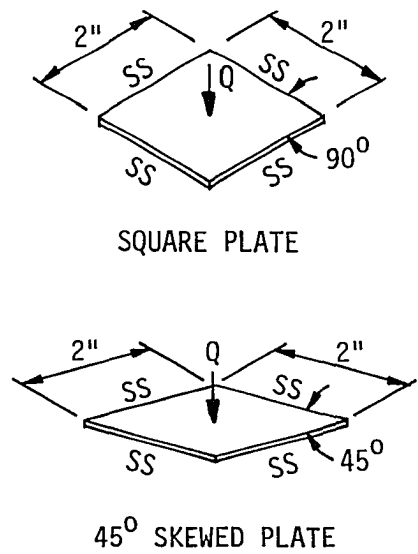
One of the convergence tests recommended by Robinson is illustrated in Figure 10. The test is for a plate simply supported on all four edges and loaded with a concentrated force at the center. Two plates were tested: a square plate and a 45-degree skewed plate which has a rhombus shape. Each plate was subdivided into SAP IV thin plate and shell elements for analysis, using first one element per quarter plate, then four elements per quarter plate, etc., as indicated on the abscissa

of the graph. The square plate was subdivided into square elements, and the 45-degree skewed plate was subdivided into 45-degree, rhombus-shaped elements. The SAP IV-computed central deflections are plotted as fractions of the theoretical deflections. For the square plate, the theoretical deflection is taken from plate theory [80] and, for the skewed plate, the theoretical deflection is taken from a conformal mapping solution by Aggarwala [1].

The graph in Figure 10 shows that the SAP IV solution for the square plate converges rapidly toward the theoretical deflection as the plate is subdivided into more elements. Even with only four elements (one element per quarter plate), the solution is quite accurate. The solution for the skewed plate is much less accurate, however. The skewed plate must be subdivided into 64 elements in order to equal the accuracy of the four-element square plate solution. As the comparison between the convergence for the square and skewed plates indicates, the accuracy of a solution for a skewed plate will be less than the accuracy of a comparable solution for a square plate. The reduced accuracy for a skewed plate will be of interest in developing the finite element model for a skewed bridge in the next chapter.

2.3.2. Model assembly

Within the range of options and elements available in the SAP IV program, a post-tensioned composite beam can be modeled with a variety of finite element configurations. For comparison purposes, the four finite element models illustrated in Figure 11 were assembled. Model A



$t = 0.05 \text{ in}$
 $E = 10 \times 10^3 \text{ ksi}$
 $G = 4 \times 10^3 \text{ ksi}$
 $\nu = 0.25$

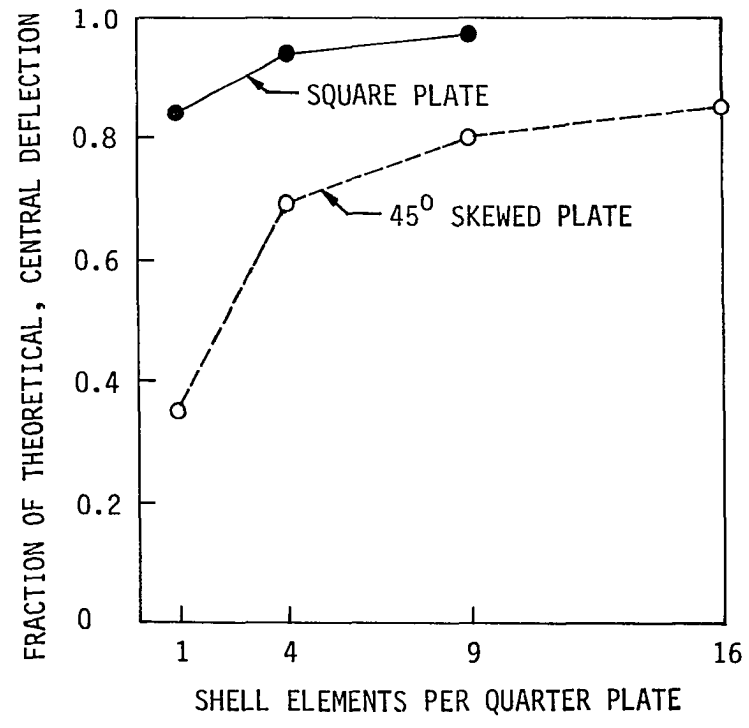


FIGURE 10. Convergence tests for a simply supported plate with a central concentrated load

in Figure 11a is a simplified model which has been utilized in previous bridge research [36,26]. The deck in the model is represented by plate elements linked through master-slave nodes to beam elements representing the steel beam. The beam elements are placed at the elevation of the centroid of the steel beam or at the elevation of the centroid of the steel beam with coverplate. Because of the rigid links created by the master-slave node relationship, the model does not allow for slip of shear connectors, and it will not give shear connector forces directly. For the post-tensioning bracket in the model, a rigid beam element is attached at a beam node and extended to the elevation of the tendon.

Model B in Figure 11b is a more complex model patterned after a finite element model developed by Tumminelli and Kostem [83]. The deck, steel beam, and bracket are modeled the same as in Model A, but the deck and beam are linked with a "shear connector linkage assembly." The shear connector linkage assembly has a stiff truss element which maintains the separation between deck and beam. Rigid beam elements are attached to deck and beam nodes which stretch or compress a flexible truss element link representing the shear connector. The flexible link is placed at the elevation of the interface between deck and top beam flange, and the link is given a small length (exaggerated in the figure) and properties so that its deformation characteristics are identical to those of the actual shear connector in a push-out test.

Model C in Figure 11c represents the deck with plate elements, the same as for Models A and B. The steel beam is modeled differently,

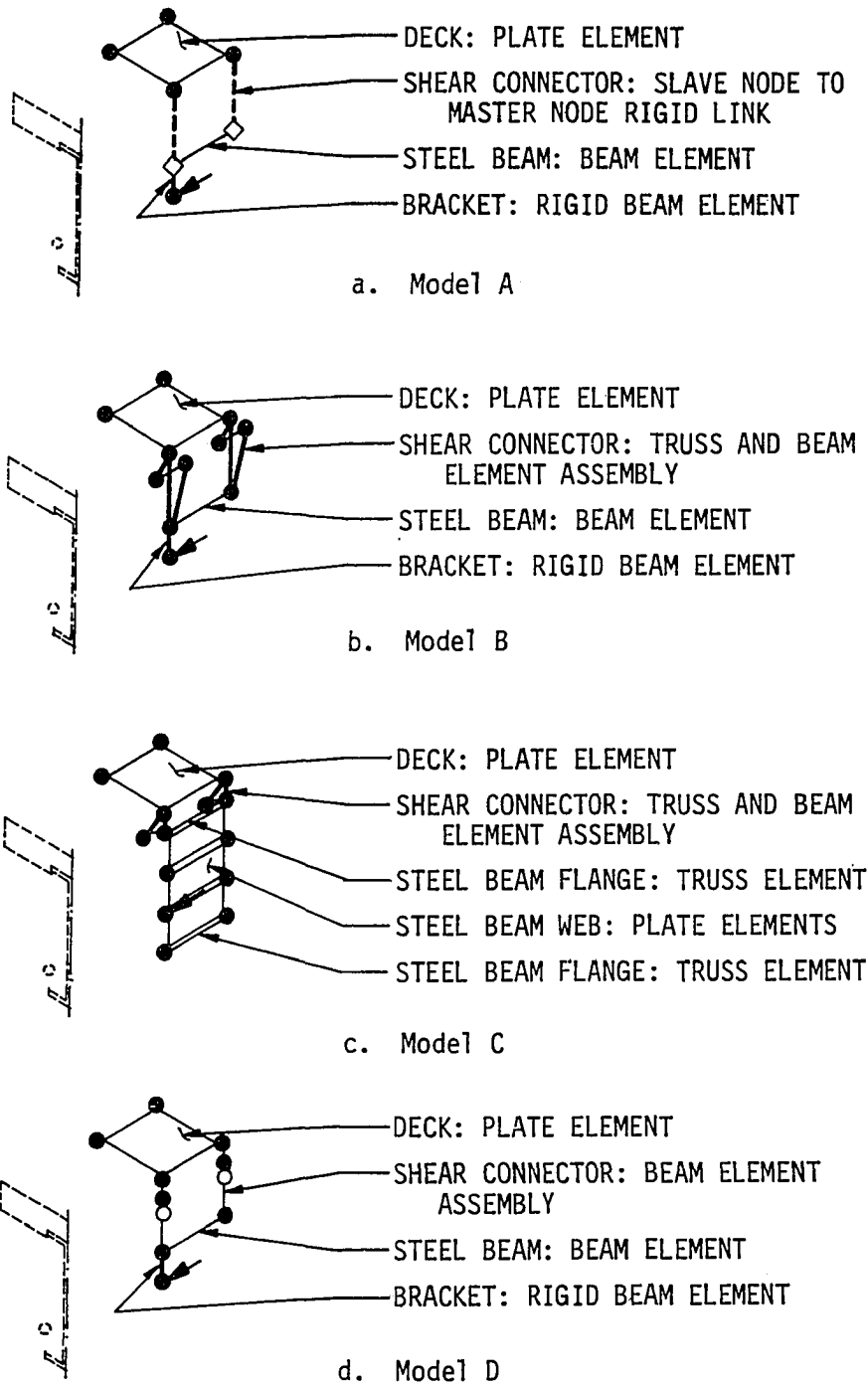


FIGURE 11. SAP IV finite element models for post-tensioned composite beams

however. The top and bottom flanges of the steel beam are modeled by truss elements, and the web of the steel beam is modeled by plate elements. Shear connectors are represented by an assembly similar to the assembly in Model B. A stiff truss element maintains separation between deck and beam flange, and a rigid beam element attached to the deck node will stretch or compress a flexible truss element at the elevation of the top flange. Since the full beam depth is represented in the model, there is no need for the rigid beam element extended to the elevation of the tendon. The post-tensioning force is simply applied at a correctly-located node on the beam web.

The fourth model, Model D in Figure 11d, is the same as Model B except for the shear connector assembly. In Model D, two flexible beam elements separate the deck and the steel beam. An end release for rotation in the lower beam element, at the elevation of the deck-top flange interface, gives the assembly the capacity to model shear connector slip and to give shear connector forces directly. This model reduces the number of nodes and elements, as compared to Model B, and thus reduces cost of analysis.

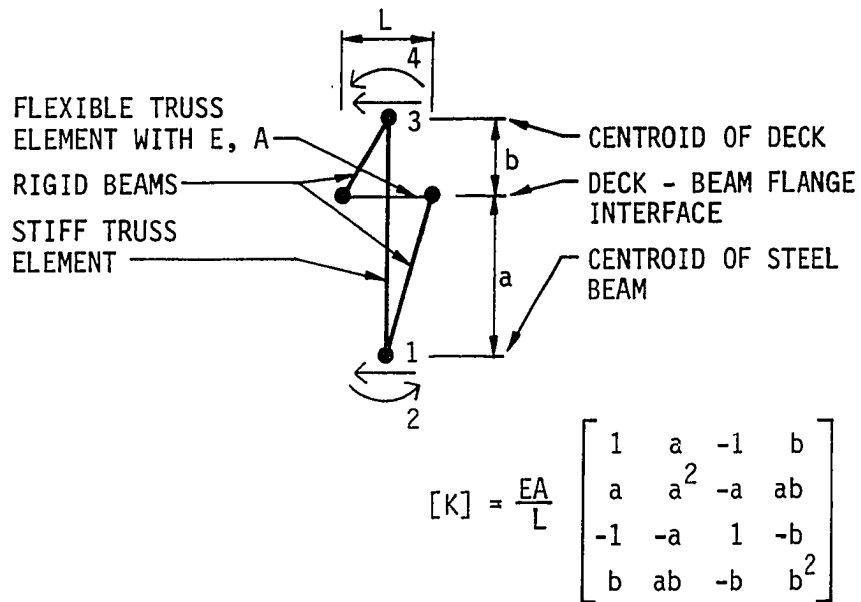
All models could have a truss element, to represent a tendon, attached at the bracket node, however, the truss element adversely affects bandwidth and solution cost. The effect of the tendon can be determined through a less expensive flexibility analysis based on separate analyses for vertical load and for a post-tensioning force applied at the bracket. For checking purposes, in several instances the

flexibility analysis was compared with SAP IV analyses with the tendons represented by truss elements.

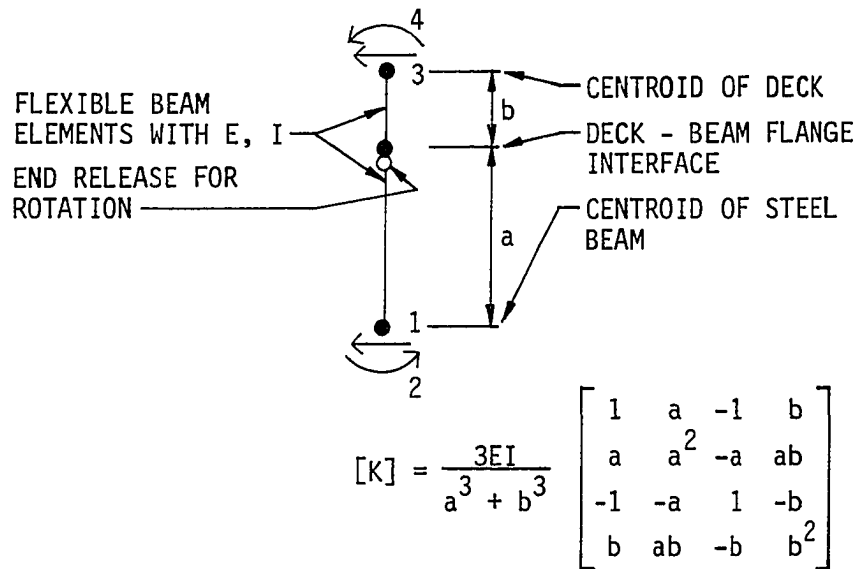
In Models B, C, and D, the shear connector assemblies could either represent a tributary portion of a shear connector or an entire shear connector. In cases when the shear connector assembly represented an entire shear connector for an analysis run, excess shear connector assemblies were disconnected by means of end releases within the assemblies.

The shear connector assemblies for Models B and D are illustrated in more detail in Figure 12. In Figure 12a, the shear connector linkage assembly developed by Tumminelli and Kostem is shown with the four degrees of freedom which affect the flexible link. The stiffness matrix for those degrees of freedom can be set equal to the push-out test stiffness of a shear connector by setting the axial stiffness of the flexible truss element. The length of the truss element, L , should be kept arbitrarily small, and the modulus of elasticity, E , and area, A , of the truss element set to match the shear connector stiffness.

The stiffness matrix derived for the flexible beam element assembly in Figure 12b is identical to the stiffness matrix in Figure 12a except for the term outside of the brackets. If that term is set to be numerically the same for both assemblies, computed stiffness terms will be the same. For the flexible beam element assembly in Figure 12b, the modulus of elasticity, E , and the moment of inertia, I , can be used to set the finite element assembly stiffness equal with a push-out test



a. Shear connector linkage assembly (Tumminelli and Kostem)



b. Flexible beam elements

FIGURE 12. SAP IV finite element models for shear connectors

stiffness. This flexible beam element assembly saved approximately 10% of the SAP IV analysis cost in a direct comparison with Model B, and Model D also has modeling advantages which will become apparent in the next chapter when the finite element model for a composite beam is extrapolated to a bridge.

2.3.3. Model verification

Models A through D were assembled to explore the effects of deck node spacing (mesh size), shear deflection, shear lag, and shear connector slip. With the objective of developing a trial composite beam model to be extrapolated to a composite bridge, the models were compared with each other and with the test results from Beams 2 and 3 cut from the model bridge constructed at Iowa State University.

Selected SAP IV analysis runs for the finite element models are summarized in Table 5. All four models were utilized for Beam 2, an interior beam, but only Models C and D were utilized for Beam 3, an interior beam with added high strength bolt shear connectors. Mesh size for the concrete deck was varied from 15 inches to 6 inches. Shear deflections were excluded or included for the steel beam elements. Shear connectors were modeled with or without slip. If shear connector slip was modeled, the connector stiffness determined from push-out tests was assigned to shear connector assemblies by one of three methods: a partial stiffness for the tributary length for the assembly, full stiffness to an assembly at the actual shear connector location, or full stiffness to the assembly at the nearest deck node.

TABLE 5. SAP IV analysis runs for post-tensioned composite beams

SAP IV RUN	BEAM (DEDIC)	MODEL ^a	CONCRETE DECK PLATE ELEMENTS, APPROXIMATE SIDE LENGTH, in	STEEL BEAM ELEMENT ASSEMBLY	SHEAR CONNECTORS	
					SLIP	STIFFNESS
1	2	A	15	i	no	-
2	2	B	10	ii	no	-
3	2	B	10	ii	yes	iv
4	2	B	10	i	yes	iv
5	2	B	15	i	yes	iv
6	2	C	7.5	iii	yes	iv
7	2	C	6	iii	no	-
8	2	C	6	iii	yes	v
9	2	D	15	i	yes	vi
10	3	C	6	iii	yes	v
11	3	D	15	i	yes	vi

i - beam element with shear deformation	iv - partial stiffness for tributary length
ii - beam element without shear deformation	v - total at exact location
iii - truss and plate elements	vi - total at nearest deck node location

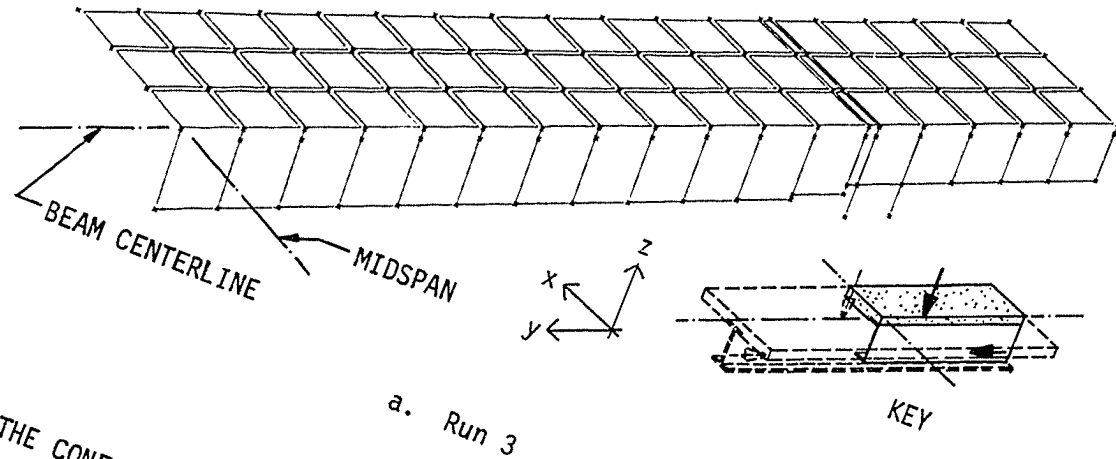
^aSee Figure 11.

The finite element models associated with four of the SAP IV analysis runs listed in Table 5 are illustrated in Figure 13. Because both post-tensioning and the vertical loading in the tests were symmetrical (except for minor variations in vertical load placement), the finite element models were assembled only for one quarter of the composite beam, as indicated in the key in Figure 13a. Boundary conditions at midspan and at the beam centerline were applied to enforce the symmetrical behavior of the finite element models.

Bottom flange coverplates for Beams 2 and 3 had tapered ends similar to those in typical Iowa bridges. In Run 5, Figure 13b, the coverplate taper is not modeled. In Run 3, Figure 13a, the taper is modeled with stepped steel beam elements, and in Runs 6 and 10, Figure 13c and 13d, the taper is modeled by truss elements of varying area. The concentrated vertical loads, actually applied through 8-inch square pads, are modeled either as a single point load or as a group of point loads, depending on the coarseness of the deck mesh. Results from the SAP IV runs are given in Table 6 for Beam 2 and in Table 7 for Beam 3. Overall, there are only minor differences among the results of the runs, except for the deflection caused by vertical load. In all cases, except one, the SAP IV-computed deflections, strains and changes in tendon force are less than those measured in the laboratory tests.

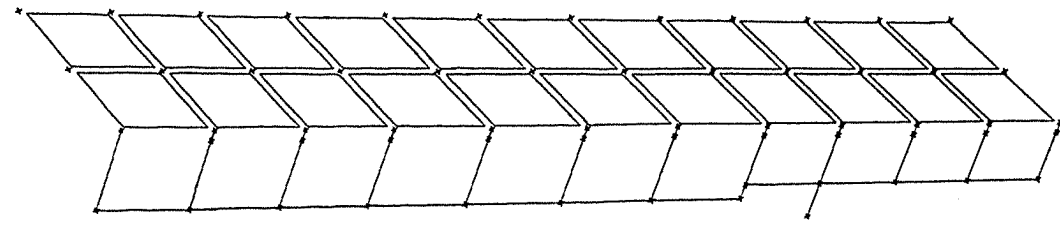
The size of the concrete deck mesh has little effect on the computed deflections and strains. Runs 1, 5, 9, and 11, which have the coarsest deck mesh give results which are comparable with those from the

NOTE: THE CONFIGURATION FOR RUNS
2 AND 4 IS SIMILAR.



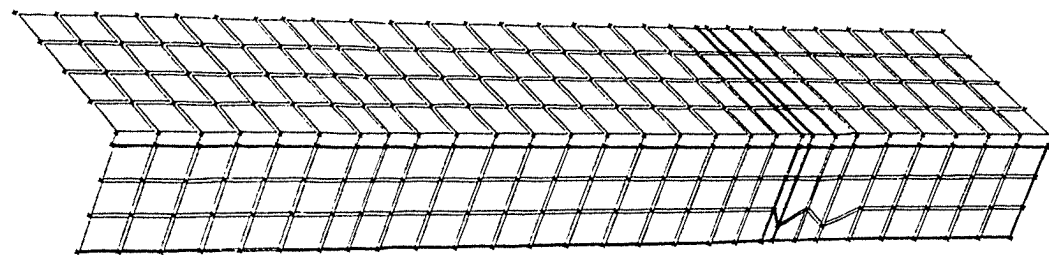
a. Run 3

NOTE: THE CONFIGURATION FOR RUNS
1, 9, AND 11 IS SIMILAR.



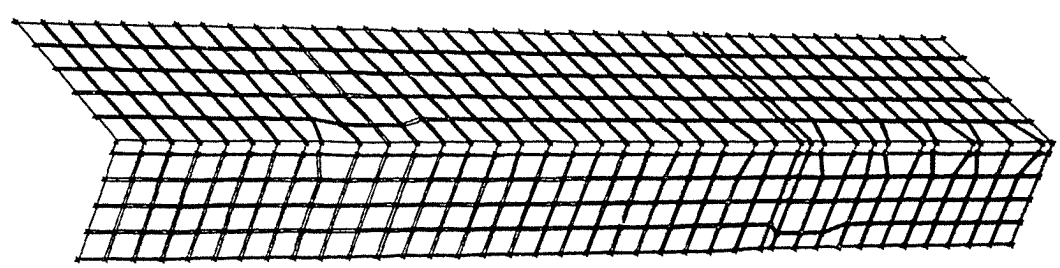
b. Run 5

FIGURE 13. SAP IV quarter symmetry post-tensioned composite beam models



c. Run 6

NOTE: THE CONFIGURATION FOR RUNS
7 AND 8 IS SIMILAR.

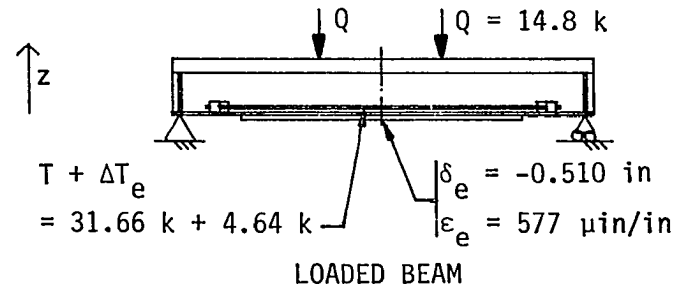
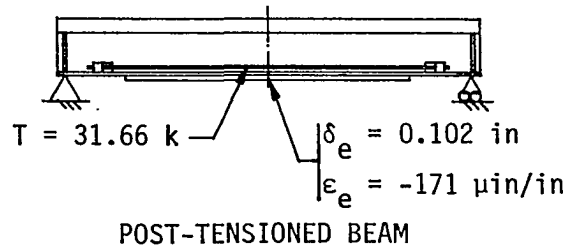


d. Run 10

FIGURE 13 (Continued)

TABLE 6. Experimental and computed midspan deflections, midspan strains, and ΔT forces for Beam 2
 -- elastic finite element models

Subscripts: e = experimental, c = computed



SAP IV RUN	δ_c in	$\frac{\delta_e}{\delta_c}$	ϵ_c $\mu\text{in/in}$	$\frac{\epsilon_e}{\epsilon_c}$	ΔT_c kips	$\frac{\Delta T_e}{\Delta T_c}$	δ_c in	$\frac{\delta_e}{\delta_c}$	ϵ_c $\mu\text{in/in}$	$\frac{\epsilon_e}{\epsilon_c}$
1	0.093	1.10	-147	1.16	4.56	1.02	-0.409	1.25	535	1.08
2	0.092	1.11	-147	1.16	4.48	1.04	-0.380	1.34	535	1.08
3	0.091	1.12	-147	1.16	4.44	1.05	-0.424	1.20	548	1.05
4	0.091	1.12	-147	1.16	4.44	1.05	-0.453	1.13	548	1.05
5	0.093	1.10	-147	1.16	4.53	1.02	-0.457	1.12	548	1.05
6	0.089	1.15	-141	1.21	4.37	1.06	-0.448	1.14	520	1.11
7	0.090	1.13	-141	1.21	4.41	1.05	-0.409	1.25	511	1.13
8	0.089	1.15	-141	1.21	4.38	1.06	-0.453	1.13	522	1.11
9	0.093	1.10	-147	1.16	4.53	1.02	-0.457	1.12	548	1.05

runs with finer mesh. It appears that the coarse mesh may actually create a slightly more flexible model, with computed deflections slightly closer to experimental deflections.

The addition of shear deflection to steel beam elements generally improves performance of the finite element model. A comparison of Run 3 without shear deflection and Run 4 with shear deflection, in Table 6, indicates that the composite beam model with shear deflection becomes about 7% more flexible and closer to the experimental deflection for vertical load. Other comparisons between runs, not as direct, indicate the same behavior. Strains and changes in tendon force are affected only slightly by beam shear deflection.

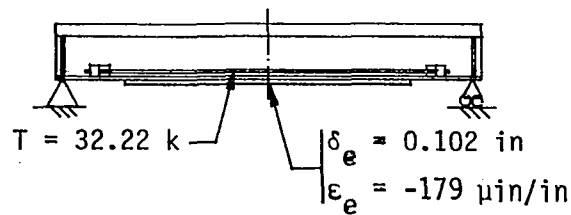
Including shear connector slip in the finite element model also improves deflection behavior for vertical loads. A comparison of Run 2 without slip and Run 3 with slip indicates that the model becomes approximately 14% more flexible for vertical loads when connector slip is included in the model. A 12% improvement in deflection behavior for vertical loads is indicated by a comparison of Runs 7 and 8. Other SAP IV-computed quantities are affected very little by shear connector slip.

Beam 2 has a deck width about 20% greater than the effective flange width permitted under the AASHTO bridge design specifications.

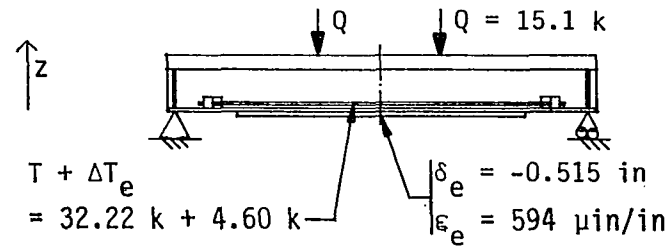
Therefore, shear lag should have some effect on the behavior of the composite beam. SAP IV-computed longitudinal membrane stresses for the deck plate elements, which should vary because of shear lag, are plotted for Beam 2 in Figures 14 and 15. In Figure 14, for post-tensioning, the

TABLE 7. Experimental and computed midspan deflections, midspan strains, and ΔT forces for Beam 3
 -- elastic finite element models

Subscripts: e = experimental, c = computed



POST-TENSIONED BEAM



LOADED BEAM

SAP IV RUN	δ_c in	$\frac{\delta_e}{\delta_c}$	ϵ_c $\mu\text{in/in}$	$\frac{\epsilon_e}{\epsilon_c}$	ΔT_c kips	$\frac{\Delta T_e}{\Delta T_c}$	δ_c in	$\frac{\delta_e}{\delta_c}$	ϵ_c $\mu\text{in/in}$	$\frac{\epsilon_e}{\epsilon_c}$
10	0.091	1.12	-143	1.25	4.47	1.03	-0.459	1.12	532	1.12
11	0.094	1.09	-149	1.20	4.62	1.00	-0.464	1.11	559	1.06

Longitudinal stresses are relatively constant across the deck width, except at Sections y_2 and y_3 , near the application of the post-tensioning and beginning of the coverplate. The stress disturbances there are modeled quite differently depending on shear connector slip, but much the same for coarse and fine deck mesh.

Figure 15 for combined post-tensioning and vertical load does indicate some shear lag. The longitudinal membrane stresses decrease with increasing distance from the beam centerline. Again the mesh size has less effect on the membrane stresses than the presence or absence of shear connector slip.

It is interesting to note that, in spite of the difference in deflected shape caused by post-tensioning vs. vertical load, the membrane stresses are compression. The deck compression for post-tensioning is caused by the applied axial force rather than the applied moment.

If shear connectors cannot slip, the concrete deck responds very quickly to application of post-tensioning or change in beam cross section. At Section y_2 in Figure 14, the Run 1 deck membrane stress is very large near the steel beam, as compared with the stress for either Run 8 or 9. In Figure 15, at Section y_4 , near the applied load, Run 1 again gives a larger stress than either Runs 8 or 9. From the membrane stress graphs, it appears that shear connector slip generally equalizes deck stresses and reduces maximum stresses.

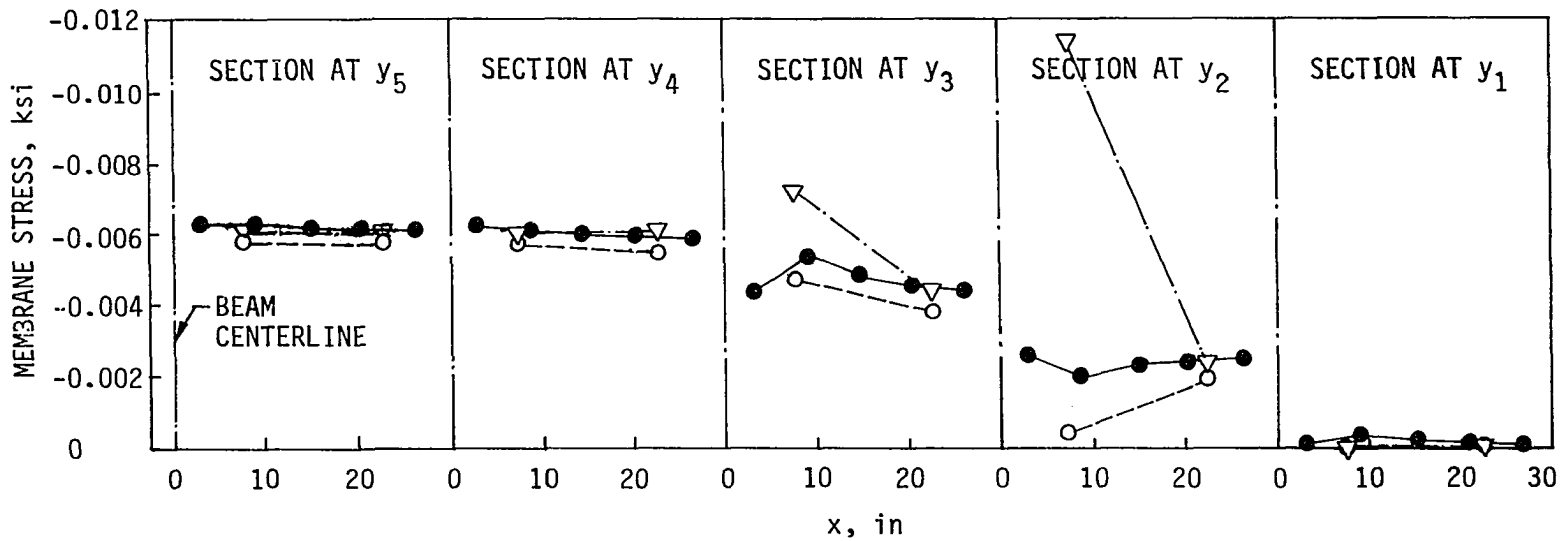
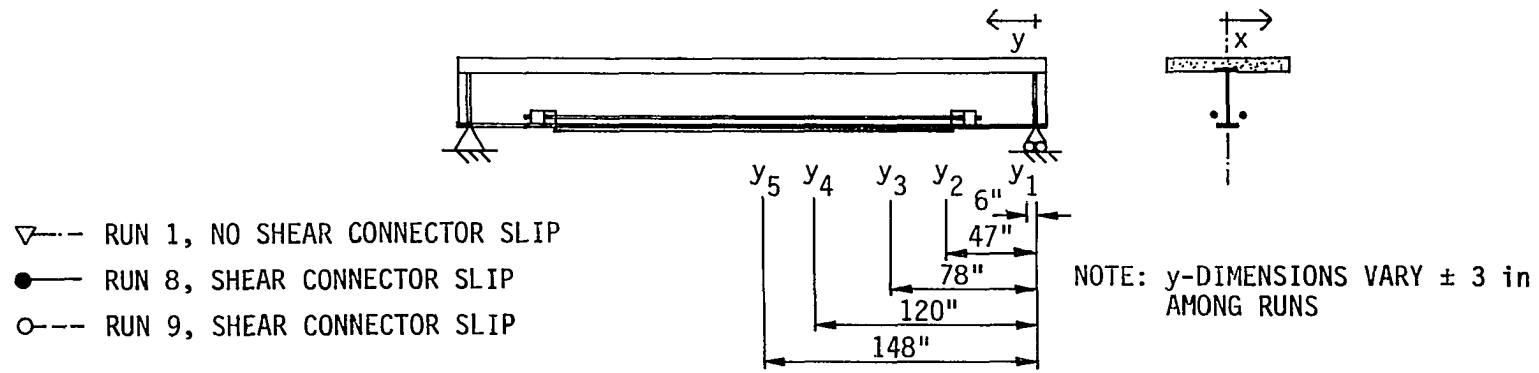


FIGURE 14. Longitudinal membrane stresses in deck for post-tensioning, Beam 2

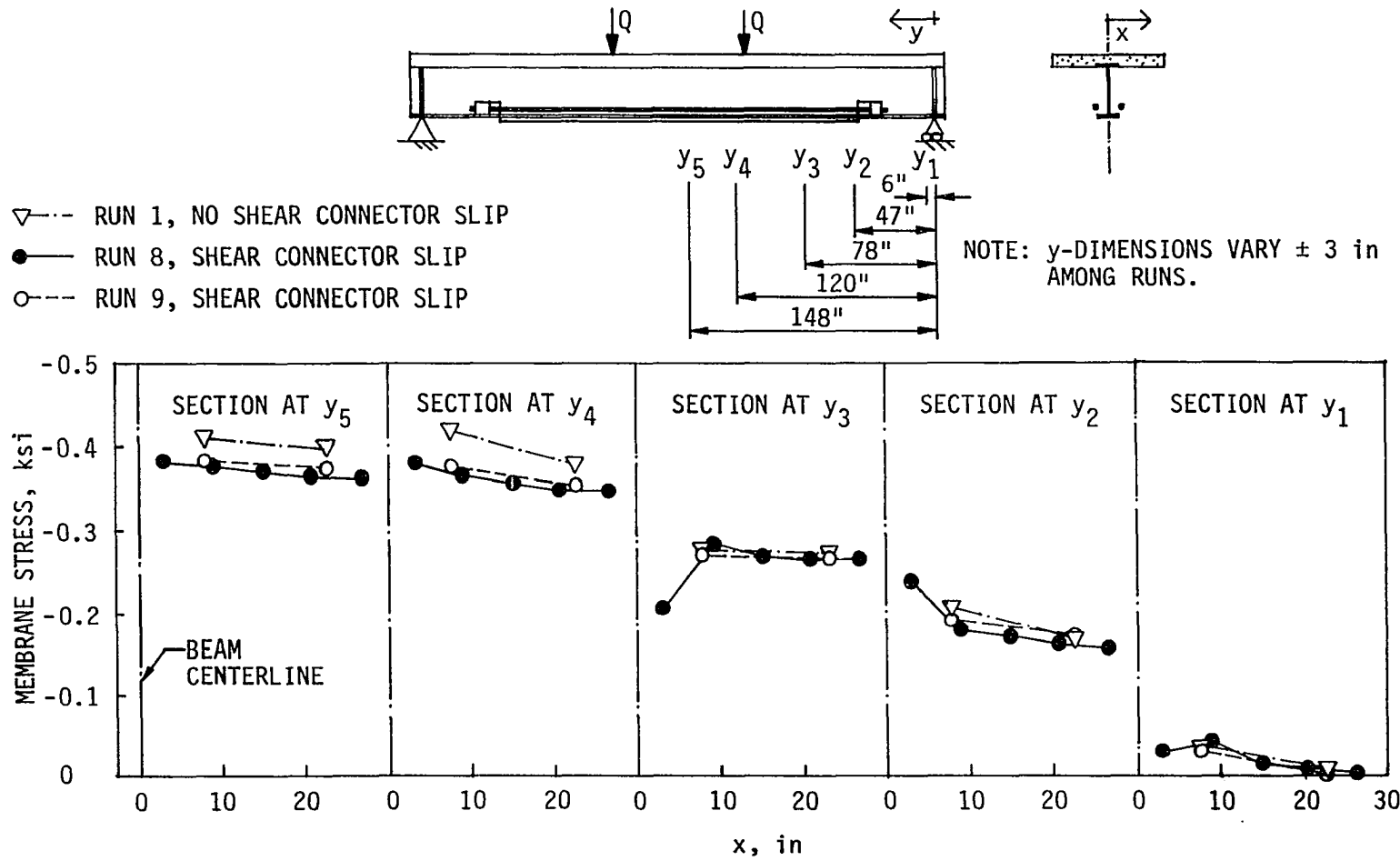
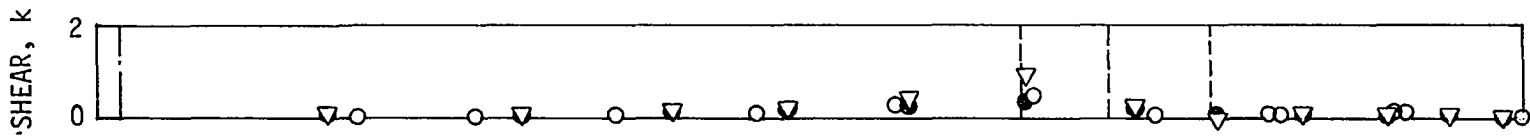


FIGURE 15. Longitudinal membrane stresses in deck for post-tensioning and vertical load, Beam 2

Shear connector slip also has the effect of equalizing shear connector forces and reducing maximum forces, as illustrated in Figure 16b. The maximum shear connector forces shown are for Run 7, for which no slip was permitted, as compared with Runs 8 and 9, for which shear connector assemblies were given stiffnesses based on push-out tests.

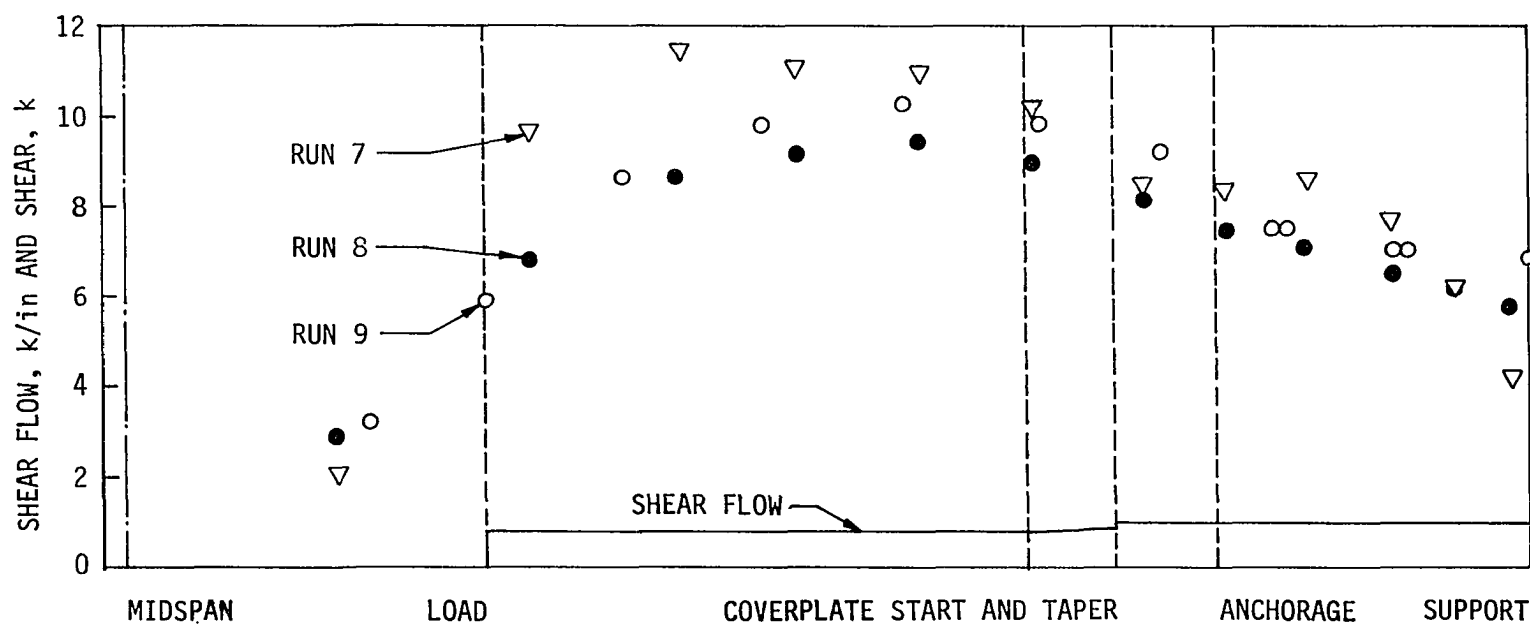
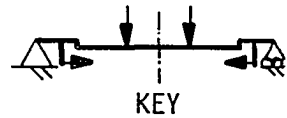
Figure 16 also illustrates several other items of interest. For post-tensioning alone, there is no vertical shear according to classical beam theory. The largest of the relatively small forces plotted in Figure 16a is near the coverplate start, where the change in post-tensioning moment occurs because of the shift in neutral axis (which does cause horizontal shear if the beam is analyzed as a frame with a vertical member connecting beam sections at the different neutral axis elevations). The force is in the direction for positive bending moment, as it should be, based on the equilibrium analysis given earlier in this chapter.

The shear connector forces toward midspan, away from the coverplate start, are those required to transmit part of the axial compression force from the steel beam to the concrete deck. The forces on the shear connectors caused by post-tensioning are generally small and can be safely neglected in design. A comparison of Run 8, for which shear connector stiffnesses were accurately located, and Run 9, for which shear connector stiffnesses were arbitrarily moved to the nearest assembly, shows that the nearest node forces are quite accurate, usually within 15% of the exact forces.



NOTE: ALL FORCES ARE FOR ANGLE-PLUS-BAR CONNECTORS.

a. Post-tensioning



b. Post-tensioning and vertical load

FIGURE 16. Shear flow and shear connector forces, Beam 2

Figure 17 for Beam 3 is intended to show the effect of adding relatively flexible high strength bolt shear connectors to a beam with the stiff, angle-plus-bar connectors. The SAP IV runs in Figure 17b indicate that the elastic forces are generally proportional to the connector stiffnesses, as theory would predict. The figure also shows that stiffnesses moved to the nearest shear connector assembly are quite accurate. When several connector stiffnesses are added to a finite element connector assembly, the computed force also can be proportioned on the basis of the connector stiffnesses.

The comparisons of SAP IV Models A through D and associated analysis runs show that the coarsest mesh, with deck plate elements approximately 15-inches square, gives accurate results. Models which utilize beam elements to represent the steel beam should include shear deflections, in order to accurately model the deflection behavior of a composite beam under vertical loading. Including shear connector slip in the finite element model also improves deflection behavior.

The shear connector assembly in Model D reduces analysis cost when compared with Model B. Moving shear connector stiffnesses to the nearest shear connector assembly generally has minimal effect on accuracy of the shear connector forces or overall behavior of the finite element model.

Finite element models with shear deflections and shear connector slip generally compare better with experimental results than the elastic analytical model given in Section 2.2. Based on the comparisons in this

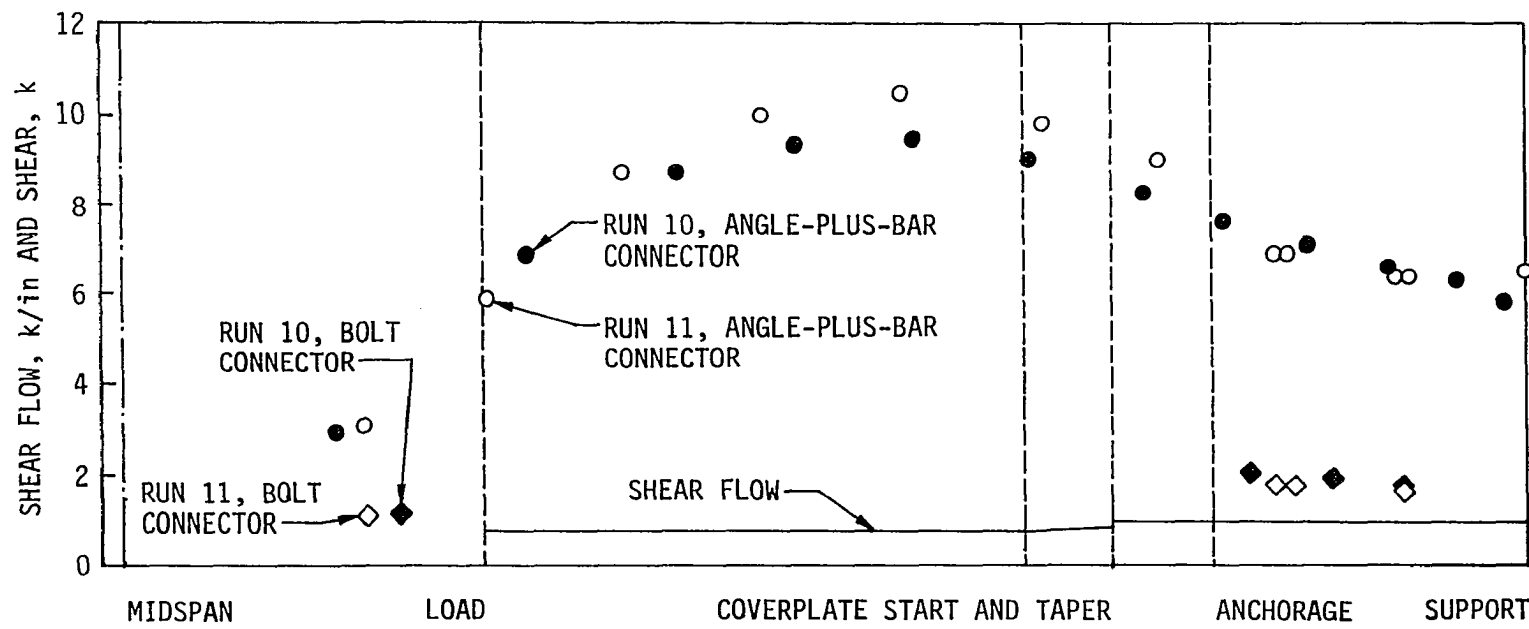
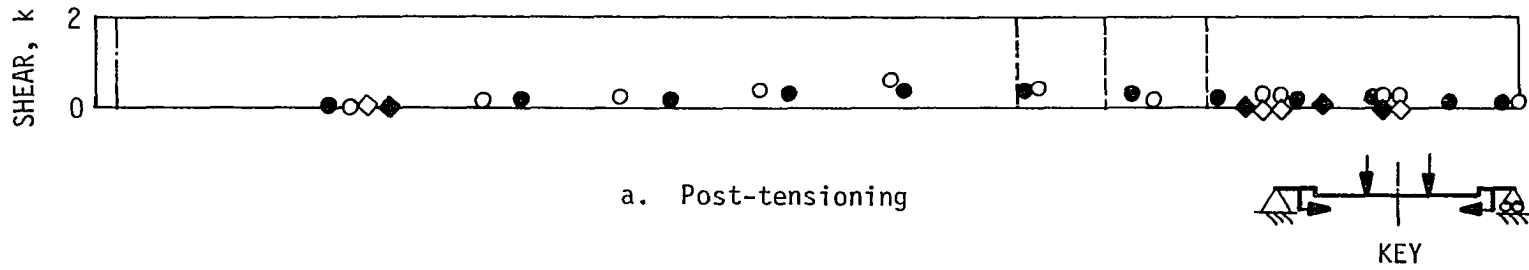


FIGURE 17. Shear flow and shear connector forces, Beam 3

section, Model D with the coarse mesh appears to be the best trial model to extrapolate to a bridge constructed of composite beams.

2.4. Inelastic Analytical Model

If a composite beam is prestressed as part of its original design or post-tensioned as part of a strengthening program, it gains capacity under both service load design and load factor or ultimate strength design. The gain in capacity is larger under service load design than under load factor or ultimate strength design, and this fact has raised questions regarding the safety of prestressed composite beams. The inelastic analytical model developed in this section and verified with experimental results can be utilized to compute the strength of a prestressed composite beam, and thus to check the safety of the beam.

2.4.1. Model development

An inelastic analytical model for a prestressed composite beam should include the inelastic behavior of a steel beam as well as the following behavior: concrete-steel composite action, partial shear connection, partial prestress, and unbonded tendons. Some of the behavior can be included in a correct failure mechanism for the beam, and the remaining behavior can be included by following the AASHTO Load Factor Design rules [3], which are based on previous composite beam research.

Experimental behavior of prestressed composite beams has been documented by Stras [76] and Dedic [54]. Reagan [68] developed a

computerized numerical method for the behavior of prestressed composite beams and studied the behavior of the Stras beams, a series of bridge beams, and a series of building beams.

Except for composite beams with partial shear connection, the failure mode for prestressed composite beams has been crushing of the concrete deck at or near midspan and formation of a hinge at that location because of localized loss of strength and yield of the steel beam. Therefore, it is reasonable to consider the beam behavior to be similar to a steel beam with a plastic hinge at midspan, if sufficient shear connectors anchor the concrete deck to the steel beam.

Because the tendons may not be restrained to deflect with the beam, some estimate of the deflection at the plastic hinge is required in order to account for $P-\Delta$ effects. The average midspan deflection at ultimate load for the three beams tested by Stras and the four beams tested by Dedic was equal to the span length, L , divided by 79. The average midspan deflection for the seven beams actually tested and two beams analyzed to failure by Reagan also was $L/79$. For estimating the deflection at the plastic hinge, the deflection can be rounded to $L/80$.

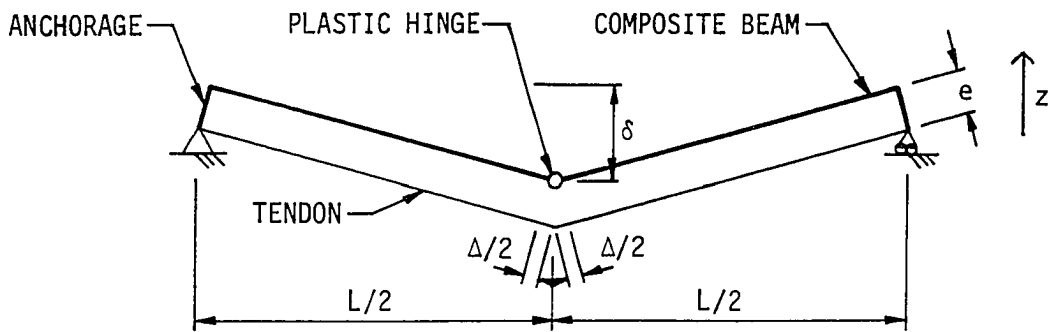
In the absence of other information, the composite beam flange width can be determined according to the AASHTO rules for effective flange width for Load Factor Design (which are the same rules as for Service Load Design). The compressive force in the deck also can be determined according to AASHTO rules, which account for reinforcing in the deck, relative capacity of the concrete deck with respect to the steel beam, and partial or full shear connection.

Change in the tendon length can be determined from the idealized failure mechanisms illustrated in Figure 18. In the Stras and Reagan beams, the tendon was restrained to deflect with the beam, and the change in length can be computed from the idealized mechanism in Figure 18a. In Figure 18b, the idealized mechanism which represents the beams tested by Dedic permits the tendon to rise. The change in tendon eccentricity must be included in the computations for flexural strength, in order to consider the P- Δ effect.

Tendon force at the ultimate moment for the composite beam can be computed from an idealized stress-strain curve for the tendon steel. The force must be based on the sum of the strain in the tendon caused by prestressing and the additional strain in the tendon caused by deformation of the beam under vertical load. Shear connector capacities can be computed from the formulas given in the AASHTO bridge design specifications or separate research data. For the Dedic beams, the angle-plus-bar connector capacity was available from push-out tests and an extrapolation formula based on the AASHTO channel connector formula [54]. The combination of the failure mechanisms, the AASHTO Load Factor Design rules, and shear connector data gives the inelastic analytical model the ability to consider all significant prestressed composite beam behavior at ultimate load.

2.4.2. Model verification

Applying the inelastic analytical model to a beam requires a certain amount of trial and error, in order to correctly locate the

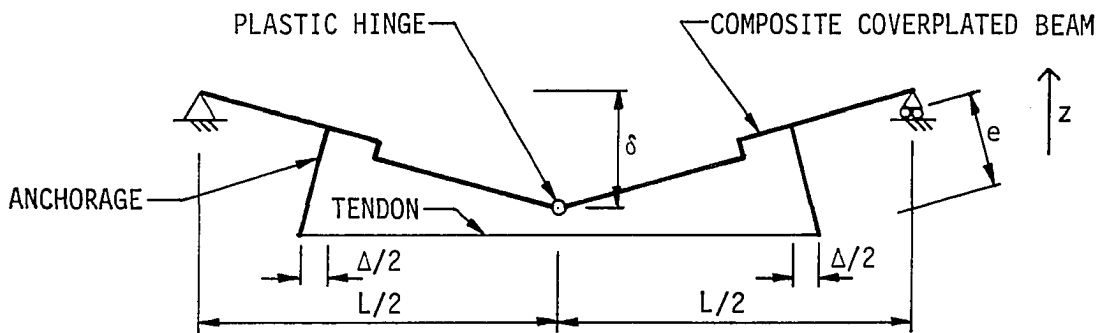


a. Stras and Reagan beams

e = ECCENTRICITY OF TENDON WITH RESPECT TO NEUTRAL AXIS AT PLASTIC HINGE

Δ = CHANGE IN TENDON LENGTH AFTER PRESTRESSING

δ = DEFLECTION AT PLASTIC HINGE, ESTIMATED TO BE $L/80$



b. Dedic beams

FIGURE 18. Prestressed composite beams -- inelastic analytical model

neutral axis. The procedure outlined below provides a guide for using the model.

1. Assume a plastic hinge at midspan with a deflection of $L/80$.
2. Compute the maximum compressive force according to AASHTO Load Factor Design rules based on slab and reinforcing; beam, coverplate, and tendon at yield; and shear connectors.
3. Compute the tendon force at ultimate load, using the sum of the initial post-tensioning strain and the strain caused by the change in tendon length as the beam deflects to $L/80$, and a stress-strain curve for the tendon steel. Correct the compressive force computed in 2, if necessary.
4. Determine the elevations of compressive and tensile force resultants, accounting for the rise in the tendon, if the tendon is unrestrained.
5. Compute the flexural strength as the product of the maximum compressive force and the distance between compressive and tensile force resultants.

The inelastic analytical model was applied to the average of the three beams tested by Stras, two beams analyzed by Reagan (one of which was a Stras beam), and the four beams tested by Dedic. Results and comparisons for the midspan deflection at failure, change in tendon force, and flexural strength are given in Table 8. Because there was some question as to the amount of prestressing on the Stras beams at the time of the ultimate load tests, the computations in the table are set

up so as to bracket the actual condition. In the first line of the table, the full prestressing is assumed for the inelastic analytical model computations and, in the second line, no prestressing is assumed. Also given in the last two columns of the table are computed moments for the composite beams without prestressing and a comparison which shows the strength increase with prestressing.

The largest difference between values determined by test (or values computed by Reagan) and values computed with the inelastic analytical model is for midspan deflection values. The actual deflection at failure is often difficult to measure accurately. During the ultimate load test of Beam 3, for example, there were problems with the instrumentation and loading jacks caused by large deflections, and the test had to be stopped and restarted, in order to obtain a complete failure of the beam [54]. In Table 8, the experimental deflection is being compared with an average computed deflection and, therefore, some differences will be apparent.

The computed midspan deflection generally affects the tendon stress in the inelastic range, where a change in tendon length does not cause as large a change in tendon force. Any midspan deflection error then should not cause as large an error in subsequent computations.

The computed change in tendon force agrees within 12%, and the computed flexural strength agrees within 7% of values determined by tests or computed by Reagan. In general, the inelastic analytical model underestimates the change in tendon force and slightly overestimates the

TABLE 8. Experimental and computed midspan deflections, ΔT forces, and flexural strengths -- inelastic analytical model

BEAM, TEST OR COMPUTED (AUTHOR)	δ_{pe} in	L/80 in	$\frac{\delta_{pe}}{L/80}$	ΔT_{pe} kips	ΔT_{pc} kips	$\frac{\Delta T_{pe}}{\Delta T_{pc}}$
Beams A, B, & C, test average (Stras) prestressed ^a	-1.90	-1.80	1.06	8.99	8.04	1.12
Beams A, B, & C, test average (Stras) restrained ^a	-1.90	-1.80	1.06	8.99	8.19	1.10
Stras Beam A, computed (Reagan)	-1.80	-1.80	1.00	8.38	8.04	1.04
Beam PH3, computed (Reagan)	-12.50	-11.85	1.06	97.47	91.67	1.06
Beam 1, test (Dedic)	-3.57	-3.84	0.93	-	35.39	-
Beam 2, test (Dedic)	-3.38	-3.84	0.88	-	28.04	-
Beam 3, test (Dedic)	-5.56 ^b	-3.84	1.45 ^b	-	27.19	-
Beam 4, test (Dedic)	-3.36	-3.84	0.87	28.83	31.25	0.92

δ = midspan deflection at
ultimate load
 ΔT = change in prestressing force
 M_u = flexural strength

Subscripts:
e = experimental or computed
by Reagan
c = computed, inelastic
analytical model
p = prestressed

^aTests were conducted with loss of prestress. Computations are for extreme conditions: full prestress or no prestress (restrained).

^bTest was stopped and restarted.

Mu_{pe} in-kips	Mu_{pc} in-kips	$\frac{Mu_{pe}}{Mu_{pc}}$	Mu_c in-kips	$\frac{Mu_{pc}}{Mu_c}$
1078	1126	0.96	948	1.19
1078	1037	1.04	948	1.09
1073	1126	0.95	948	1.19
42591	42472	1.00	31650	1.34
4140	4176	0.99	3876	1.08
5813	6269	0.93	5561	1.13
6102	6359	0.96	5635	1.13
4503	4530	0.99	4036	1.12

flexural strength. The model is quite accurate considering the variation in tendon type and placement, the variation in beam cross section, and the variation in shear connection.

The last column in Table 8 gives the comparison of flexural strength between the prestressed and unprestressed conditions. The increase in strength with prestressing varies from 8% to 34%. For the two prestressed beams analyzed by Reagan, the increase in strength averages 26%. The prestressing for those beams was greater than the post-tensioning proposed for strengthening the Iowa bridges. For exterior beams, Beams 1 and 4, similar to those to be post-tensioned in the Iowa bridges, the increase in strength averages 10%. This increase is less than the capacity increase computed under AASHTO Service Load Design which would be 30% to 35%.

The inelastic analytical model, verified by experimental work, does predict that the ultimate flexural capacity of a composite beam will be increased by prestressing. The increase in ultimate capacity, however, is less than the increase in capacity computed under a service load design method. The factor of safety for a prestressed composite beam, therefore, will be reduced. Because the small exterior beams in the Iowa bridges to be strengthened will be post-tensioned to overcome a relatively moderate overstress, the reduction in factor of safety will not be large. Thus, in the opinion of the author, AASHTO Service Load Design is an acceptable method for designing the post-tensioning for strengthening a bridge.

The inelastic analytical model is accurate for isolated prestressed composite beams but does not account for the restraints and load redistribution mechanisms which affect the beam when it is part of a bridge superstructure. The inelastic prestressing distribution which would allow extrapolation of the inelastic analytical model to a bridge was not part of this research study. Thus, additional study is required if strengthening by post-tensioning were to be designed by AASHTO Load Factor Design.

3. BEHAVIOR OF POST-TENSIONED COMPOSITE BRIDGES

In this chapter, the finite element model for a post-tensioned, composite beam, developed in Section 2.3, is extrapolated to post-tensioned composite bridges. Several bridge characteristics, not encountered in isolated beams, require alteration and refinement of the model. The finite element model for a bridge, as it is developed and refined, is verified with the model bridge constructed and tested in the Iowa State University Structural Research Laboratory.

The model bridge was carefully supported on hinges and rollers so as to create simple supports with virtually no end rotation or longitudinal displacement restraints. Because of practical considerations, highway bridges were connected at abutments with little regard to theoretical, simple support conditions. As a consequence, when the finite element bridge model analyses were compared with field tests for two highway bridges, there were significant differences between the analysis and test results. The field results, however, were bracketed by two separate finite element analyses for simple support and fixed support conditions. When reasonable estimates of the guard rails and end restraints were included in the finite element model, the computed strains and deflections correlated well with the values measured in the field.

After the verification of the finite element bridge model in this chapter, it will be utilized to develop the post-tensioning distribution required for the strengthening of simple span composite bridges. The

finite element bridge model also has been utilized for analysis of bridges different from the typical Iowa bridges [14].

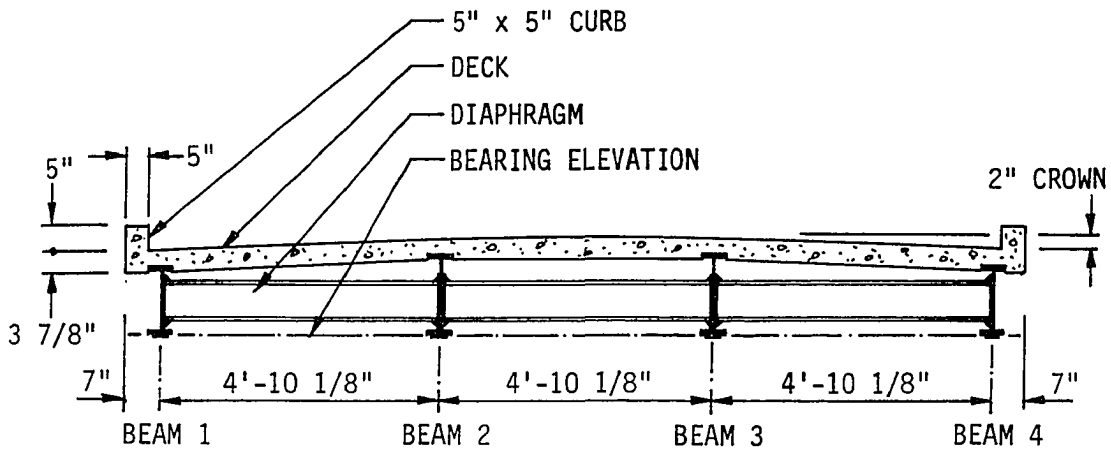
3.1. Bridge Descriptions

The finite element model developed in the next section was verified with three bridges: the model bridge, a right-angle highway bridge, and a 45-degree skewed highway bridge. Throughout this chapter and subsequent chapters, the right-angle highway bridge will be referred to as Bridge 1, and the 45-degree skewed bridge will be referred to as Bridge 2. The prototype highway bridge on which the model bridge was patterned is a composite bridge in Appanoose County, Iowa. Bridge 1 and the Appanoose County bridge have identical superstructures.

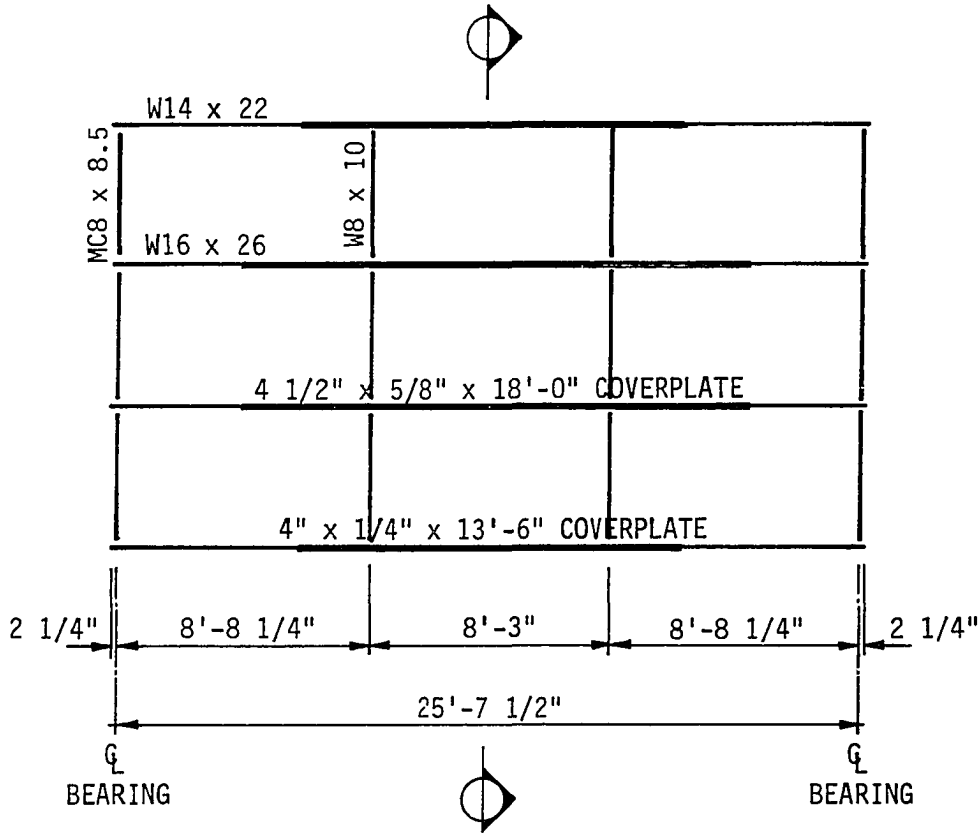
3.1.1. Model bridge

The cross section and framing plan for the model bridge are given in Figure 19. All plan dimensions, deck thickness, and curb depth were set at half the prototype dimensions. The curb cross section for the model was modified to 5 inches by 5 inches for ease of forming. Reinforcing bar diameters were selected to be half those of the prototype, and were placed at half the dimensions given on the plans for the prototype.

Because the choice of steel sections was limited to those available in 1980, model beam and diaphragm sections were selected to most nearly match half-size prototype sections. Beam coverplate cross section dimensions for the model were varied slightly from half-size, in order



a. Cross section at midspan



b. Framing plan

FIGURE 19. Model bridge

to make use of steel plate in commonly available thicknesses. In general, the properties of the steel members for the model agreed within 10% of the desired scale properties computed from the prototype. Material properties for the model curb, deck, and beams are given in Tables 1 and 2. Because the deck concrete mixture contained only small aggregate, it was more susceptible to shrinkage than normal structural concrete. Quite possibly the shrinkage caused cracking in the deck, which increased the flexibility of the bridge model.

Other construction details of the prototype were replicated as nearly as possible to half scale. Angle-plus-bar shear connectors and bearing stiffeners were accurately replicated. Approximately correct camber of model bridge beams resulted from the continuous coverplate welds. Diaphragm connections were modified somewhat from the prototype, primarily to accommodate 1/2-inch diameter bolts rather than half-scale 3/8-inch diameter bolts.

Post-tensioning brackets had to be enlarged beyond half size because of the diameter of the hollow-core cylinders used for the post-tensioning in the laboratory. The enlarged brackets reduced post-tensioning moments slightly, but the reduction was partially offset by the slightly oversized beam depths. Further details of the model bridge are given in Reference 55.

Abutments, hinge supports, and roller supports were constructed so as not to cause rotational or longitudinal restraint of the model bridge beams. Because of the scale of the model bridge, dead load stresses in

the steel beams were only half those of the prototype bridge. In order to more correctly model the dead load stresses, and in order to prevent uplift of beam ends, the composite bridge model was weighted with sandbags. The sandbag weight caused tensile dead load stresses in the steel beams comparable with those in the prototype. The sandbag weight also, however, caused small compressive stresses in the concrete deck which do not exist in the prototype, since there is no equivalent load applied to the prototype composite bridge.

Preliminary computations showed that the prototype bridge would require post-tensioning forces of 80 kips per exterior beam. Therefore, model beams, by principles of similitude, required forces of 20 kips. In some tests, the forces were increased to 40 kips to check the response of the model to excessive post-tensioning.

The laboratory testing of the model bridge was extensive. The model was tested with or without diaphragms and with or without curbs. The model was subjected to vertical loads, post-tensioning, and combinations of vertical loads and post-tensioning. Further details of the testing program, instrumentation utilized on the model bridge, and test results are given in Reference 55.

3.1.2. Bridge 1

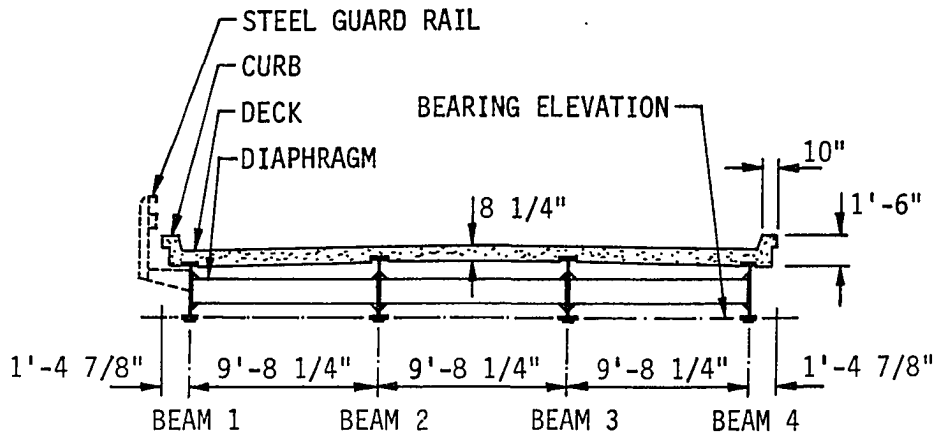
Bridge 1, for which copies of design plans are given in Figure 1, is located in Dickinson County, Iowa, on the secondary road system, 2.2 miles north of Terril on county road N14. It is a four-beam, right-angle bridge with a nominal width of 30 feet and a nominal span of 50

feet. Figure 20 gives the cross section and framing plan with actual dimensions for the bridge. The cross section at midspan in Figure 20a illustrates the deck crown, the curb configuration, and the steel guard rail.

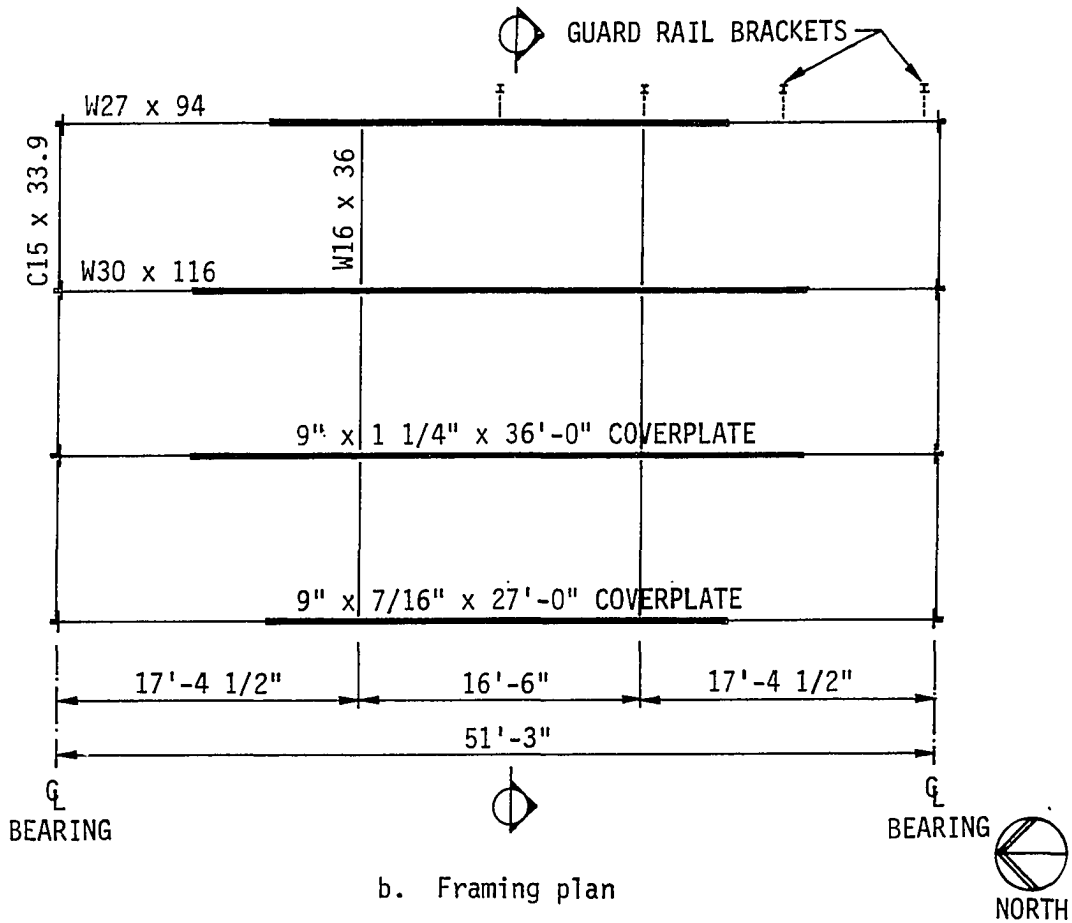
The condition of the deck on Bridge 1 was excellent; tests of three cores taken from the deck gave an average concrete compressive strength of 7140 psi. The steel frame of Bridge 1 needed painting in 1982 but was not severely corroded. Frame members were assumed to be of A7 steel, with a yield point of 33 ksi. In order to bring the shear connector capacity up to current ultimate strength standards, 26 high strength bolt connectors were added to each exterior beam by the method described in Reference 54.

Bridge 1 was instrumented, post-tensioned, and tested in both 1982 and 1984. In 1982, the strains and deflections for the following loading conditions were measured and recorded: an overloaded truck (60.54 kips) at various predetermined positions, post-tensioning of the exterior beams (182.0 kips, average per exterior beam), and the same truck in the same predetermined positions on the post-tensioned bridge. Details of the testing program are given in Reference 54.

In 1984, the testing program was more extensive. Strains and deflections were measured and recorded for an overloaded truck (63.98 kips) at predetermined positions on the post-tensioned bridge, removal of post-tensioning (172.0 kips per exterior beam), the same overloaded truck on the bridge, re-application of post-tensioning (196.8 kips per



a. Cross section at midspan



b. Framing plan

FIGURE 20. Bridge 1

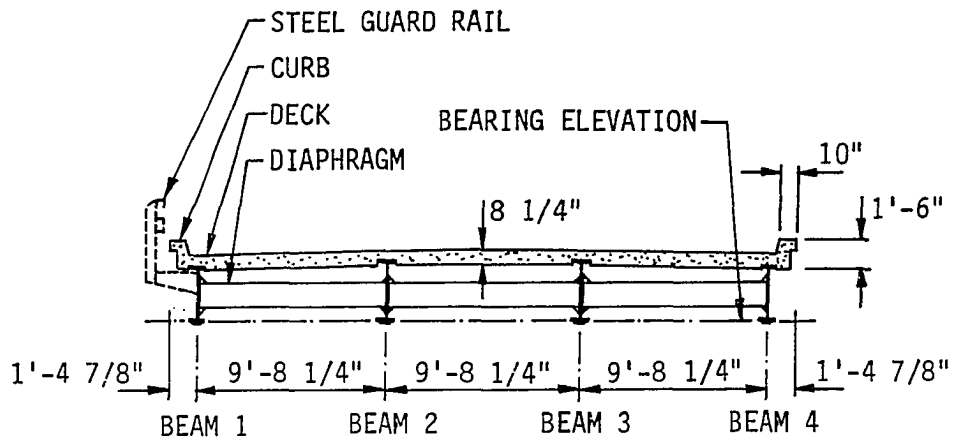
exterior beam), and the same truck on the post-tensioned bridge. Test details and results are given in Reference 28.

3.1.3. Bridge 2

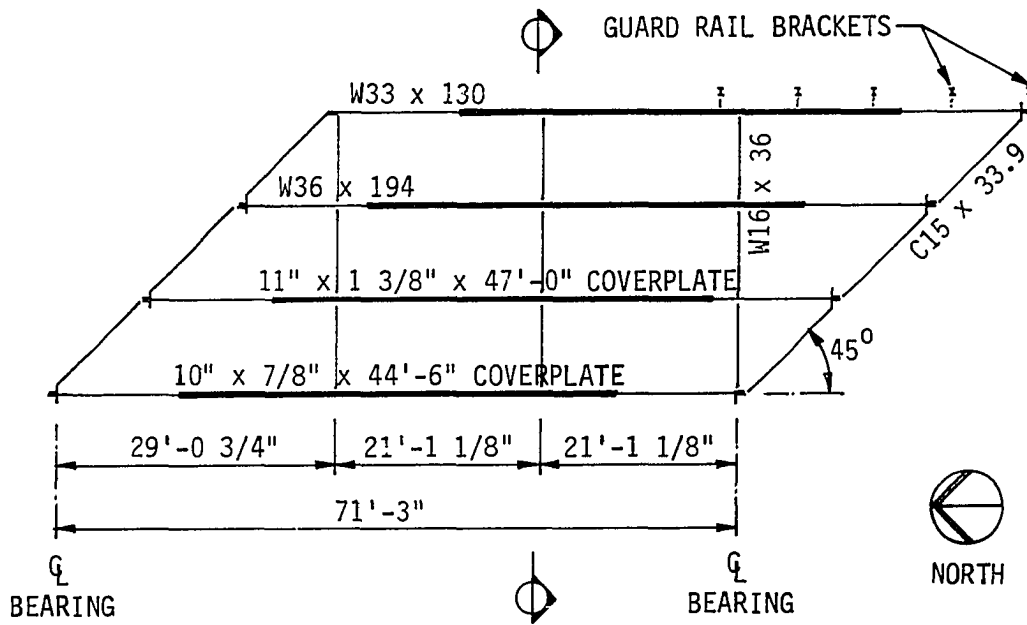
Bridge 2 is on the primary highway system, in Greene County on Iowa 144, a few yards south of the Greene-Webster County line. The bridge is a four-beam, 45-degree skewed bridge with a nominal width of 30 feet and a nominal span of 70 feet. The cross section given in Figure 21a is identical to the cross section for Bridge 1. The steel frame configuration and actual dimensions are shown in Figure 21b. The deck surface on Bridge 2, prior to the 1982 testing, was badly spalled, and a few reinforcing bars were exposed. The average concrete compressive strength obtained from six deck cores was 6430 psi. After the bridge was post-tensioned in the summer of 1982, the deck and curbs were extensively repaired during the summer of 1983. Portions of the deck and curbs were removed and replaced prior to the retesting of the bridge in 1984.

The steel frame for Bridge 2 had been repainted prior to 1982, and the frame was in excellent condition. As for Bridge 1, the frame was assumed to be of A7 steel. Shear connector capacity was increased by adding 28 high strength bolt connectors to each exterior beam and 26 high strength bolt connectors to each interior beam, as documented in Reference 54.

The testing and post-tensioning procedures for Bridge 2 were similar to those for Bridge 1. In 1982, the bridge was instrumented and



a. Cross section at midspan



b. Framing plan

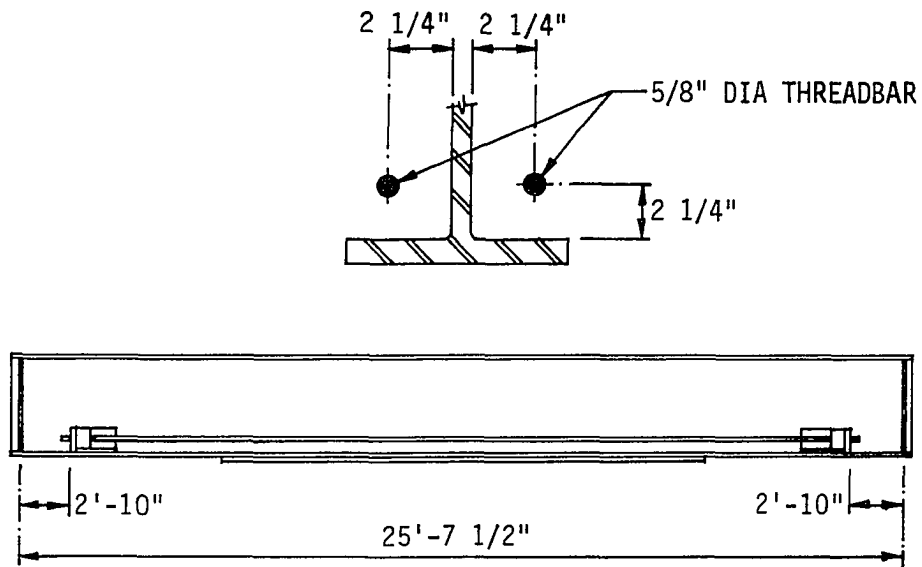
FIGURE 21. Bridge 2

its response measured and recorded for an overloaded truck (60.50 kips) at predetermined locations, post-tensioning (305.6 kips, average per exterior beam), and the same truck at the same locations. In 1984, the bridge was again tested for an overloaded truck (61.18 kips) on the post-tensioned bridge, removal of post-tensioning (271.5 kips per exterior beam), the same truck on the bridge, re-application of post-tensioning (371.2 kips per exterior beam), and the same truck on the post-tensioned bridge. Test details and results are given in References 54 and 28.

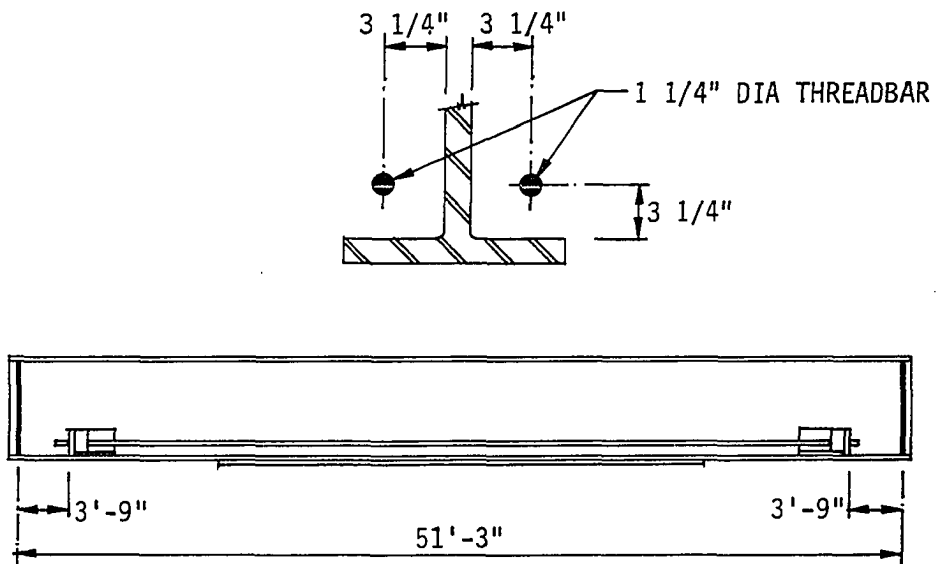
3.1.4. Post-tensioning details

Details of the post-tensioning for all three bridges are given in Figure 22. In all cases tendons are Dywidag high strength steel threadbars. The nominal ultimate tensile strength for the 5/8-inch diameter bars for the model bridge tendons is 157 ksi, and the nominal ultimate tensile strength for the 1-inch and 1 1/4-inch diameter bars for Bridge 1 and 2 tendons is 150 ksi. Final tendon forces in all cases were less than 60% of ultimate forces, as recommended by the tendon manufacturer.

The tendons for the model bridge, as shown in Figure 22a, were placed 2 1/4 inches from the exterior beam web and flange in order to allow clearance for the hollow-core jacking cylinder. The 3 1/4-inch dimensions given in Figure 22b for Bridge 1 and in Figure 22c for Bridge 2 are also for jacking cylinder clearance.

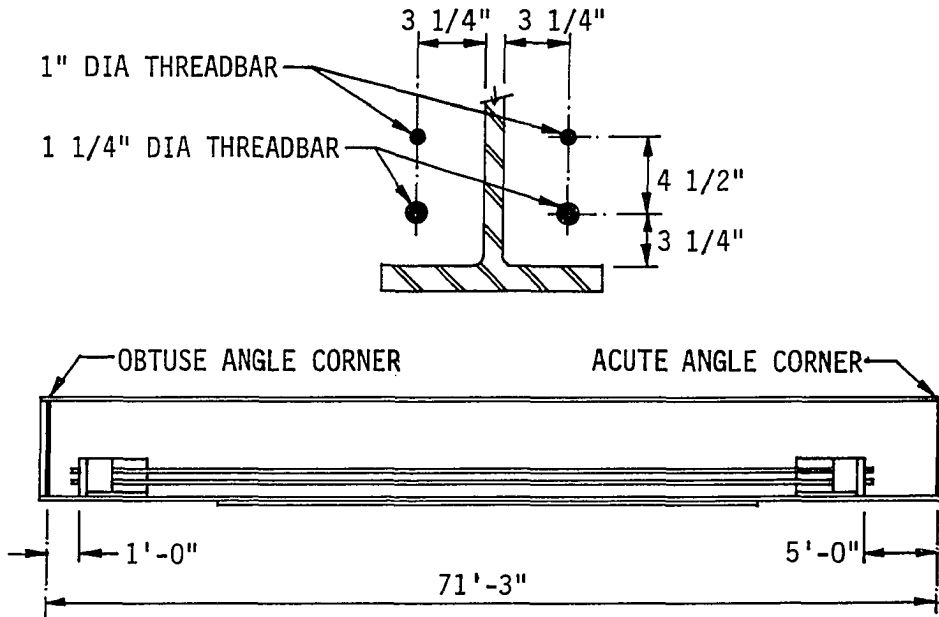


a. Tendon location for model bridge



b. Tendon location for Bridge 1

FIGURE 22. Post-tensioning details



c. Tendon location for Bridge 2

FIGURE 22 (Continued)

Because the design methodology presented in Chapter 5 was not available during early stages of this research, post-tensioning forces for all bridges were approximated by means of orthotropic plate theory. Post-tensioning of the model bridge and Bridge 1 required only two tendons per exterior beam, but the post-tensioning for Bridge 2 required four tendons per exterior beam. The four tendons for Bridge 2 were arranged in a group with the larger tendons at the bottom, as shown in Figure 22c, in order to maximize the moment effect of the post-tensioning.

The anchorage brackets for the tendons were located on the span so as to provide post-tensioning at midspan and also at coverplate cutoffs. The brackets were placed far enough from midspan so that the bolt holes for attachment of the brackets would not cause overstress of the bottom flanges of the exterior beams. Jacking clearance also was considered when planning the bracket locations. For each exterior beam in Bridge 2, one bracket was arbitrarily placed as close to the support as possible at the obtuse corner of the bridge deck. The post-tensioning then could counteract vertical loads shifted toward that corner as a result of the skew of the bridge.

3.2. Elastic Finite Element Model

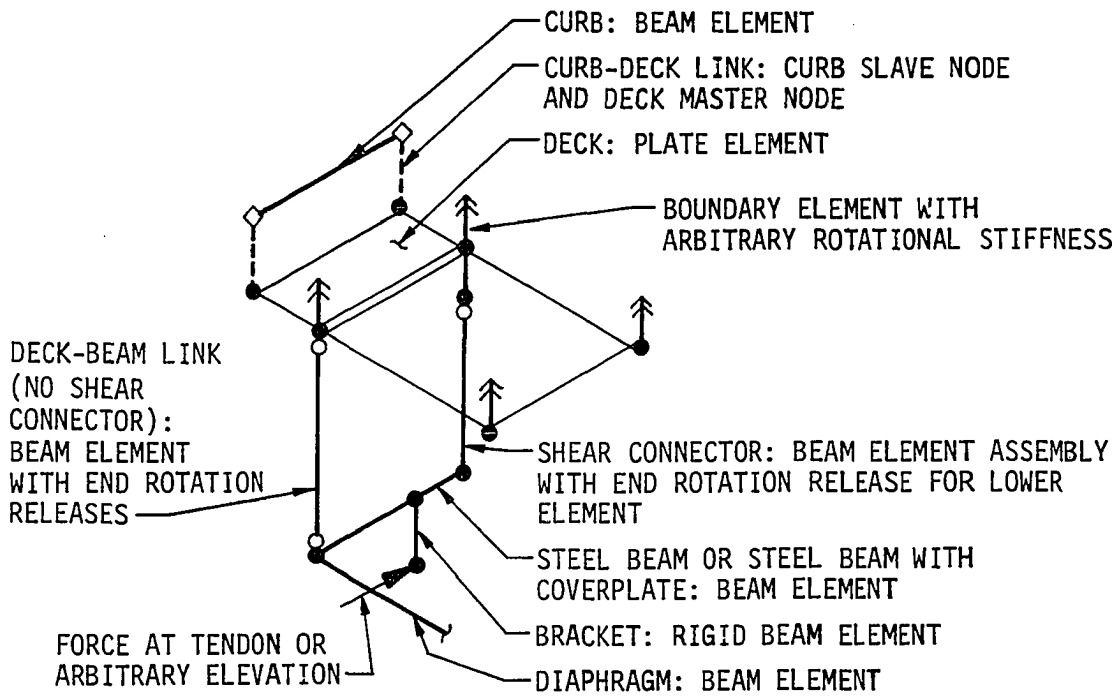
3.2.1. Model development

For the initial finite element model of a composite bridge, Model D, developed in Section 2.3.2, was adapted to each bridge beam, and the

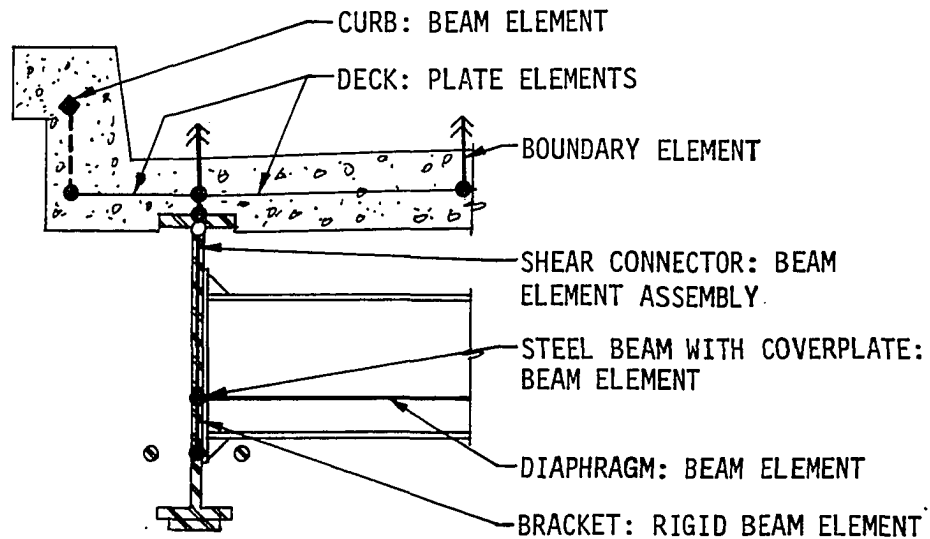
individual beams were joined to form the bridge. The concrete bridge deck was modeled with approximately square plate elements, the steel beams were modeled with beam elements including shear deflection, and the shear connectors were modeled with beam element assemblies as illustrated in Figure 23.

Because the concrete deck in the typical Iowa composite bridge has a crown of approximately 3 inches, and because the crown can change the effect of the post-tensioning, the crown was included in the finite element model for the bridge. The crown increases the eccentricity of the tendons and thus the moment effect as shown in Figure 24a. Because of the crown, it was necessary to add boundary elements for deck nodes at which sloped plate elements were joined. Without the boundary elements with small rotational stiffnesses, there would be numerical difficulties during analysis because the SAP IV plate and shell element has an undefined rotational stiffness perpendicular to its surface. The amount of reinforcing in the deck is quite small and, therefore, it was neglected in determining the properties for the deck plate elements.

Curbs were not included in the composite beam model developed earlier but are part of the typical Iowa composite bridge. Since there is very little opportunity for the curb to slip with respect to the deck, the curbs were modeled as beam elements with shear deflections and linked to the edge of the deck with the SAP IV slave-master node option as shown in Figure 23a. The position of the curb with respect to the exterior beam required that a row of rectangular deck plate elements be placed along the edge of the bridge.

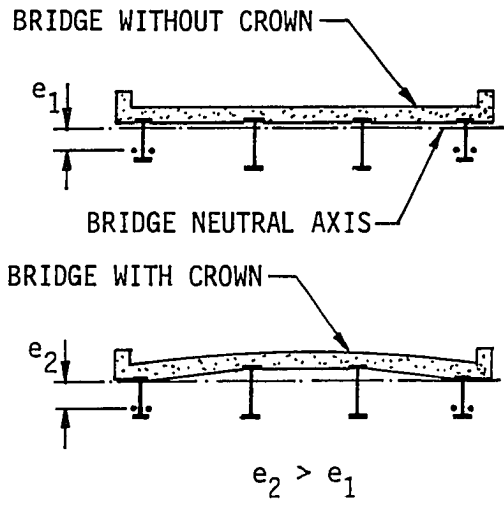


a. Isometric view



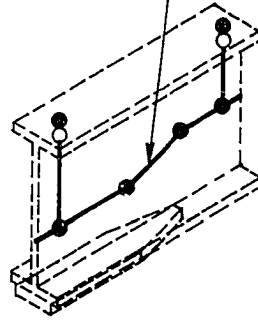
b. Section through exterior bridge beam

FIGURE 23. SAP IV finite element model for post-tensioned composite bridge beam



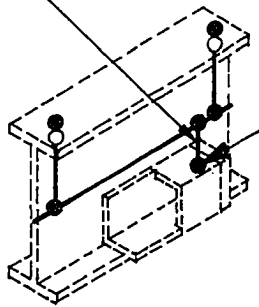
a. Bridge crown

SLOPED BEAM ELEMENT TO REPRESENT TAPERED COVERPLATE

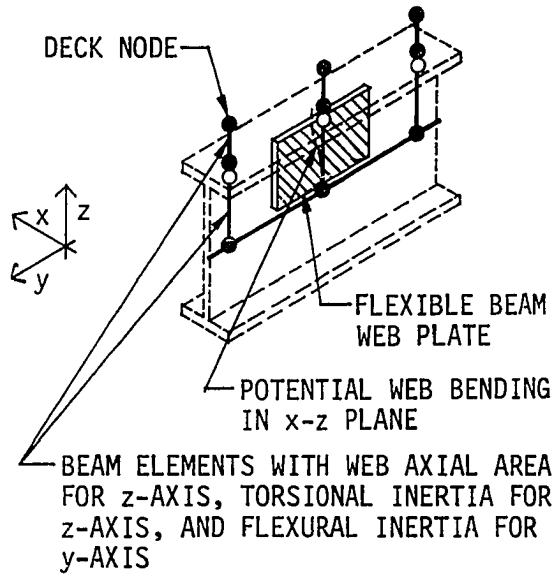


b. Beam coverplate taper

RIGID BEAM ELEMENT LOCATED AT BEARING FACE OF BRACKET PLATE



c. Tendon anchorage



d. Beam web

FIGURE 24. SAP IV bridge model details

Diaphragms also were not included in the composite beams model but are part of the steel frame for most Iowa composite bridges. Because the diaphragms generally are steel wide flange or channel shapes, they can be accurately modeled by beam elements with shear deflections. Interior diaphragms usually are detailed with rigid connections to beam webs but, due to the web flexibility, the connections are less than perfectly rigid. For the finite element model, the connections were taken to be rigid, and the diaphragms were moved to the elevations of the bridge beam elements. There is then some modeling error in the rigidity of the connection and the slight change in elevation, which is usually 3 inches or less.

In Model D, the change in section from beam to coverplated beam was modeled as a change in cross section, with a short, vertical rigid beam element making the step in vertical elevation. In order to correct for the typical tapered coverplate end, a sloped beam element was used for the transition as shown in Figure 24b. The sloped element was given the average properties of the beam and coverplated beam.

For modeling the post-tensioning bracket, the short, rigid beam element could be placed either at the center of the bracket, where the bracket transfers the post-tensioning to the beam, or at the anchorage, where the tendon transfers its force to the bracket. As indicated in Figure 24c, the beam element was placed at the anchorage location.

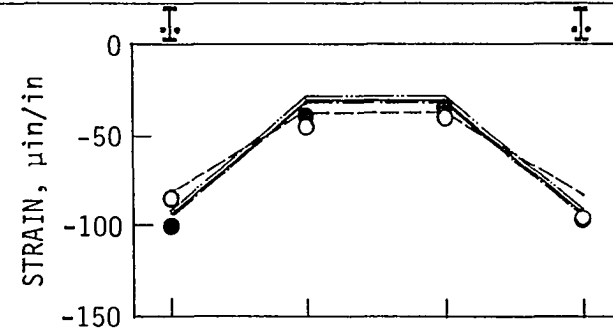
Based on the recommendation of Johnson [51], the shear connector assemblies were given the stiffness computed from the force and slip at

one-half the ultimate shear connector capacity in a push-out test. As in Model D, the shear connector stiffnesses were moved to the nearest connector assembly in the finite element model. Shear connector assemblies which had no assigned stiffness were disconnected by means of end releases as illustrated in Figure 23a.

Initially, the lateral rigidity of the shear connector assemblies was set at an arbitrarily large value. The stiff connector assemblies, however, did not recognize the flexibility of the steel beam web. That flexibility is indicated in Figure 24d. When the SAP IV model for the post-tensioned model bridge with curbs and diaphragms was analyzed, the computed exterior beam coverplate strains and deflections were 15% to 25% less than the corresponding test values. The test values and finite element values given in the first three lines of Tables 9 and 10 can be compared directly. When the beam web stiffness was included in the finite element model, the analysis results were generally within 5% to 10% of the test results, as a comparison of the first, second, and fourth lines in the tables will show.

Two other comparisons can be made from the results given in Tables 9 and 10. In order to check the accuracy of the finite element model, the size of the deck plate elements was reduced from 15 inches to 10 inches. The maximum difference between two comparable analyses was less than 1%, which would indicate that the 15-inch deck mesh was fine enough for accurate analysis. Also, based on the convergence tests given in Figure 10, it can be inferred that the 15-inch mesh will give accuracy within 10% for a bridge skewed no more than 45 degrees.

TABLE 9. Experimental and computed midspan coverplate strains for post-tensioned model bridge
 -- elastic finite element model



TEST	SAP IV	CROWN	BEAM WEB	DECK ELEMENT SIZE, in	SYMBOL	BEAM 1 ϵ $\mu\text{in/in}$	BEAM 2 ϵ $\mu\text{in/in}$	BEAM 3 ϵ $\mu\text{in/in}$	BEAM 4 ϵ $\mu\text{in/in}$
Intermediate ^a	-	yes	flexible	-	●	-101	-40	-36	-99
Final ^b	-	yes	flexible	-	○	-85	-45	-41	-98
-	yes	yes	rigid	15	-----	-82	-37	-37	-82
-	yes	yes	flexible	15	—————	-93	-31	-31	-93
-	yes	yes	flexible	10	-----	-93	-31	-31	-93
-	yes	no	flexible	15	-----	-89	-29	-29	-89

^aFor this test, post-tensioning forces were increased in approximately 2.5 kip stages to 10 kips per tendon and beyond. Strains in the table are for 10 kips per tendon or 20 kips per beam.

^bFor this test, post-tensioning forces were increased rapidly to 10 kips per tendon.

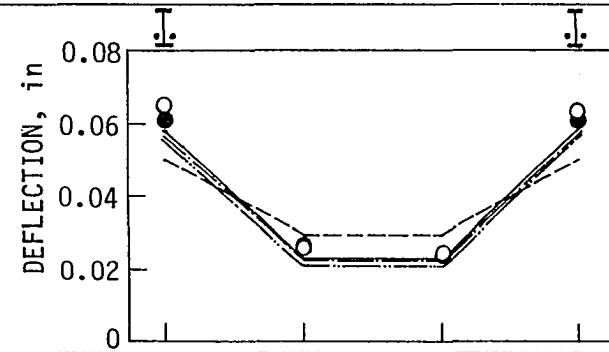
The sixth line in the tables, for an analysis without deck crown, shows that neglecting the crown will reduce the computed midspan strains and deflections by 5% to 10%. For best accuracy, then, the crown should be included in the finite element model.

Although the finite element bridge model permits adjustment for the points of application of post-tensioning forces, it does not adapt easily for vertical loads placed on the deck at arbitrary locations. For that reason it is desirable to have some means of computing equivalent nodal loads. The tributary area method illustrated in Figure 25 is a method recommended by Davis for such situations [25]. Because the tributary area method considers only nodal forces and not also nodal moments, the method is only approximate. The vertical loads applied to the model bridge and truck tire loads are actually patch loads applied over some finite area and, therefore, the tributary area method is accurate enough for purposes of this research, which is not concerned with local stress concentrations.

3.2.2. Quarter symmetry model

For symmetrical, right-angle bridges and for symmetrical loading conditions such as post-tensioning of exterior beams, the entire bridge need not be modeled. Only one-quarter of the bridge, with correct rotational and translational boundary conditions at midspan and bridge centerline, is required for finite element analysis. Quarter symmetry reduces bandwidth and analysis cost considerably and, therefore, a quarter symmetry finite element model was used for the post-tensioning distribution analyses described in Chapter 4.

TABLE 10. Experimental and computed midspan deflections for post-tensioned model bridge
 -- elastic finite element model



TEST	SAP IV	CROWN	BEAM WEB	DECK ELEMENT SIZE, in	SYMBOL	BEAM 1 δ in	BEAM 2 δ in	BEAM 3 δ in	BEAM 4 δ in
Intermediate ^a	-	yes	flexible	-	●	0.0611	0.0266	0.0237	0.0611
Final ^b	-	yes	flexible	-	○	0.0654	0.0261	0.0243	0.0635
-	yes	yes	rigid	15	-----	0.0492	0.0288	0.0288	0.0492
-	yes	yes	flexible	15	—————	0.0582	0.0231	0.0231	0.0582
-	yes	yes	flexible	10	-----	0.0578	0.0231	0.0231	0.0578
-	yes	no	flexible	15	-----	0.0563	0.0207	0.0207	0.0563

^aFor this test, post-tensioning forces were increased in approximately 2.5 kip stages to 10 kips per tendon and beyond. Strains in the table are for 10 kips per tendon or 20 kips per beam.

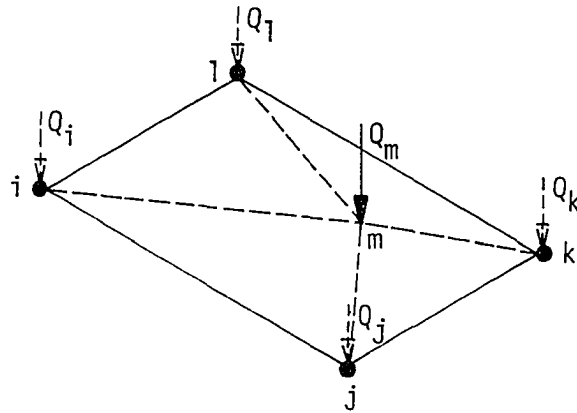
^bFor this test, post-tensioning forces were increased rapidly to 10 kips per tendon.

A quarter symmetry finite element model for Bridge 1 is illustrated in Figure 26. Deck elements in the figure are drawn with an arbitrarily reduced size so that they may be distinguished from beam elements. The deck plate elements are approximately 30 inches square and give accuracy comparable to that for the 15-inch square elements used for the model bridge. The change in elevation for bridge beam elements representing steel beams with and without coverplates, and the sloped beam elements for the tapered coverplate ends are clearly visible in the figure. Extra rows of nodes, off the bridge near the abutment and the curb, provide for the correct orientation of deck node boundary elements and of beam and diaphragm elements. Although not very obvious in the figure, the deck between the exterior and interior beams is sloped in order to simulate the deck crown.

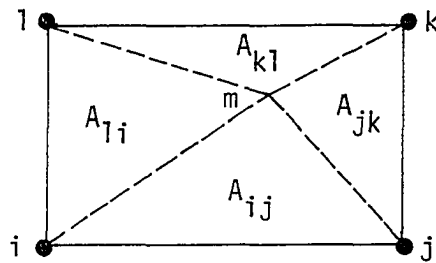
The quarter symmetry SAP IV model for Bridge 1 contains more than 170 nodes and more than 210 elements. For accuracy and convenience in constructing such a complex model, a preprocessing program was written which takes the basic bridge data, such as beam spacing, and generates the SAP IV model with correct boundary conditions. Provisions in the preprocessing program do allow for the addition of unique features such as guard rails and beam end restraints.

3.2.3. Complete model

The quarter symmetry model cannot be applied to skewed bridges or to right-angle bridges with unsymmetrical loads. For those analysis conditions, the finite element model must be complete. An example of a



a. Loaded deck plate element



$$Q_i = \frac{A_{kl}}{(A_{kl} + A_{ij})} \cdot \frac{A_{jk}}{(A_{jk} + A_{li})} Q_m$$

b. Equivalent load at node i by tributary area

FIGURE 25. Equivalent nodal loads

NOTE: BOUNDARY ELEMENTS
ARE NOT SHOWN.

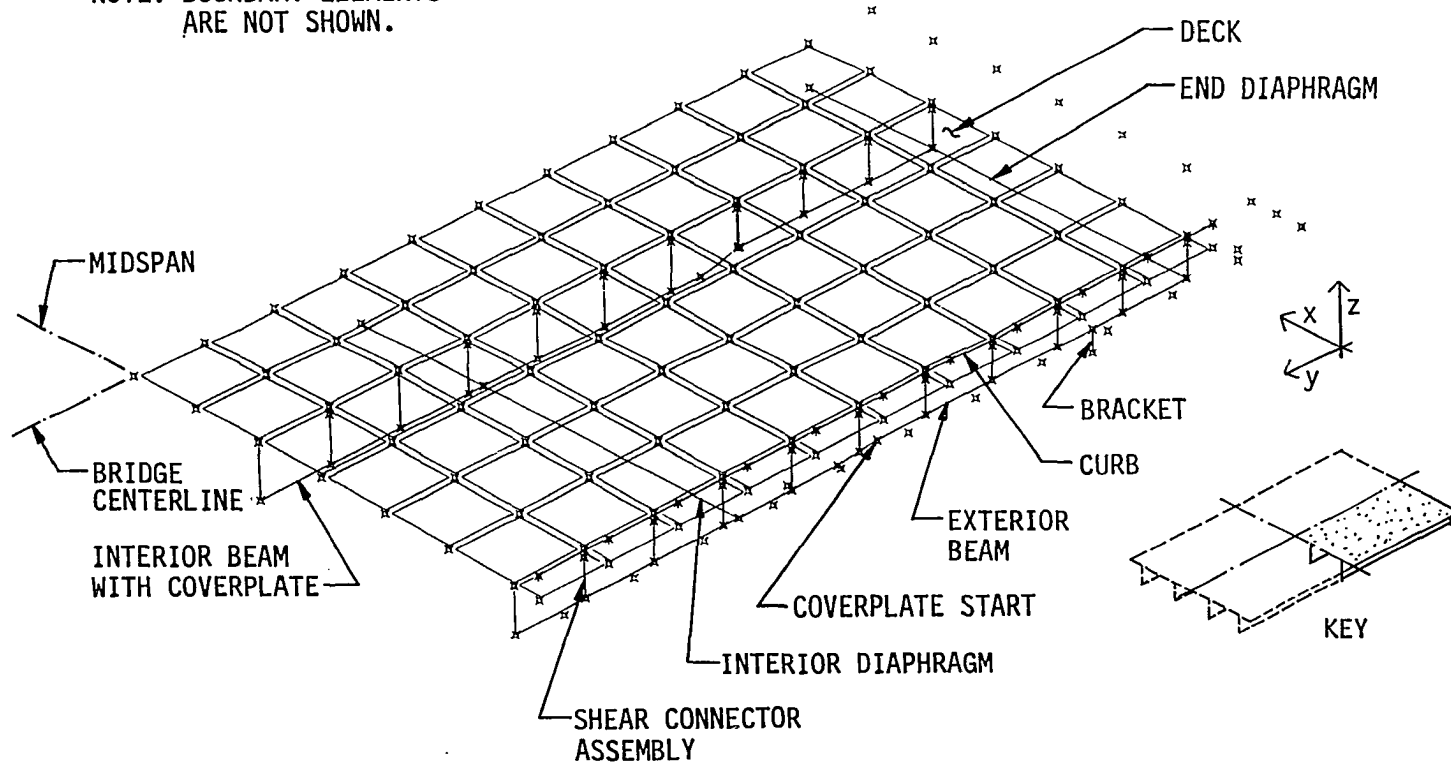


FIGURE 26. SAP IV quarter symmetry model for Bridge 1

complete model for Bridge 2 is given in Figure 27. For the model illustrated, guard rails and end restraints have been added to the basic model most often used for structural analysis. Guard rails and rail brackets have been modeled with beam elements; frictional restraints at beam bearing pads have also been modeled with beam elements.

Although not obvious in the figure, all deck elements are parallelogram-shaped plate elements. Each side of the element is approximately 30 inches in length. Interior diaphragms are perpendicular to bridge beams, although perspective distortion seems to indicate otherwise. The deck is sloped between exterior and interior beams, and is level between interior beams, in order to simulate the deck crown.

The complete finite element model is considerably more complex than the quarter symmetry model. A preprocessing program generated the basic model, to which the guard rails and bearing pad restraints were added. Guard rails and interior diaphragms create links between different parts of the finite element model, and thereby increase bandwidth and analysis cost considerably.

3.2.4. Model verification

3.2.4.1. Model bridge In order to verify the finite element model and to determine the behavior of a composite bridge under various loading conditions, computed strains and deflections from the quarter symmetry and complete finite element models were compared with laboratory test results. The comparisons often show noticeable

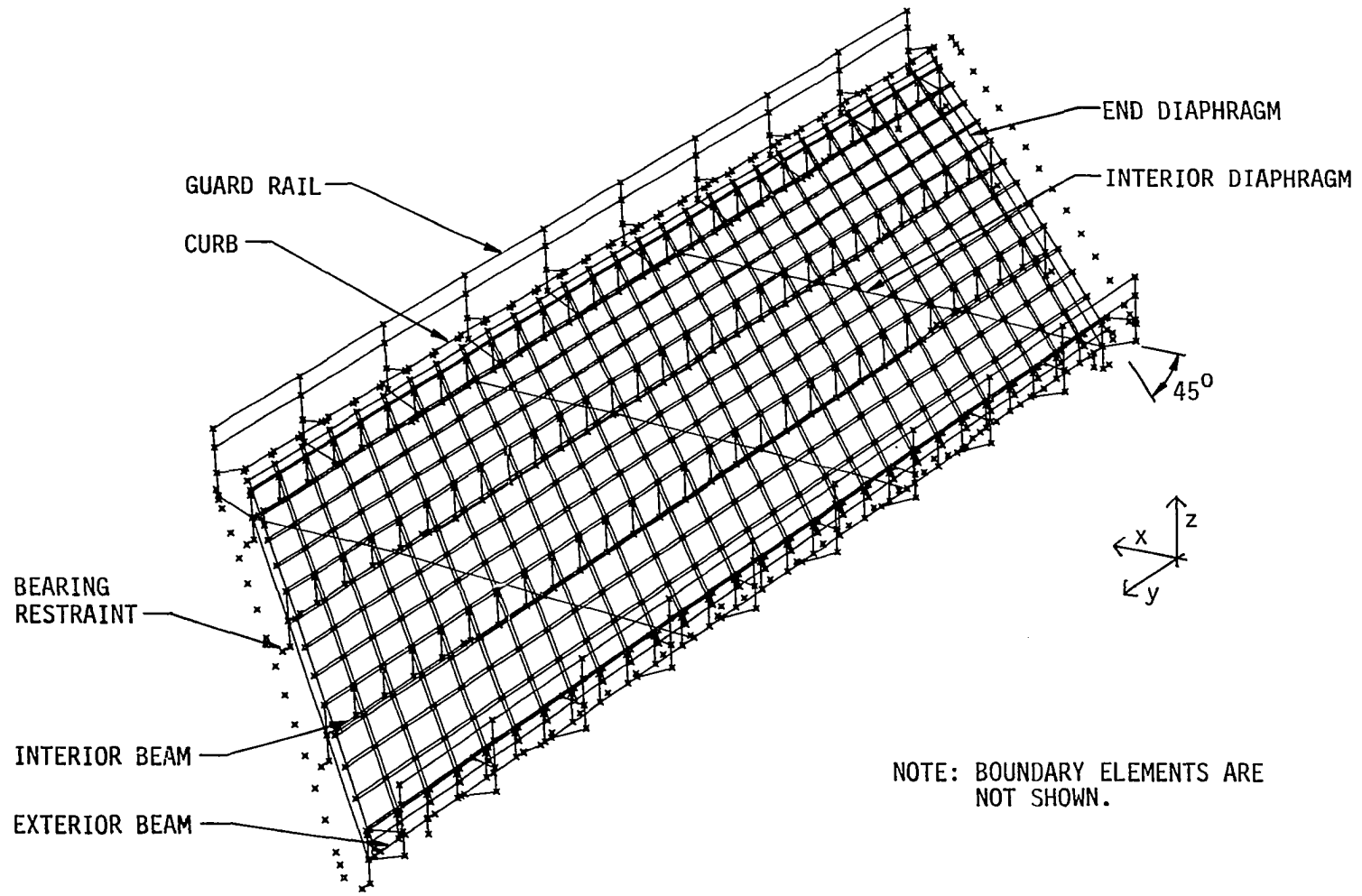


FIGURE 27. SAP IV complete model for Bridge 2

differences between the computed and experimental values. Some of the differences can be attributed to scatter and inaccuracies in the experimental data. Some of the laboratory tests were repeated over a period of several months during the time when shrinkage was taking place in the concrete deck. Repeated testing cracked the concrete deck and quite probably released some of the surface bond between deck and top beam flanges. The data acquisition system which recorded strain gage readings sometimes was subject to drift. For these reasons and minor construction imperfections in the bridge model, there is scatter among the experimental data which generally is limited to 10% but which may be as much as 20% in a few instances.

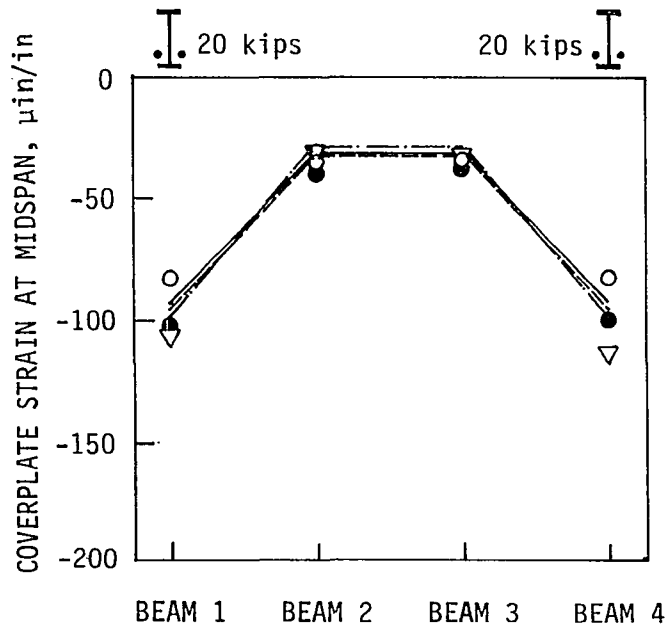
Because of the scatter among the experimental data, the data was averaged for two or more tests when possible. The comparisons between computed and experimental values generally have differences on the same order as the scatter among the experimental data. In most cases, the differences between computed and experimental values are on the same order and in the same direction as those for the composite beam finite element model and laboratory tests. Except as noted otherwise in this section, the comparisons are for the model bridge with curbs and diaphragms, which simulates the prototype bridge.

One of the objectives of the testing program for the model bridge was to test the effects of curbs and diaphragms on the behavior of the bridge. The strains and deflections at midspan in the post-tensioned model bridge, plotted in Figure 28, show minor differences, depending on

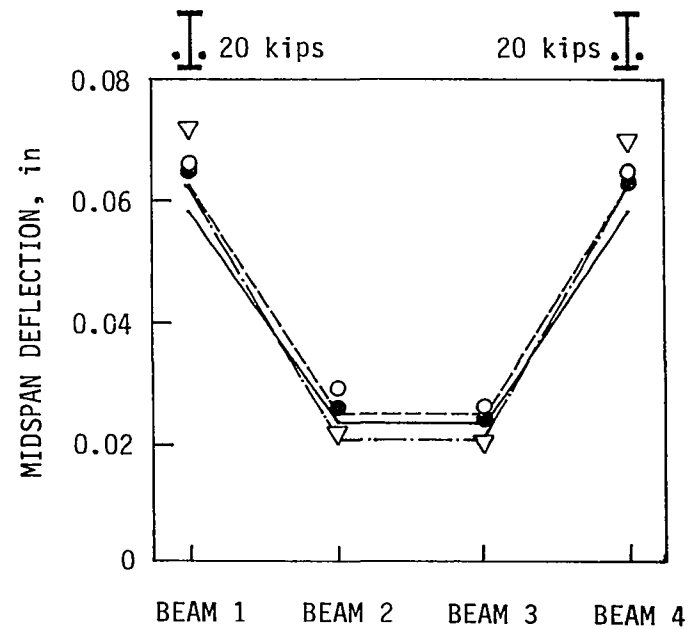
the presence or absence of curbs and diaphragms. Experimental values show more difference than SAP IV-computed values, probably due to the time difference between tests. Curbs were added to the model after approximately six months of testing and after much of the deck shrinkage and cracking had taken place. The test values for diaphragms only, which are from the period before the curbs were added, show smaller strains and deflections for the exterior beams than indicated by the other test values.

The finite element model indicates that addition of both curbs and diaphragms reduces strains and deflections for exterior beams. Because curbs increase the composite beam section moduli for exterior beams, the curbs can be expected to reduce strains. This effect apparently dominates a reverse effect: stiffer beams retain more post-tensioning. Diaphragms increase the transverse stiffness of a bridge, causing it to behave more as a unit and, therefore, they can be expected to reduce strains and deflections for the exterior beams.

In Figure 29, strains and deflections for the post-tensioned model bridge at quarterspan are illustrated. Exterior beam coverplates terminate at approximately the quarterspan points and, consequently, some increase in strain above the midspan strain can be expected, as illustrated in Figure 29a. Another reason for the increase in strain at quarterspan is that the quarterspan points are closer to the tendon anchorages, and the bridge has not distributed as much of the post-tensioning to the interior beams.



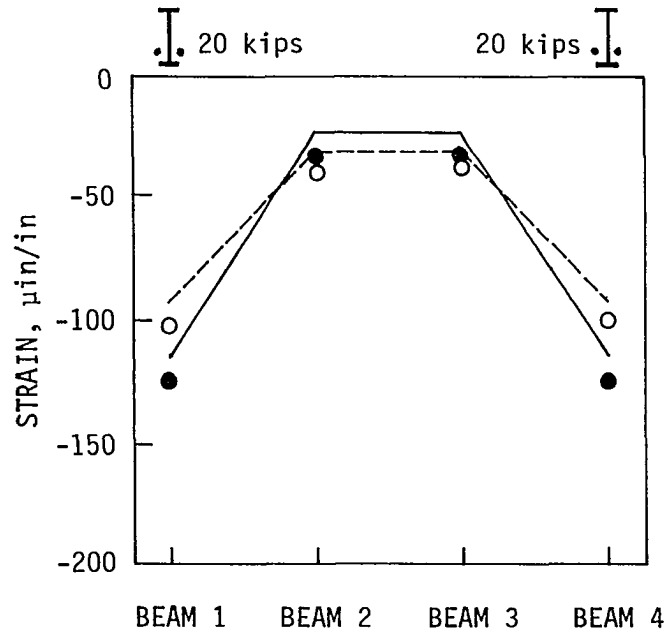
a. Strains



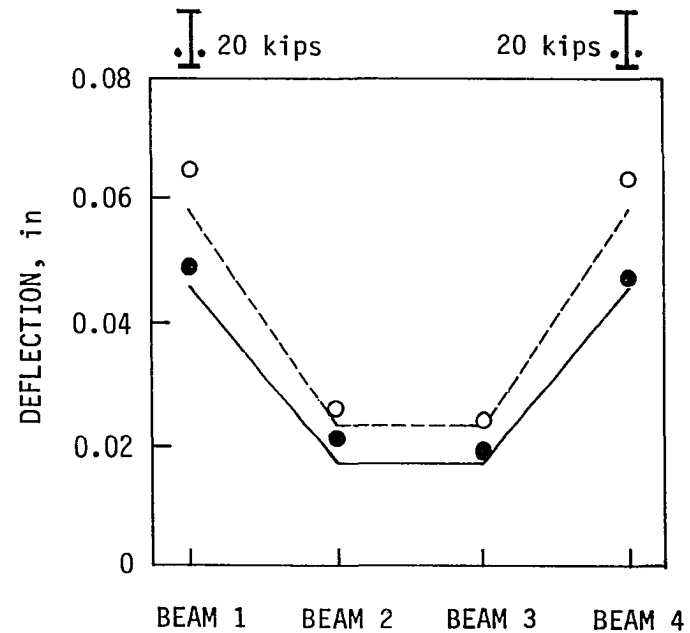
b. Deflections

CONDITION	TEST	SAP IV
WITH CURBS	∇	— — —
WITH DIAPHRAGMS	\circ	- - - - -
WITH CURBS AND DIAPHRAGMS	\bullet	—————

FIGURE 28. Midspan strains and deflections for model bridge with post-tensioned exterior beams



a. Strains



b. Deflections

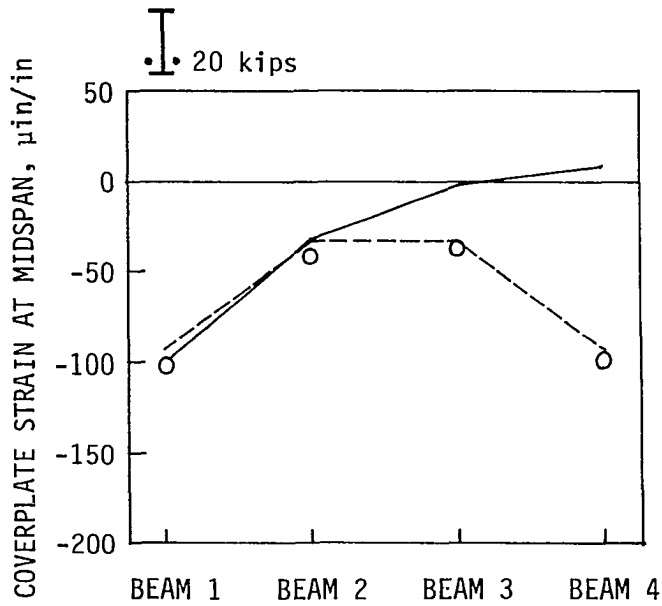
CONDITION	TEST	SAP IV
MIDSPAN	○	----
QUARTERSPAN	●	----

FIGURE 29. Quarterspan strains and deflections for model bridge with post-tensioned exterior beams

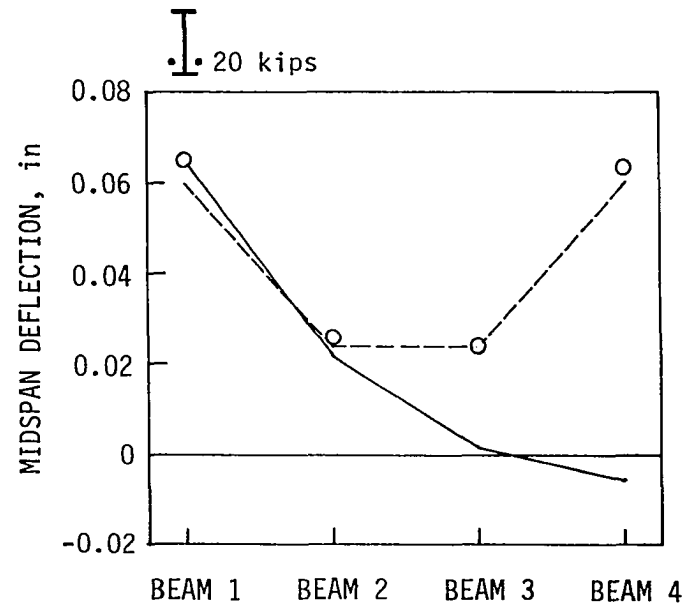
Deflections at quarterspan are less than the deflections at midspan, as shown in Figure 29b. The exterior beam deflections are approximately three times the interior beam deflections at both midspan and quarterspan. The figure also indicates that the finite element model is stiffer than the model bridge, a fact which was noted previously for the composite beams cut from the model bridge.

Occasionally, because of damage or unusual construction, it may be necessary to strengthen only one exterior beam by post-tensioning. Figure 30 illustrates the strain and deflection distributions for that condition. The post-tensioned exterior beam, of course, has the largest compression strain and midspan deflection. Of more importance, however, is the strain and deflection on the far side of the bridge in Beam 4. As shown in Figure 30a, post-tensioning of Beam 1 actually creates a small amount of tension strain in Beam 4, caused by a positive bending moment, in the same direction as for a vertical load. The deflections plotted in Figure 30b indicate that the bridge twists at midspan due to the unsymmetrical post-tensioning. Beam 4, at the far side of the bridge, will actually rise a small amount when Beam 1 is post-tensioned. Unsymmetrical post-tensioning should be used with caution for strengthening a bridge, due to undesirable behavior on the opposite side of the bridge from the post-tensioning.

A deflected shape for the symmetrically post-tensioned model bridge without curbs is given in Figure 31. The shape indicates a doubly curved region near the center of the model bridge. Exterior beams



a. Strains



b. Deflections

CONDITION	TEST	SAP IV
ONE BEAM POST-TENSIONED		—————
TWO BEAMS POST-TENSIONED	○	- - - - -

FIGURE 30. Midspan strains and deflections for model bridge with one post-tensioned exterior beam

deflect upward more than interior beams because of larger negative moments. The larger upward deflections of the exterior beams cause positive moments in the deck and interior diaphragms and, thus, the opposite curvature perpendicular to the span of the bridge.

The response of the model bridge to a concentrated vertical load at midspan of the exterior beam is similar to, but in the opposite direction to, the response of the bridge to post-tensioning of one exterior beam. Figure 32 shows the relatively large strain and deflection for Beam 1, the loaded beam, and the opposite strain and deflection for Beam 4, the beam on the far side of the bridge. Experimental and computed values are in excellent agreement except for the loaded beam. Part or all of the difference at the load is caused by the fact that the finite element model was loaded at a single node, but the model bridge was loaded through a 9-inch square pad.

The midspan strains and deflections in Figure 32 have been plotted for two separate conditions: the loaded model bridge and the loaded, post-tensioned model bridge. There is virtually no difference illustrated for the two conditions -- either in the experimental or in the computed values. For design purposes, therefore, a post-tensioned composite bridge can be assumed to respond the same to vertical load as the same composite bridge without post-tensioning.

A deflected shape for the composite bridge without curbs or post-tensioning is given in Figure 33. The loaded beam deflects more than any other beam and has a slight reverse curvature near the supports caused by the restraining effect of the bridge deck.

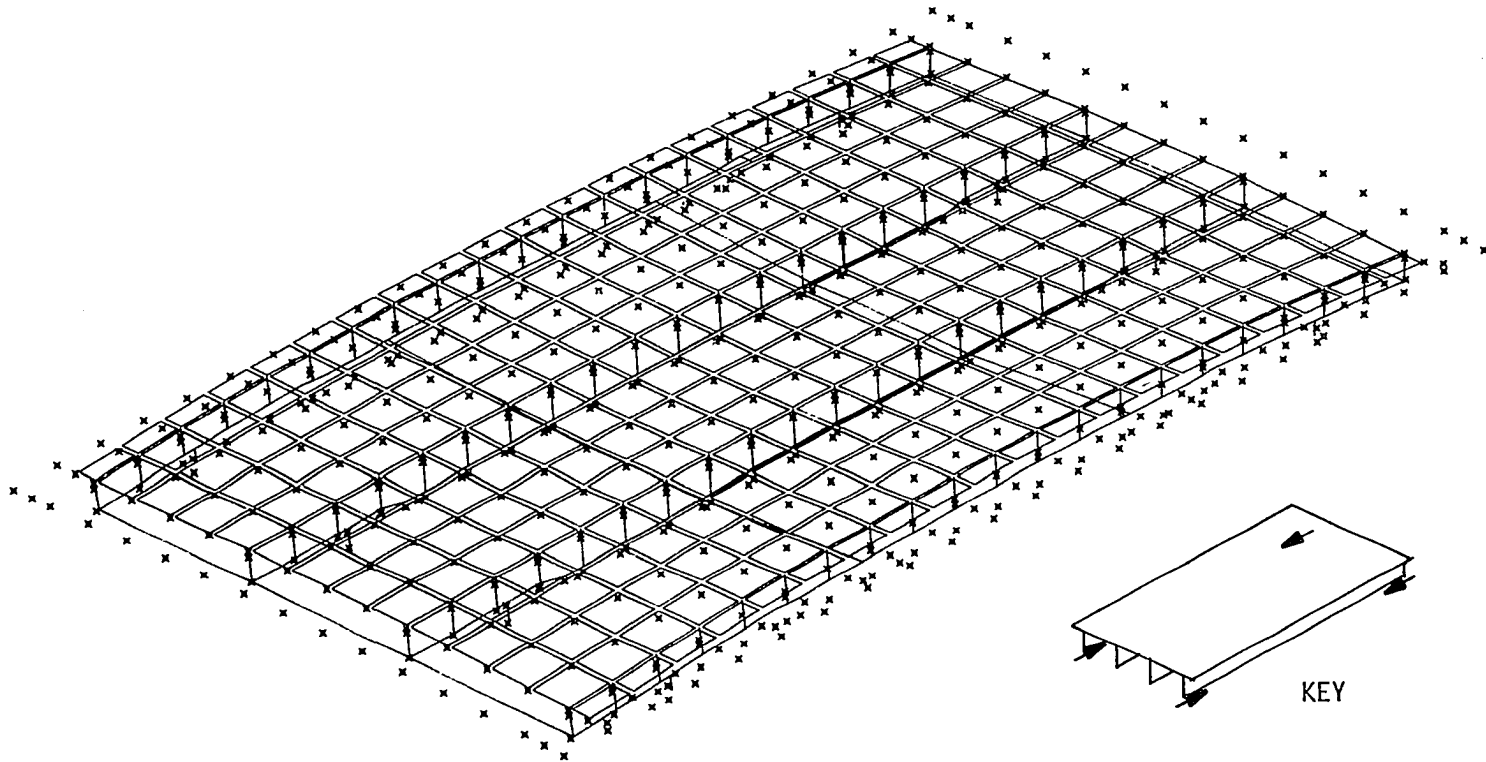
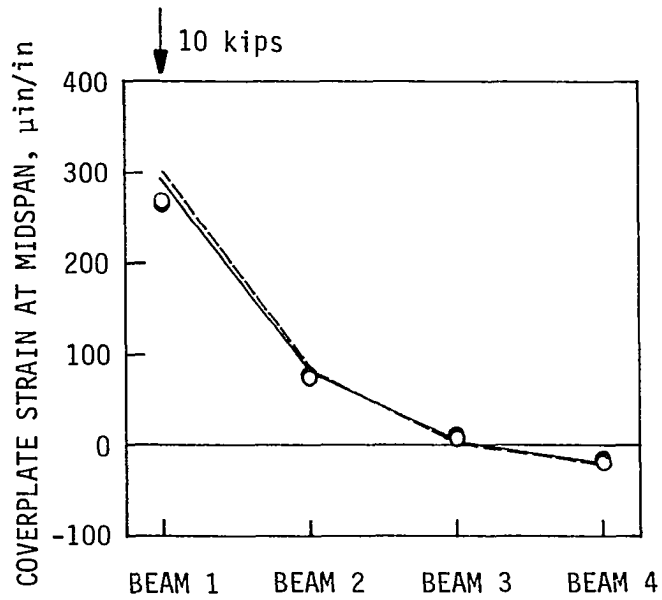
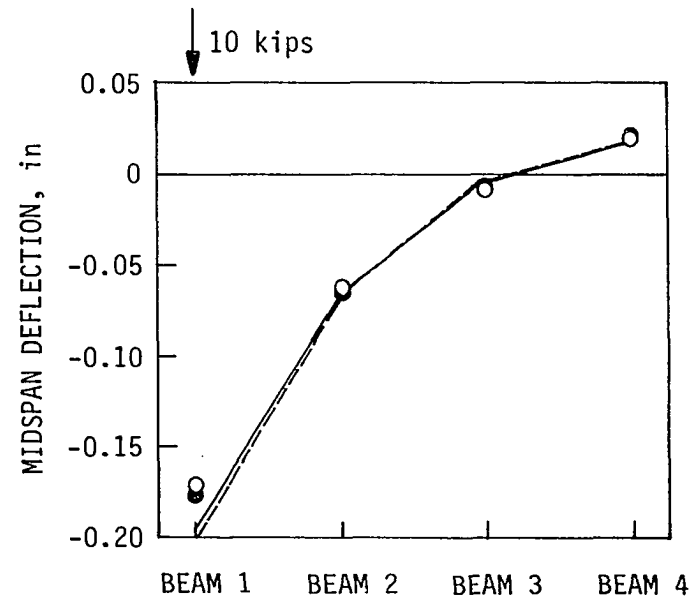


FIGURE 31. Deflected shape for model bridge with post-tensioned exterior beams



a. Strains



b. Deflections

CONDITION	TEST	SAP IV
WITH POST-TENSIONING	●	—
WITHOUT POST-TENSIONING	○	- - -

FIGURE 32. Midspan strains and deflections for model bridge with concentrated load at midspan of exterior beam

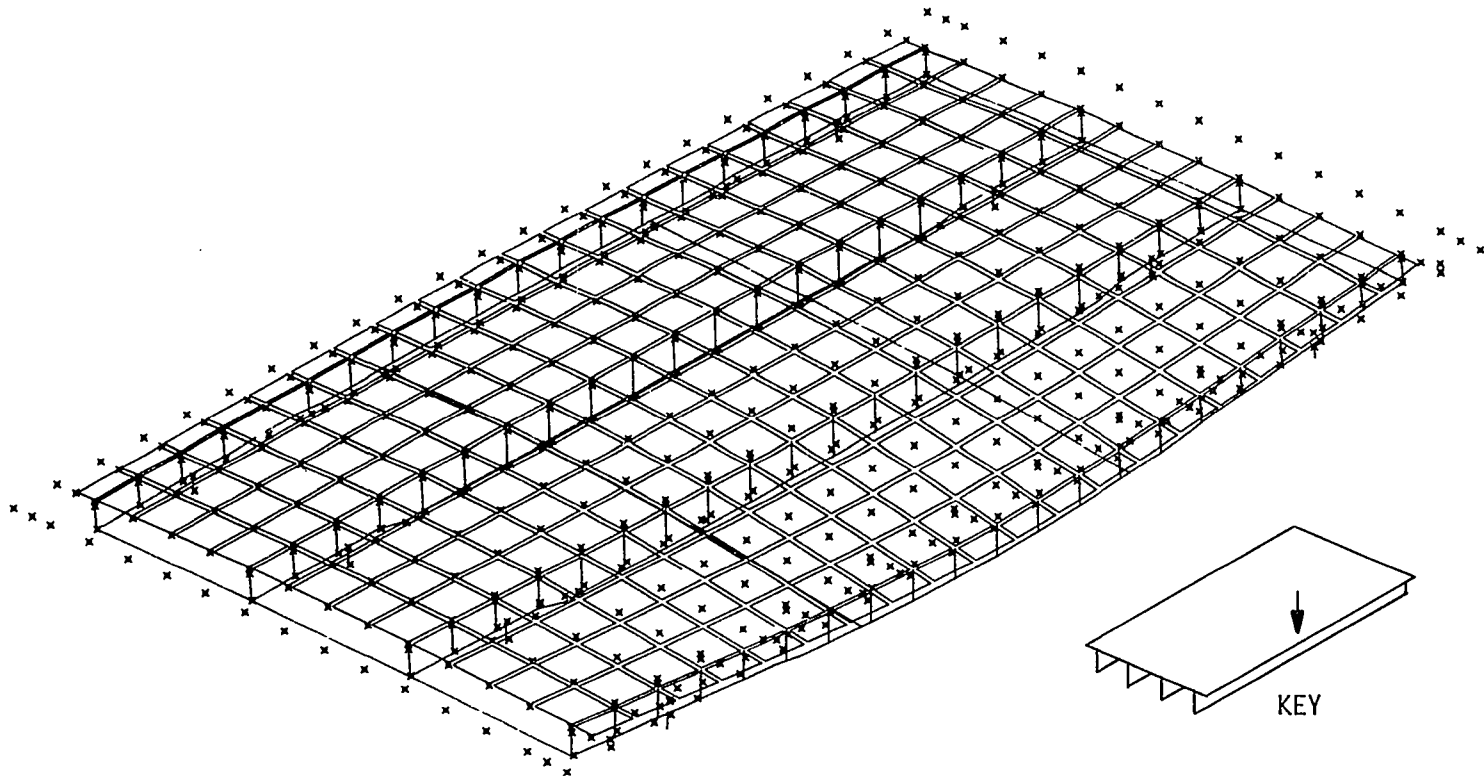
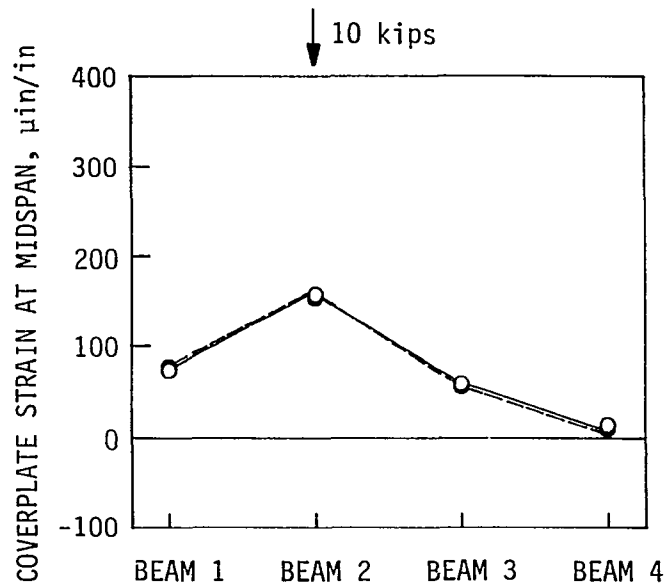


FIGURE 33. Deflected shape for model bridge with concentrated load at midspan of exterior beam

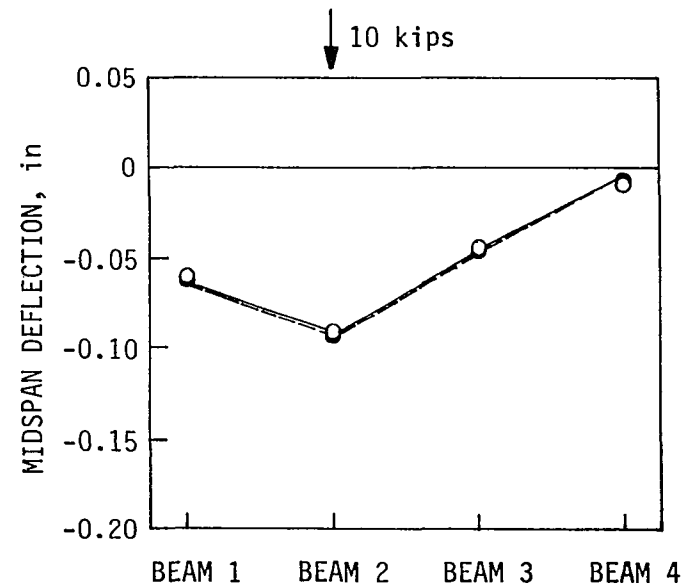
When the 10-kip vertical load is placed at midspan of Beam 2, an interior beam, that beam responds more than any other bridge beam. Because Beam 2 has adjacent beams on each side, its response is not so extreme as when an exterior beam is loaded. The midspan strains and deflections plotted in Figure 34 again indicate that post-tensioning has virtually no effect on the response of the bridge to vertical load.

Although the response of a composite bridge to vertical load is essentially the same before and after post-tensioning, tendon forces do change when vertical load is applied to a post-tensioned bridge. The graph in Figure 35 has the same general shape as the strain and deflection graphs for post-tensioning or vertical load on one exterior beam. When Beam 1, one of the two post-tensioned beams, is loaded, the tendon force increases much more than when Beam 2, the adjacent beam, is loaded. When Beam 4 on the far side of the bridge is loaded, the tendon force in Beam 1 actually decreases slightly. Because the change in tendon force is caused by a load which can be classified as a live load, there is no problem with loss of post-tensioning. For the tendon length and elevation in the model bridge, the maximum increase in tendon force is approximately 17% of the applied load.

Overall, the quarter symmetry or complete finite element model, once refined as described in Section 3.2.1, accurately predicts the behavior of the model bridge for both post-tensioning and vertical loads. The largest differences between experimental and computed values tend to be for members directly subjected to post-tensioning or load.



a. Strains



b. Deflections

CONDITION	TEST	SAP IV
WITH POST-TENSIONING	●	——
WITHOUT POST-TENSIONING	○	----

FIGURE 34. Midspan strains and deflections for model bridge with concentrated load at midspan of interior beam

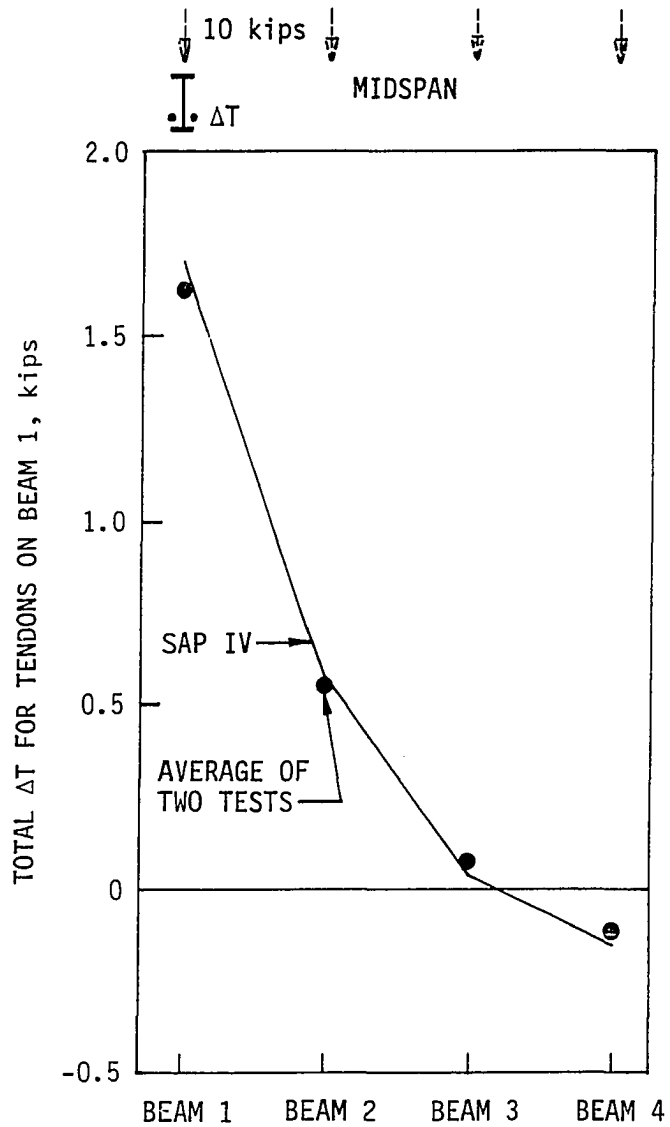


FIGURE 35. Change in tendon force for vertically loaded, post-tensioned model bridge

The composite bridge finite element model is clearly as accurate as the composite beam finite element model.

3.2.4.2. Bridge 1 For preliminary design, the distribution of post-tensioning for Bridge 1 was approximated from orthotropic plate theory for a simply supported plate with a vertical load at midspan of each exterior beam. During post-tensioning of the bridge in 1982, it became obvious that the bridge was not responding as much, in terms of strains or deflections, as predicted by theory. Two probable explanations for the reduced response were the approximation in loading (vertical load vs. eccentric load) and restraints caused by construction details.

The guard rails shown in Figure 1a on the transverse cross sections and in Figure 36 are steel rigid frames usually neglected in design or rating computations for the bridge. The rails do stiffen the edges of the bridge and, therefore, can reduce the effect of post-tensioning or vertical loads on the bridge. When frames consisting of beam elements and representing the guard rails were added to a simply supported finite element model of Bridge 1, the rails accounted for about 20% of the difference between strains and deflections measured in the field and computed from a finite element model without rails.

Guard rails account for part of the difference between computed and experimental values, but there must be other factors which cause restraint. Figure 36 illustrates three other potential restraints. Bridge 1 was designed and constructed with reinforcing bars continuous

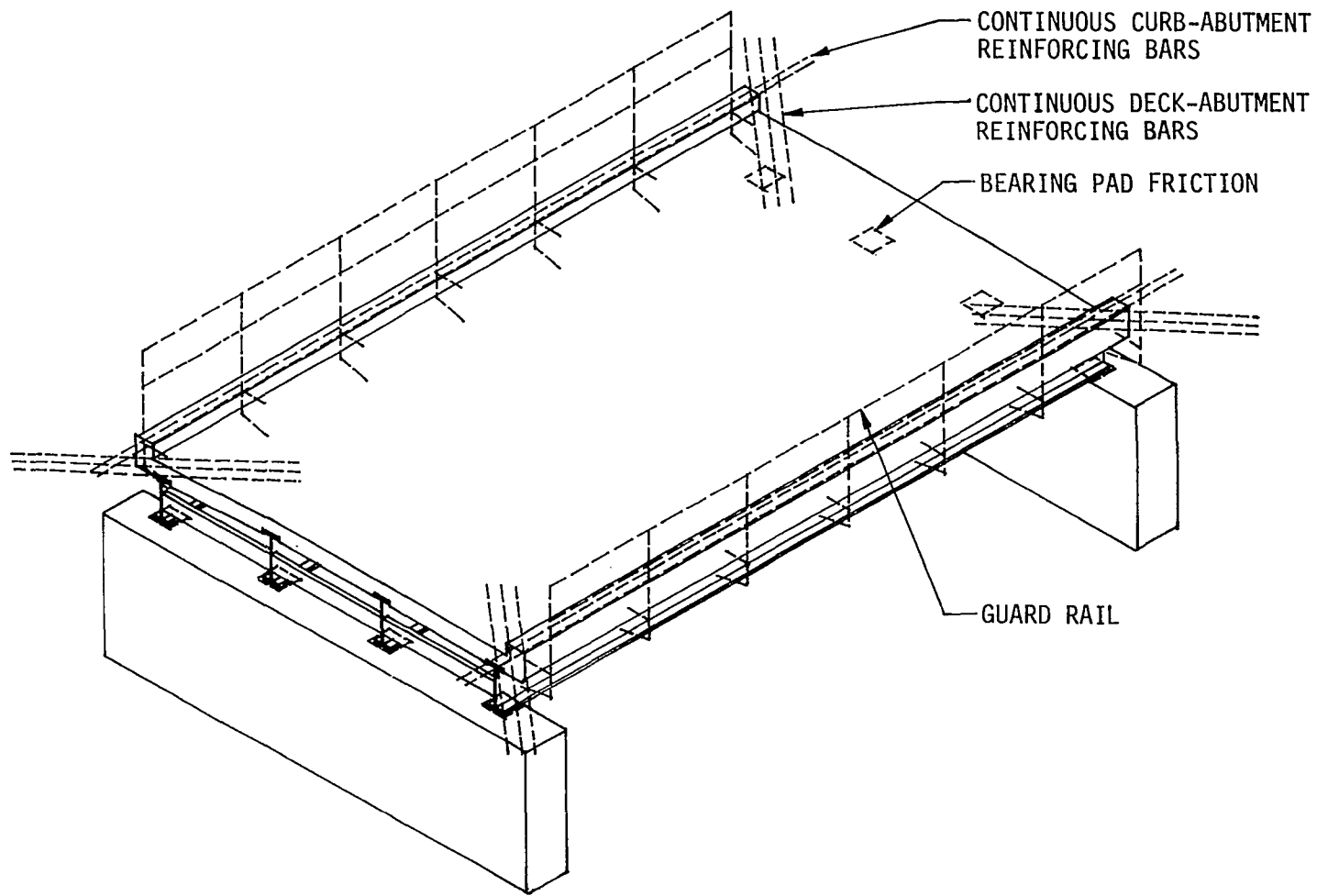


FIGURE 36. Guard rail and end restraints for Bridge 1

from curbs into abutments and from corners of deck into abutments. These bars are shown on the wing wall section in Figure 1a as well as in Figure 36. The reinforcing bars will provide restraint for both axial forces and moments in the bridge. In the field, some cracks were visible in 1984 where the bars were continuous from the bridge to the abutments, as if the bars had provided restraint for tension stresses.

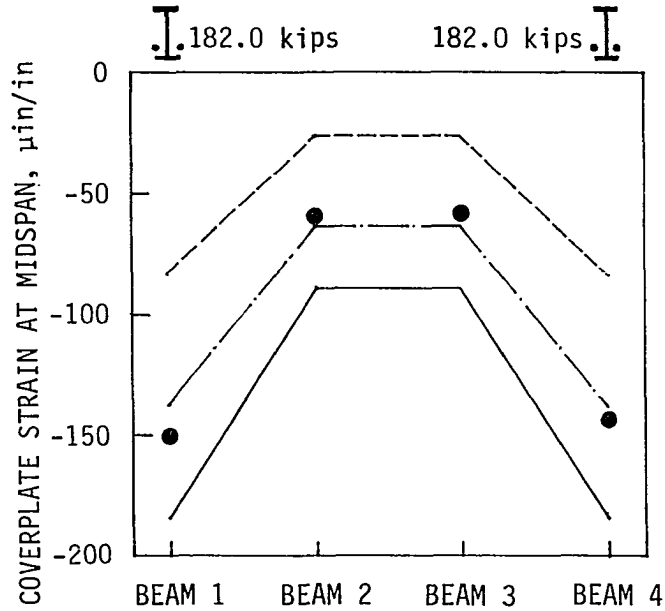
A third potential restraint is friction between the bridge beams and abutments at points of bearing. Design details for Bridge 1 do not suggest any attempt to provide restraint at bearing pads, but there can be forces due to friction at the pads, and at bearing locations for the concrete cast with the bridge end diaphragms.

In attempting to model the field conditions, all three restraints caused by reinforcing bars and bearing pad friction were modeled with beam elements. The stiffnesses of the beam elements were set at values based on reinforcing bar properties and potential frictional forces for dead loads at bearing pads. After some adjustment, the partial restraint model fit the field data very closely, especially for post-tensioning. Some of the frictional forces were slightly higher than could be expected due to dead load, but it is possible that beam and curb end details could create prying forces which would add to the dead load forces at bearing pads.

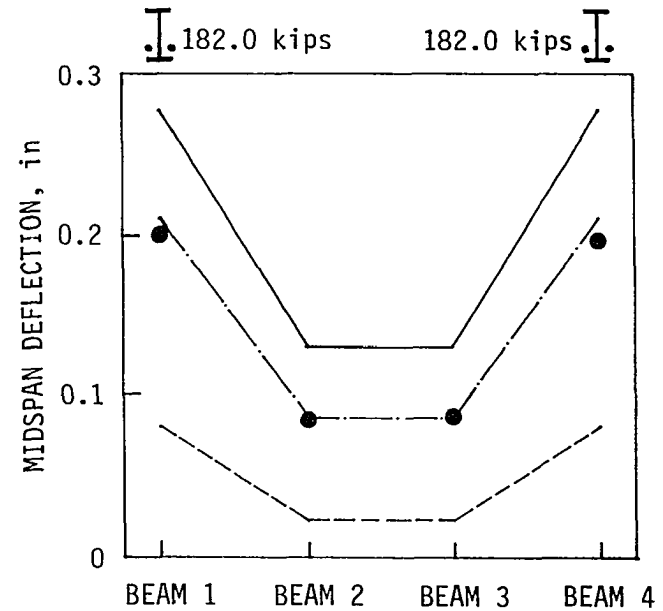
Additional restraints could exist beyond those illustrated in Figure 36. There are effectively no expansion joints at the ends of the bridge deck, and the deck could bear against the pavement when the

bridge is subjected to negative bending. What restraint mechanisms do exist may not be the same for both post-tensioning and vertical load. Experimental data for post-tensioning more nearly match the partial restraint model than experimental data for truck loads. The initial approach to checking field data against the finite element model was to compute strains and deflections for both simple support and fixed support conditions, to insure that the computations for the extreme conditions would bracket the field data. As shown in Figure 37, strains and deflections computed for simple support and fixed support conditions do bracket the experimental values. The partial restraint model, with the restraints illustrated in Figure 36, gives strains and deflections which are in excellent agreement with those measured in the field.

In order to illustrate the effect of post-tensioning along the span of Bridge 1, bottom flange and coverplate strains for interior and exterior beams are plotted in Figure 38. The SAP IV-computed strains are discontinuous at most beam nodes because of attached shear connector assemblies or changes in beam element properties or elevation. Figure 38a shows a very large discontinuity in strain at each tendon anchorage. Even for the strains computed for simple support conditions there is some tensile strain in the short region between each anchorage and support. The tensile strains in the same short regions, computed for fixed support conditions, are large, even larger than the desired compressive strains in the post-tensioned region. For any support conditions, therefore, a portion of the post-tensioning will be lost as



a. Strains



b. Deflections

CONDITION	1982 TEST	SAP IV
SIMPLE SUPPORT		—
PARTIAL RESTRAINT	●	- · - · -
FIXED SUPPORT		- - -

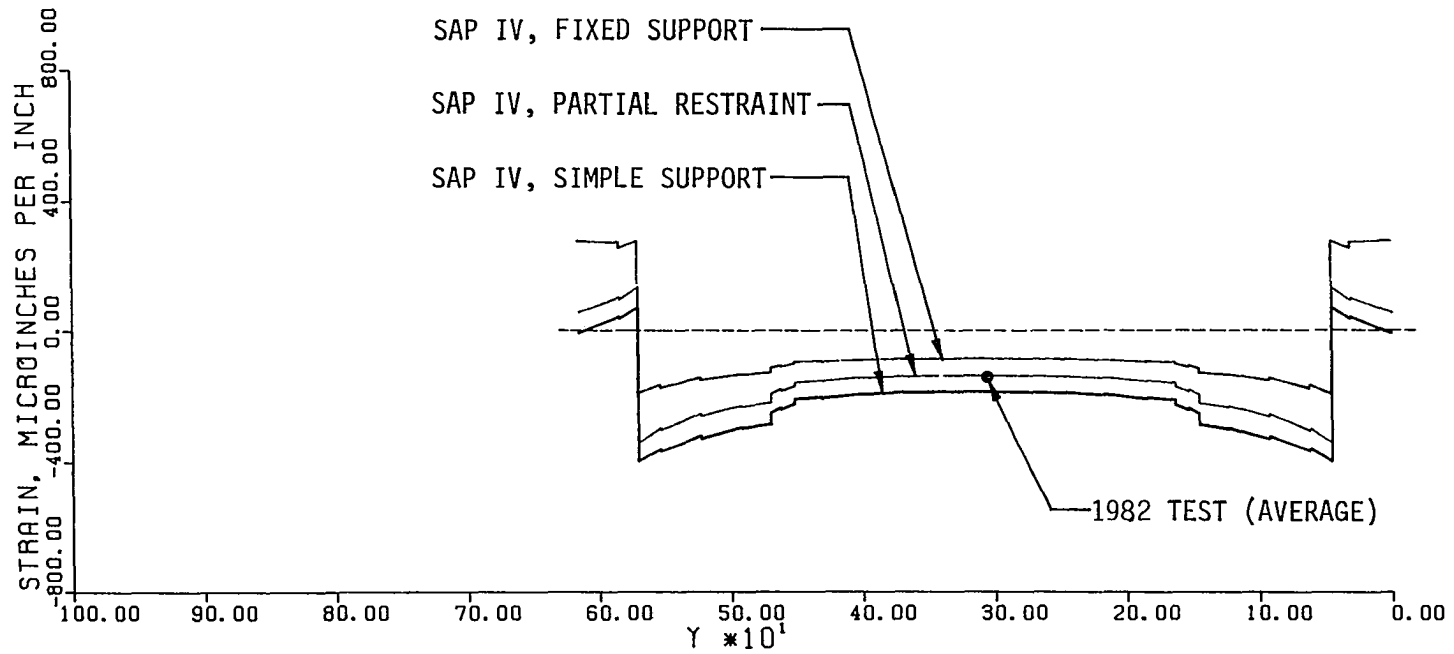
FIGURE 37. Midspan strains and deflections for Bridge 1 with post-tensioned exterior beams

a result of end restraint, if tendon anchorages are located away from the supports.

The reduction in strain toward midspan is caused by the coverplate and the distribution effect of the deck and diaphragms. The relatively sharp drop in strain near quarterspan points is caused by the increase in beam cross section when the coverplate is added. The gradual upward curve toward midspan for all three strain plots is caused by the distribution effect. For three reasons, then, post-tensioning effects on the exterior beams are reduced at midspan.

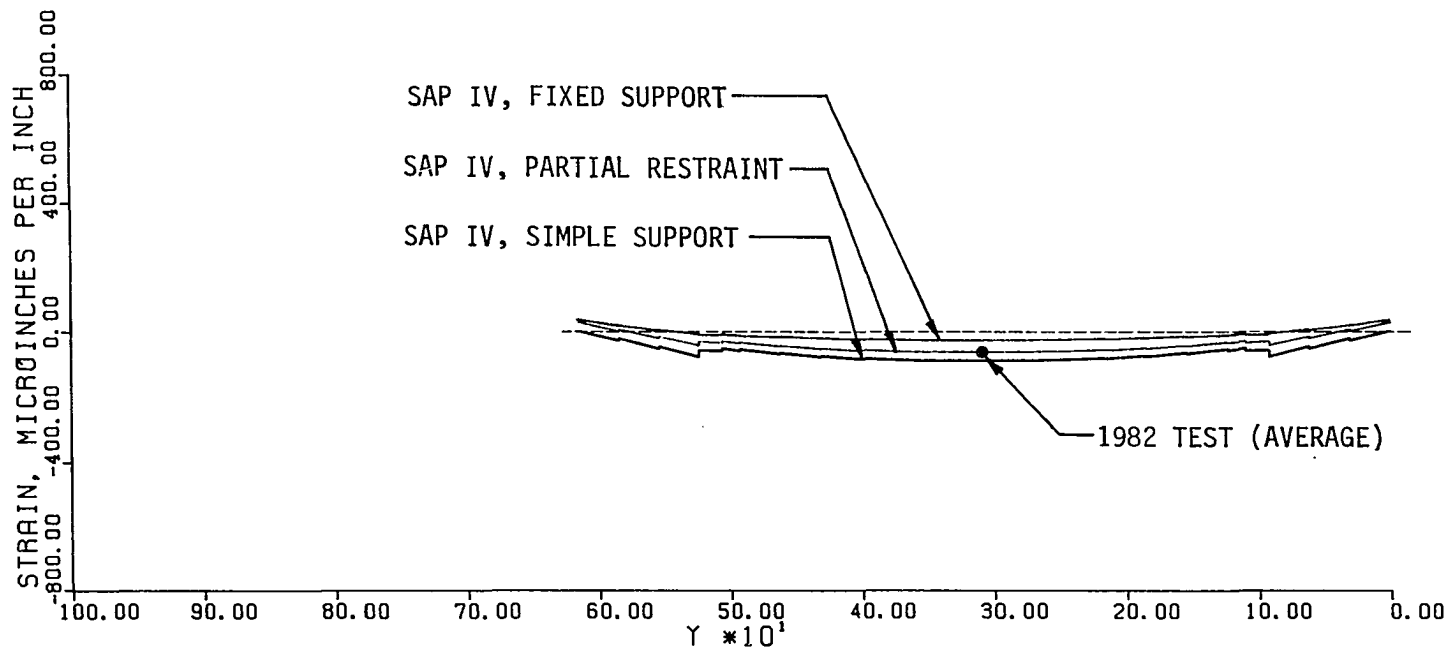
Figure 38b, for an interior beam, shows that a small amount of the post-tensioning is distributed to the beam. The amount distributed decreases at the two points where the coverplate begins, but the amount generally increases toward midspan. The increase in strain toward midspan complements the decrease in strain for the exterior beam.

The post-tensioning for Bridge 1 was released in 1984 and larger post-tensioning forces were applied. In order to check for end restraint, strain gages were attached to bottom flanges of the bridge beams at 9 inches from one support. The end strains plotted in Figure 39b clearly indicate presence of end restraint. The end strains for the exterior beams are of the opposite sense and are larger than the midspan strains for the exterior beams plotted in Figure 39a. The strains both at midspan and near the supports fall about halfway between the simple support and fixed support values. Strains and deflections measured in both 1982 and 1984 indicate that the bridge was being restrained significantly during post-tensioning.



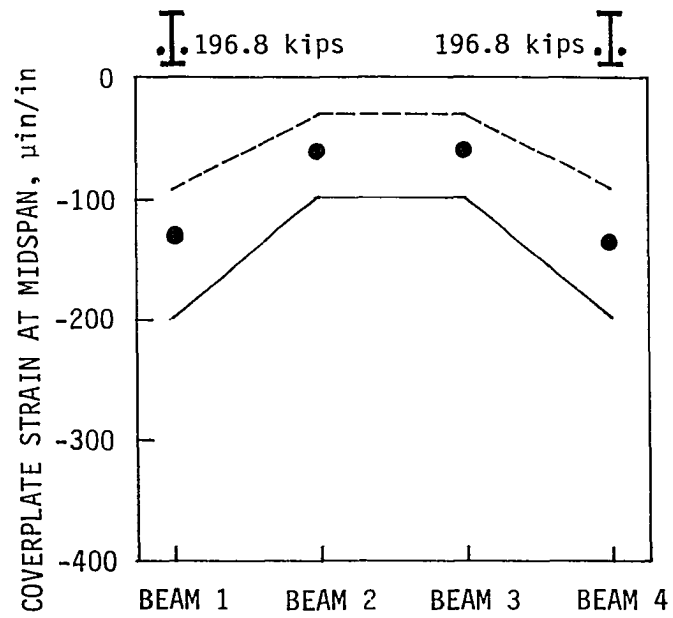
a. Exterior beam

FIGURE 38. Bottom flange and coverplate strains for Bridge 1 with post-tensioned exterior beams

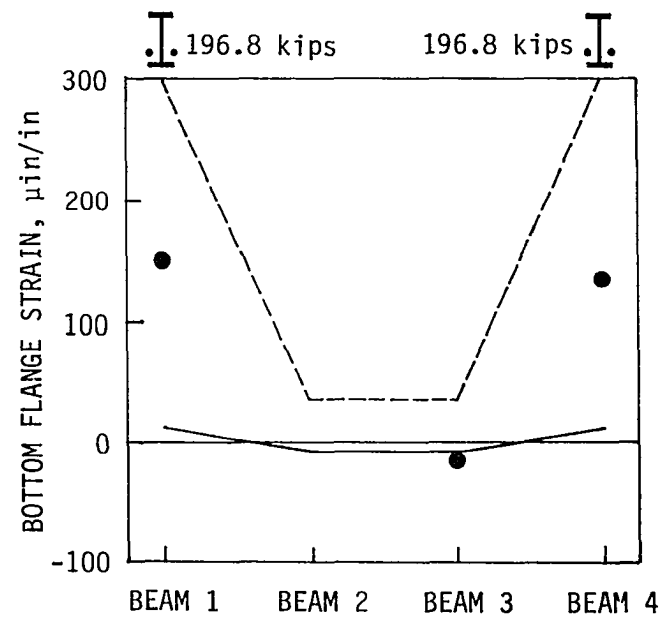


b. Interior beam

FIGURE 38 (Continued)



a. Midspan



b. 9 inches from support

CONDITION	1984 TEST	SAP IV
SIMPLE SUPPORT		—
PARTIAL RESTRAINT	●	—
FIXED SUPPORT		- - -

FIGURE 39. Midspan and end strains for Bridge 1 with post-tensioned exterior beams

Deflected shapes for the post-tensioned bridge with the extreme support conditions, simple and fixed, are illustrated in Figures 40 and 41. The shape in Figure 40 for simple supports is very similar to that for the post-tensioned model bridge. Because the deflected shape for fixed supports given in Figure 41 is plotted to the same vertical scale as Figure 40, the doubly curved portion of the deck at midspan is much less apparent. In both figures, the curbs remain in their undeflected shape because the SAP IV master-slave node option does not output deflections at the slave nodes.

During the 1982 and 1984 testing of Bridge 1, an overloaded truck was placed at a series of predetermined locations on the bridge both before and after post-tensioning, as described in References 54 and 28. The strain and deflection results from the 1982 test for an eccentric truck (wheel line 2 feet from curb, and center of gravity at midspan) and corresponding SAP IV analyses are given in Figures 42 and 43. From the graphs in Figure 42, the end restraint again is obvious. Field-measured strains plot closest to the fixed support analysis, and field-measured deflections plot closest to the partial restraint analysis. Since the experimental strains fall closer to the fixed support analysis for the truck load than for post-tensioning, there is evidence that the bridge restraints for positive and negative bending are slightly different.

In Figures 44 and 45, the strain and deflection values for a central truck (center of gravity at midspan and at bridge centerline)

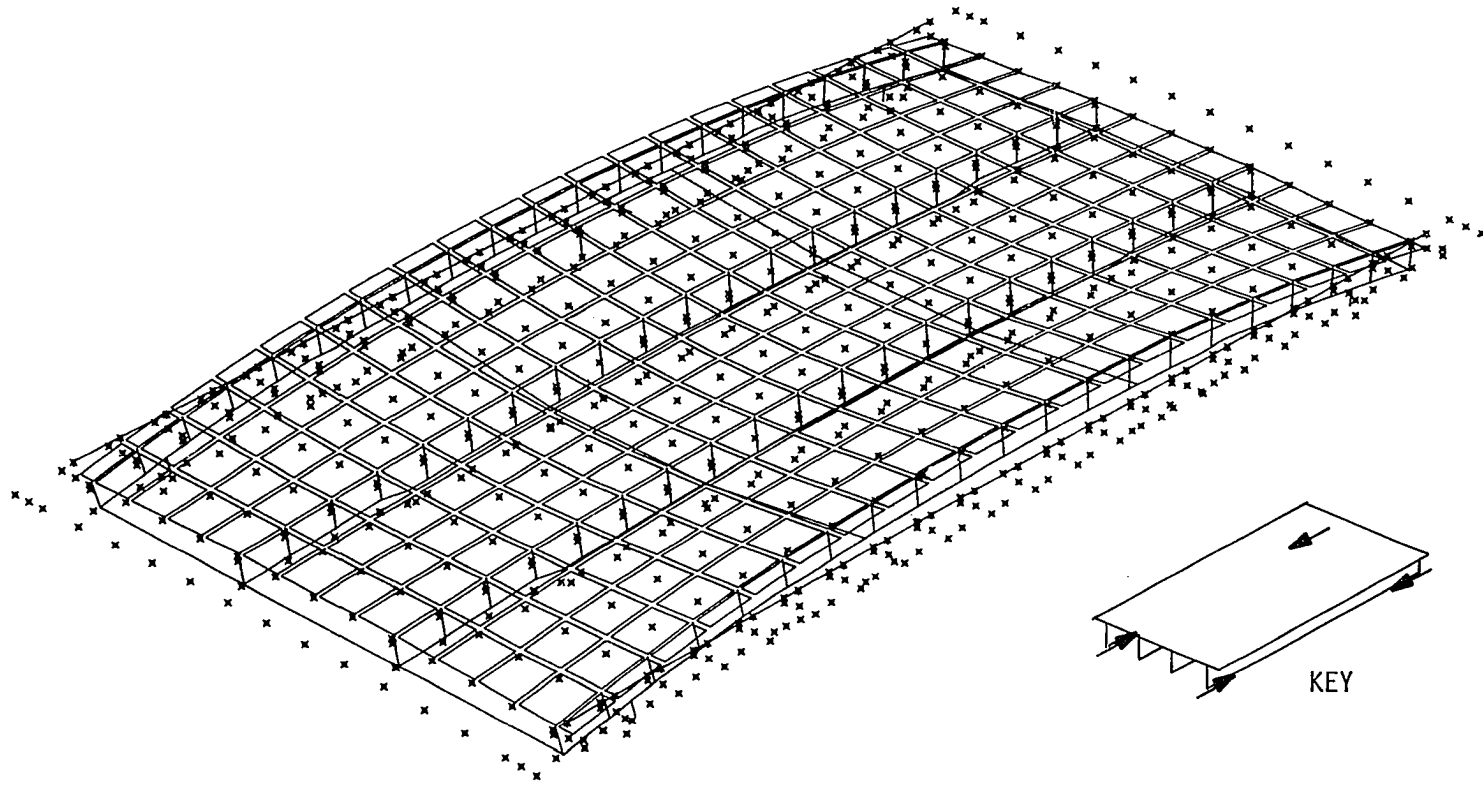


FIGURE 40. Deflected shape for Bridge 1 with post-tensioned exterior beams and simple supports

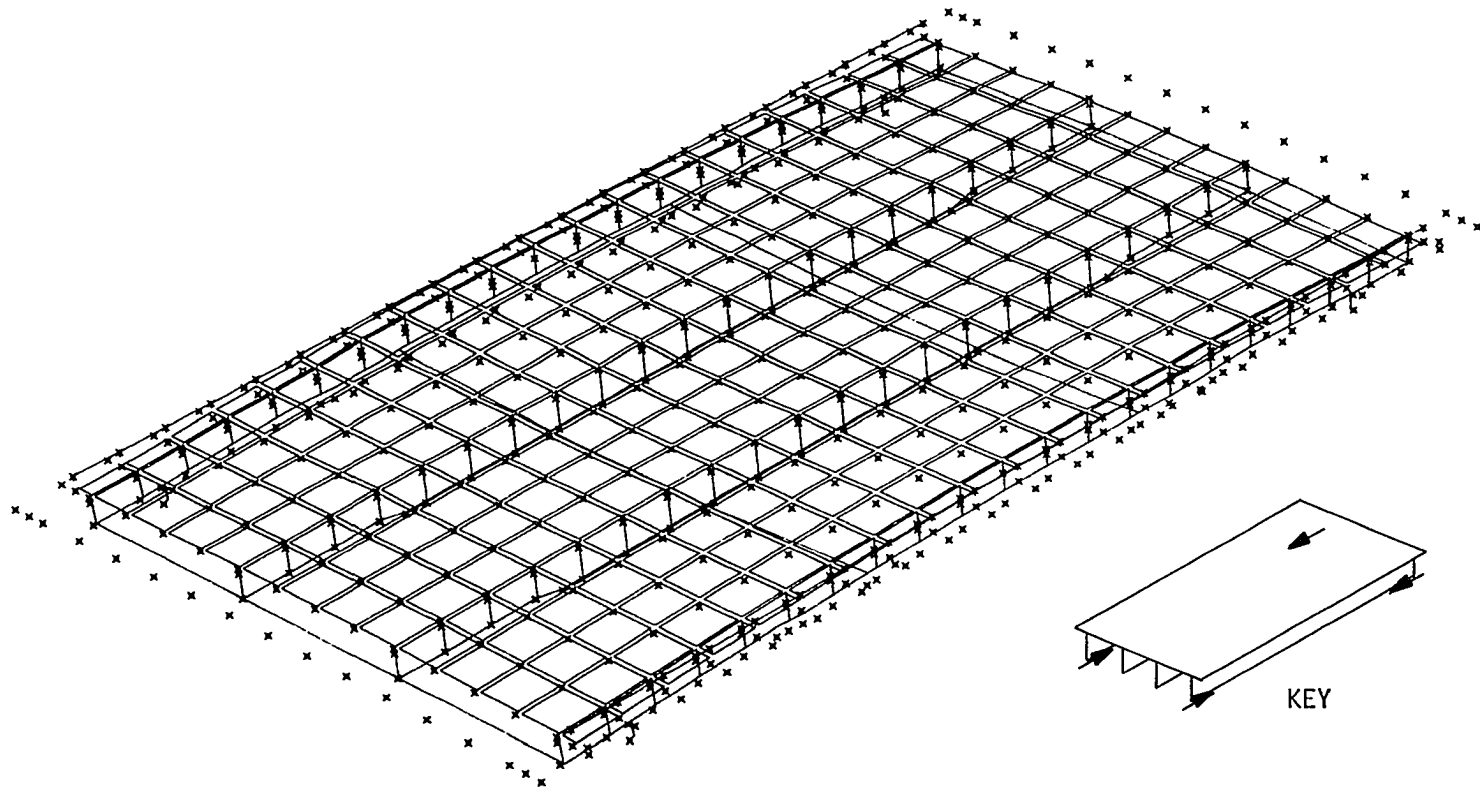
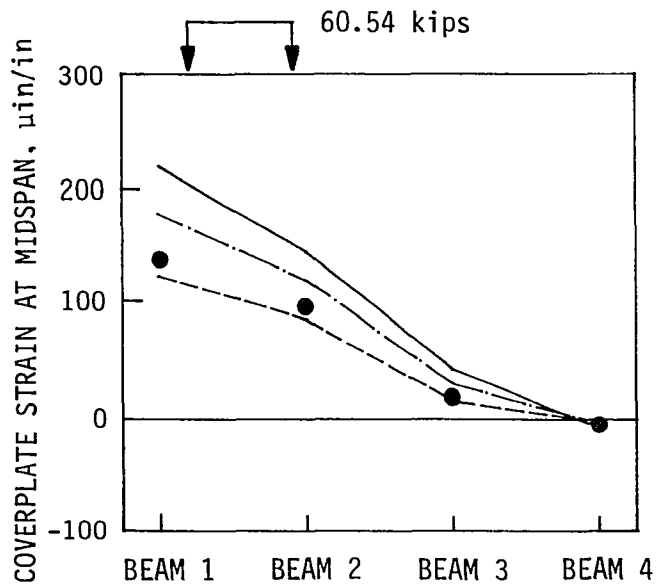
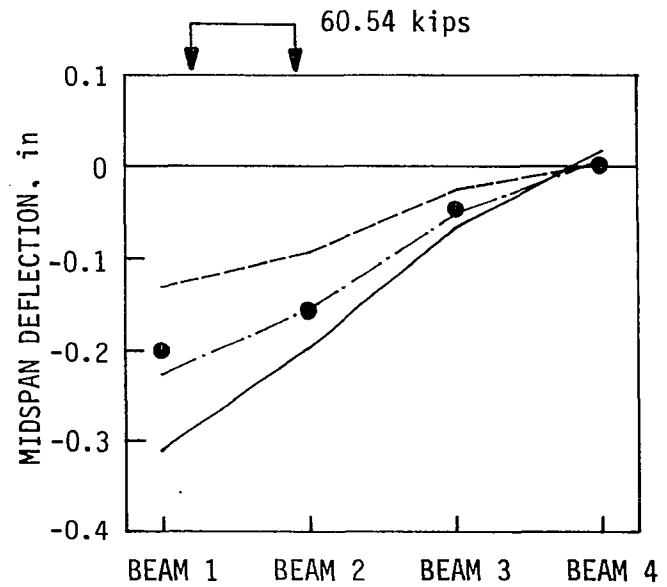


FIGURE 41. Deflected shape for Bridge 1 with post-tensioned exterior beams and fixed supports



a. Strains



b. Deflections

CONDITION	1982 TEST (AVERAGE)	SAP IV
SIMPLE SUPPORT		—
PARTIAL RESTRAINT	●	· · ·
FIXED SUPPORT		- - -

FIGURE 42. Midspan strains and deflections for Bridge 1 with eccentric truck load

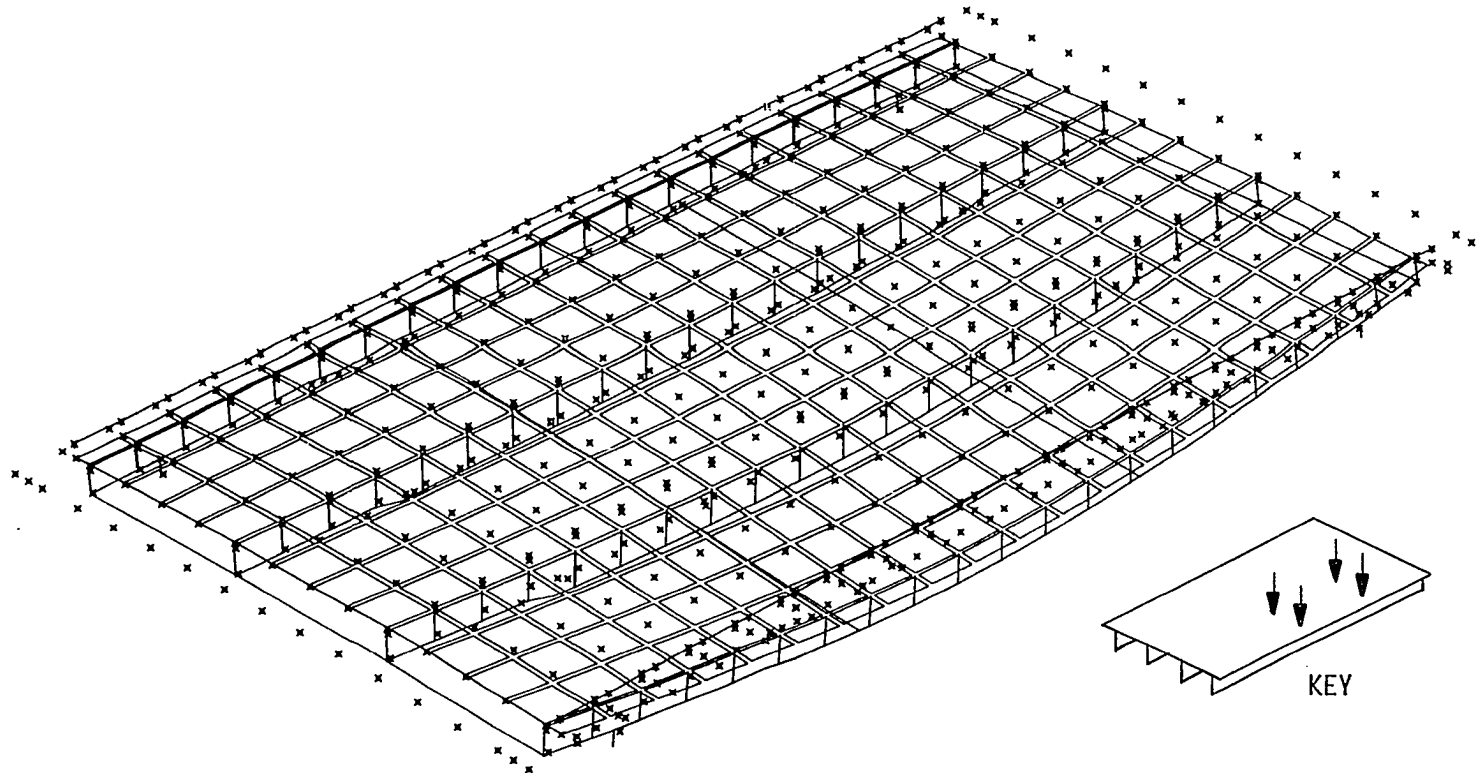


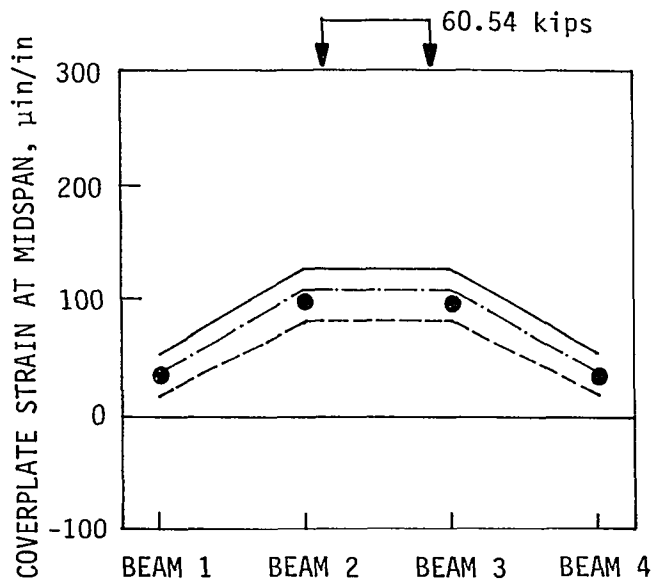
FIGURE 43. Deflected shape for Bridge 1 with eccentric truck load

are illustrated. Experimental deflections in Figure 44b fall approximately halfway between simple and fixed support analyses. Experimental strains in Figure 44a fall slightly closer to the fixed support analysis values, as they did for the eccentric truck. The deflected shape at midspan, as illustrated in Figure 45, is doubly curved at midspan, with both curvatures indicating positive bending moment.

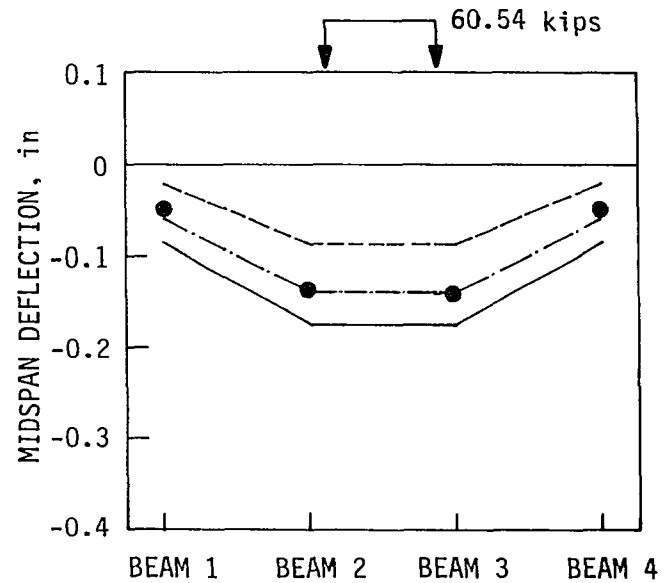
Changes in tendon forces were measured separately from the bridge strains in 1982. Due to drift in the strain indicator, much of the field data were unreliable. From the reliable data and from comparable SAP IV computations, the maximum change in tendon force, for an eccentric truck, was approximately 4 kips. The 4 kips represents about 6% of the applied load. The 6% is about one-third of the 17% measured and computed for the model bridge with an eccentric load. The decrease is due to the fact that the truck load is not as eccentric as the concrete weight placed at midspan of the exterior beam of the model bridge.

With partial restraints, the finite element model gives an accurate analysis for Bridge 1. The finite element model with either simple supports or fixed supports gives values which bracket the field-measured strains and deflections. Thus, the finite element model correlates well with Bridge 1.

3.2.4.3. Bridge 2 Because Bridge 2 is skewed at 45 degrees, it will have end restraint caused by staggered beam ends and the attached



a. Strains



b. Deflections

CONDITION	1982 TEST (AVERAGE)	SAP IV
SIMPLE SUPPORT		————
PARTIAL RESTRAINT	●	- · - · - ·
FIXED SUPPORT		-----

FIGURE 44. Midspan strains and deflections for Bridge 1 with central truck load

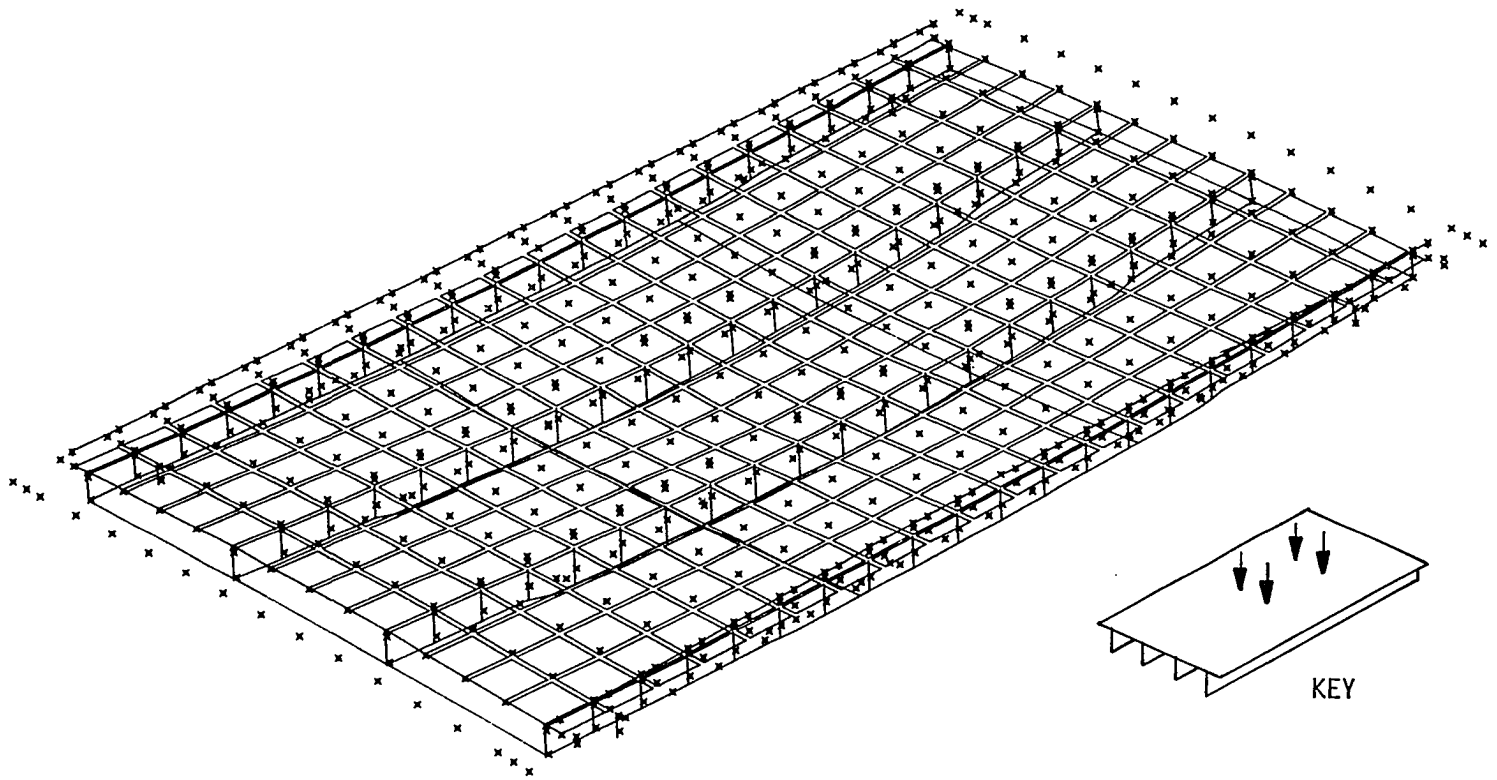
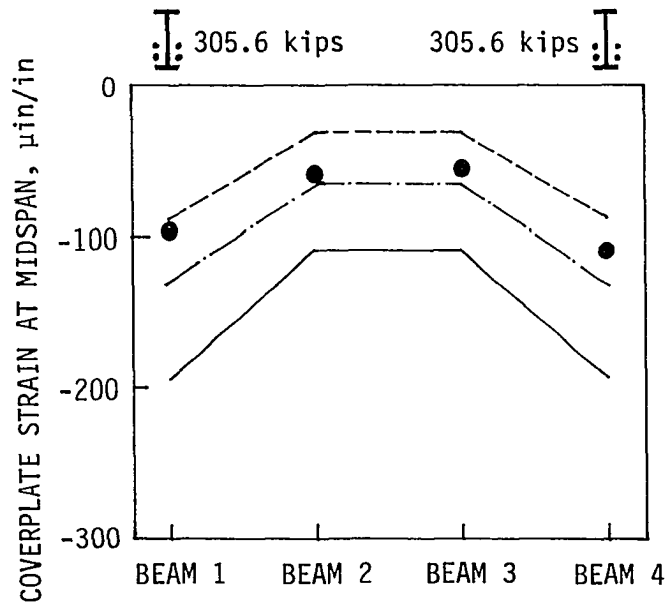


FIGURE 45. Deflected shape for Bridge 1 with central truck load

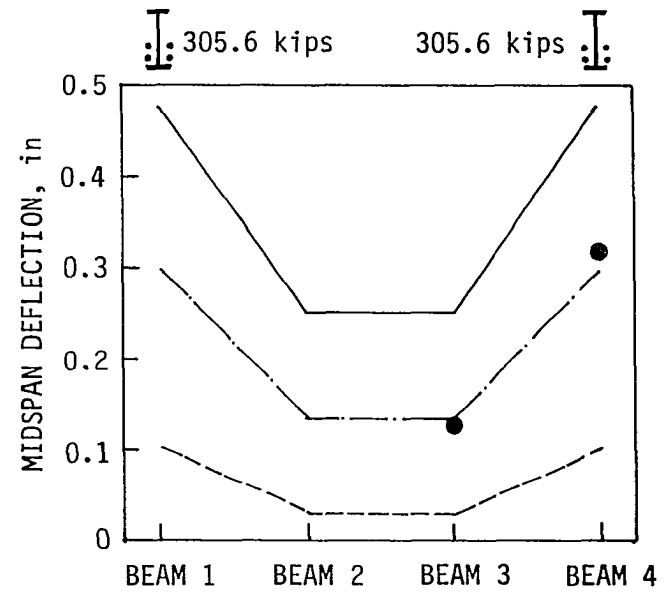
deck. The staggered beam ends and deck create a restraint similar to that of a rotary spring. In addition, Bridge 2 has guard rails similar to those on Bridge 1, which offer restraint along the edges of the bridge deck. No reinforcing bars extend from deck or curbs into abutments, but bearing pad restraints can exist, similar to those for Bridge 1. For the partial restraint finite element model analyses for Bridge 2, the guard rail and bearing pad restraints were included in the model.

Midspan strains and deflections for Bridge 2 with post-tensioning are presented in Figure 46. Field-measured deflections follow the partial restraint analysis, but field-measured strains approach the fixed support analysis. Similar observations can be made regarding the quarterspan strains and deflections presented in Figure 47. Although the strains and deflections are symmetrical at midspan, they are unsymmetrical at quarterspan.

The lack of symmetry in strains at the two quarterspan points also is apparent in Figure 48, in which the bottom flange and coverplate strains are plotted for exterior and interior beams. The lack of symmetry is caused by the staggered beam placement and the change in tendon anchorage locations from one end of the span to the other. The anchorage at the left end of the exterior beam in Figure 48a is located at 5 feet from the support, whereas the anchorage at the right end is located at 1 foot from the support. In general, however, the strain plots are very similar to those for Bridge 1 given in Figure 38.



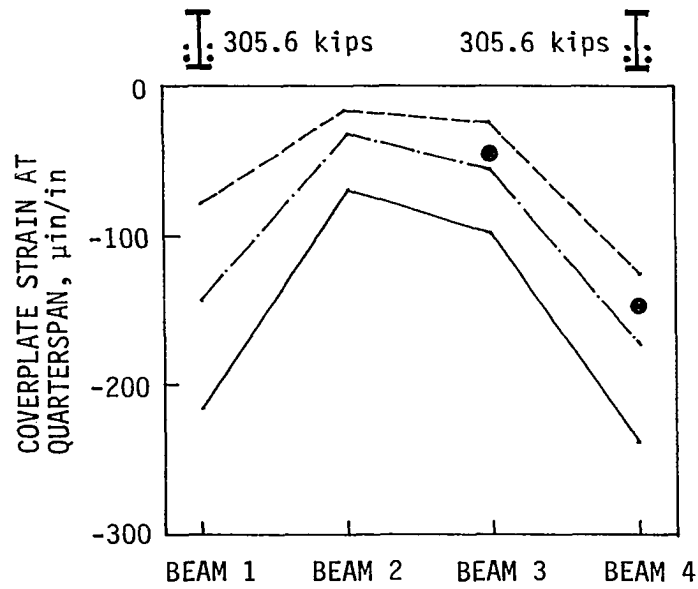
a. Strains



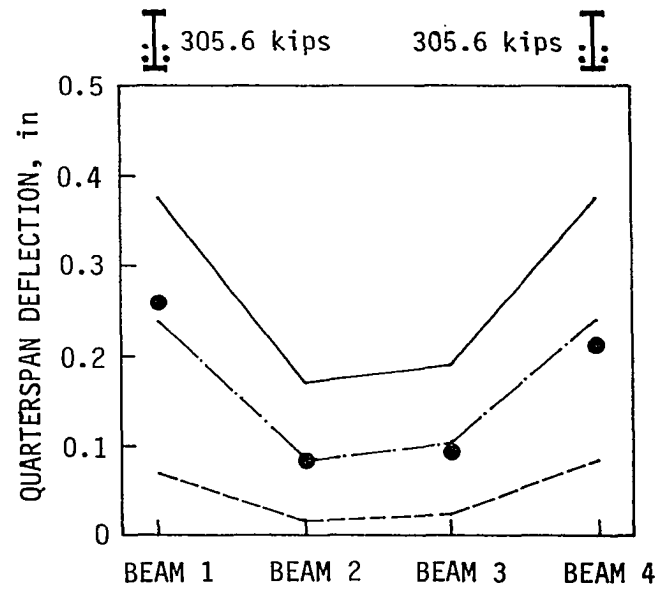
b. Deflections

CONDITION	1982 TEST	SAP IV
SIMPLE SUPPORT		————
PARTIAL RESTRAINT	●	- · - · - · -
FIXED SUPPORT		-----

FIGURE 46. Midspan strains and deflections for Bridge 2 with post-tensioned exterior beams



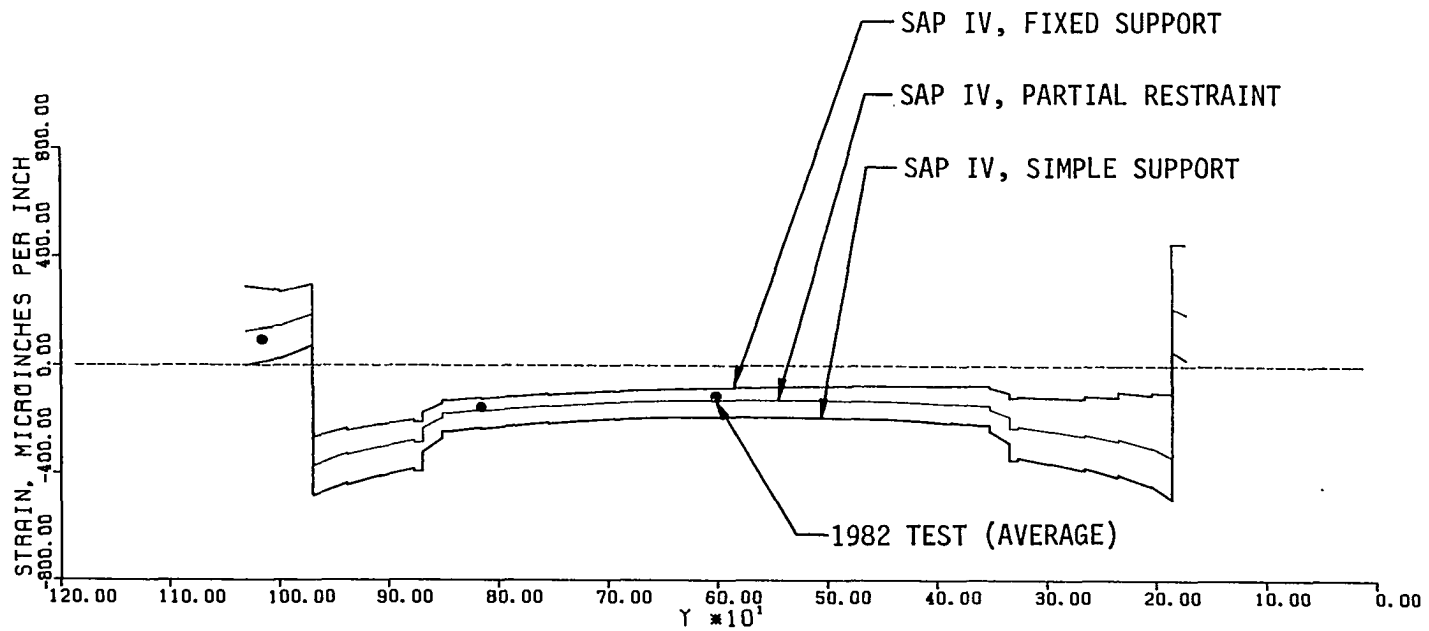
a. Strains



b. Deflections

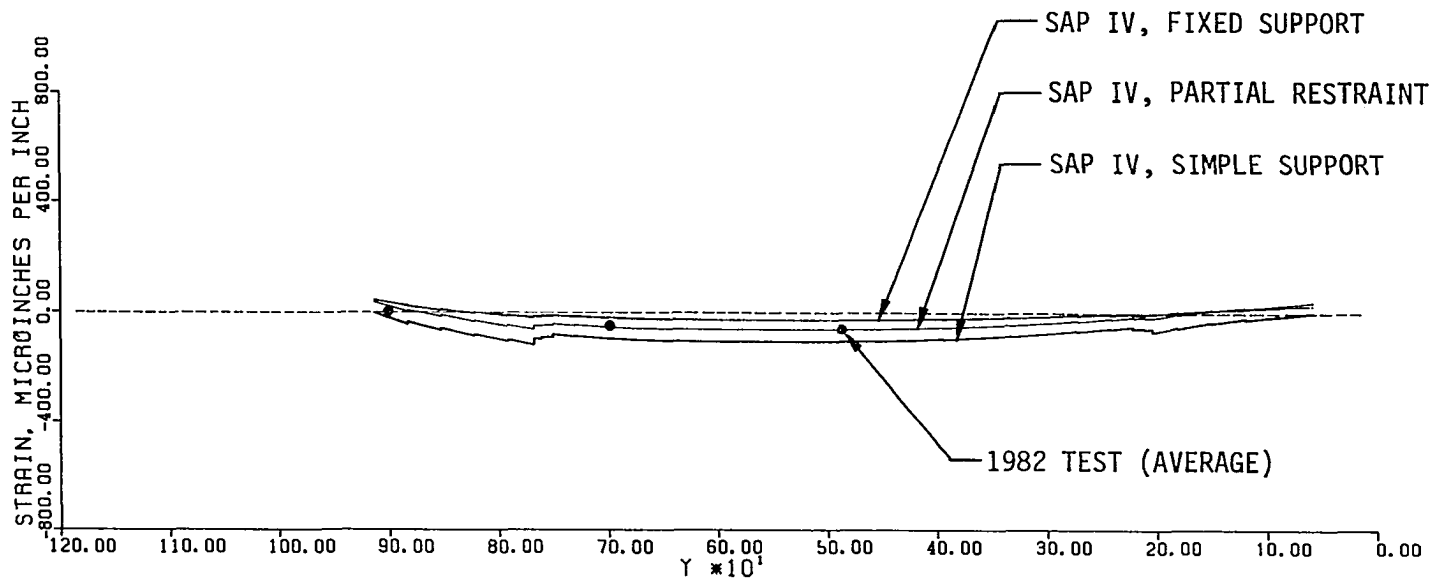
CONDITION	1982 TEST	SAP IV
SIMPLE SUPPORT		————
PARTIAL RESTRAINT	●
FIXED SUPPORT		-----

FIGURE 47. Quarterspan strains and deflections for Bridge 2 with post-tensioned exterior beams



a. Exterior beam

FIGURE 48. Bottom flange and coverplate strains for Bridge 2 with post-tensioned exterior beams



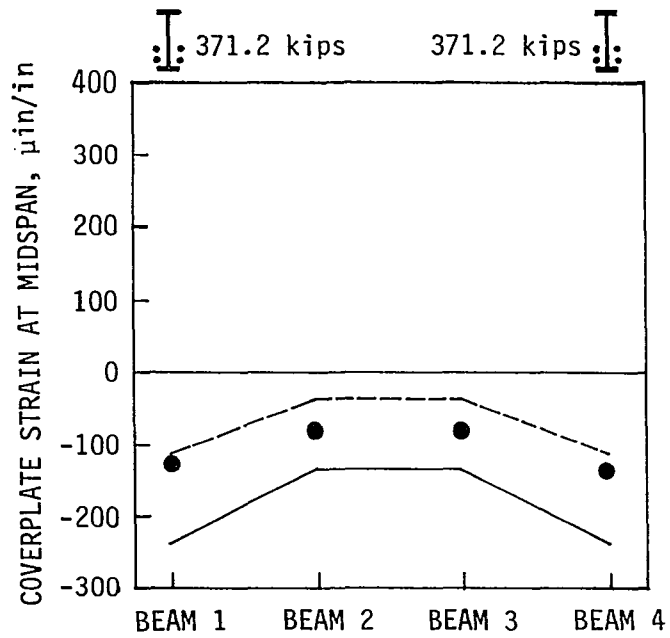
b. Interior beam

FIGURE 48 (Continued)

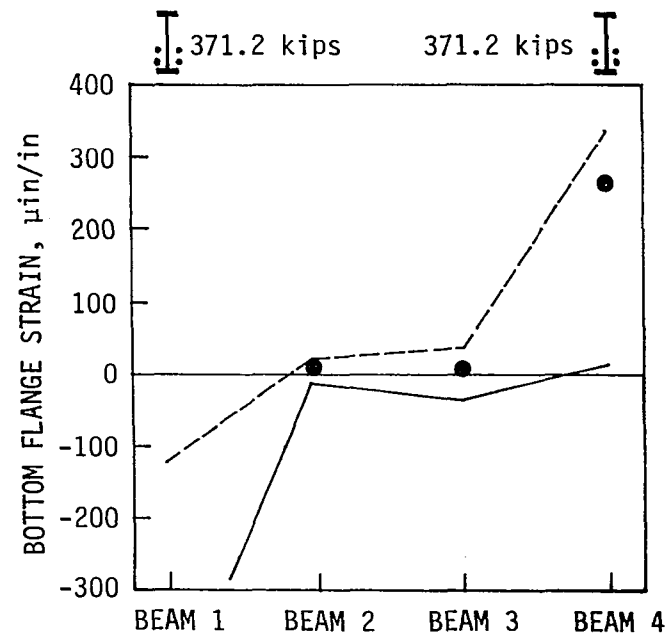
In 1984, strain gages were placed on the bottom flanges of all four beams for Bridge 2 at 15 inches from one support. The gages for Beam 1 were within the post-tensioned region, did not give reliable results and, therefore, are not included in Figure 49b. The strains measured at midspan and at 15 inches from the support fall closer to the fixed support than to the simple support analysis, as shown in Figure 49. For Beam 4 at the support, the strain is of the opposite sense and numerically about twice as large as the strain measured at midspan. In general, there appeared to be more restraint in Bridge 2 than in Bridge 1.

A deflected shape for Bridge 2 with post-tensioned exterior beams is given in Figure 50. The viewpoint for the perspective causes some distortion of the view, and the skew is not very apparent. The post-tensioning causes a symmetrical deflection pattern at midspan but causes alternate twists between midspan and the supports. The deflected shape is more complex than the shape for a right-angle bridge such as Bridge 1.

Test and analysis results for Bridge 2 with an eccentric truck (wheel line 2 feet from curb, and center of gravity at midspan) are given in Figures 51 and 52. Measured strains and deflections fall very close to the fixed support analysis values, more so than for post-tensioning. As for Bridge 1, there appears to be more end restraint for vertical loads than for post-tensioning, which suggests that end restraint mechanisms are slightly different for negative and positive bending moments.



a. Midspan



b. 15 inches from support

CONDITION	1984 TEST	SAP IV
SIMPLE SUPPORT		—
PARTIAL RESTRAINT	●	
FIXED SUPPORT		- - -

FIGURE 49. Midspan and end strains for Bridge 2 with post-tensioned exterior beams

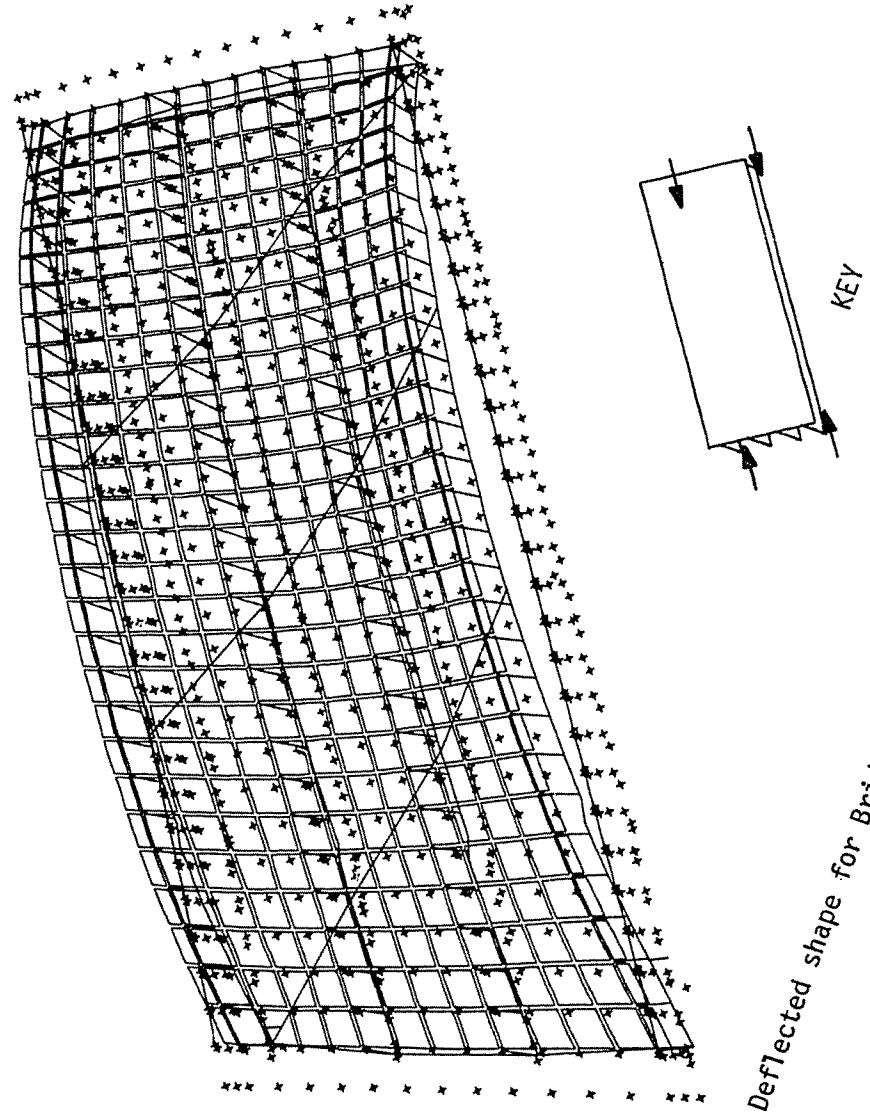
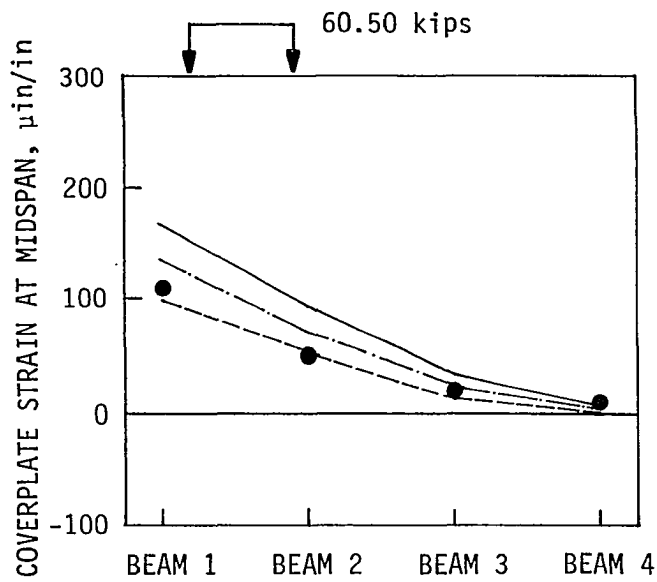
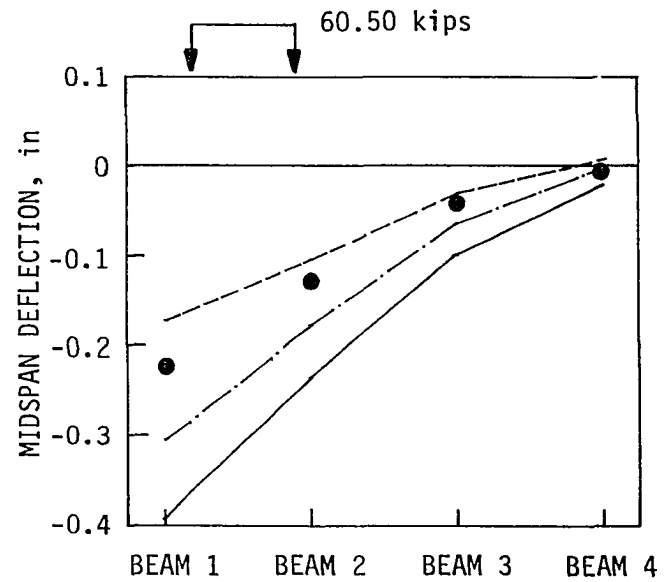


FIGURE 50. Deflected shape for Bridge 2 with post-tensioned exterior beams



a. Strains



b. Deflections

CONDITION	1982 TEST (AVERAGE)	SAP IV
SIMPLE SUPPORT		————
PARTIAL RESTRAINT	●	- · - · - · -
FIXED SUPPORT		-----

FIGURE 51. Midspan strains and deflections for Bridge 2 with eccentric truck load

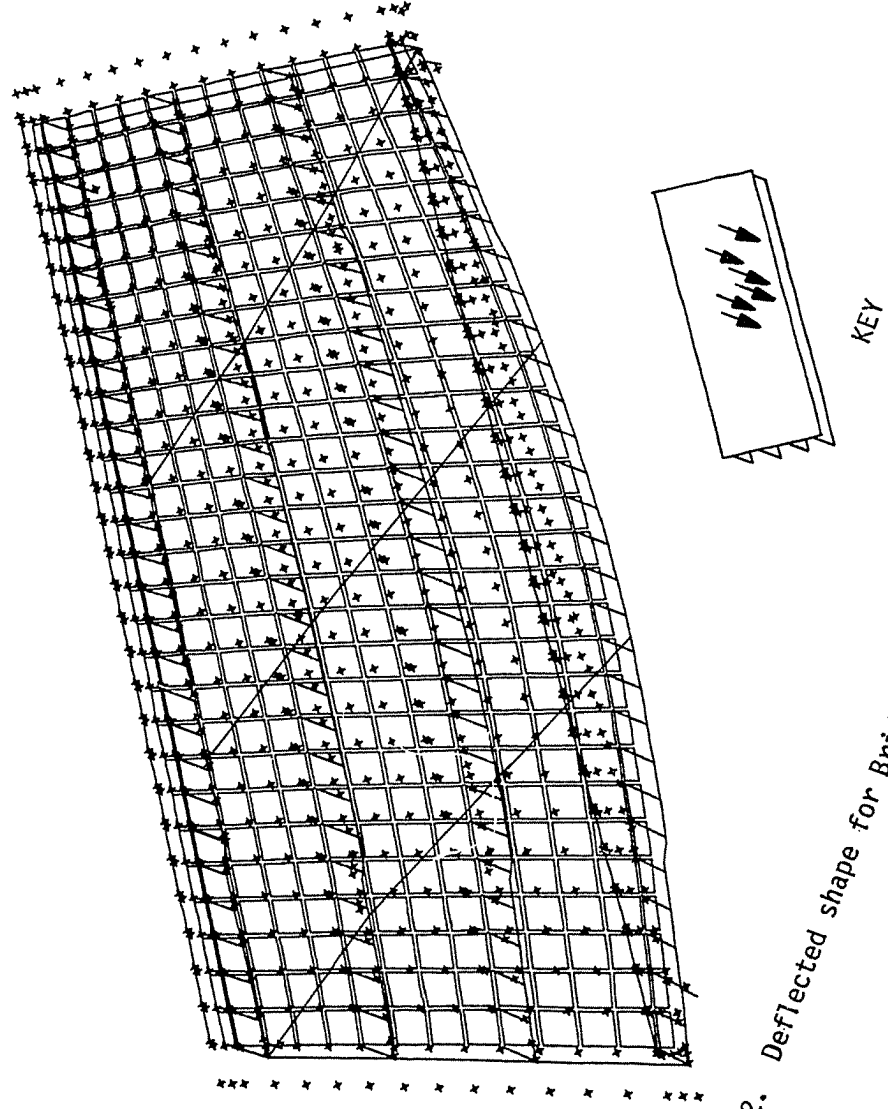
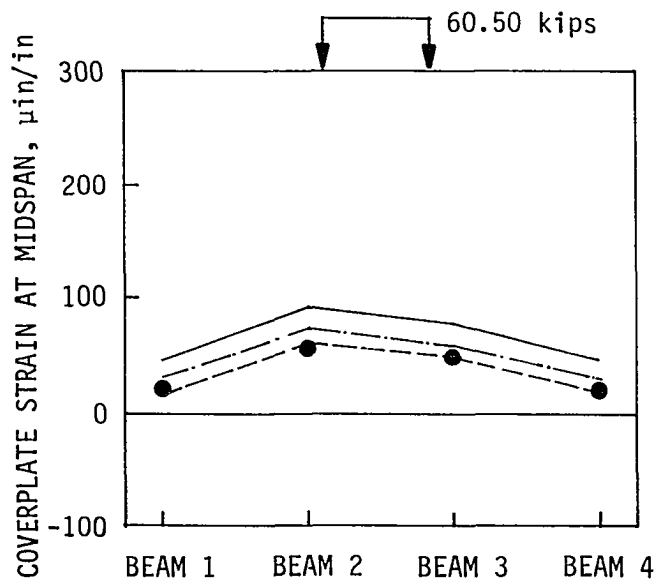


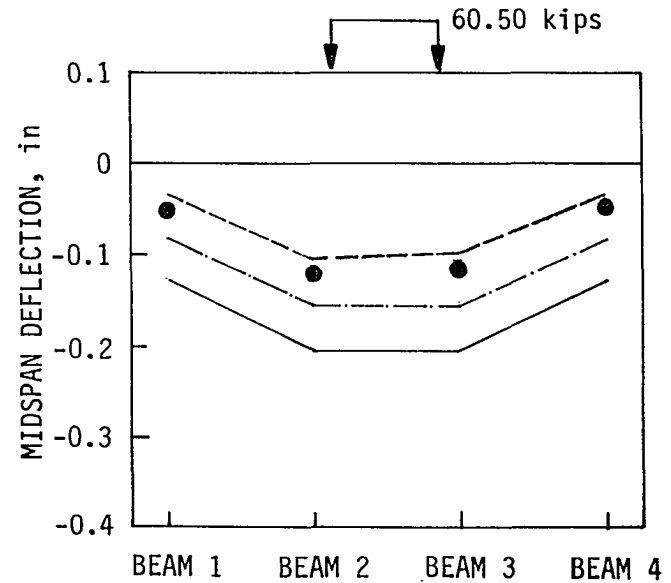
FIGURE 52. Deflected shape for Bridge 2 with eccentric truck load

Figures 53 and 54 for Bridge 2 with a central truck load (center of gravity at midspan and bridge centerline) show behavior similar to that for Bridge 2 with the eccentric truck. Field-measured strains and deflections plotted in Figure 53 fall very close to the analysis for fixed supports. Again, it appears that Bridge 2 has more restraint than Bridge 1.

Overall, the SAP IV finite element model accurately predicts the strain and deflection behavior of post-tensioned and vertically loaded composite bridges. For the model bridge, with accurately modeled simple supports, the finite element model gives results which are in very good agreement with laboratory test results. Bridges 1 and 2, with supports designed and constructed for practical conditions, exhibit some restraint, which can be bracketed between simple support and fixed support finite element analyses. Finite element models with partial restraint can be adjusted to closely model the field-measured behavior of the bridges.



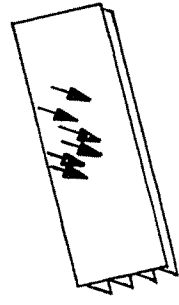
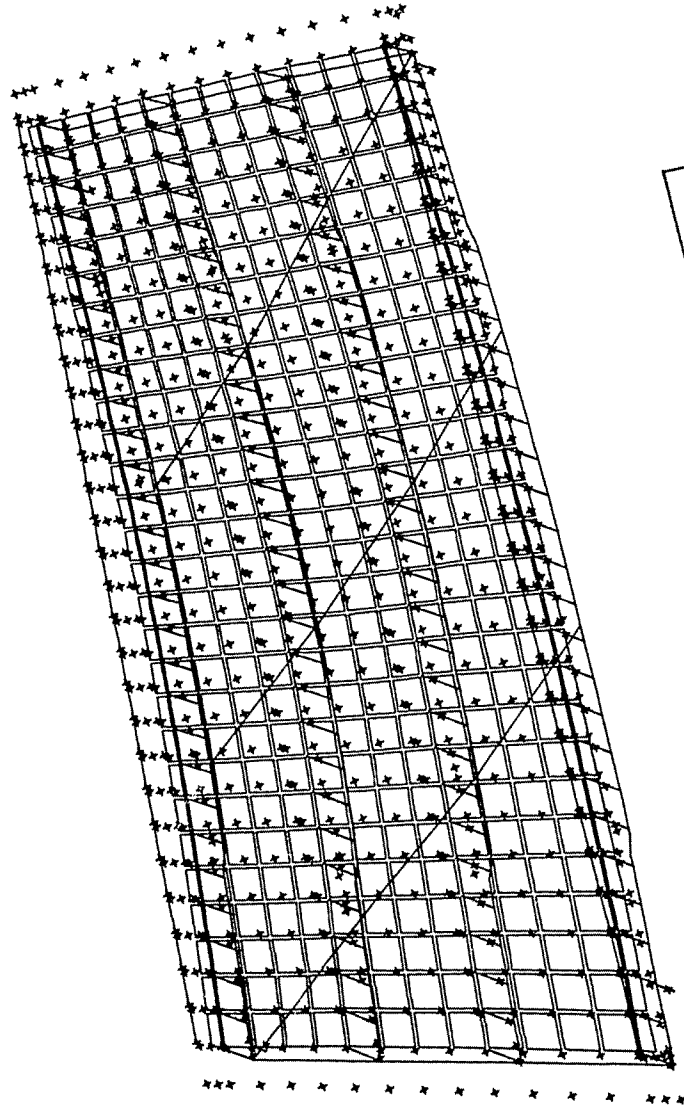
a. Strains



b. Deflections

CONDITION	1982 TEST (AVERAGE)	SAP IV
SIMPLE SUPPORT		————
PARTIAL RESTRAINT	●	- - - - -
FIXED SUPPORT		· · · · ·

FIGURE 53. Midspan strains and deflections for Bridge 2 with central truck load



KEY

FIGURE 54. Deflected shape for Bridge 2 with central truck load

4. POST-TENSIONING DISTRIBUTION

The composite bridge finite element model developed in the previous chapter is capable of accurately analyzing a specific bridge for a variety of loading conditions, including post-tensioning. Use of the model, however, requires access to preprocessing programs, SAP IV, and a large computer with associated hardware. Since the programs and large computer would not be readily available to many Iowa practicing engineers, this research study focused on providing a relatively simple means of determining the post-tensioning distribution.

The distribution for use in design of post-tensioning could be developed as tables, charts, or formulas by means of many analysis methods. Efforts by the author to develop a very general method for determining the distributions for bridges with any reasonable number of beams were not productive. Accuracy was poor, and use of the method would have been more cumbersome than desired. As a result, efforts were focused more specifically on the Iowa bridges in need of strengthening. The Iowa DOT provided series of standard plans for the typical composite three-beam and four-beam bridges with small exterior beams and standard plans for four-beam composite bridges with beams of equal size. For the standard bridge designs and other individual designs, the SAP IV bridge model was utilized to generate post-tensioning distribution data, and that data was then used with multiple linear regression to develop simple distribution fraction formulas. The distribution fraction formulas are relatively easy to use, not significantly more difficult to

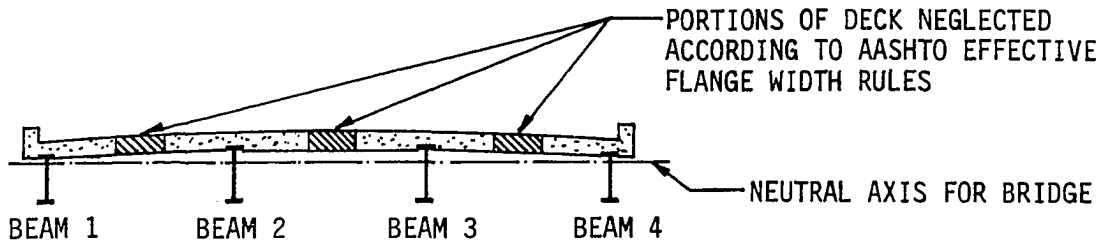
use than the AASHTO wheel load distribution fractions. Distribution fractions for bridges beyond the range of the regression data on which the formulas are based must, however, be determined from finite element analysis or another suitable analysis method.

4.1. Distribution Fractions

In general, a distribution fraction can be defined as the ratio of a quantity for a single bridge beam to the total quantity for a bridge. For the Iowa composite bridges in need of strengthening, the critical location is the bottom flange or coverplate at midspan, and that location was adopted as the reference for all distribution fractions.

Specific distribution fractions for axial force and bending moment for an exterior bridge beam, Beam 1, are defined in Figure 55. The force fraction, FF_1 , is defined as the axial force applied to Beam 1 divided by the sum of the axial forces applied to all bridge beams, Beams 1 through 4. The definition can be extended, as shown in the figure, to strains or stresses. For strains or stresses, the force fraction then is dependent on relative composite beam areas.

Also in Figure 55, the moment fraction for Beam 1, MF_1 , is defined. If the definition is extended to strains or stresses, the moment fraction is dependent on the relative composite beam section moduli. Not shown in Figure 55, but also feasible is the definition of moment fraction in terms of midspan deflections, in which case the fraction is dependent on relative composite beam moments of inertia [55].



a. Bridge cross section

$$FF_1 = \frac{P_1}{\Sigma P} = \frac{E(\epsilon_1 A_1)}{E(\Sigma \epsilon A)} = \frac{f_1 A_1}{\Sigma f A}$$

$$MF_1 = \frac{M_1}{\Sigma M} = \frac{E(\epsilon_1 S_1)}{E(\Sigma \epsilon S)} = \frac{f_1 S_1}{\Sigma f S}$$

WHERE FF = FORCE FRACTION FOR A COMPOSITE BEAM
 MF = MOMENT FRACTION FOR A COMPOSITE BEAM
 P = AXIAL FORCE FOR A COMPOSITE BEAM SECTION
 M = MOMENT FOR A COMPOSITE BEAM SECTION
 E = MODULUS OF ELASTICITY FOR A TRANSFORMED COMPOSITE SECTION
 ϵ = STRAIN IN BOTTOM FLANGE OR COVERPLATE
 A = AREA OF TRANSFORMED COMPOSITE SECTION
 S = SECTION MODULUS FOR TRANSFORMED COMPOSITE SECTION WITH RESPECT TO BRIDGE NEUTRAL AXIS AND BOTTOM FLANGE OR COVERPLATE
 f = STRESS IN BOTTOM FLANGE OR COVERPLATE
 Σ INDICATES SUM OF QUANTITIES FOR ALL COMPOSITE BRIDGE BEAMS
 SUBSCRIPT 1 INDICATES QUANTITY FOR BEAM 1

b. Force and moment fractions for Beam 1

FIGURE 55. Distribution fractions for axial force and moment

The alternate definitions of distribution fractions, in terms of strains or stresses, permit interpretation of field strain data and SAP IV stress computations. Because an eccentric post-tensioning force causes both axial force and moment, interpretation of field data or SAP IV computations for that eccentric force cannot be exact. For the model bridge, Bridge 1, and Bridge 2, approximately two-thirds of the midspan coverplate stress caused by post-tensioning was due to moment, and the remainder was due to axial force. Since the moment effect is dominant, and since relative section moduli were nearly the same as relative areas, there is little error in interpreting field-measured strains as if they were caused only by moment.

Force fractions and moment fractions will not be exact due to the portions of the deck neglected as illustrated in Figure 55. The AASHTO effective flange width rules, intended to correct for shear lag caused by bending, are only approximate, and would probably be different if intended to correct for an axial force distribution mechanism comparable to shear lag. For consistency in design computations, the effective flange width was set according to the AASHTO rules for either section modulus or area computations.

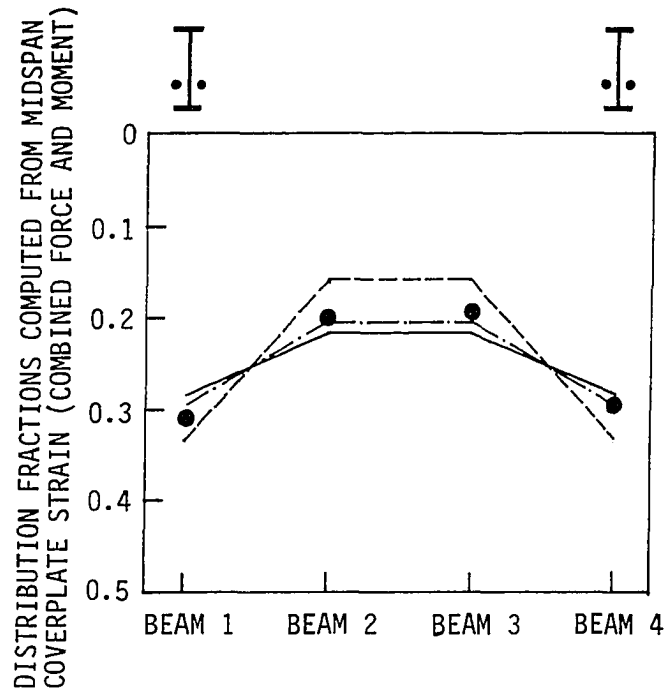
A further difficulty with force fractions is the variation in cross section of the bridge beams due to the partial-length coverplates. Because the elevation of the neutral axis of a bridge varies along the span, a force which is applied at the centroid near the support will not be axial with respect to midspan. Experiments with the SAP IV model

showed that it was impossible to obtain an undeflected shape for a bridge with partial-length coverplates or impossible to obtain purely axial forces in all bridge beams at midspan. A definition which is compatible with the purpose of the research study, and which was used for interpreting results from the composite bridge finite element model, is to apply axial forces to the bridge model at the elevation of the bridge centroid at midspan. That elevation for the axial forces is correct for most of the post-tensioned region of the bridge.

Variations among bridges will cause post-tensioning to be distributed differently from one bridge to another. Distribution factors will be more sensitive to some bridge variables than to others. In order to identify the more important variables for further study, a series of experiments were conducted with the SAP IV model.

Figure 56 illustrates the variation in post-tensioning distribution at midspan depending on end restraint for Bridge 1. Each exterior beam retains approximately 29% of the total post-tensioning effect under simple support conditions, approximately 31% of the effect under field conditions, and approximately 34% of the effect under fixed support conditions. It can be noted that the simple support distribution is conservative for the exterior beams, with respect to the actual condition.

The partial beam end restraints caused by construction details are difficult to quantify and vary from bridge to bridge. The field end restraints generally affect both post-tensioning and live load, although



CONDITION	1982 TEST	SAP IV
SIMPLE SUPPORTS		——
PARTIAL RESTRAINT	●
FIXED SUPPORTS		-----

FIGURE 56. Post-tensioning distribution at midspan for Bridge 1

not necessarily to the same degree. Since the simple support condition is easy to apply, is consistent with usual design practice, and is conservative with respect to post-tensioning distribution to the exterior beams, partial end restraint will be neglected in the determination of distribution fractions for use in design.

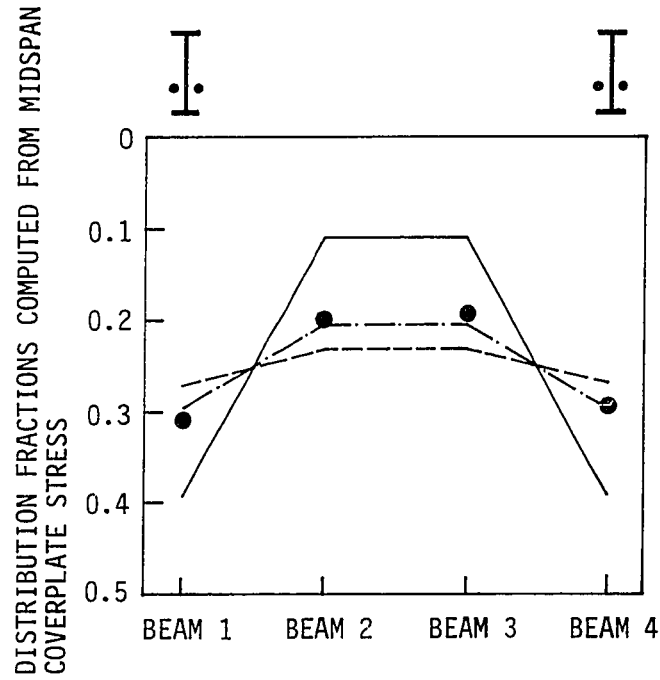
Experiments with the SAP IV model showed that shear connector stiffness, coverplate length, and crown had little effect on post-tensioning distribution. Two separate finite element analyses, one with the test load-slip value for shear connectors and one with an arbitrarily large value, gave almost identical beam stresses and deflections. Two separate analyses, one with actual-length coverplates and one with full-length coverplates differed very little in terms of post-tensioning distribution at midspan. Although crown affects the eccentricity of the post-tensioning force, crown does not affect the distribution significantly, as determined by comparing two SAP IV analyses.

Post-tensioning of the model bridge and Bridges 1 and 2 was not applied in such a manner as to examine the distribution for axial force vs. moment. Experiments with the SAP IV model, however, were quite easy to perform, and the results for Bridge 1 are given in Figure 57. The figure shows that a much greater amount of the axial force than moment remains on the exterior beams at midspan. The force fractions and moment fractions bracket the eccentric force fractions, as they should, and the eccentric force fractions are closer to the moment fractions.

There is enough difference between the force and moment fractions that they should definitely be kept separate for design.

Post-tensioning distribution is not constant over the entire post-tensioned region. At the anchorages, where post-tensioning is applied, most of the moment and axial force remains on the exterior beams. Toward midspan, however, the transverse stiffness of the deck and diaphragms cause much of the post-tensioning to be distributed to the interior of the bridge. The change in distribution, for moment applied to Bridge 1, is shown in Figure 58. As the figure indicates, near the anchorages more than 40% of the total applied moment remains with each exterior beam, but at midspan less than 30% of the moment remains. The moment distribution is relatively constant over the center half of the post-tensioned region and then changes rapidly toward the anchorages.

Two other effects are apparent in Figure 59. The greater change in distribution occurs due to change in span length for the bridge, as shown in Figure 59a. For the short span bridge with a 23.75-foot span, almost all of the applied post-tensioning moment remains on the exterior beams at midspan; whereas, for the bridge with a 71.25-foot span, the exterior beams retain less moment than is distributed to the interior beams at midspan. Given a constant span as in Figure 59b, as the anchorages are moved toward the supports, more moment is distributed away from the exterior beams. The distribution, then, appears to be highly dependent on the length of the post-tensioned region between anchorages.



APPLIED LOAD	1982 TEST	SAP IV
AXIAL FORCE		————
ECCENTRIC FORCE	●	- · - · - ·
MOMENT		-----

FIGURE 57. Force, eccentric force, and moment distribution at midspan for Bridge 1

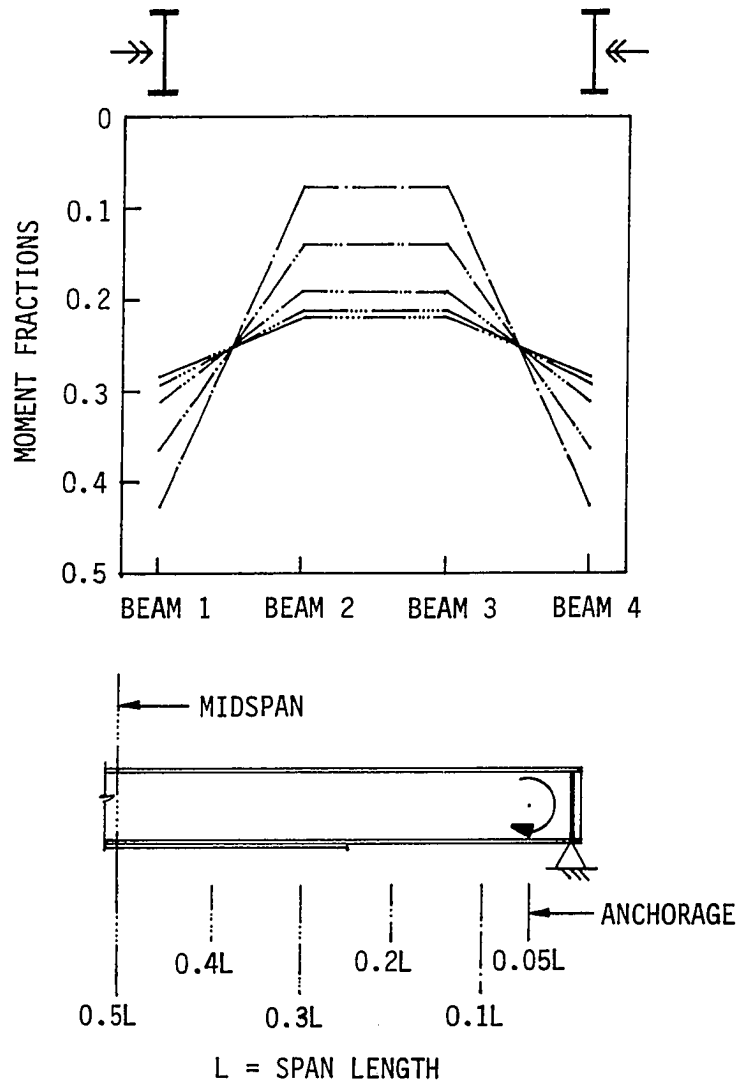
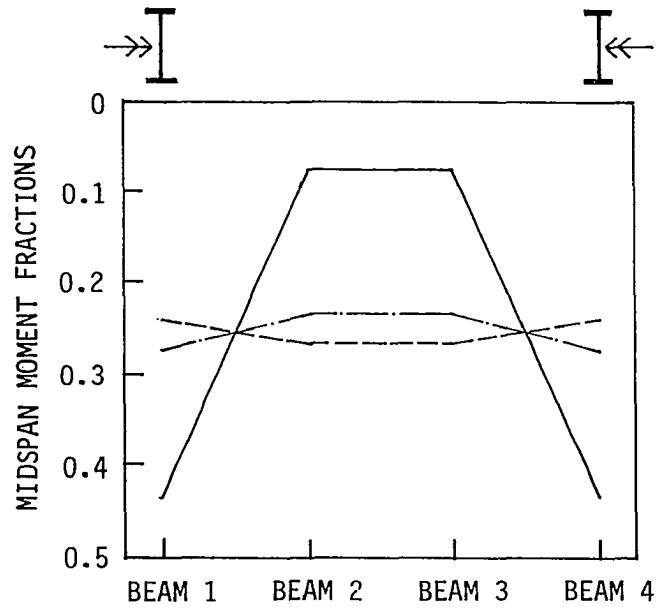
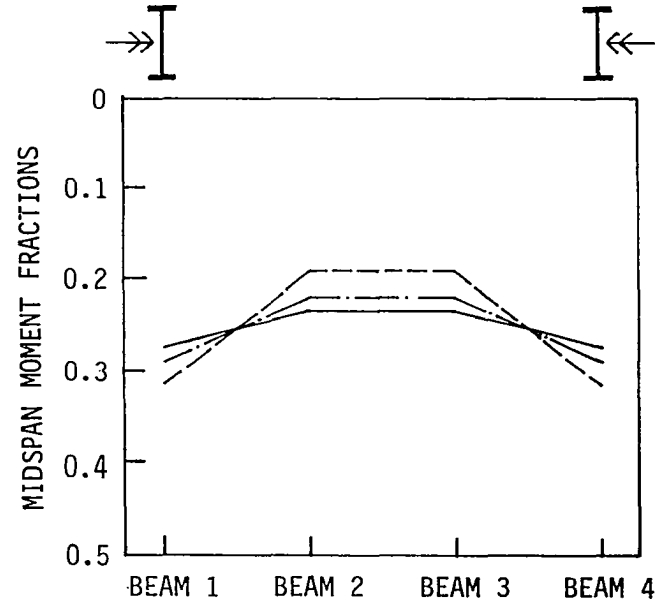


FIGURE 58. Moment distribution at selected span locations for Bridge 1



SPAN, feet	SAP IV
23.75	—————
51.25 (BRIDGE 1)	- · - · - · -
71.25	-----

a. Effect of span



ANCHORAGE LOCATION, DISTANCE FROM SUPPORT, inches	SAP IV
(SPAN = 51.25 feet, BRIDGE 1)	
45	—————
90	- · - · - · -
135	-----

b. Effect of anchorage location

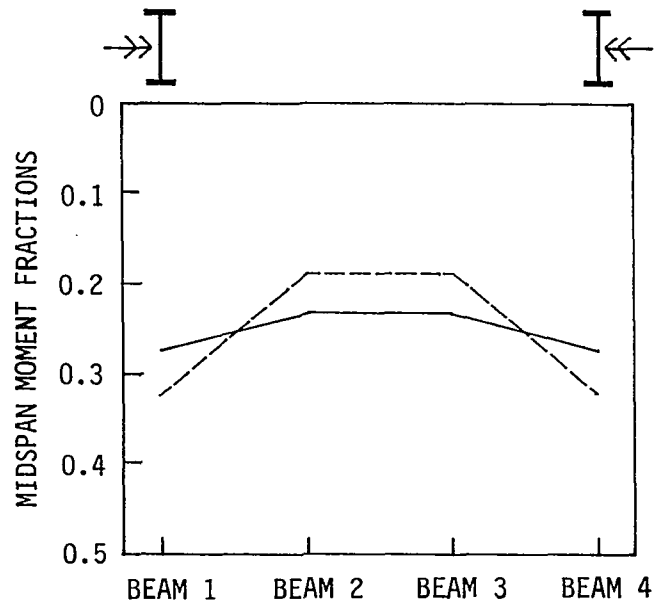
FIGURE 59. Effects of span and anchorage location on moment distribution

Stiffer exterior beams retain more post-tensioning, as shown in Figure 60a. The bridge with all steel beams of the same size [14] has larger moment fractions for exterior beams at midspan than Bridge 1 with the smaller exterior beams. Moment distribution is, therefore, dependent on relative beam stiffness.

Skew had a small effect on moment distribution at midspan. Skew tends to add end restraint to bridge beams, and the effect shown in Figure 56 for simple vs. fixed support conditions is shown again in Figure 60b for the end restraint caused by skew. The maximum effect of skew on moment distribution occurs for short spans, such as the 23.75-foot span in Figure 60b. Because the effect of skew is relatively small at the usual spans for the Iowa composite bridges in need of strengthening, and because neglecting the skew gives conservative moment distribution factors for exterior beams, the author recommends neglecting the effects of skew for skews of 45 degrees or less.

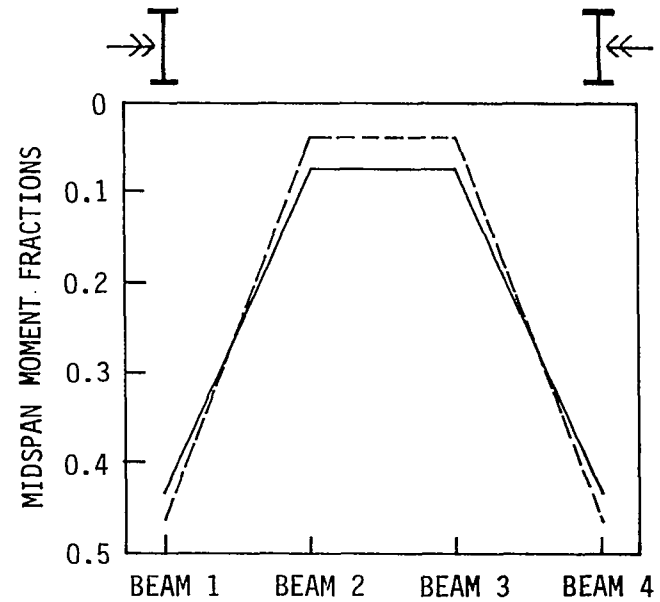
4.2. Iowa Standard Bridge Designs

The Iowa composite bridges in need of strengthening have a relatively limited range of characteristics determined by previous AASHTO bridge design specifications, by the composite bridge type, and by standard steel shapes. The plans for the bridges designed by the Iowa State Highway Commission are very consistent in terms of dimensions and details, probably because of standards established by the commission. The commission also provided standard plans to counties, which promoted



BEAM SIZE	SAP IV
EXTERIOR < INTERIOR (SPAN = 51.25 feet, BRIDGE 1)	————
EXTERIOR = INTERIOR (SPAN = 49.00 feet)	-----

a. Effect of relative beam stiffness



SKEW (SPAN = 23.75 feet)	SAP IV
0° (RIGHT ANGLE)	————
45°	-----

b. Effect of skew

FIGURE 60. Effects of relative beam stiffness and skew on moment distribution

uniformity of design. Because all of the bridge beams were wide flange sections, maximum spans were limited to 80 feet. Culverts and other bridge types were more appropriate and economical for very short spans and, consequently, the standard bridge design plans show minimum spans of 23.75 feet.

The range of three-beam and four-beam bridges to be used for developing the post-tensioning distribution fraction formulas is summarized in Table 11. The V9 series [48], for one-lane, three-beam bridges, has six standard spans which range from 23.75 feet to 80 feet. Beam spacing is set at 9.50 feet, and deck thickness without wearing surface is 6.94 inches. The bridges have integral curbs and partial-length coverplates and are designed for an H 15-44 truck. In order to provide for post-tensioning anchorages at different locations on the span, each bridge in the series was analyzed separately for anchorages at 5% and 20% of the span.

For the two-lane, four-beam bridges, there is considerably more range in the standard series and individual designs for which plans are currently available. Also, to give more range to the data on which the distribution fractions are to be based, a modern series, V15 [45], with all bridge beams of the same size, was included. The V11 series [49], V13 series [50], V15 series, and individual designs have spans which range from 23.75 to 80 feet, beam spacings which range from 7.67 to 9.69 feet, and deck thicknesses which range from 6.25 to 8.00 inches. Beams are of equal or unequal size, and beams have or do not have partial-

TABLE 11. Bridges included in multiple linear regression analysis for distribution fractions

IDOT SERIES, DATE (EARLIEST USE OF SERIES)	NUMBER OF BEAMS/ NUMBER OF LANES	SMALLER EXTERIOR BEAMS	BEAM SPACING, feet	COVER- PLATE LENGTH
V9, 1964 (1950)	3/1	yes	7.67	partial
V11, 1964 (1957)	4/2	yes	7.67	partial
V13, 1964 (1960)	4/2	yes	9.00	partial
V15, 1975 (1975)	4/2	no	9.33	no plate or partial
Individual designs, 1946 - 1948	4/2	yes	9.69	partial

^aWearing surface has been deducted from deck thickness in the table.

^bFor each bridge span there are separate SAP IV runs for the anchorage at 0.05L and 0.20L.

DECK THICKNESS ^a , inches	INTEGRAL CURBS	SPANS, L, feet	DESIGN LIVE LOAD	NUMBER OF SAP IV RUNS ^b
6.94	yes	23.75, 30, 42.5, 55, 67.5, 80	H 15-44	12
6.25	yes	23.75, 30, 42.5, 55, 67.5, 80	H 15-44	12
6.78	yes	23.75, 30, 42.5, 55, 67.5, 80	H 20-44	12
8.00	yes	23.75, 30, 42.5, 55, 67.5, 80	H 20-44	12
8.00	yes	41.25, 51.25, 71.25, 79.04	H 20-44	8

length coverplates. All bridges have low curbs integral with the bridge deck. Live loads range from an H 15-44 to an H 20-44 truck. In order to generate a range of distribution data, post-tensioning anchorages were placed separately at 5% and at 20% of the span for each four-beam bridge.

4.3. Multiple Linear Regression

Statistical Analysis System (SAS) [72], was available through the Iowa State University Computation Center and, consequently, SAS was used for all of the regression computations. The SAS procedure RSQUARE provided the coefficient of multiple determination for single bridge variables and combinations of variables. The multiple linear regression for the most promising variable combinations was performed with procedure GLM. For checking data patterns and residuals, the SAS graphics procedure PLOT was utilized with a standard line printer.

4.3.1. Bridge variables

The distribution fraction comparisons in Section 4.1 indicated that several factors caused significant changes in distribution: length of span, location of anchorage on the span, and relative beam stiffness. The comparisons also showed that deck crown, coverplate length, shear connector stiffness, and skews of 45 degrees or less had little effect on the distribution and could be neglected.

From the significant factors, several other bridge variables can be developed or inferred. The anchorage locations can be used to compute

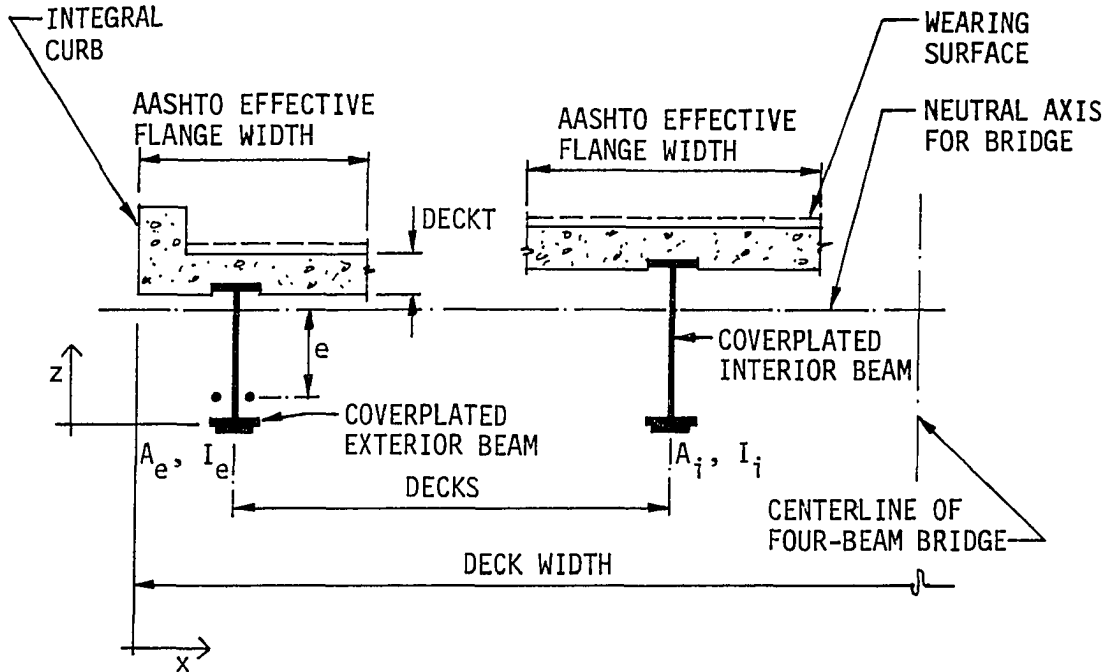
an aspect ratio which includes both the width and length of the post-tensioned region of the bridge. Relative stiffness of the bridge beams was significant for moment fractions; therefore, relative area of bridge beams could be significant for determining force fractions. Vertical live load distribution factors for the Ontario Highway Bridge Design Code [8] are based on the orthotropic plate theory flexural parameter, θ , and the torsional parameter, α ; thus these parameters also could be significant for post-tensioning distribution. A simpler variable than the orthotropic plate torsional parameter, such as a depth-span ratio for the deck, might also account for the transverse stiffness of the bridge deck.

The variables identified above as potentially significant are defined in Figure 61. In developing the multiple linear regression formulas for distribution fractions, DECKT and DECKS were treated as separate variables as well as a depth-span ratio, in order to determine the best variables for the formulas.

4.3.2. Midspan distribution fractions

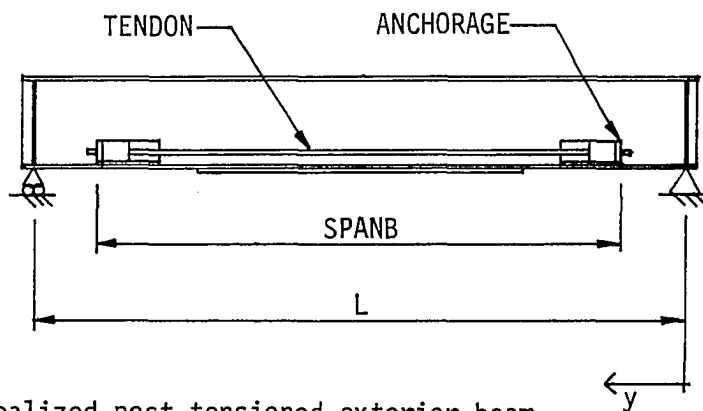
Midspan force and moment fractions were computed from SAP IV analyses of the bridges listed in Table 11; all of the potentially significant bridge variables were computed for the various bridges. From the computations, separate data sets were assembled for three-beam and four-beam bridges.

Because the form of an appropriate regression formula for each distribution fraction was unknown, many experiments with linear,



NOTE THAT SUBSCRIPT e INDICATES VARIABLE FOR EXTERIOR BEAM, AND THAT SUBSCRIPT i INDICATES VARIABLE FOR INTERIOR BEAM.

a. Idealized beam cross sections



b. Idealized post-tensioned exterior beam

FIGURE 61. Bridge variables

DECKT = THICKNESS OF BRIDGE DECK WITHOUT WEARING SURFACE, inches

DECKS = SPAN OF DECK OR BEAM SPACING, inches

SPANB = LENGTH BETWEEN TENDON ANCHORAGES, inches

AR = ASPECT RATIO = $\frac{\text{DECK WIDTH}}{\text{SPANB}}$, DIMENSIONLESS

WHERE: DECK WIDTH = WIDTH OF DECK, INCLUDING CURBS, inches

AET = $\frac{2(A_e)}{\Sigma A}$, DIMENSIONLESS

WHERE: A = TRANSFORMED AREA OF COMPOSITE BEAM, inches²

IET = $\frac{2(I_e)}{\Sigma I}$, DIMENSIONLESS

WHERE: I = MOMENT OF INERTIA OF COMPOSITE BEAM, inches⁴

THETA = FLEXURAL PARAMETER FOR ORTHOTROPIC PLATE THEORY

= $\frac{\text{DECK WIDTH}/2}{L} \sqrt[4]{\frac{i}{j}}$, DIMENSIONLESS

WHERE: L = BRIDGE SPAN, inches

i = UNIT, AVERAGE LONGITUDINAL FLEXURAL STIFFNESS

= $\frac{\Sigma I}{\text{DECK WIDTH}}$, inches³

j = UNIT, AVERAGE TRANSVERSE FLEXURAL STIFFNESS,
inches³

ALPHA = TORSIONAL PARAMETER FOR ORTHOTROPIC PLATE THEORY

= $\frac{G(i_o + j_o)}{2E\sqrt{ij}}$, DIMENSIONLESS

WHERE: E = MODULUS OF ELASTICITY, ksi

G = MODULUS OF RIGIDITY, ksi

i_o = UNIT, AVERAGE DECK TORSIONAL STIFFNESS
WITH RESPECT TO LONGITUDINAL DIRECTION, inches³

j_o = UNIT, AVERAGE TORSIONAL STIFFNESS FOR DECK AND
DIAPHRAGMS WITH RESPECT TO TRANSVERSE DIRECTION
inches³

c. Variable definitions

FIGURE 61 (Continued)

product, logarithmic, and exponential terms were tried. The most effective technique for developing the regression formulas proved to be transformation of each independent bridge variable by means of a ladder of powers for transformations [16]. If a plot of a distribution fraction vs. an independent variable exhibited a curve, the curve was straightened by re-expressing the independent variable to some power other than one.

An example of the re-expression of one of the bridge variables is illustrated in Figure 62. When the moment fraction for four-beam bridges was plotted against the variable AR, the data points showed a definite bulge toward the upper left, as indicated by the dotted line in the figure. However, when the moment fraction was plotted against the variable AR expressed to the $-1/2$ power, the data points follow the straight line drawn in the figure. The coefficient of multiple determination for the re-expressed variable also is greater than the coefficient for the original variable.

The magnitude of the improvement in the coefficient of multiple determination and, therefore, the fit of the regression, is indicated in Figure 63. In the figure, the results from several SAS RSQUARE runs are graphed for four-beam bridge moment fractions and force fractions. Linearizing the bridge variables by power transformations increases the coefficient of multiple determination by about 10% for regression models containing one or two variables and by smaller percentages for models with more variables. The figure also shows that using more than three

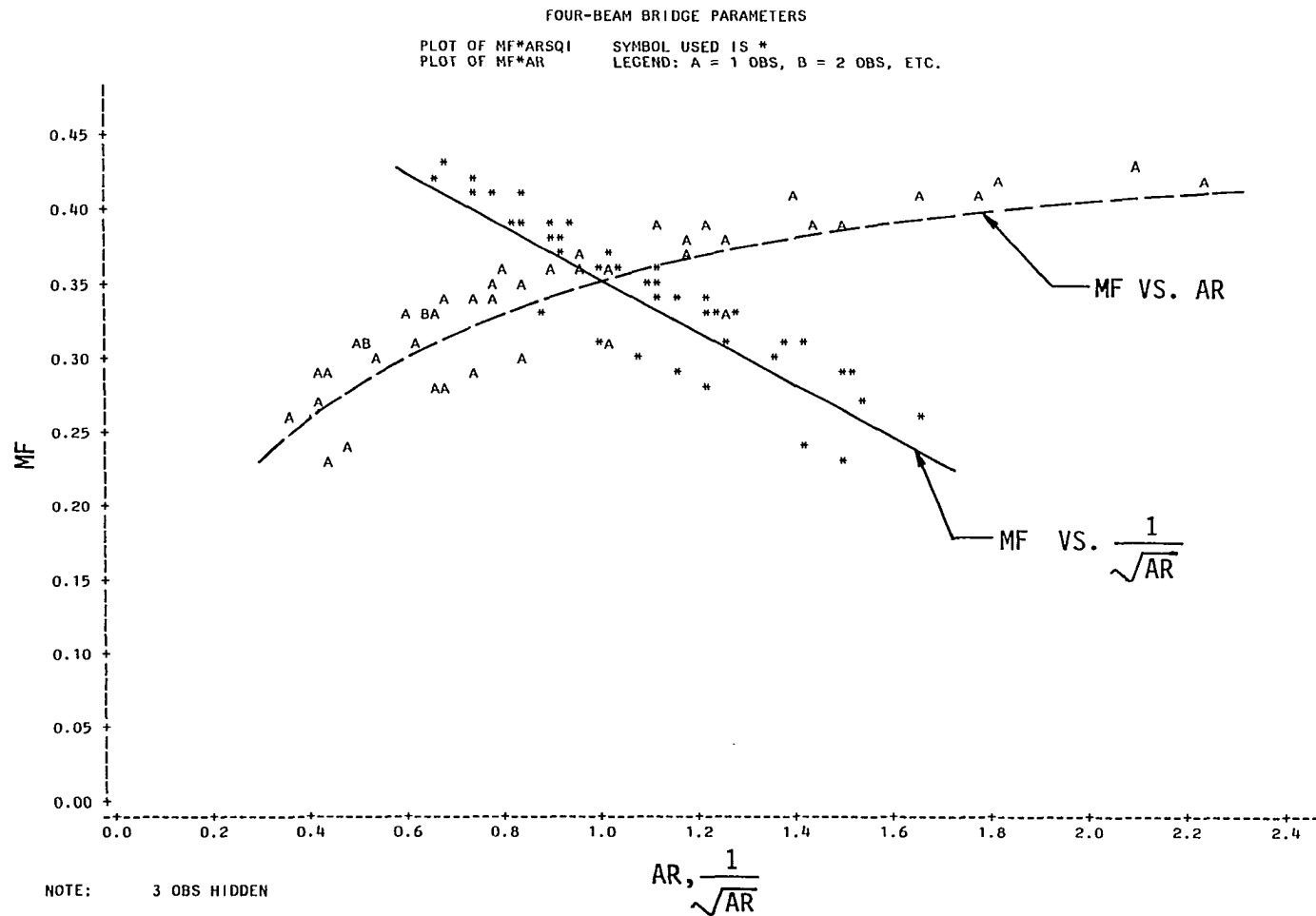


FIGURE 62. Transformation for aspect ratio vs. moment fractions for four-beam bridges

independent variables in the regression model for a four-beam bridge distribution fraction is not effective in improving the fit of the model to the data.

4.3.2.1. Three-beam bridges In developing the multiple linear regression formulas, the objectives were to achieve a coefficient of multiple determination of at least 0.95, to minimize the number of variables in each formula, and to have as much consistency as possible among the three-beam and four-beam bridge formulas. Both of the distribution fraction formulas for three-beam bridges in Figure 64 have coefficients of multiple determination of 0.98 or greater, and each formula uses only two variables, one of which is the same for both formulas. Comparisons of coefficients of partial determination indicated that THETA explained more of the variation in the force fraction than AR, and that AR explained more of the variation in the moment fraction than IET.

According to the coefficients of multiple determination and the error ranges, the formula for the moment fraction is more accurate, a desirable situation since eccentric post-tensioning forces typically create more bending moment stress than axial force stress. Scatter plots of residuals vs. predicted values and residuals vs. each of the regression variables showed no consistent patterns. The lack of patterns gives a favorable check on the regression models. The analysis of variance tables provided with the SAS GLM procedure showed that the independent variables contributed significantly to the models, which gives another favorable check on the regression models.

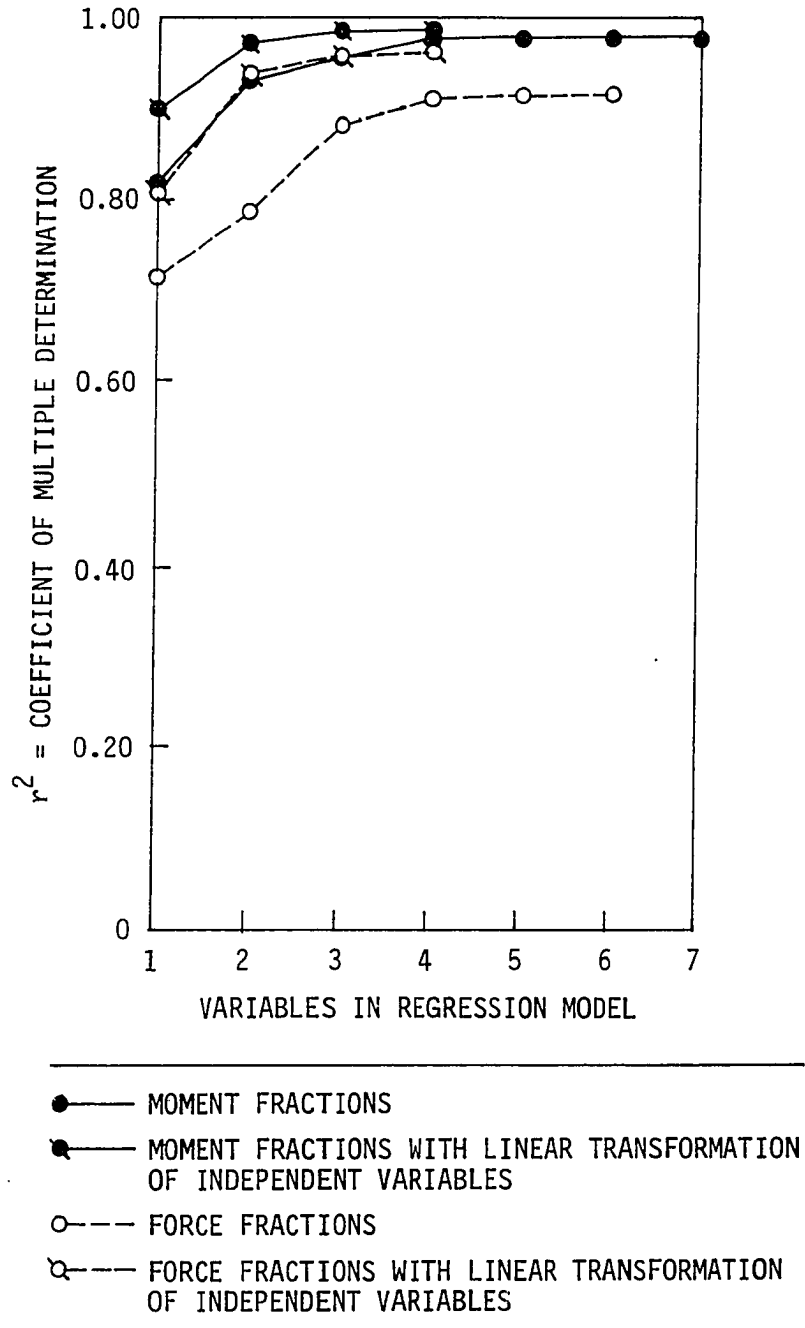
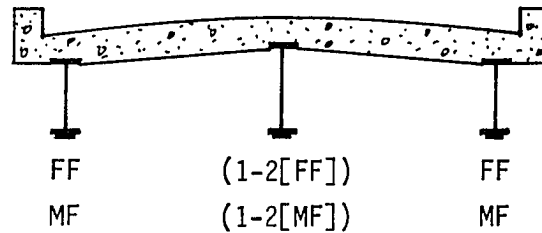


FIGURE 63. Multiple linear regression models for four-beam bridge distribution fractions



$$FF = 0.741 - 0.175 \frac{1}{\sqrt{\text{THETA}}} - 0.0624 \frac{1}{\sqrt{AR}}$$

$$r^2 = 0.986, \text{ ERROR RANGE } +2\%, -3\%$$

$$MF = 0.816 - 0.245 \frac{1}{\sqrt{IET}} - 0.0755 \frac{1}{\sqrt{AR}}$$

$$r^2 = 0.991, \text{ ERROR RANGE } +2\%, -2\%$$

RANGES OF REGRESSION $0.417 \leq \text{THETA} \leq 0.893$
 VARIABLES: $0.456 \leq \text{IET} \leq 0.571$
 $0.306 \leq \text{AR} \leq 1.544$

NEGATIVE ERROR RANGE INDICATES THAT SAP IV VALUE IS LESS THAN REGRESSION FORMULA-PREDICTED VALUE.

VARIABLES ARE DEFINED IN FIGURE 61.

r^2 = COEFFICIENT OF MULTIPLE DETERMINATION

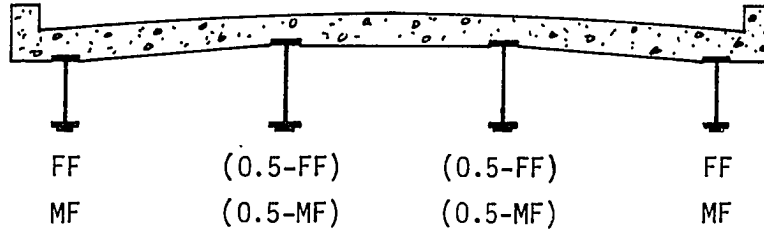
FIGURE 64. Midspan distribution fractions for three-beam bridges

The formulas in Figure 64 are then appropriate for the Iowa DOT V9 series of standard bridge designs. The formulas may also be appropriate for other bridges which have similar details, regression variables which fall within the ranges given at the bottom of the figure, and which have similar deck thickness to span ratios. The formulas are not likely to be accurate, however, for bridges which have regression variables beyond the ranges given.

4.3.2.2. Four-beam bridges The formulas for four-beam bridge distribution fractions in Figure 65 require an additional regression variable, the ratio of the deck thickness to span, for accuracy. For the four-beam bridges, the range of data is much more extensive than for the three-beam bridges and, therefore, there is need for an additional variable. Comparisons of coefficients of partial determination indicated that THETA explained more of the variation in the force fraction than other variables, and that AR explained more of the variation in the moment fraction than other variables.

Based on the coefficients of multiple determination and error ranges, the moment fraction formula again is the more accurate of the two formulas. Scatter plots showed no patterns, and analysis of variance tables indicated that the independent variables contributed significantly to the regression models.

The distribution fraction formulas should be used only for bridges for which the regression variables fall within the ranges listed at the bottom of Figure 65. To be conservative during design, the negative



$$FF = 0.605 - 0.323 \frac{1}{\sqrt{\text{THETA}}} - 0.0720 \frac{1}{\sqrt{\text{AR}}} + 3.87 \frac{\text{DECKT}}{\text{DECKS}}$$

$r^2 = 0.954$, ERROR RANGE +9%, -6%

$$MF = 0.963 - 0.221 \frac{1}{\sqrt{\text{IET}}} - 0.145 \frac{1}{\sqrt{\text{AR}}} - 2.18 \frac{\text{DECKT}}{\text{DECKS}}$$

$r^2 = 0.983$, ERROR RANGE +4%, -7%

RANGES OF REGRESSION	0.516	≤	THETA	≤	1.329
VARIABLES:	0.379	≤	IET	≤	0.600
	0.361	≤	AR	≤	2.246
	6.25	≤	DECKT	≤	8.00
	92.00	≤	DECKS	≤	116.25

NEGATIVE ERROR RANGE INDICATES THAT SAP IV VALUE IS LESS THAN REGRESSION FORMULA-PREDICTED VALUE.

VARIABLES ARE DEFINED IN FIGURE 61.

r^2 = COEFFICIENT OF MULTIPLE DETERMINATION

FIGURE 65. Midspan distribution fractions for four-beam bridges

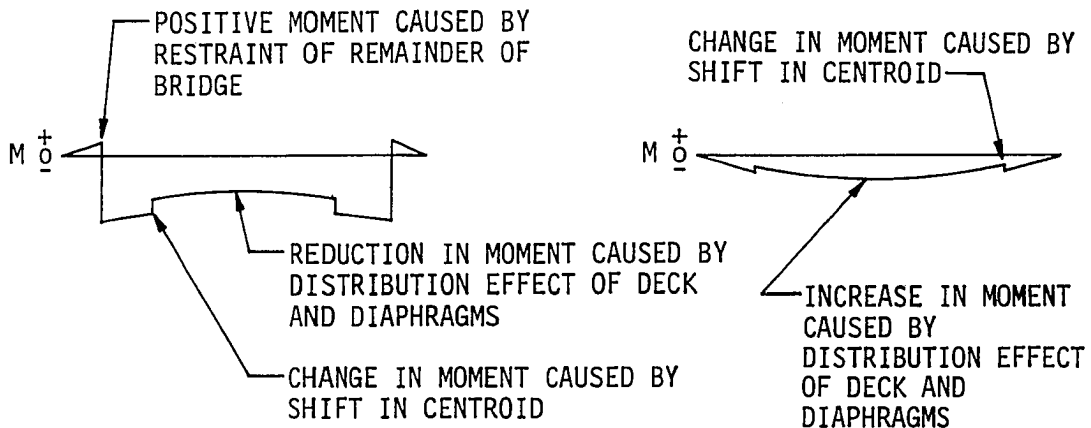
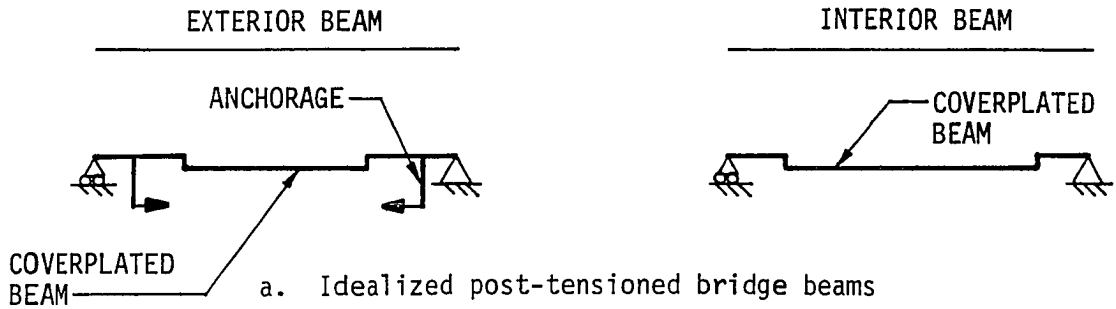
error ranges can be used to increase the required post-tensioning, in order to compensate for the potential error between the formulas and the SAP IV analyses. The computed moment fraction, for example, can be reduced by 7%, or the 7% can be treated as a post-tensioning loss during design.

4.4. Distribution Fraction Interpolation and Verification

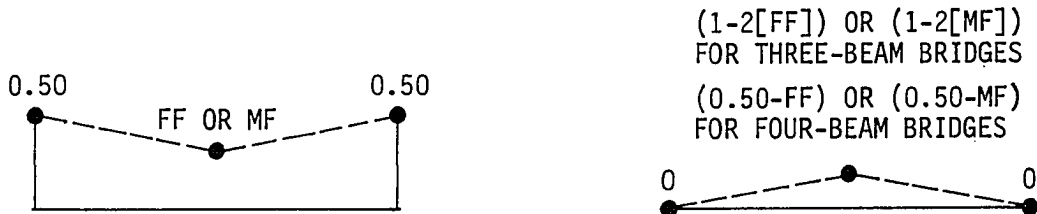
The distribution fractions computed from the regression formulas apply only at midspan. Original design of the Iowa composite bridges required checks of flexural stresses at midspan and at coverplate cutoffs. For the design of post-tensioning, a check of the stresses at the anchorage is required. Thus, there is need for distribution fractions at several locations on the bridge span.

The general distribution of the post-tensioning moment (which is similar to the distribution of axial force) is illustrated in Figure 66b for exterior and interior beams. The moment applied to the exterior beam at the anchorage does not remain constant within the post-tensioned length. The moment varies for two reasons: the coverplate on the exterior beam causes a downward shift in neutral axis, thereby reducing the eccentricity of the post-tensioning force, and the transverse stiffness of the bridge deck and diaphragms causes moment to be gradually shifted from the exterior beam to the interior beam.

In order to account for the change in force fractions and moment fractions for design purposes, the linear interpolation in Figure 66c is



b. Moment diagrams



FF = FORCE FRACTION FROM FIGURE 64 FOR THREE-BEAM BRIDGES
OR FROM FIGURE 65 FOR FOUR-BEAM BRIDGES

MF = MOMENT FRACTION FROM FIGURE 64 FOR THREE-BEAM BRIDGES
OR FROM FIGURE 65 FOR FOUR-BEAM BRIDGES

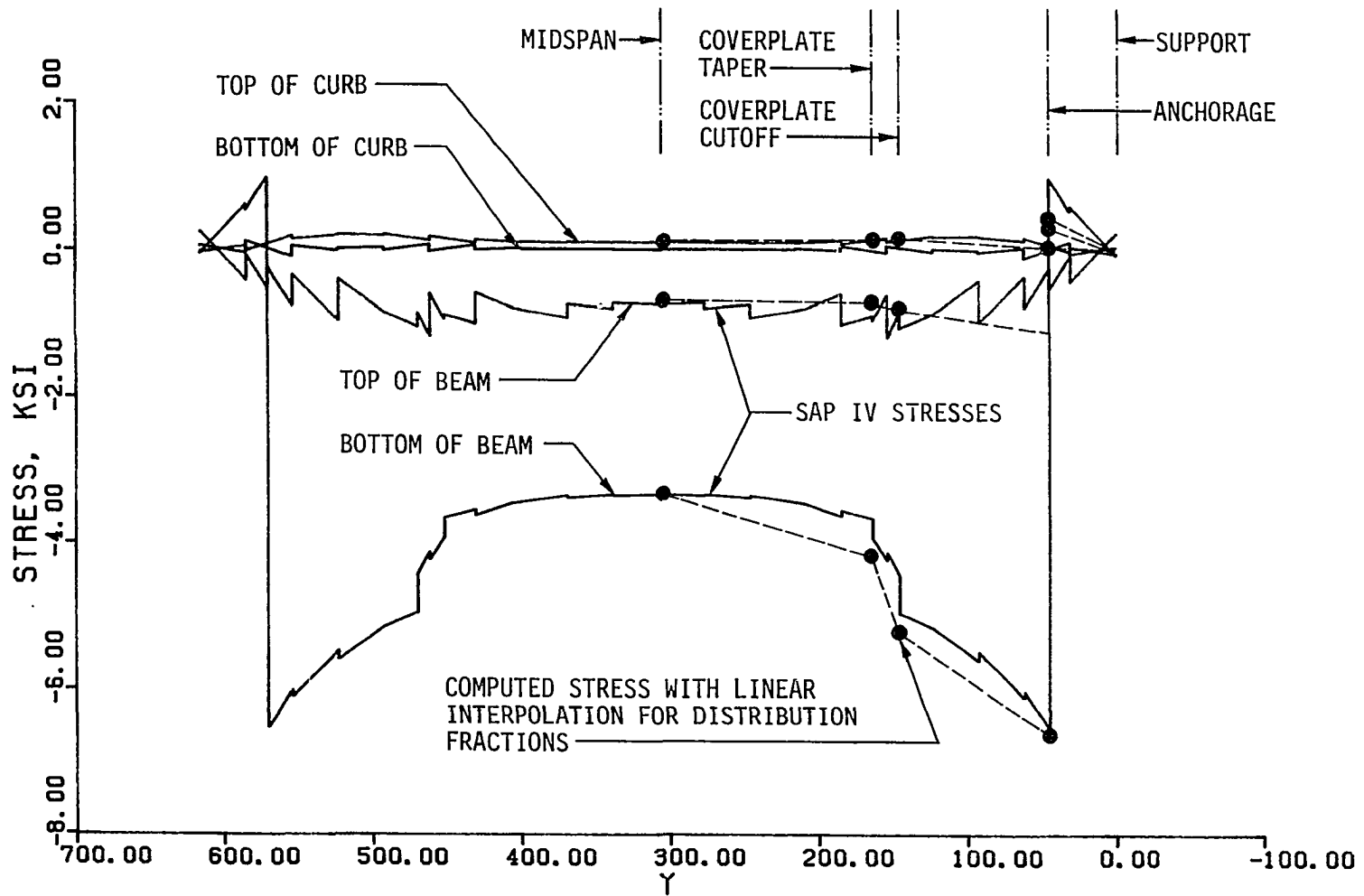
c. Linear interpolation for distribution fractions

FIGURE 66. Interpolation for distribution fractions at locations other than midspan

recommended. Because the beam supports are used for known distribution fractions of 0.5 for the exterior beam and 0 for the interior beam, the anchorage locations are independent of the interpolation, an advantage during design. Using the supports for known points also partially accounts for the small positive moments between anchorages and supports for the exterior beam.

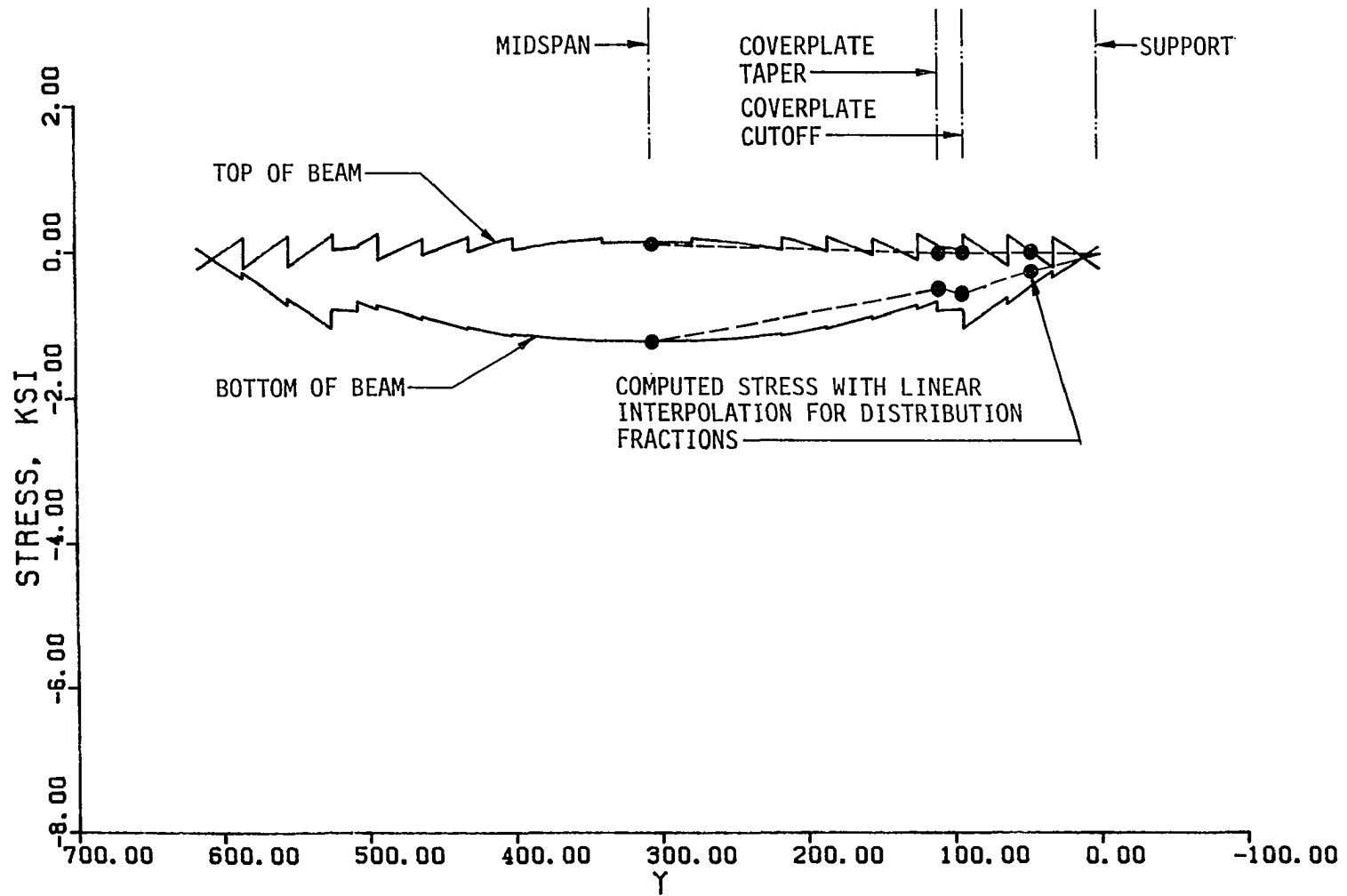
The accuracy of the distribution fractions and the interpolation is evident in Figure 67. Figure 67a is plotted for the SAP IV stresses at top and bottom of curb and at top and bottom of beam or coverplate for the exterior beam. Figure 67b is plotted for the SAP IV stresses at the top and bottom of the beam or coverplate for the interior beam. The especially jagged nature of the SAP IV beam stresses is caused by the shear connector assemblies. Those assemblies take part of the moment at each beam node and, therefore, there is a discrepancy between the moments on either side of the node.

Superimposed on the SAP IV stresses for Bridge 1 are the stresses computed using classical beam theory with distribution fractions from the regression formulas and interpolations. As the figure shows, the SAP IV and classical beam theory stresses are in excellent agreement at midspan and at the exterior beam anchorage. At the coverplate taper and cutoff for the exterior beam, the interpolation procedure causes the classical beam theory stresses to be unconservative by about 10%. In general, the distribution fraction formulas and linear interpolation give stresses which compare well with a SAP IV analysis for Bridge 1.



a. Exterior beam and curb stresses

FIGURE 67. Stresses for Bridge 1 with post-tensioning of 100 kips on each exterior beam



b. Interior beam stresses

FIGURE 67 (Continued)

5. DESIGN METHODOLOGY

The midspan distribution fractions and interpolation procedures developed in Chapter 4 provide the information required for designing the post-tensioning for strengthening the Iowa composite bridges. The distribution fractions and interpolation procedures give the information in a simplified form, which does not require extensive analysis by the designer. Because the rating and design of bridges must meet AASHTO specifications, the suggested design procedure and the design example contained in this chapter have been developed to be compatible with those specifications. The distribution fractions are based on the elastic behavior of composite bridges and, therefore, all procedures and computations given in this chapter are for the AASHTO Service Load Design Method [3].

5.1. Design Procedure

The design procedure outlined below provides a framework for organizing the bridge strengthening computations. Dead, long-term dead, and live plus impact stresses are computed with individual, isolated beam section properties, in accordance with usual rating and design practice. Post-tensioning forces and stresses, however, are computed with composite beam properties referenced to the neutral axis for the bridge.

The post-tensioning design requires checks of the bending stresses at several locations on the span. The tables of moments for 1980 Iowa

DOT rating trucks, an H 20-44 truck, and an HS 20-44 truck given in the appendix to Reference 29 aid considerably in making the bending stress checks. Post-tensioning anchorage brackets of several configurations were tested during the feasibility part of the research program, and those bracket tests are described in Reference 55. The final bracket configurations for Bridges 1 and 2 are given in Reference 54. If existing shear connectors are inadequate, additional shear connector capacity may be gained by installing high strength bolt connectors as described in Reference 54.

For the post-tensioning design, the following procedure is recommended; references are noted for live loads, post-tensioning brackets, and shear connectors:

1. Determine all loads and load fractions for dead load, long-term dead load, impact load, and live load for both exterior and interior beams.
2. Compute moments for dead load, long-term dead load, and live load plus impact [29] at midspan, coverplate cutoffs, and approximate anchorage location (only for exterior beams) for exterior and interior beams.
3. Compute section properties for steel beam, steel beam with coverplate, composite beam, composite beam with coverplate, composite beam with concrete creep, and composite beam with coverplate and concrete creep for exterior and interior beams. Also compute section properties for composite beam

and composite beam with coverplate for exterior and interior beams with respect to the bridge neutral axis at several locations, as required by the coverplate configuration.

4. Compute tension stress to be removed by post-tensioning at midspan of exterior beam. Determine approximate tendon elevation. Compute force and moment fractions. (Figures 64, 65 and 66) Solve for P, the total post-tensioning force for the bridge, using:

$$f_b = FF \frac{P}{A} + MF \frac{Pec}{I}$$

Select tendons, and account for losses in determining tendon forces to be specified.

5. Check stresses at top of curb, top of deck, top of beam, and bottom of beam or coverplate at midspan, coverplate cutoff, and bracket (only for exterior beam) for exterior beam and interior beam.
6. Design brackets and anchorages [54,55].
7. Check other design factors such as beam shear, shear connectors [54], deflection, fatigue, and beam strength.

5.2. Design Example

The design example given here is summarized from the example in Reference 29. More detailed computations for loads, wheel load distribution fractions, moments, section properties, effective flange

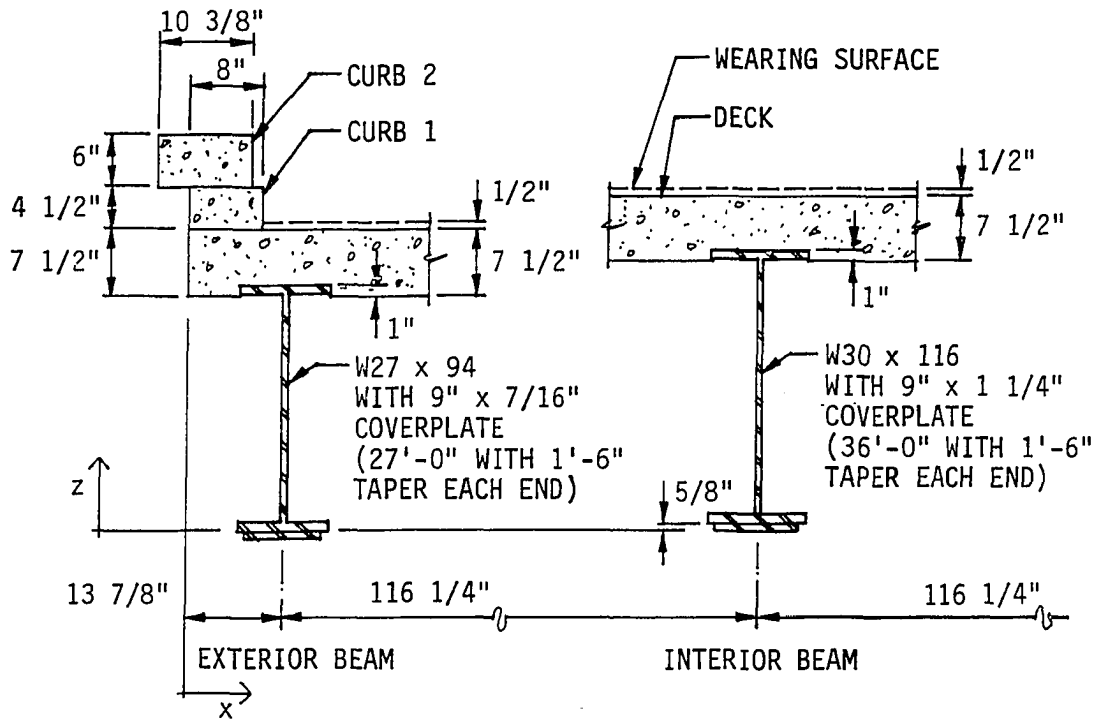
widths, distribution fractions, post-tensioning losses, and stresses are contained in the reference.

5.2.1. Bridge description

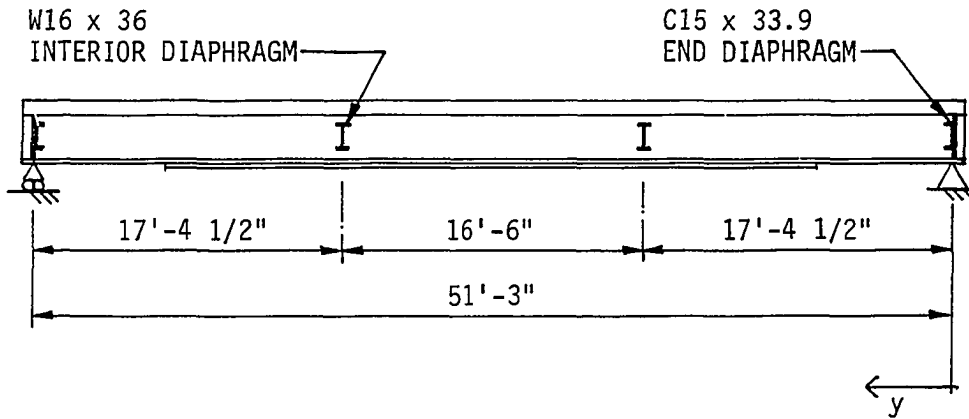
The design example is for the strengthening of Bridge 1, a single-span, two-lane, four-beam bridge. Several of the original plan drawings are given in Figure 1, and other drawings and specifications are given in Figure 20 and Reference 54. The transverse and longitudinal sections for the bridge are idealized in Figure 68. The curb cross section is idealized as two rectangles. The deck is assumed to be of 3000 psi concrete. The deck is adjusted to be level with respect to each of the steel beams, and the 1/2-inch wearing surface is removed from the deck. Steel sections and coverplates are assumed to be of A7 steel with a yield point of 33 ksi. Properties for the steel sections will be taken from Reference 5.

The composite bridge is to be strengthened to meet the current legal load standards for Iowa. Live load moments will be interpolated from the table for maximum moments for 1980 Iowa DOT rating trucks in the appendix to Reference 29. Wheel load distribution fractions, impact load fraction, dead loads, and dead load moments will be computed in accordance with the AASHTO bridge design specifications [3].

For the post-tensioning, threadbars [30] with an ultimate strength of 150 ksi will be selected for the tendons. Experience has shown that the tendon anchorages should be at about 7% and 93% of the span, and that brackets will be about 2 feet in length. High strength bolts of



a. Idealized transverse section



b. Idealized longitudinal section

FIGURE 68. Four-beam composite bridge (Bridge 1)

1-inch diameter will be used for attachment of brackets to exterior beams.

5.2.2. Loads and load distribution fractions

Dead loads and long-term dead loads are summarized in Table 12. Dead loads are those loads applied to the steel bridge beams, whereas long-term dead loads are those loads applied to the composite bridge. As permitted by the AASHTO bridge design specifications [3], the long-term dead loads are distributed equally to all beams.

According to the AASHTO specifications, live loads are to be increased by an impact fraction. Computations for Bridge 1 show that fraction to be 0.284. Exterior beam wheel load fractions are to be computed as the larger of the load fraction for a simple beam condition and the load fraction from an AASHTO formula. The larger fraction, from the formula, is 1.51. For the interior beam, the AASHTO wheel load fraction formula gives 1.76. Although the AASHTO bridge design specifications require that an exterior beam have at least the carrying capacity of an interior beam, it is the author's interpretation that the rule refers to future widening rather than strengthening. Consequently, the exterior beam wheel load fraction will be taken as 1.51.

5.2.3. Moments

The post-tensioning design stress and stress checks at critical locations require moments at midspan and coverplate cutoff points for exterior and interior beams, and at post-tensioning anchorages for

TABLE 12. Dead and long-term dead loads

BRIDGE PART	EXTERIOR BEAM		INTERIOR BEAM	
	DEAD LOAD	LONG-TERM DEAD LOAD	DEAD LOAD	LONG-TERM DEAD LOAD
	plf	plf	plf	plf
Steel beam	94		116	
Steel coverplate (assumed full length)	13		38	
Steel shear connectors (average)	2		3	
Reinforced concrete deck	600		969	
Reinforced concrete curb	98		-	
Steel interior diaphragms (average for central portion of span)	10		21	
Steel rail (average)	48		-	
Steel tendons and brackets ^a (estimated average)		8		8
Future wearing surface (19 psf) ^a		143		143
Total dead load	865		1147	
Total long-term dead load		151		151

^aLong-term dead loads are distributed equally to all beams as permitted by the AASHTO bridge design specifications [3].

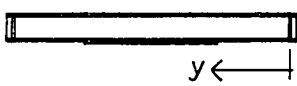
exterior beams. Exterior and interior beam coverplates for Bridge 1 have different lengths and, therefore, the coverplate cutoff points are not the same for all beams. The anchorage location, based on previous experience, is approximately 7% of the span, which is 3.59 feet for Bridge 1. In order to give some flexibility for subsequent computations for bracket locations, moments will be computed at 2 feet and 6 feet from the support.

Dead load and long-term dead load moments are computed from standard formulas, and live load moments are based on the AASHTO impact fraction, AASHTO wheel load distribution fractions, and the 1980 Iowa DOT rating truck moment tables in the appendix to Reference 29. Maximum truck load moments, although they actually occur a few feet from midspan, are conservatively assumed to act at midspan. Moments at the various critical locations are summarized for the exterior bridge beam in Table 13, and the moments for the interior bridge beam are summarized in Table 14.

5.2.4. Section properties

For computing the section properties for composite beams, the modular ratio, n , will be taken to be 9, as required by the AASHTO bridge design specifications for concrete with a strength of 3000 psi. Effects of creep on the composite section for long-term dead load will be considered by taking n as 27, three times the usual value, as required by the AASHTO specifications. Areas, centroid locations, and moments of inertia are then computed with concrete deck and curbs transformed or reduced by the appropriate modular ratio.

TABLE 13. Dead, long-term dead, and live load moments for exterior beam



LOCATION	y ft	LOAD	MOMENT ft-kips
Midspan	25.625	dead	284.00
		long-term dead	49.58
		live plus impact ^a	534.73
Coverplate cutoff ^b	13.625	dead	221.77
		long-term dead	38.71
		live plus impact ^a	430.71
Anchorage (estimate plus approximately 2 feet)	6.000	dead	117.42
		long-term dead	20.50
		live plus impact ^a	244.62
Anchorage (estimate minus approximately 2 feet)	2.000	dead	42.60
		long-term dead	7.44
		live plus impact ^a	93.65

^a1980 Iowa DOT rating truck load moment is interpolated from Table A-1 in Reference 29. An impact fraction of 0.284 and a wheel load fraction of 1.51 are computed according to AASHTO bridge design specifications [3].

^bCoverplate cutoff is taken to be at the end of the full width plate.

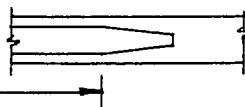
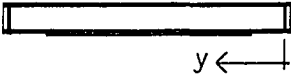


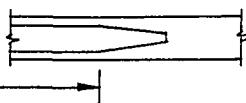
TABLE 14. Dead, long-term dead, and live load moments for interior beam



LOCATION	y ft	LOAD	MOMENT ft-kips
Midspan	25.625	dead	376.58
		long-term dead	49.58
		live plus impact ^a	623.26
Coverplate cutoff ^b	9.125	dead	220.54
		long-term dead	29.03
		live plus impact ^a	385.78

^a1980 Iowa DOT rating truck load moment is interpolated from Table A-1 in Reference 29. An impact fraction of 0.284 and a wheel load fraction of 1.76 are computed according to the AASHTO bridge design specifications [3].

^bCoverplate cutoff is taken to be at the end of the full width plate.



The exterior beam is not at the edge of the deck and therefore may be considered to have a flange on both sides. Based on the AASHTO specifications, the effective flange width is to be taken as the smallest of widths computed from simple rules based on beam span, beam spacing, and deck thickness. For the exterior beam, the width based on deck thickness controls, and the width is 58.88 inches. Areas, centroid elevations, and moments of inertia computed for the exterior beam are summarized in Table 15.

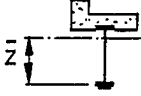
The AASHTO rules for effective flange width for interior beams give the width as 90.00 inches. Areas, centroid elevations, and moments of inertia for an interior beam are summarized in Table 16.

Centroid elevations and moments of inertia with respect to the neutral axis of the bridge are listed in Table 17. For Bridge 1, neutral axis elevations for exterior and interior beams and for the bridge fall within a relatively narrow range. With different curb and crown configurations, however, the neutral axis elevations can have more variation, and the recomputation of the moments of inertia with respect to the neutral axis for the bridge would have more significance.

5.2.5. Post-tensioning design

For several reasons -- because the exterior beam is the critical member; because more post-tensioning is required at midspan due to the larger, coverplated beam; and because more post-tensioning is distributed away from the exterior beam at midspan -- computation of the required post-tensioning force can be based on the exterior beam's

TABLE 15. Section properties for exterior beam

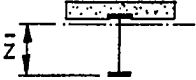


The diagram shows a cross-section of an exterior beam. It consists of a vertical web and a horizontal flange. A horizontal dashed line represents the centroidal axis, and a vertical arrow labeled \bar{z} indicates the distance from the top surface of the flange to this centroidal axis.

DESCRIPTION	A = AREA ^a in ²	\bar{z} = CENTROID ELEVATION ^a in	$I_{\bar{z}}$ = MOMENT OF INERTIA ^a in ⁴
Steel beam	27.65	13.46	3266.70
Steel beam with coverplate	31.59	11.75	3915.64
Composite beam with deck and curb, n = 9	87.64	25.71	10,438.91
Composite beam with deck, curb, and coverplate, n = 9	91.58	24.60	12,949.70
Composite beam with deck and curb, n = 27	47.65	20.97	7357.81
Composite beam with deck, curb, and coverplate, n = 27	51.59	19.35	8995.94

^aEffective flange width of 58.88 inches (based on deck thickness without wearing surface) is computed according to the AASHTO bridge design specifications [3]. See Reference 29 for computations.

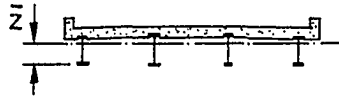
TABLE 16. Section properties for interior beam



DESCRIPTION	A = AREA ^a in ²	\bar{z} = CENTROID ELEVATION ^a in	$I_{\bar{z}}$ = MOMENT OF INERTIA ^a in ⁴
Steel beam	34.13	15.63	4919.10
Steel beam with coverplate	45.38	11.76	6998.58
Composite beam with deck, n = 9	109.13	27.83	12,653.18
Composite beam with deck and coverplate, n = 9	120.38	25.23	20,564.68
Composite beam with deck, n = 27	59.13	23.13	9595.38
Composite beam with deck and coverplate, n = 27	70.38	19.44	14,649.77

^aEffective flange width of 90.00 inches (based on deck thickness without wearing surface) is computed according to the AASHTO bridge design specifications [3]. See Reference 29 for computations.

TABLE 17. Section properties with respect to composite bridge neutral axis



BRIDGE BEAM CONDITION, n = 9	\bar{z} = BRIDGE CENTROID ELEVATION in	$I_{\bar{z}}$ = MOMENT OF INERTIA FOR BEAM WITH RESPECT TO BRIDGE NEUTRAL AXIS in ⁴	
		EXTERIOR BEAM	INTERIOR BEAM
Coverplates on all beams	24.95	12,960.92	20,574.12
Coverplates on interior beams only	25.43	10,445.78	20,569.50
No coverplates	26.89	10,560.94	12,749.61

flexural tension stress at midspan. In Table 18, when the total computed tension stress of 24.33 ksi is compared with the AASHTO allowable inventory stress [2] of 18 ksi, the difference, an overstress of 6.33 ksi, is the stress which must be relieved by post-tensioning.

In order to determine the required post-tensioning force, it is necessary to assume tendon elevation and anchorage locations. If the tendons are placed above the bottom flange of the exterior beam, but as close to the flange as possible, the size of the jacking cylinder must be considered. One brand of hollow-core hydraulic cylinder with a capacity of 120 kips has a diameter of 6 1/4 inches. With a 1/8-inch clearance, the tendons can be placed 3 1/4 inches above the bottom flange, as diagrammed in Figure 69. The eccentricity of the post-tensioning force then will be 20.95 inches.

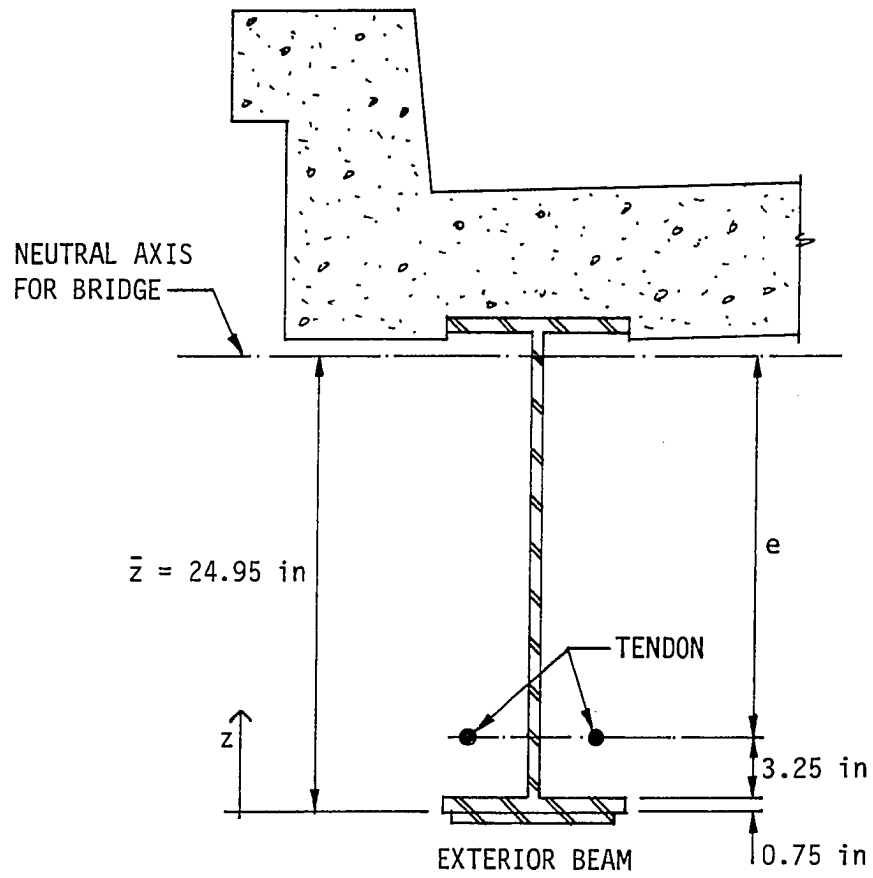
With the previous assumption that the anchorages will be located at 7% and 93% of the span, sufficient information is available to compute the distribution fractions at midspan, and interpolate for the fractions at the coverplate cutoffs. Computed bridge variables and distribution fractions are given in Table 19. All of the bridge variables fall within the variable ranges for the midspan distribution fraction formulas determined by multiple linear regression. The force fraction for the exterior beam is larger than the moment fraction for the beam, as is typically the case.

Because the tension stress to be relieved, distribution fractions, section properties, and eccentricity of post-tensioning force are either

TABLE 18. Tension stresses in exterior beam coverplate at midspan

STRESS CONDITION	TENSION STRESS ksi
Dead load	10.61
Long-term dead load	1.31 ^a
Live plus impact load	12.41
Total computed	24.33
Allowable	18.00
Overstress to be relieved by post-tensioning	6.33

^aUse of section properties for $n = 9$ gives a smaller stress.



$$e = 24.95 - 0.75 - 3.25 = 20.95 \text{ in}$$

FIGURE 69. Tendon elevation and eccentricity

TABLE 19. Distribution fractions

BRIDGE VARIABLES ^a		
$i = 178.14 \text{ in}^3$		
$j = 6.10 \text{ in}^3$		
THETA = 0.712		
AR = 0.712		
$\frac{\text{DECKT}}{\text{DECKS}} = 0.0645$		
IET = 0.386		
LOCATION	FF	MF
Exterior beam, midspan	0.39 ^b	0.29 ^b
Exterior beam, coverplate cutoff	0.44 ^c	0.39 ^c
Interior beam, midspan	0.11	0.21
Interior beam, coverplate cutoff	0.04 ^c	0.07 ^c

^aVariables are computed from definitions given in Figure 61.

^bDistribution fractions for exterior beam at midspan are computed from formulas in Figure 65.

^cDistribution fractions at coverplate cutoffs are interpolated on the basis of Figure 66c.

known or assumed, the required post-tensioning forces can be computed as outlined in Table 20. P , the total post-tensioning force for the bridge, is computed as 392 kips, and P_e , the post-tensioning force for each exterior beam, is simply half of the total force for the bridge.

Due to potential error in the distribution fraction formulas, post-tensioning losses, and the ΔT effect, the force applied to the tendons for each exterior beam should be adjusted. For the distribution fraction formulas, there is a potential, unconservative error of 6% for the force fractions and 7% for the moment fractions (Figure 65). In Table 20, the error is conservatively taken as 7%.

Relaxation loss for the threadbar tendons stressed to 60% of ultimate strength for 57 years is 3.7% [44]. If an adverse temperature difference (tendons warmer than bridge beams) of 10 degrees Fahrenheit is assumed, the temporary post-tensioning loss can be computed as 2.1% [29]. Based on a limited amount of testing as part of the bridge strengthening research program, the temperature difference is not likely to exceed 10 degrees Fahrenheit [28].

Based on field testing, the ΔT effect can be estimated as 6% of the total weight of a truck placed eccentrically on the bridge. That gain in post-tensioning, in terms of tendon force, is 2.4% [29], as shown in Table 20.

After accounting for potential error, losses, and ΔT effect, the force to be applied to each exterior beam is 219 kips, and the force to be applied to each tendon is 110 kips. Stressed to 60% of ultimate

TABLE 20. Required post-tensioning tendon force

CONDITION	COMPUTATION	FORCE kips
Total post-tensioning for bridge (Tables 15, 17, 18, and 19, Figure 69)	$f_b = FF \frac{P}{A} + MF \frac{Pec}{I}$	392
Total post-tensioning for each exterior beam	$P_e = \frac{P}{2}$	196
Potential error in distribution factor formulas (Figure 65)	$0.070P'_e$	
Loss caused by relaxation [44]	$0.037P'_e$	
Loss caused by 10°F adverse temperature differential [29]	$0.021P'_e$	
Gain caused by ΔT in tendon, 6% of truck weight [29]	$0.024P'_e$	
Total initial post-tensioning for each exterior beam	$P'_e = \frac{P_e}{1.0 - \text{losses} + \text{gain}}$	219
Initial post-tensioning force for each tendon	$P'_t = \frac{P'_e}{2}$	110

strength, two threadbars of 1 1/4-inch diameter have a capacity of 225 kips [30]. Therefore, for the post-tensioning, specify two 1 1/4-inch diameter threadbar tendons per exterior beam with an initial force of 110 kips in each of the tendons.

5.2.6. Stress checks and bracket location

In order to check the post-tensioning design at all critical locations except the anchorage, for which the location is as yet unknown, stresses at top of curb, top of deck, top of beam, and bottom of beam or coverplate are checked in Tables 21 through 26. Allowable stresses are given at the bottom of Table 21. Some tension is permitted by the AASHTO bridge design specifications for prestressed concrete, and the more restrictive value for severe exposure conditions has been selected as a basis for the stress checks. In the author's opinion, the severe exposure condition adequately covers the salt and freeze-thaw conditions to which the curb and top of the deck are subjected.

If the anchorage brackets are bolted to the bottom flange of the exterior beam, the flange cross section will be reduced by the bolt holes. If the average stress in the flange is not to exceed 18 ksi, the computed stress must be less at the holes. In Table 27, the reduced stress is computed as a product of the 18 ksi allowable stress and the ratio of the net flange width to gross flange width. The reduced stress is 13.95 ksi, slightly larger than the stress at 6 feet from the support. Any set of two 1-inch diameter bolt holes, therefore, can be located no farther than 6 feet from the support.

TABLE 21. Stress checks for exterior beam at midspan

LOAD	STRESS AT TOP OF CURB ksi	STRESS AT TOP OF DECK ksi	STRESS AT TOP OF BEAM ksi	STRESS AT BOTTOM OF COVERPLATE ksi
1. Dead	-	-	-13.19	+10.61
2. Long-term dead	-0.060	-0.034	- 0.50	+ 1.31
3. Live plus impact	-1.063	-0.485	- 1.14	+12.41
4. Post- tensioning, axial	-0.185	-0.185	- 1.67	- 1.67
5. Post- tensioning, flexural	+0.387	+0.173	+ 0.36	- 4.67
1+2+4+5	+0.142 < +0.164 OK	-0.046 > -1.200 OK	-15.00 > -18.00 OK	+ 5.58 < +18.00 OK
1+2+3+4+5	-0.921 > -1.200 OK	-0.531 > -1.200 OK	-16.14 > -18.00 OK	+17.99 < +18.00 OK

AASHTO allowable stresses [3]:

for steel: $F_b = 18$ ksi for extreme fiber in tension or extreme fiber in compression with lateral support

for concrete: $f_c = 0.40f'_c = 1.200$ ksi for extreme fiber in compression

$f_t = 3\sqrt{f'_c} = 0.164$ ksi for tension in precompressed tensile zone, bonded reinforcing, severe exposure conditions

TABLE 22. Stress checks for exterior beam with coverplate at coverplate cutoff

LOAD	STRESS AT TOP OF CURB ksi	STRESS AT TOP OF DECK ksi	STRESS AT TOP OF BEAM ksi	STRESS AT BOTTOM OF COVERPLATE ksi
1. Dead	-	-	-10.30	+ 8.28
2. Long-term dead	-0.047	-0.027	- 0.39	+ 1.02
3. Live plus impact	-0.856	-0.391	- 0.92	+ 9.99
4. Post- tensioning, axial	-0.209	-0.209	- 1.88	- 1.88
5. Post- tensioning, flexural	+0.521	+0.232	+ 0.48	- 6.27
1+2+4+5	+0.265 \geq +0.164 ^a	-0.004 $>$ -1.200 OK	-12.09 $>$ -18.00 OK	+ 1.15 $<$ +18.00 OK
1+2+3+4+5	-0.591 $>$ -1.200 OK	-0.395 $>$ -1.200 OK	-13.01 $>$ -18.00 OK	+11.14 $<$ +18.00 OK

^aReinforcing bars provided in the curb, not considered in the computations, should be capable of resisting the tension overstress. See also footnote for Table 28.

TABLE 23. Stress checks for exterior beam without coverplate at coverplate cutoff

LOAD	STRESS AT TOP OF CURB ksi	STRESS AT TOP OF DECK ksi	STRESS AT TOP OF BEAM ksi	STRESS AT BOTTOM OF BEAM ksi
1. Dead	-	-	-10.96	+10.96
2. Long-term dead	-0.054	-0.029	- 0.37	+ 1.32
3. Live plus impact	-1.001	-0.424	- 0.59	+12.73
4. Post- tensioning, axial	-0.219	-0.219	- 1.97	- 1.97
5. Post- tensioning, flexural	+0.644	+0.278	+ 0.46	- 7.98
1+2+4+5	+0.371 +0.164 ^a	+0.030 < +0.164 OK	-12.84 > -18.00 OK	+ 2.33 < +18.00 OK
1+2+3+4+5	-0.630 > -1.200 OK	-0.394 > -1.200 OK	-13.43 > -18.00 OK	+15.06 < +18.00 OK

^aReinforcing bars provided in the curb, not considered in the computations, should be capable of resisting the tension overstress. See also footnote for Table 28.

TABLE 24. Stress checks for interior beam at midspan

LOAD	STRESS AT TOP OF DECK	STRESS AT TOP OF BEAM	STRESS AT BOTTOM OF COVERPLATE
	ksi	ksi	ksi
1. Dead	-	-12.18	+ 7.99
2. Long-term dead	-0.027	- 0.45	+ 0.81
3. Live plus impact	-0.481	- 1.96	+ 9.40
4. Post-tensioning, axial	-0.040	- 0.36	- 0.36
5. Post-tensioning, flexural	+0.113	+ 0.48	- 2.14
1+2+4+5	+0.046 < +0.164 OK	-12.51 > -18.00 OK	+ 6.30 < +18.00 OK
1+2+3+4+5	-0.435 > -1.200 OK	-14.47 > -18.00 OK	+15.70 < +18.00 OK

TABLE 25. Stress checks for interior beam with coverplate at coverplate cutoff

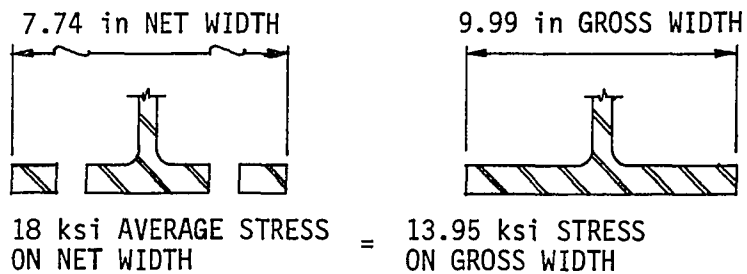
LOAD	STRESS AT TOP OF DECK	STRESS AT TOP OF BEAM	STRESS AT BOTTOM OF COVERPLATE
	ksi	ksi	ksi
1. Dead	-	- 7.14	+ 4.68
2. Long-term dead	-0.016	- 0.27	+ 0.48
3. Live plus impact	-0.298	- 1.22	+ 5.82
4. Post-tensioning, axial	-0.014	- 0.13	- 0.13
5. Post-tensioning, flexural	+0.037	+ 0.15	- 0.74
1+2+4+5	+0.007 < +0.164 OK	- 7.34 > -18.00 OK	+ 4.29 < +18.00 OK
1+2+3+4+5	-0.291 > -1.200 OK	- 8.61 > -18.00 OK	+10.11 < +18.00 OK

TABLE 26. Stress checks for interior beam without coverplate at coverplate cutoff

LOAD	STRESS AT TOP OF DECK	STRESS AT TOP OF BEAM	STRESS AT BOTTOM OF BEAM
	ksi	ksi	ksi
1. Dead	-	- 8.07	+ 8.07
2. Long-term dead	-0.019	- 0.27	+ 0.82
3. Live plus impact	-0.378	- 1.02	+ 9.95
4. Post-tensioning, axial	-0.016	- 0.14	- 0.14
5. Post-tensioning, flexural	+0.056	+ 0.18	- 1.29
1+2+4+5	+0.021 < +0.164 OK	- 8.30 > -18.00 OK	+ 7.46 < +18.00 OK
1+2+3+4+5	-0.357 > -1.200 OK	- 9.32 > -18.00 OK	+17.41 < +18.00 OK

TABLE 27. Bracket bolt location

LOAD	BOTTOM FLANGE STRESS AT $y = 2$ ft ksi	BOTTOM FLANGE STRESS AT $y = 6$ ft ksi
Dead	+ 2.11	+ 5.81
Long-term dead	+ 0.25	+ 0.70
Live plus impact	+ 2.77	+ 7.23
Total	+ 7.48	+13.74



At $y = 6$ feet, the bottom flange stress is 13.74 ksi < 13.95 ksi. Therefore, two 1-inch diameter bolts may be safely located at any cross section no farther than 6 feet from the support.

Based on experience, the anchorage brackets will be approximately 2 feet long. Thus, the anchorage for the tendons will occur at about 4 feet from the support. That anchorage location is 7.8% of the span, acceptably close to the assumed 7%.

Stress checks for the exterior beam at the anchorage are given in Table 28. The top of the curb is overstressed when no vehicles are on the bridge and, if the curb concrete is neglected, the curb reinforcing is overstressed. If the entire curb is neglected, as if the concrete had cracked and the bars had yielded, the maximum deck tension remains within the allowable tension stress. Without the curbs at the anchorages, therefore, the concrete stresses remain within the allowable stress range. The same reasoning can be used to show that the curb overstress at the coverplate cutoff indicated in Tables 22 and 23 can be neglected.

In the bottom flange of the exterior beam at the anchorage, the post-tensioning causes compression stress. The allowable compression stress, due to lack of bracing of the compression flange, is reduced. According to the AASHTO bridge design specifications, the compression stress permitted on the compression flange with bracing at the support and the interior diaphragm can be computed as 15.41 ksi. The allowable is greater than the computed stress -- with or without the curb. Therefore, the post-tensioning does not overstress the bottom flange in compression at the anchorage.

TABLE 28. Stress checks for exterior beam at anchorage ($y = 4$ feet)

LOAD	STRESS AT TOP OF CURB ksi	STRESS AT TOP OF DECK ksi	STRESS AT TOP OF BEAM ksi	STRESS AT BOTTOM OF BEAM ksi
1. Dead	-	-	- 3.95	+ 3.95
2. Long-term dead	-0.019	-0.010	- 0.14	+ 0.48
3. Live plus impact	-0.393	-0.166	- 0.23	+ 5.00
4. Post- tensioning, axial ^a	-0.244	-0.244	- 2.19	- 2.19
5. Post- tensioning, flexural ^b	+0.771	+0.295	+ 0.01	-10.97
1+2+4+5	+0.508 ^c +0.164	+0.041 < +0.164 OK	- 6.27 > -18.00 OK	- 8.73 ^d -15.41
1+2+3+4+5	+0.115 < +0.164 OK	-0.125 > -1.200 OK	- 6.50 > -18.00 OK	- 3.73 ^d -15.41

^aFF is interpolated to be 0.49.

^bMF is interpolated to be 0.48.

^cWithout the truck load, the curb concrete is overstressed, and the two #5 bars would be overstressed to 42 ksi, if the concrete is neglected. If the entire curb is neglected, the maximum deck tension is 0.100 ksi < 0.164 ksi. Maximum compression at the bottom of the beam is 10.75 ksi < 15.41 ksi. Even if the curb cracks and the reinforcing bars yield, the bridge itself will remain within the allowable stress range.

^dThe bottom flange, subjected to varying axial and flexural compression, is effectively braced only at the support and the interior diaphragm. The 15.41 ksi allowable stress is computed for an unbraced compression flange subjected to bending, according to the AASHTO formula in Table 10.32.1A [3]. See Reference 29 for the allowable stress computation.

A review of the stress check tables and the stress diagrams presented in Figure 70 indicates that the post-tensioning produces a finely tuned bridge. Application of the post-tensioning relieves the tension overstress in the exterior beams at midspan and also removes a slight tension overstress in the interior beams at midspan. If the post-tensioning force were increased significantly, it could overstress the top flange of the exterior beam in compression at midspan. There also would be some danger of compression overstress near the tendon anchorages.

Application of the post-tensioning generally causes a net tension in the curbs and, in a few locations, tension in the deck. If the post-tensioning force were increased or lowered (in terms of elevation), the curb and deck tension would increase. With curbs as part of the bridge, the deck tension fell within the allowable range for concrete with bonded reinforcement, but the curb tension generally did not. Without a truck load on the bridge, the curb reinforcing apparently is overstressed, an undesirable condition. Observations during the bridge strengthening research program, did not indicate any problems, quite possibly because various restraints, higher-than-assumed concrete strength, and the wearing surface are neglected in the computations. A curb tension greater than the allowable should not be permitted, however, without a check of the bridge with curbs removed.

The post-tensioning design for Bridge 1 is summarized in Figure 71.

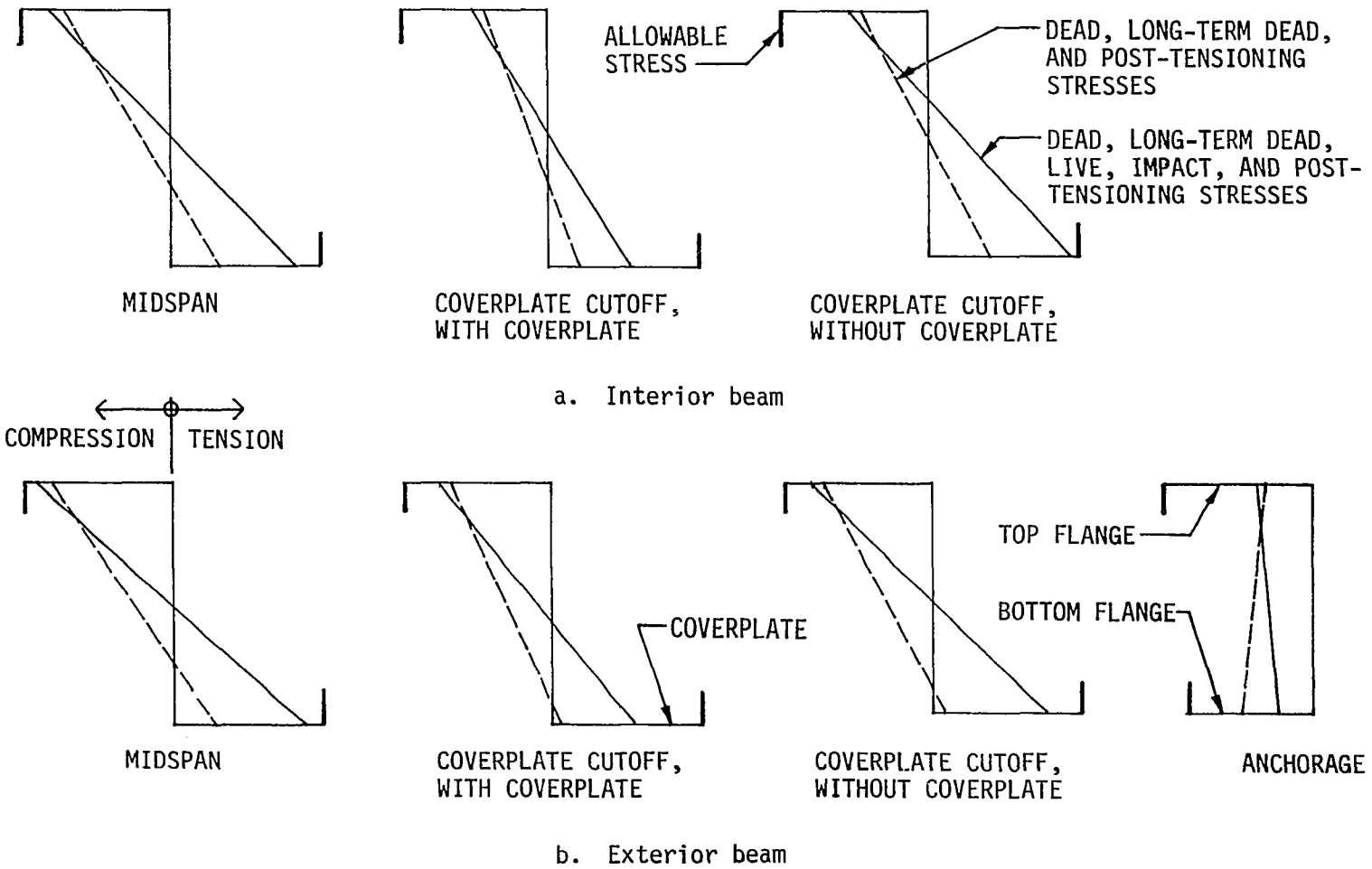
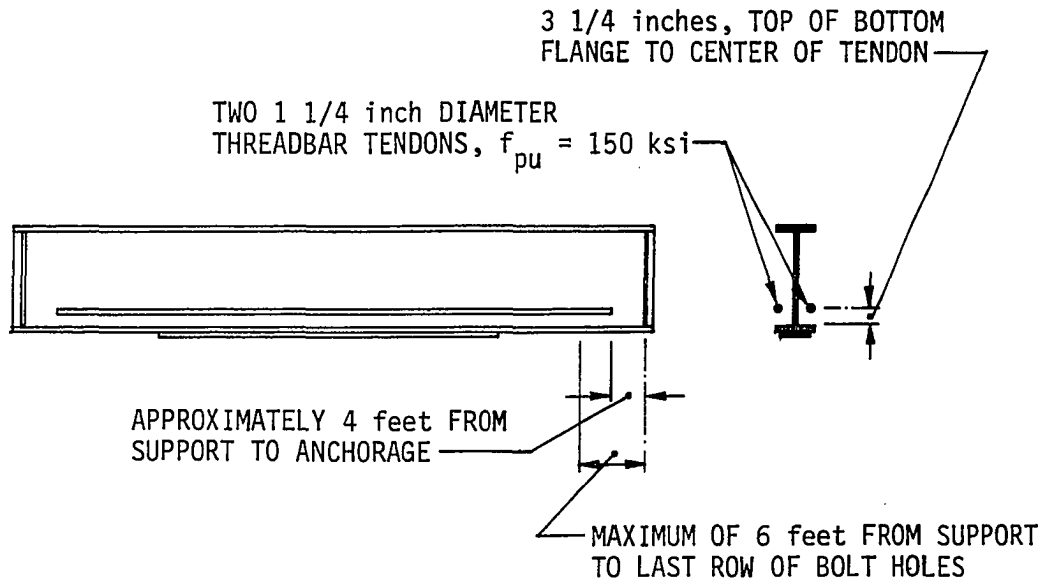


FIGURE 70. Stress diagrams for steel bridge beams



TENDONS ARE TO BE STRESSED TO 110 kips EACH AT TIME OF POST-TENSIONING.

BRACKETS MAY BE BOLTED TO BOTTOM FLANGE OF EXTERIOR BEAM WITH 1 inch DIAMETER BOLTS AT ANY LOCATION WITHIN 6 feet OF SUPPORT.

FIGURE 71. Post-tensioning design

5.2.7. Brackets and anchorages

In general, the bracket design would proceed within the limitations of tendon elevation, region for location of bracket bolts, and manufacturer's hardware. The AASHTO bridge design specifications [3] require that the bracket connection be designed for a force greater than the specified tendon force, if the tendon is considered to be a member. Welds within the bracket must be designed for axial and flexural stresses, and bolts must be designed for both shear and tension forces, depending on the configuration of the bracket. Because the stress in the bracket will vary only because of the change in tendon force when a truck comes onto or leaves the bridge, stress ranges will be small, and fatigue should not control.

Brackets and anchorages for Bridge 1 will not be designed here. An example of the bracket actually used for the post-tensioning of the bridge is given in Reference 54.

5.2.8. Additional design considerations

Post-tensioning can relieve only the bending stress deficiencies in a given bridge. Other potential deficiencies, such as shear connectors, also may require strengthening. At the time some Iowa bridges were designed, the shear connection often was assumed to consist of both shear connectors and bond between the deck and top flanges of the beams. Since bond is no longer considered a valid shear connection, additional shear connectors may be required. Reference 54 contains information for the design of retrofit high strength bolt shear connectors which can be used to supplement the existing shear connectors for a bridge.

From experience gained during the bridge strengthening research program, it is the author's opinion that a well-maintained bridge of the type in the example generally will not require additional strengthening beyond the post-tensioning and the addition of shear connectors. Every bridge must be rated and evaluated individually, however, and the strengthening program tailored to the specific bridge deficiencies.

6. SUMMARY AND CONCLUSIONS

6.1. Summary

Iowa has a considerable inventory of understrength single span composite bridges. The bridges are understrength for two reasons: beams were designed according to out-dated AASHO wheel load distribution standards which permitted use of small exterior beams, and the bridges were designed for live loads less than the recently increased Iowa legal loads.

One method of strengthening the bridges economically is to post-tension only the exterior beams. If only the exterior beams are post-tensioned, distribution of post-tensioning becomes important because some of the post-tensioning will be lost to other parts of the bridge. The distribution problem generally has been avoided in previous bridge strengthening, by post-tensioning all bridge beams equally.

Because no information was available in the literature for post-tensioning distribution, this research study was initiated to determine the distribution and develop a design methodology of use to practicing engineers. The study involved construction and testing of a half-scale model bridge, strengthening of two Iowa bridges by post-tensioning, and development of the design methodology.

The design methodology was developed through study of the behavior of composite beams and bridges, based on analytical and finite element models. Classical beam theory with AASHTO effective flange width,

modular ratio, and a formula for change in tendon force derived by means of Castigliano's Theorem, provided a reasonable estimate of the elastic behavior of isolated, post-tensioned composite beams. With shear deflection of beam elements and load-slip of shear connectors included, finite element models accurately predicted the behavior of prestressed composite beams, as verified by experimental results.

The finite element analyses of composite beams showed that shear connector forces are increased very little by post-tensioning, and the increase may be safely neglected in design. Secondary $P-\Delta$ and ΔT effects were small and could be neglected in design or credited against post-tensioning losses.

For inelastic behavior of post-tensioned composite beams, a simple analytical beam model with a plastic hinge at midspan gave accurate estimates of the ultimate flexural strength. The model indicated that post-tensioning did increase the ultimate flexural strength of a composite beam, but the increase was less than the increase in capacity computed under AASHTO Service Load Design.

When the composite beam finite element model was extrapolated to a composite bridge, it quickly became apparent that the finite element model was too stiff and did not agree well with experimental data from the half-scale model bridge. When the finite element model was refined by including a reasonable estimate for the lateral stiffness of each beam web, the finite element model gained the flexibility necessary to correlate well with the experimental data.

Initially, the refined finite element model did not agree well with field data from the post-tensioning of Bridges 1 and 2. The model bridge in the laboratory was carefully supported so as to have simple support conditions, but guard rails and construction details at bridge abutments in the field caused some restraint. Separate finite element analyses, for simple support and fixed support conditions, bracketed the field data for both bridges. When reasonable estimates for guard rails and construction details were included in the finite element model, the model agreed well with the field data.

The verified finite element model was utilized to determine which bridge variables significantly affected post-tensioning distribution. Although field restraints affected the distribution, neglecting those restraints was shown to be conservative for exterior beams. Comparisons showed that axial force and moment were distributed differently and, on that basis, all distribution was referenced separately to axial force and moment fractions.

The distribution varied depending on location on the bridge span. More force or moment remained on the post-tensioned exterior beams at the anchorages than at midspan. Length of the post-tensioned region, dependent on both the span length and anchorage locations, was determined to be the most significant variable which controlled the distribution for moment. Relative beam stiffness also was important in determining the distribution for moment. Skew had relatively little effect on the distribution for moment, and neglecting skew of 45-degrees or less was shown to be conservative for exterior beams.

Standard designs for the three-beam and four-beam bridges in need of strengthening were obtained from the Iowa DOT. The standard bridge designs were analyzed by means of the finite element model for force and moment distribution data. The distribution data were analyzed by multiple linear regression to develop simple force fraction and moment fraction formulas. The distribution fraction formulas were developed separately for midspan of three-beam and four-beam bridges. Distribution fractions for locations other than midspan, obtained by linear interpolation, were shown to be accurate.

For organizing the structural computations, a design procedure was developed which is compatible with the AASHTO Service Load Design Method. For determining the stresses caused by dead, long-term dead, live, and impact loads, the procedure recommends computing section properties for individual composite beams, which is the usual practice in rating bridges. For determining the eccentricity of tendons and computing post-tensioning stresses, however, the procedure recommends that eccentricity and section properties be computed with respect to the neutral axis of the bridge.

The design procedure was applied to a typical right-angle composite bridge. The example indicated that the post-tensioning would produce a finely tuned bridge. Tension overstress in the exterior and interior beams was eliminated, but compression stresses at the tops of the steel beams were increased, almost to the point of exceeding the allowable stress. Curb stresses exceeded the allowable tension stress but, if the

curbs were neglected, deck stresses remained within the allowable tension stress. At the anchorages, compression stresses were relatively large but within the allowable stress computed for an unbraced compression flange.

The design methodology, verified by field experience, provides a means for accurately determining the required post-tensioning for strengthening the Iowa composite bridges. The basic post-tensioning concept can be used to strengthen other types of bridges, if the distribution of the post-tensioning is included in the design. Any bridges, however, which are not within the range of the distribution factor data, from which the formulas were derived, must be analyzed individually.

6.2. Conclusions

1. Iowa single span composite bridges with small exterior beams can be strengthened to meet current AASHTO and Iowa legal load standards by post-tensioning only the exterior beams. Post-tensioning of the exterior beams requires consideration of the post-tensioning lost to the interior beams.
2. A finite element model was developed which accurately predicted the behavior of a composite bridge under post-tensioning and vertical load. The model was verified with test results from a half-scale model bridge, and the model was more accurate than previous finite element models which

did not account for the flexibility of the webs of the steel beams.

3. Comparison of the finite element analyses with field data obtained during post-tensioning of two Iowa bridges indicated that typical construction details caused considerable restraint. The field-measured strains and deflections generally fell about halfway between the values computed for theoretical simple support and fixed end conditions.
4. For distribution of post-tensioning to exterior beams, it is conservative to neglect the effects of field restraints and skews of 45 degrees or less.
5. Deck crown, shear connector stiffness, and coverplate length has virtually no effect on the post-tensioning distribution for typical Iowa bridges.
6. Length of post-tensioned region, relative stiffness of exterior beams, and transverse stiffness of deck and diaphragms generally have the largest effects on post-tensioning distribution.
7. Force fractions and moment fractions for midspan of exterior beams in typical Iowa three-beam and four-beam bridges can be determined accurately from the formulas given in this research study.
8. Post-tensioning distribution varies along the span of a bridge. Distribution fractions at any point on the span can be computed accurately by linear interpolation.

9. Post-tensioning the exterior beams can relieve the tension overstress in exterior beams at midspan and at coverplate cutoff points. An excess of post-tensioning, however, can overstress exterior and interior beams in compression and can overstress curbs and deck in tension.
10. Vertical live load distribution is virtually the same for a composite bridge with or without post-tensioning.
11. The simple beam model with a plastic hinge at midspan accurately predicts the ultimate flexural strength of a post-tensioned composite beam. The increase in ultimate strength due to post-tensioning is less than the increase in capacity computed under AASHTO Service Load Design.

7. ACKNOWLEDGMENTS

The research study presented in this dissertation was conducted by Engineering Research Institute at Iowa State University as part of several research projects sponsored by the Highway Division, Iowa DOT and the Iowa Highway Research Board. Primary facilities used at Iowa State University include the Structural Research Laboratory and the Computation Center.

I wish to express my appreciation to my major professor, Dr. F. Wayne Klaiber for his assistance and guidance over more than five years. I also wish to thank my committee members, Drs. Lowell F. Greimann, Wallace W. Sanders, Jr., Frederick M. Graham, and Christian P. Burger (oral examination substitute Dr. Loren W. Zachary) for their assistance. Drs. Klaiber and Greimann deserve special thanks for promptly reviewing eighteen research memos on which this dissertation is based. Dr. Sanders aided in interpreting the AASHTO bridge design specifications and in obtaining several bridge research reports from Dr. Kostem at Lehigh University.

John Harkin at the Iowa DOT provided considerable advice for bridge rating and design checks and provided the Iowa standard bridge designs on which the distribution formulas are based. Vernon Marks and Charles Pestotnik aided in the coordination and funding of the various research projects.

Dr. Carl E. Ekberg provided considerable support and assisted in arranging my teaching schedules to meet the demands of the research

projects. Former graduate student David J. Dedic is to be commended for keeping excellent and well-organized test records which were critical to verifying the finite element models. Graduate students Brad Beck, Doug Wood, and others assisted in many ways during the laboratory and field testing.

I also wish to thank my parents for their interest and encouragement.

8. REFERENCES

1. Aggarwala, B. D. "Bending of Parallelogram Plates." Journal of the Engineering Mechanics Division, ASCE, 93, No. EM4 (Aug. 1967), 9-18.
2. American Association of State Highway and Transportation Officials. Manual for Maintenance Inspection of Bridges 1978. Third edition. Washington, D. C.: American Association of State Highway and Transportation Officials, 1979.
3. American Association of State Highway and Transportation Officials. Standard Specifications for Highway Bridges. 13th edition. Washington, D. C.: American Association of State Highway and Transportation Officials, 1983.
4. American Association of State Highway Officials. Standard Specifications for Highway Bridges. 7th edition. Washington, D. C.: American Association of State Highway Officials, 1957.
5. American Institute of Steel Construction. Manual of Steel Construction. 6th edition. New York: American Institute of Steel Construction, Inc., 1963.
6. Arendts, J. G. "Study of Experimental and Theoretical Load Distribution in Highway Bridges." M.S. Thesis. Iowa State University, Ames, Iowa, 1968.
7. Badaruddin, S. "Analyses of Slab and Girder Highway Bridges." Ph.D. Dissertation. University of Illinois, Urbana, Illinois, 1965.
8. Bakht, B., M. S. Cheung and T. S. Aziz. "Application of a Simplified Method of Calculating Longitudinal Moments to the Ontario Highway Bridge Design Code." Canadian Journal of Civil Engineering, 6 (1979), 36-50.
9. Bares, R. Berechnungstafeln für Platten und Wandscheiben/Tables for the Analysis of Plates, Slabs and Diaphragms Based on the Elastic Theory. Wiesbaden and Berlin: Bauverlag GMBH., 1971.
10. Bares, R. and C. Massonnet. Analysis of Beam Grids and Orthotropic Plates. New York: Frederick Ungar Publishing Co., 1966.
11. Barnard, P. F. "Prestressed Steel Bridges." Iowa State Highway Commission, Ames, Iowa, 1960.

12. Barnett, R. L. "Prestressed Truss-Beams." Journal of the Structural Division, ASCE, 83, No. ST2 (Mar. 1957), 1191-1 - 1191-22.
13. Bathe, K-J., E. L. Wilson and F. E. Peterson. "SAP IV, A Structural Analysis Program for Static and Dynamic Response of Linear Systems." Report No. EERC 73-11, Revised April 1974. College of Engineering, University of California, Berkeley, California, 1974.
14. Beck, B. L., F. W. Klaiber and W. W. Sanders, Jr. "Field Testing of County Road 54 Bridge over Anclote River, Pasco County, Florida." Engineering Research Institute, Iowa State University, Ames, Iowa, 1984.
15. Belenya, E. I. and D. M. Gorovskii. "The Analysis of Steel Beams Strengthened by a Tie Rod." International Civil Engineering, 2, No. 9 (Mar. 1972), 412-419.
16. Berenson, M. L., D. M. Levine and M. Goldstein. Intermediate Statistical Methods and Applications. Englewood Cliffs: Prentice-Hall, Inc., 1983.
17. Berridge, P. S. A. and D. H. Lee. "Prestressing Restores Weakened Truss Bridge." Civil Engineering (London), 26, No. 9 (Sep. 1956), 578-579.
18. Botzler, P. W., J. Colville and C. P. Heins. "Ultimate Load Tests of Continuous, Composite Bridge Models." Report No. FHWA-MD-R-76-14. Civil Engineering Department, University of Maryland, College Park, Maryland, 1976.
19. Carskaddan, P. S. "Evaluation of Load Distribution in Multi-Girder Straight and Curved Steel Bridge Structures with the MSC/NASTRAN Program." Seminar 1, the National Engineering Conference, AISC, Tampa, Florida, 29 and 30 March 1984.
20. Cheung, M. S. and M. Y. T. Chan. "Finite Strip Evaluation of Effective Flange Width of Bridge Girders." Canadian Journal of Civil Engineering, 5, No. 2 (June 1978), 174-185.
21. Clark, L. A. and R. West. The Behaviour of Solid Skew Slab Bridges under Longitudinal Prestress. London: Cement and Concrete Association, 1974.
22. Coff, L. "American Engineer Studies Prestressing of Structural Steel." Civil Engineering (London), 20, No. 11 (Nov. 1950), 64.

23. Commonwealth of Pennsylvania, Bridge Unit, Department of Highways. "Composite Prestressed Steel WF Beam Bridge over Quittaphilla Creek." Commonwealth of Pennsylvania, Bridge Unit, Department of Highways, Harrisburg, Pennsylvania, 1965.
24. Cusens, A. R. and R. P. Pama. Bridge Deck Analysis. New York: John Wiley and Sons, Inc., 1975.
25. Davis, R. E. "Design of a Skew, Reinforced Concrete, Box Girder Bridge Model." Unpublished paper. University of California, Berkeley, California, ca. 1978.
26. DeCastro, E. S. and C. N. Kostem. "Load Distribution in Skewed Beam-Slab Highway Bridges." Report No. 378A.7. Fritz Engineering Laboratory, Lehigh University, Bethlehem, Pennsylvania, 1975.
27. Dischinger, F. "Stahlbrücken im Verbund mit Stahlbeton Druckplatten bei gleichzeitiger Vorspannung durch hochwertiger Seile." Bauingenieur, 24, Nos. 11 and 12 (Nov. and Dec. 1949), 321-332 and 364-376.
28. Dunker, K. F., F. W. Klaiber, B. L. Beck and W. W. Sanders, Jr. "Strengthening of Existing Single-Span Steel-Beam and Concrete Deck Bridges." Final Report -- Part II. Engineering Research Institute, Iowa State University, Ames, Iowa, 1985.
29. Dunker, K. F., F. W. Klaiber and W. W. Sanders, Jr. "Design Manual for Strengthening Single-Span Composite Bridges by Post-tensioning." Final Report -- Part III. Engineering Research Institute, Iowa State University, Ames, Iowa, 1985.
30. DYWIDAG Systems International. "DYWIDAG Threadbar Posttensioning System." DYWIDAG Systems International, USA, Inc., Lincoln Park, New Jersey, 1983.
31. Ekberg, C. E. "Development and Use of Prestressed Steel Flexural Members, Subcommittee 3 Report on Prestressed Steel of Joint ASCE-AASHO Committee on Steel Flexural Members." Journal of the Structural Division, ASCE, 94, No. ST9 (Sep. 1968), 2033-2060.
32. Ferjencik, P. "Czechoslovak Contribution in the Field of Prestressed Steel Structures." International Civil Engineering, II, No. 11 (May 1972), 481-491.
33. Finn, E. V. and F. H. Needham. "The Use of Prestressed Steel in Elevated Roadways." Structural Engineer, 42, No. 1 (Jan. 1964), 5-18.

34. Fritz, B. "Über die Berechnung und Konstruktion vorgespannter, stahlerner Fachwerktrager." Stahlbau, 24, No. 8 (Aug. 1955), 169-174.
35. Gurbuz, O. "Theories of Transverse Load Distribution on Simple Span, (Non-Skewed) Beam-and-Slab and Slab Bridges." M.S. Thesis. Iowa State University, Ames, Iowa 1968.
36. Gustafson, W. C. and R. N. Wright. "Analysis of Skewed Composite Girder Bridges." Journal of the Structural Division, ASCE, 94, No. ST4 (Apr. 1968), 919-941.
37. Hadley, H. M. "Heavy Duty Composite Bridge." Civil Engineering, 30, No. 5 (May 1960), 44-48.
38. Hadley, H. M. "Steel Bridge Girders with Prestressed Composite Tension Flanges." Civil Engineering, 36, No. 5 (May 1966), 70-72.
39. Hambly, E. C. Bridge Deck Behavior. New York: John Wiley and Sons, Inc., 1976.
40. Heins, C. P. "LFD Criteria for Composite Steel I-Beam Bridges." Journal of the Structural Division, ASCE, 106, No. ST11 (Nov. 1980), 2297-2312.
41. Hoadley, P. G. "Behavior of Prestressed Composite Steel Beams." Journal of the Structural Division, ASCE, 89, No. ST3 (Jun. 1963), 21-34.
42. Hondros, G. and J. G. Marsh. "Load Distribution in Composite Girder-Slab Systems." Journal of the Structural Division, ASCE, 86, No. ST11 (Nov. 1960), 79-109.
43. "How to Keep that Old Bridge Up." American City and County, 96, No. 1 (Jan. 1981), 29-32.
44. Institut für Bautechnik. "Official Approval Specification for Hot Rolled, Stretched and Tempered Post-tensioning Steel, St 1080/1230." Institut für Bautechnik, Berlin, West Germany, 1982.
45. Iowa Department of Transportation, Highway Division. "Standard Design -- 30 ft. Roadway, Simple Span I-Beam Bridges, H 20-44 Loading." Iowa Department of Transportation, Highway Division, Ames, Iowa, 1975.
46. Iowa Department of Transportation, Office of Bridge Design. "Bridge Rating and Posting Criteria." Iowa Department of Transportation, Office of Bridge Design, Ames, Iowa, 1980.

47. Iowa State Highway Commission. "Design for 50' x 30' I-Beam Bridge, Project F.A. 905, Dickinson County." Iowa State Highway Commission, Ames, Iowa, 1947.
48. Iowa State Highway Commission. "Standard Design, Simple Span I-Beam Bridges, 20 ft. Roadway, Concrete Floor, Steel Rail, H 15 Loading." Iowa State Highway Commission, Ames, Iowa, 1964.
49. Iowa State Highway Commission. "Standard Design, Simple Span I-Beam Bridges, 24 ft. Roadway, Concrete Floor, H 15 Loading." Iowa State Highway Commission, Ames, Iowa, 1964.
50. Iowa State Highway Commission. "Standard Design, Simple Span I-Beam Bridges, 28 ft. Roadway, Concrete Floor, H 20 Loading." Iowa State Highway Commission, Ames, Iowa, 1964.
51. Johnson, R. P. Composite Structures of Steel and Concrete, Volume 1. New York: John Wiley and Sons, Inc., 1975.
52. Kandall, C. "Increasing the Load-Carrying Capacity of Existing Steel Structures." Civil Engineering, 38, No. 9 (Oct. 1968), 48-51.
53. Kennedy, J. B. and D. S. R. Gupta. "Bending of Skew Orthotropic Plate Structures." Journal of the Structural Division, ASCE, 102, No. ST8 (Aug. 1976), 1559-1574.
54. Klaiber, F. W., D. J. Dedic, K. F. Dunker and W. W. Sanders, Jr. "Strengthening of Existing Single Span Steel Beam and Concrete Deck Bridges." Final Report -- Part I. Engineering Research Institute, Iowa State University, Ames, Iowa, 1983.
55. Klaiber, F. W., K. F. Dunker and W. W. Sanders, Jr. "Feasibility Study of Strengthening Existing Single Span Steel Beam Concrete Deck Bridges." Final Report. Engineering Research Institute, Iowa State University, Ames, Iowa, 1981.
56. Knee, D. W. "The Prestressing of Steel Girders." Structural Engineer, 44, No. 10 (Oct. 1966), 351-353.
57. Knowles, P. R. Composite Steel and Concrete Construction. New York: John Wiley and Sons, Inc., 1973.
58. Kostem, C. N. and E. S. DeCastro. "Effects of Diaphragms on Lateral Load Distribution in Beam-Slab Bridges." Transportation Research Record 645, TRB, Bridge Tests, 6-9.
59. Lamberson, E. A. "Posttensioning Concepts for Strengthening and Rehabilitation of Bridges and Special Structures." DYWIDAG Systems International, USA, Inc., Lincoln Park, New Jersey, 1983.

60. Lee, D. H. "Prestressed Concrete Bridges and Other Structures." Structural Engineer, 30, No. 12 (Dec. 1952), 302-313.
61. Lee, D. J. and E. C. Chaplin. "Design and Analysis of Skew Bridge Structures." Proceedings -- Symposium on Prestressed Concrete in Short to Medium Span Bridges. Sydney: FIP/Concrete Institute of Australia, 1976.
62. Magnel, G. P. "Long Prestressed Steel Truss Erected for Belgian Hangar." Civil Engineering (London), 24, No. 10 (Oct. 1954), 38-39.
63. Magnel, G. "Prestressed Steel Structures." Structural Engineer, 28, No. 11 (Nov. 1950), 285-295.
64. Mancarti, G. D. "Strengthening California's Bridges by Prestressing." Transportation Research Record 950, Volume 1, TRB, (1984), 183-187.
65. McCormac, J. C. Structural Analysis. 3rd edition. New York: Harper and Row, Publishers, 1975.
66. Newmark, N. M., C. P. Siess and W. M. Peckham. "Tests of Simple-Span Skew I-Beam Bridges." Studies of Slab and Beam Highway Bridges, Part II, Bulletin Vol. 45, No. 31, Series No. 375. University of Illinois, Urbana, Illinois, 1948.
67. Palmer, R. A. "Emergency Bridge Repair in Minnesota." Journal of the Prestressed Concrete Institute, 19, No. 1 (Jan-Feb. 1974), 73-75.
68. Reagan, R. S. "An Analytical Study of the Behavior of Prestressed Composite Beams." M.S. Thesis. Rice University, Houston, Texas, 1966.
69. Reagan, R. S. and N. W. Krahl. "Behavior of Prestressed Composite Beams." Journal of the Structural Division, ASCE, 93, No. ST6 (Dec. 1967), 87-107.
70. Robinson, J. "Element Evaluation -- A Set of Assessment Points and Standard Tests." Proceedings of the Second World Congress on Finite Element Methods. Dorset: Robinson and Associates, 1978.
71. Sanders, W. W., Jr. and H. A. Elleby. "Distribution of Wheel Loads on Highway Bridges." Report 83. National Cooperative Highway Research Program, Washington, D. C., 1970.
72. SAS Institute. SAS User's Guide, 1979 Edition. Cary: SAS Institute, Inc., 1979.

73. Seim, C., R. Zimmerman, T. Jee and M. Walters. "Bonners Ferry: A Pioneering Prestressed Steel Bridge." Welding Innovation Quarterly, 1, No. 2 (Fall 1984), 12-13, 21.
74. "Steeling the Tension Arch." Engineering News-Record, 11 October 1984, pp 18-19.
75. Sterian, D. S. "Introducing Artificial Initial Forces into Steel Bridge Decks." Acier-Stahl-Steel, 34, No. 1 (Jan. 1969), 31-37.
76. Stras, J. C., III. "An Experimental and Analytical Study of Prestressed Composite Beams." M.S. Thesis. Rice University, Houston, Texas, 1964.
77. Szilard, R. "Design of Prestressed Composite Steel Structures." Journal of the Structural Division, ASCE, 85, No. ST9 (Nov. 1959), 97-123.
78. Tamberg, K. G. "The Analysis of Right, Multi-Girder Simple-Span Bridge Decks as Equivalent Torsionally-Weak Grid Systems." D. H. O. Report No. 102. Department of Highways, Downsview, Ontario, Canada, 1965.
79. Timoshenko, S. P. and J. N. Goodier. Theory of Elasticity. 3rd edition. New York: McGraw-Hill Book Company, 1970.
80. Timoshenko, S. and S. Woinowsky-Krieger. Theory of Plates and Shells. 2nd edition. New York: McGraw-Hill Book Company, 1959.
81. Tochacek, M. and F. G. Amrhein. "Which Design Concept for Prestressed Steel?" Engineering Journal, AISC, 8, No. 1 (Jan. 1971), 18-30.
82. Tochacek, M. and C. L. Mehta. "Economical Design of Prestressed Plate Girder." Journal of the Structural Division, ASCE, 98, No. ST6 (Jun. 1972), 1273-1289.
83. Tumminelli, S. C. and C. N. Kostem. "Finite Elements for the Elastic Analysis of Composite Beams and Bridges." Report No. 432.3. Fritz Engineering Laboratory, Lehigh University, Bethlehem, Pennsylvania, 1978.
84. Vernigora, et al. "Bridge Rehabilitation and Strengthening by Continuous Post-Tensioning." Prestressed Concrete Institute Journal, 14, No. 2 (Apr. 1969), 88-104.
85. Wei, B. C. F. "Load Distribution of Diaphragms in I-Beam Bridges." Journal of the Structural Division, ASCE, 85, No. ST5 (May 1959), 17-55.

86. Whipple, S. A Work on Bridge Building. Utica: H. H. Curtiss, 1847.
87. Yam, L. C. P. Design of Composite Steel-Concrete Structures. London: Surrey University Press, 1981.

9. APPENDIX. DERIVATION OF ΔT FORMULA FOR POST-TENSIONED BEAM WITH
PARTIAL-LENGTH COVERPLATE

After a simply supported beam is prestressed, it becomes a first-degree indeterminate structure. Hoadley [41] derived the change in tendon force for a beam of constant cross section, but that analysis is incorrect for the Iowa composite bridge beams which have partial-length coverplates.

The formula for the change in tendon force, given in Figure 8 for a beam with a partial-length coverplate, is derived below. Refer to Figure 8 for a view of the post-tensioned beam and definitions of the variables.

Take the change in tendon force, ΔT , caused by vertical load moment applied after post-tensioning, to be the redundant. Cut the tendons to release the structure, and measure the distance between the cut ends as δ .

By Castigliano's Theorem [65], δ may be computed with a partial derivative as follows:

$$\delta = \frac{\partial U}{\partial \Delta T}$$

where U is the strain energy.

For the beam,

$$U = U_{\text{moment}} + U_{\text{axial force}}$$

and, for the tendons,

$$U = U_{\text{axial force}}$$

Since δ must be zero for the post-tensioned beam,

$$\delta_{\text{beam}} + \delta_{\text{tendons}} = 0$$

or,

$$\frac{\partial U_{\text{bending, beam}}}{\partial \Delta T} + \frac{\partial U_{\text{axial force, beam}}}{\partial \Delta T} + \frac{\partial U_{\text{axial force, tendons}}}{\partial \Delta T} = 0$$

The strain energy listed in the numerators above can be computed as follows:

$$\begin{aligned} U = & \int_{y_1}^{y_2} \frac{(M - \Delta T e_{12})^2}{2EI_{12}} dy + \int_{y_2}^{y_3} \frac{(M - \Delta T e_{23})^2}{2EI_{23}} dy \\ & + \int_{y_3}^{y_4} \frac{(M - \Delta T e_{12})^2}{2EI_{12}} dy + 2 \left[\int_{y_1}^{y_2} \frac{(\Delta T)^2}{2A_{12}E} dy \right] \\ & + \int_{y_2}^{y_3} \frac{(\Delta T)^2}{2A_{23}E} dy + \int_{y_1}^{y_4} \frac{(\Delta T)^2}{2A_R E_R} dy \end{aligned}$$

Performing the differentiation, and integrating where possible,

$$\begin{aligned} - \frac{e_{12}}{EI_{12}} \int_{y_1}^{y_2} M dy + \frac{\Delta T (e_{12})^2 L_{12}}{EI_{12}} - \frac{e_{23}}{EI_{23}} \int_{y_2}^{y_3} M dy + \frac{\Delta T (e_{23})^2 L_{23}}{EI_{23}} \\ - \frac{e_{12}}{EI_{12}} \int_{y_3}^{y_4} M dy + \frac{\Delta T (e_{12})^2 L_{12}}{EI_{12}} + \frac{2\Delta T L_{12}}{A_{12}E} + \frac{\Delta T L_{23}}{A_{23}E} + \frac{\Delta T L_{14}}{A_R E_R} \end{aligned}$$

Solving for ΔT ,

$$\Delta T = \frac{\frac{e_{12}}{EI_{12}} \left[\int_{y_1}^{y_2} M dy + \int_{y_3}^{y_4} M dy \right] + \frac{e_{23}}{EI_{23}} \int_{y_2}^{y_3} M dy}{\frac{2(e_{12})^2 L_{12}}{EI_{12}} + \frac{(e_{23})^2 L_{23}}{EI_{23}} + \frac{2L_{12}}{A_{12}E} + \frac{L_{23}}{A_{23}E} + \frac{L_{14}}{A_R E_R}}$$

where,

$$\int_{y_1}^{y_2} M \, dy$$

represents the area of the moment diagram from y_1 to y_2 .